

https://dspace.org/

Synthesis of nitrogen doped carbon nanotubes using ferrocenes

Nxumalo, Edward Ndumiso

2011-10-12
http://hdl.handle.net/10539/10541

Downloaded from a DSpace repository. https://dspace.org/

Synthesis of nitrogen doped carbon nanotubes using ferrocenes

Edward Ndumiso Nxumalo

A thesis submitted to the Faculty of Science, University of the Witwatersrand, Johannesburg, in fulfilment of the requirements for the Degree of Doctor of Philosophy

April 2011

Declaration

I, the undersigned, declare that the work presented in this thesis was carried out by myself under the supervision of Professor Neil. J. Coville. All sources used in this work have been duly acknowledged. It is being submitted for the degree of Doctor of Philosophy in the University of the Witwatersrand, Johannesburg, and has not been submitted before for any degree or examination at this or any other university.



Edward Ndumiso Nxumalo

On this 22nd day of April 2011

Dedication

This work is dedicated to my mum, brother and sisters, my lovely wife and my grandmother who passed on in 2009.

Acknowledgments

This research work was carried out at the University of the Witwatersrand (Wits), School of Chemistry in the period (March 2007 – June 2010) as part of my PhD studies and would not have been conceived without the support and contributions from many people. I would like to express my sincere gratitude to everyone who contributed anything whatsoever to this thesis.

I am extremely grateful for the unique opportunity of having been one of Prof. Neil Coville's students in the School of Chemistry at Wits. Thank you very much Neil for being a mentor and friend. You have made my span in the School a very pleasant one. For those who do not know: 'Neil is naturally a very nice and humble personality'. It was a pleasure to work in your group and under your guidance. Your ideas, collaborations and professional advices have been put to good use and are wrapped up nicely in this manuscript.

There are several other individuals who contributed to this work from their different perspectives: Vincent Nyamori (for his contributions on the three papers we have published together), Amit Deshmukh (for his ideas on the catalysis work which is ongoing), Sabelo Mhlanga and Srinivasu Vallabhapurapu (for running ESR spectra and help analyzing the data), Paul Franklyn (for his great contribution to the work involving HRTEM), Rudolph Erasmus (for Raman spectroscopy measurements) and John Werner from the CSIR (for XPS analysis). Special thanks go to Basil Chassoulas (for the technical help with furnaces and those 'ancient' GCs) and Steve Gannon and Barry Fairbrother - the glassblowers (for providing all the glassware that was

required to conduct experiments and more especially for the injecting equipment). I am particularly grateful to the Electron Microscopy and Microanalysis Unit personnel *i.e.* Professor Michael Witcomb, Abe Seema and Caroline Lalkhan for the assistance and patience throughout the years I spent with you. Actually, I just cannot explicitly thank everyone.

The component of this project involving the influence of nitrogen sources on CNTs was a joint collaboration with our colleagues at the University of Johannesburg (UJ), especially Leskey Cele and Phatu Lestoalo. Phato performed most of the experiments in this component and published some in his MTech work. Guys, thanks for your contributions towards this work. The paper has finally been accepted for publication after many attempts. Whew..!

Further, I enjoyed the involvement of some B.Sc. Honours and M.Sc. students in the School who inspired some parts of this work: Mahaleao Kao, Vongane Chabalala, Terisha Rampersadh, Myron Johnson and Nafise Ghadimi.

My acknowledgements would not be complete if I did not express my gratitude to the CATOMAT research group members who were always there to give social support. Guys, thanks for the good times and those clownish moments we shared: Prof. Mike, Tsenolo, Haifeng, Justice, Ahmed, Ketulo, Sibongile, Myriam, Ella, Wonga, Themba, Messai, Thabiso, Nikiwe, Manoko, Moses, Mahluli, Ellen, Staton, Linda, Nthabiseng, Dean, Isaac, *etc.* I have been delighted to work with all of you guys. Keep that good working spirit! I would also like to give credit to our administrators, Colleen Courts, Agnes Pointer, Kitty Banda and Amanda Morgan. Keep up the good work!

I am very grateful to the School of Chemistry for the opportunity to have tutored and demonstrated for undergraduate students; it enhanced my teaching skills. Financial support for this research was provided by CoE/NRF in Strong Materials, Mellon Foundation, Canon Collins and MSSA trust. I am so grateful to all these funding programmes.

I would like to specially thank Prof. Bhekie Mamba (UJ) and his family for always being there for me. I still remember the first day I came and slept over in your house in 2004. Actually, that is how all these started. Many thanks!! I look forward to re-joining you soon at UJ. To our family friends (Sabelo and Phindile), we enjoy your everyday presence in our life. I am also indebted to my Church in Johannesburg, Jesus Calls Worship Centre. To my family and friends - thank you so much for always being there for me, especially very recently when I was wedding. For those that I did not mention here, thank you so much; all of you equally provided a fruitful working environment for my studies.

My most heartfelt thanks go to my lovely wife, who is naturally a very nice and warm person. Bongiwe, you are that spark of light in my life. Thanks NKHABANHLE! This work is my tribute to you.

Finally, I would like to thank God Almighty for making me what I am today. I'm wiser, I'm stronger, I'm better!! To Him be all the Glory and the Honour forever and ever.

Brief CV for Edward Nxumalo

Objective and interests

- Seeking a competitive position in the field of nanotechnology (nanomaterials or nanochemistry) in academia, industry or research arena
- Interested in nanotechnology research (application of nanomaterials in catalysis, fuel cells and water treatment); nanotechnology consultation; commercialization of nanotechnology in SA; teaching basic Chemistry at tertiary level; willing to consider travel and further training.

Current engagement (2010/2011)

Post-doctoral Research Fellow; Univ. Johannesburg

- Host: Prof. Bhekie Mamba
- CNT/polymer membranes for water purification and use of doped carbon systems in catalysis. - Co-supervising UJ and Wits M.Sc. students

Recent education

2007 - 2010 Wits University - PhD - Chemistry

- Nanotechnology - Synthesis of nitrogen doped shaped carbon nanomaterials using organometallic complexes; their properties and applications
- Supervisor: Prof. Neil Coville; - Co-supervised several B.Sc. Honours students

2004 - 2006 UJ – MTech in Chemistry

- Area: Cyclodextrin polymers for the removal of organic pollutants from water
- Supervisors: Prof. B.B. Mamba and Prof. R.W. Krause; Co-supervised B-Tech students

Research articles emanating from this thesis

- E.N. Nxumalo, V.O. Nyamori, N.J. Coville, *J. Organomet. Chem.* 693 (2008) 2942.
- V.O. Nyamori, E.N. Nxumalo, N.J. Coville, J. Organomet. Chem. 694 (2009) 2222.
- E.N. Nxumalo, V.P. Chabalala, V.O. Nyamori, M.J. Witkomb, N.J. Coville, *J. Organomet. Chem.* 695 (2010), 1451.
- E.N. Nxumalo, P.J. Letsoala, L.M. Cele, N.J. Coville, *J. Organomet. Chem.* 695 (2010), 2596.
- E.N. Nxumalo, N.J. Coville, *Materials*, 3 (2010) 2141.
- S.D. Mhlanga, E.N. Nxumalo, N.J. Coville, S.V. Vallabhapurapu, *Materials Chemistry and Physics* (2010), *submitted.*
- N.J. Coville, S.D. Mhlanga, E.N. Nxumalo, A. Shaikjee, *S. Afr. J. Sci.* 107 (2011) 1.
- E.N. Nxumalo, A. Shaikjee, M. Mamo, N.J. Coville, Facile method towards the fabrication of gold/nitrogen doped carbon nanotube hybrids, *submitted (2010).*
- E.N. Nxumalo, P. Frankylin, N.J. Coville, HRTEM studies of nitrogen doped carbon nanotubes, *submitted (2011).*

Other publications

- B.B. Mamba, R.W. Krause, T.J. Malefetse, E.N. Nxumalo, *Environ. Chem. Lett.* 5(2) (2007) 79.
- B.B. Mamba, R.W. Krause, T.J. Malefetse, S.D Mhlanga, S.P. Sithole, K.L. Salipira and E.N. Nxumalo, *Water SA* 33(2) (2009), ISSN 0378.
- Co-author of the Water Research Commission (WRC) report entitled: Cyclodextrin for the removal of pollutants from water, 2005.
- S.D. Mhlanga, E.N. Nxumalo, M. Zamxaka, Careers in Nanoscience and Nanotechnology, SASTSA, DST/NRF, South Africa, 2010.
- E.N. Nxumalo, S.D. Mhlanga, M. Zamxaka, Nanotechnology: A solution to South Africa's Five Grand Changes? SASTSA, DST/NRF, South Africa, 2010.
- S.D. Mhlanga, E.N. Nxumalo, C. Pretorius, S. Bergh, Nanotechnology in food and agriculture, Afgriland, AFGRI Operations LTD, South Africa, 2010.

Appointments

- Safety representative - 2008/9 (Wits University – School of Chemistry)
- Co-founder of SabiNano Trading cc (a company concerned with commercialization of nanotechnology products and consultation in South Africa)
- Co-editor of the Nanonewsletter (South Africa)
- Secretary of the Board: Jesus Calls Worship Centre (Church Affiliation)

Awards received

- SACI Sasol Postgraduate Medal – 2010
- Best PhD student presenter at Nanotechnology Young Researcher Symposium (NYRS) CSIR (Pretoria) – 2009
- Finalist (top 5) in the Moola for Amanzi business plan competition – an event organized by WISA and Netherlands Water Partnership
- Awarded the Mellon Foundation for 2009
- Best student for DST/Centre of Excellence (Carbon nanotubes and strong composites) for 2008.
- Award 3rd Position in the NIC innovation competition (SabiNano cc.) - 2008
- NRF/DST Centre of Excellence Bursary (2007 and 2008)
- Best 2004 Student Poster Presentation in Technikon Witwatersrand, during the Technikon Research Day
- Others: MSSA Trust, Canon Collins Trust, University of Johannesburg Postgraduate Award 2004-2005.

Conferences/workshops attended

- PhD Seminar, Wits University, Johannesburg, October 2010
- Presentation at the MSSA conference in December 2009 in UKZN (South Africa)
- Presentation in the NanoTech Insight Conference in Barcelona (Spain) in March 2009
- Presentation at the NanoAfrica Conference held in Pretoria-CSIR (South Africa) in February 2009
- Presentation at the Nanotechnology Young Researchers' Symposium (NYRS) CSIR in September 2009

- Presentation in the ICMR workshop for structure and properties for nanomaterials held in Richards Bay (July-August 2007)
- Several oral presentations at the CATOMMAT group meeting at Wits (Chemistry)
- Presented a poster at the 6th European Meeting for Environmental Chemistry (EMEC-6), December 2005 at Serbia and Montenegro (Belgrade) in Europe
- Presented a poster at the SACI Conference in CSIR (Pretoria in 2004).

Professional associations

1. Member of the South African Chemical Institute (SACI)
2. Member of the Water Institute of South Africa (WISA)
3. International Water Institute (IWA)
4. South African Nanotechnology Initiative (SANi)
5. CATOMAT member (CATOMAT is a research group on catalysis, organometallics and materials based at Wits University)
6. Member of the Centre of Excellence in Strong Materials (CoE-SM).

……

Abbreviations and symbols

Ar	argon
at.%	atomic concentration by percentage
Au	Gold
BET	Brunauer, Emmett and Teller
CNTs	carbon nanotubes
CNSs	carbon nanospheres
CVD	chemical vapour deposition
C_2H_2	acetylene
Co	cobalt
CO_2	carbon dioxide
CoE	Centre of Excellence
DP	deposition-precipitation
DWCNTs	double walled carbon nanotubes
EDX	energy dispersive X-ray spectroscopy
EFTEM	energy filtered TEM
ESR	electromagnetic spin resonance
EM	electron microscopy
FcH	ferrocene
FTIR	Fourie transform infrared
f-N-CNTs	functionalized nitrogen doped CNTs
Fe	iron
HNO_3	nitric acid
HRTEM	high resolution TEM
ID	inner diameter

IR	infrared spectroscopy
ml/min	millilitre per minute
ml/hr	millilitre per hour
MWCNTs	multi walled CNTs
N_2	nitrogen
N-CNSs	nitrogen-doped CNSs
N-CNTs	nitrogen-doped CNTs
N-SCNMs	nitrogen-doped SCNMs
nm	nanometre
NRF	National Research Foundation
mm	micrometre
OD	outer diameter
PXRD	powder X-ray diffraction spectroscopy
sccm	standard cubic centimetres per minute
SCNMs	shaped carbon nanomaterials
SEM	scanning electron microscopy
SWCNTs	single walled CNTs
wt.%	weight percentage
XPS	X-ray photoelectron spectroscopy
XRD	X-ray diffraction
TEM	transmission electron microscopy
TGA	thermogravimetric analysis
T	temperature
t	time

Abstract

Nitrogen doped carbon nanotubes (N-CNTs) have become a topic of increased importance in the study of carbonaceous materials. This arises from the physical and chemical properties that are created when N is embedded into a CNT. These properties include modified chemical reactivity, modified conductivity and changed mechanical, electronic and magnetic properties.

This thesis covers the analysis of the catalytic growth of N-CNTs under well defined conditions and the optimization of reaction conditions to produce N-CNTs. Herein, a range of methodologies have been devised to synthesize N-CNTs. One of the procedures used in this work uses a floating catalyst in which an organometallic complex is decomposed in the gas phase in the presence of a nitrogen containing reactant to give the N-CNTs. This thesis focuses on the use of ferrocene and ring substituted ferrocenes in the formation of N-CNTs and other shaped carbon nanostructures. It talks of the effects that physical parameters such as temperature, pressure, gas flow rates and the type and concentration of N source have on the N-CNT type, size and yields as well as the nitrogen content incorporated into the tubes that are produced using the organometallic complexes. Proposed growth models for N-CNT synthesis are also reported.

This work reveals that the N-CNTs produced are less stable (thermal gravimetric analysis measurements), less graphitic and more disordered (transmission electron microscope measurements) than their undoped counterparts. The ratio of the Raman D- and G-band intensities increase with the nitrogen concentration used during the CNT growth. Furthermore, the transmission electron microscopy (TEM) studies reveal that the CNTs are multi-walled, and that the diameters of the N-CNTs can be controlled by systematically varying the concentrations of the nitrogen source. Furthermore, X-ray photoelectron spectroscopy (XPS) and CHN analysis demonstrate that substitutional N is indeed present in the CNTs mainly as pyridinic and pyrrolic

N (and is sp^2 and sp^3 coordinated). The TEM analysis also revealed that when ferrocenylaniline and ferrocene/aniline reactions are compared at similar Fe/N molar ratios, higher N doping levels are achieved when ferrocenylaniline is the catalyst. Investigations of surface and interior imaging of N-CNTs was carried out by high resolution TEM (HRTEM) and identification of N-rich regions were performed by Energy filtered TEM (EFTEM).

We also investigated the solid state pyrolysis of ferrocenylmethylimidazole or a mixture of ferrocene (FcH)/methylimidazole at 800 ^{o}C at different ratios in sealed quartz tubes. TEM studies showed bamboo compartments are present in the CNTs. An investigation of the bamboo structures revealed that three methylimidazole structural isomers led to tubes with different individual bamboo compartment distances and different morphologies including different N contents. It was observed that when diverse N containing hydrocarbons were used the amount of N in the nitrogen containing reagent is more important than the source and type of the N atoms used as revealed by trends in the morphology of the N-CNTs produced. We have also studied the effect of arylferrocene ring substituents on the synthesis of CNTs and other shaped carbon nanomaterials in subsequent chapters.

Magnetic properties of different N doped carbon structures produced in the earlier chapters were investigated using electron spin resonance (ESR) spectroscopy. Most importantly, we observed a large *g*-factor shift in samples of N-CNTs from that of the free electron. Further, the shift is temperature dependant.

A facile method for attaching Au nanoparticles to the surface of pristine N-CNTs and functionalized N-CNTs has been developed. The Au nanoparticles incorporated in the N-CNTs have a wide range of diameters (10 – 35 nm) and possess different shapes. The method offers certain advantages, such as providing Au nanoparticles in good yields and ease of use. The Au/N-CNT nanohydrids are being employed in catalytic reactions *e.g.* the oxidation of styrene.

Table of contents

Declaration i

Dedication ii

Acknowledgments iii-v

Brief CV for Edward Nxumalo vi-ix

Abbreviations and symbols x-xi

Abstract vii-xiii

Table of content xiv-xv

.....

Chapter 1

Introduction 1-11

Chapter 2

A review of shaped carbon nanomaterials: A personal perspective 12-31

Chapter 3

Experimental section 32-38

Chapter 4

Nitrogen doped carbon nanotubes from organometallic compounds: A review 39-83

Chapter 5

CVD synthesis of nitrogen doped carbon nanotubes using ferrocene/aniline mixtures 84-107

Chapter 6
Influence of methylimidazole isomers on ferrocene-catalysed nitrogen doped carbon nanotube synthesis 108-131

Chapter 7
The influence of nitrogen sources on nitrogen doped multi-walled carbon nanotubes 132-162

Chapter 8
The effect of arylferrocene ring substituents on the synthesis of multi-walled carbon nanotubes 163-182

Chapter 9
Nitrogen doping of CVD multi-walled carbon nanotubes: Observation of a large *g*-shift 183-199

Chapter 10
Facile method towards the fabrication of gold/nitrogen doped carbon nanotube hybrids 200-211

Chapter 11
HRTEM studies of nitrogen doped carbon nanotubes 212-227

Chapter 12
Conclusions and perspectives 228-232

Appendices 233-251

Chapter 1
Introduction

1.1 General overview

Shaped carbon nanomaterials (SCNMs) have been actively studied over the past two decades because of their unique properties. These SCNMs typically include carbon nanotubes (CNTs), nanospheres (CNSs), nanofibers, nanohorns, nanocages, nanocoils, *etc.* CNTs have by far been regarded as the most central and pivotal type of the SCNMs and have been in the forefront of nanotechnology based research for many years [1-3]. These CNTs have remarkable electronic, magnetic, thermal, chemical and mechanical properties [4-11]. Although the properties of CNTs are tremendous, there are still many areas of application where pristine CNTs are not the 'best'. Quite recently, nanotube scientists have shifted their focus to modifying CNTs using several approaches in order to enhance their properties [12-14]. By modifying the CNT structure, one can form CNTs of defined morphology, with subsequent control of the CNT properties. Several strategies have been employed in the structural modification of CNTs. These strategies include among others, surface functionalization [15-16] and *substitutional doping* [17-18]. The present work focuses mainly on the doping of SCNMs, in particular CNT doping.

Doping entails the intentional introduction of foreign atoms ('heteroatoms') into the CNT lattice. The study of doping of SCNMs with heteroatoms has recently attracted considerable interest, since doping is known to induce exciting electronic properties into the nanomaterials and provide a means of tuning the field emission of CNT emitters [19-22]. It has been shown theoretically and experimentally that nitrogen and boron doping significantly enhance the mechanical, conducting, magnetic, field emission, energy storage and electron transport properties as well as the catalytic activity in oxidation reactions of SCNMs [23-29]. Interestingly, the doped CNT material leads to enhanced electronic performance (for example electrical conductivity) due to the participation of an additional lone pair of electrons in the delocalised system of the hexagonal framework. Nowadays, the study of CNT doping has entered explosion growth regime due to their potential use as field effect transistors, logic circuits, sensors, in gas storage and adsorption, and as fillings of reinforced composites, *etc.* [17,25,27].

Nitrogen behaves as an electron donor when doped into the graphitic structure and this enhances the CNT conductivity. Thus, the chemical structure of the nitrogen doped CNT (N-CNT) is expected to be strongly dependent on its synthesis route. Many researchers have demonstrated that the morphology and chemical composition of N-CNTs and N-CNT growth depend largely on the experimental procedures used [30-33]. To date, a comparative study on the influence of different synthesis conditions (*i.e.* catalyst, temperature, nitrogen source and gas flow) for incorporating N into the CNT lattice is lacking. Thus considerable effort is being brought to bear on the study of the fabrication, controlled synthesis and the growth mechanism of the related carbon nanostructures with nitrogen used as a dopant.

The methods for the synthesis of N-CNTs have often been limited to chemical vapour deposition (CVD) [34] and closed systems (*i.e.* autoclave systems or sealed quartz tubes) under autogenous pressure [35]. Among these techniques, the CVD process is generally the most widely used technique because it is cost effective, commercially viable and gives purer materials. The

floating catalyst [36-41] and supported catalyst [42] methods are the most common of the CVD techniques. However, the production of doped carbons using novel precursors and reproducible techniques is still highly desired. *Organometallic complexes* have recently been the focal point of N-CNT synthesis using in particular the floating catalyst method [43-44].

This research work focuses on the introduction of N into CNT structures using organometallic complexes. It describes the synthetic strategies used to produce N doped SCNMs (N-SCNMs), in particular N-CNTs using a range of organometallic precursors. The focus of this work is mainly on the use of ferrocene, and substituted ferrocenes for N-CNT production. Conventional characterization techniques (*e.g.* transmission electron and scanning microscopies, Raman and X-ray photoelectron spectroscopies, *etc.)* have been used to establish the presence of N in the N-CNTs. The introduction of a dopant atom into the SCNMs, in particular CNTs, can be achieved by adding the dopant atom as part of the catalyst or as part of the carbon source. All these procedures will be discussed in this thesis. In each section, an explanation of mechanistic models proposed to explain the formation of N-CNTs or N-SCNMs is discussed. The studies reported in this thesis have involved the synthesis and evaluation of the multi-walled type of CNTs (MWCNTs).

1.2 Objectives of the research project

The main objectives of this study are as follows:

i. To synthesize *ferrocene compounds* containing nitrogen functional groups. These materials were to be characterized by Fourie transform infrared (FTIR) and nuclear magnetic resonance (NMR) spectroscopic and crystallographic techniques at our disposal.

ii. To synthesize N-doped carbon nanotubes using a range of synthetic techniques. The catalyst (ferrocene compounds), the carbon sources and nitrogen sources were introduced as solutions into the reactor through a suitable carrier gas.

iii. To study the effect of the variation of the reaction conditions (temperature, reaction times, gas flow rate) on the types and yield of carbon nanotubes produced.

iv. To determine the precise conditions for optimal production of N-CNTs. This necessitated fine-tuning of the experimental parameters to yield quality N-CNTs with high yields at low cost.

v. To characterize the synthesized N-doped CNTs by transmission electron microscopy (TEM), high resolution TEM (HRTEM), energy filtered TEM (EFTEM), scanning electron microscopy (SEM), thermogravimetric analysis (TGA), Raman spectroscopy as well as other instrumental techniques at our disposal.

vi. To collaborate with colleagues on investigating the physical properties (*i.e.* magnetic) of the new N-doped CNTs using electron spin resonance (ESR) spectroscopy.

vii. To synthesize gold/N-CNT hybrid nanostructures. The methods involved surface functionalization of N-CNTs followed by fabrication of the hybrids by sonication procedures.

This work primarily focused on the use of different nitrogen containing substituents and ferrocene or ferrocene derivatives for N-CNT synthesis. The major objective of this research work was to specifically produce nitrogen doped CNTs. However, the variety of parameters used during the synthesis, inevitably led on occasion to the production of N-doped carbon nanospheres and other related nanomaterials. These compounds were to be characterized in a similar manner.

1.3 Structure of the thesis

This thesis is divided into 12 chapters. A brief explanation of the aims of each chapter is given below.

Chapter 1

This chapter (the current chapter) gives a general outlook of the work presented in this thesis. The main objectives of the study as well as the thesis outline are also presented in this chapter.

Chapter 2

Chapter 2 gives a general literature review on shaped carbon nanomaterials and especially on CNT production. The chapter gives a general overview of the worldwide carbon nanotube market. Introduction in CNT modification (including surface functionalization and doping) is also done in this part of the thesis. Emphasis on this review was placed on work carried out in South Africa. This work is a section of a review published recently: N.J. Coville, S.D. Mhlanga, E.N. Nxumalo, A. Shaikjee, *S. Afr. J. Sci.* 107 (2011) 1.

Chapter 3

This chapter summarizes all the methods and the techniques used in the synthesis of N-CNTs, although each chapter also gives specific details of experimental strategies pertinent to that chapter.

Chapter 4

This section covers the synthesis (and properties) of N-CNTs and other shaped carbon nanomaterials produced using organometallic complexes. It summarizes the effects that physical parameters such as temperature, pressure, gas flow rates, type and concentration of N source *etc.* have on the N-CNT type, size and yields as well as the nitrogen content incorporated into the tubes that are produced from organometallic complexes. Proposed growth models for N-CNT synthesis are also reported. This

chapter has also been published as a separate review: E.N. Nxumalo, N.J. Coville, *Materials*, 3 (2010) 2141.

Chapter 5

Chapter 5 reveals the effects of varying the N source concentration on the production of N-CNTs and other SCNMs in a CVD reactor. The work presented here demonstrates that the diameters of the tubes could be controlled by systematically varying the N source concentration. Further, it reveals that a higher N content is achieved by using the aniline substituted ferrocene as a catalyst when compared to ferrocene/aniline mixtures. A full manuscript is available: E.N. Nxumalo, V.O. Nyamori, N.J. Coville, *J. Organomet. Chem.* 693 (2008) 2942.

Chapter 6

Chapter 6 entails the formation of N-CNTs by the pyrolysis of ferrocenes and imidazoles in a confined environment. The work shows that the position of the methyl group attached to the imidazole can greatly influence the size distribution and the type of SCNMs produced in the 'autoclave' systems. The results presented in this chapter demonstrate that the control of N-CNTs is determined by fragments produced by decomposition of reactants at high temperature. This work has been published: E.N. Nxumalo, V.P. Chabalala, V.O. Nyamori, M.J. Witkomb, N.J Coville, *J. Organomet. Chem.* 695 (2010), 1451.

Chapter 7

In this chapter, we present the synthesis of N-CNTs by a nebulised floating catalyst method using a range of nitrogen containing complexes. It is shown that the amount of N in the nitrogen containing reagent is more important than the source and type of the N atoms used to make CNTs. A full manuscript is available: E.N. Nxumalo, P.J. Letsoala, L.M. Cele, N.J. Coville, *J. Organomet. Chem.* 695 (2010), 2596.

Chapter 8

Chapter 8 gives a study of the role of *para*-substituted ferrocene complexes on the production of SCNMs. The overall finding of this work is that the presence of Br and O in the organometallic complexes used to form SCNMs significantly reduces CNT growth. It is also shown that variations in the concentrations of precursor catalysts, the injection rate and pyrolysis temperature affected the type, distribution and dimensions of the SCNMs produced. This chapter has also been published: V.O. Nyamori, E.N. Nxumalo, N.J. Coville, J. Organomet. Chem. 694 (2009) 2222.

Chapter 9

In this chapter, we explore the magnetic properties of N-CNTs using electron spin resonance spectroscopy. We look at the variations in the spectral line shape, the *g*-factor shift and the line width at different temperatures and different N concentrations. These variations are analysed in terms of Elliott-Wagoner and the Bottleneck models. This work has been submitted for publication: S.D. Mhlanga, E.N. Nxumalo, N.J. Coville, S.V. Vallabhapurapu, *Materials Chemistry and Physics* (2010), *submitted.*

Chapter 10

This short chapter presents a facile method to attach varying amounts of gold nanoparticles to the surface of N-CNTs. The procedure involved two steps namely; the surface functionalization of the N-CNTs using the 'Prato' reaction and formation of the Au/N-CNT hybrid nanostructures using the sonication method. Characterization was performed by TEM and energy disperse X-ray (EDX) spectroscopy. This work has also been submitted for publication: E.N. Nxumalo, A. Shaikjee, M. Mamo, N.J. Coville, Facile method towards the fabrication of gold/nitrogen doped carbon nanotube hybrids, *submitted (2010).*

Chapter 11

This chapter explores the structural properties of the N-CNTs such as diameters, number of layers, interlayer spacing, using HRTEM. EFTEM was used to identify N-rich environments in the CNT lattice. This work has been submitted for publication: E.N. Nxumalo, P. Frankylin, N.J. Coville, HRTEM studies of nitrogen doped carbon nanotubes, *submitted (2010).*

Chapter 12

Chapter 12 gives general conclusions obtained from the research work presented in subsequent chapters. The chapter highlights the successes as they relate to the objectives of the project and zooms at potential future directions of the subject.

References

1. S. Iijima, Nature 354 (1991) 56.

2. D.S. Bethune, C.-H. Kiang, M. de Vries, G. Gorman, R. Savoy, J. Vazquez, R. Beyers, Nature 363 (1993) 605.

3. S. Iijima, T. Ichihashi, Nature 363 (1993) 603.

4. M.S. Fuhrer, J. Nygard, L. Shih, M. Forero, Y. Yoon, M. Mazzoni, H. Joon, J. Choi, S. Loui, A. Zettl, P. McEuen, Science 288 (2000) 494.

5. B.G. Demczyk, Y.M. Wang, J. Cumings, M. Hetman, W. Han, A. Zettl, R.O. Ritchie, Mater. Sci. Eng., A 334 (2002) 173.

6. C.P. Ewels, M.J. Glerup, Nano Sci. Nanotech. 5 (2005) 1345.

7. J. Tang, A. Matsushita, T. Tikegawa, M. Yudusaka, S. Bandow, S. Iijima, Mater. Rec. Soc. Symp. Proc. (2000) 593.

8. P. Serp, M. Corrias, P. Kalck, Appl. Catal. A 253 (2003) 337.

9. M.-F. Yu, O. Lourie, M.J. Dyer, K. Moloni, T.F. Kelly, R.S. Ruoff, Science 287 (2000) 637.

10. R. Pagani C & EN 1 (1999) 31.

11. M.M.J. Treacy, T.W. Ebbesen, J.M. Gibson, Nature 381 (1996) 678.

12. Y.-P. Sun, K. Fu, Y. Lin, W. Huang, Acc. Chem. Res. 35 (2002) 1096.

13. Y.-T. Liu, W. Zhao, Z.-Y. Huang, Y.-F. Gao, X.-M. Xie, X.-H. Wang, X.-Y. Ye, Carbon 44 (2006) 1613.

14. U. Vohrer, N.P. Zschoerper, Y. Koehne, S. Langowski, C. Oehr, Plasma Process. Polym. 4 (2007) S871.

15. A. Hirsch, O. Vostrowsky, Chem. Mater. Science 245 (2005) 193.

16. M. Vesali Naseh, A.A. Khodadadi, Y. Mortazavi, O. Alizadeh Sahraei, F. Pourfayaz, S. Mosadegh Sedghi, WASET 49 (2009) 117.

17. J. Tsang, M. Freitag V. Perebeinos, J. Liu, P. Avouris, Nature Nanotech. 2 (2007) 725.

18. H. Kang, S. Jeong, Phys. Rev. B 70 (2004) 233411.

19. H. Choi, J. Ihm, S. Louie, M. Cohen, Phys. Rev. Lett. 84 (2000) 2917.

20. O. Stephan, P. Ajayan, Science 266 (1994) 1863.

21. J.Y. Yi, J. Bernholc, Phys. Rev. B 47 (1993) 1708.

22. R. Czerw, M. Terrones, J. Charlier, X. Blasé, B. Foley, R. Kamalakaran, *et al.*, Nano Lett. 1 (2001) 457.

23. P. Ayala, A. Gruneis, T. Gemming, B. Buchner, M.H. Rummeli, D. Grimm, *et al.*, Chem. Mat. 19 (2007) 6131.

24. Y. Miyamoto, A. Rubio, M. Cohen, S. Louie, Phys. Rev. B 50 (1994) 4976.

25. P. Ghosh, M. Tanemura, T. Soga, M. Zamri, T. Jimbo, Solid State Commun. 147 (2008) 15.

26. M. Terrones, N. Grobert, H. Terrones, Carbon 40 (2002) 1665.

27. D. Golberg, Y. Bando, C.C. Tang, C.Y. Zhi, Adv. Mater. 19 (2007) 2413.

28. F. Villalpando-Paez, A. Zamudio, A.L. Elias, H. Son, E.B. Barros, S.G. Chou, Y.A. Kim, H. Muramatsu, T. Hayashi, J. Kong, H. Terrones, G. Dresselhaus, M. Endo, M. Terrones, M.S. Dresselhaus, Chem. Phys. Lett. 424 (2006) 345.

29. R. Chetty, S. Kundu, W. Xia, M. Bron, W. Schuhmann, V. Chirila, W. Brandl, T. Reinecke, M. Muhler, Acta 54 (2009) 4208.

30. R. Sen, B. Satishkumar, A. Govindaraj, K.R. Harikumar, M. Renganathan, C.N.R. Rao, J. Mater. Chem. 7 (1997) 2335.

31. Y. Lee, N. Kim, S. Bae, J. Park, S. Yu, H. Ryu, *et al.*, J. Phys. Chem. B 107 (2003) 12958.

32. A.A. Koos, M. Dowling, K. Jurkschat, A. Crossley, N. Grobert, Carbon 47 (2009) 30.

33. P. Ayala, A. Gruneis, C. Kramberger, M.H. Rummeli, Jr. F.L. Freire, I.G. Solorzano *et al.*, J. Chem. Phys. 127 (2007) 184709.

34 (a) P. Ayala, R. Arenal, M. Rummeli, A. Rubio, T. Pichler, Carbon 48 (2010) 575;

(b) C.P. Ewels, M. Glerup, J. Nanosci. Nanotechnol. 5 (2005) 1345.

35 (a) T. Cheng, Z. Fang, G. Zou, Q. Hu, B. Hu, X. Yang, Y. Zhang, Bull. Mater. Sci. 29 (2006) 701;

(b) J. Zhang, J. Li, J. Cao, Y. Qian, Mater. Lett. 62 (2008) 1839;

(c) V.G. Pol, S.V. Pol, J.M.C. Moreno, A. Gedanken, Carbon 44 (2006) 3285.

36. J. Liu, S. Webster, D. Carroll, J. Phys. Chem. B 109 (2005) 15769.

37. Z. Yang, Y. Xia, R. Mokaya, Chem. Mater. 17 (2005) 4502.

38. C. Tang, Y. Bando, D. Golberg, F. Xu, Carbon 42 (2004) 2625.

39. Y. Hao, L. Qingwen, Z. Jin, L. Zhongfan, Chem. Phys. Lett. 380 (2003) 347.

40. (a) X. Wu, Y. Tao, Y. Lu, L. Dong, Z. Hu, Diam. Rel. Mat. 15 (2006) 164.

(b) X. Wu, Y. Tao, C. Mao, L. Wen, J. Zhu, Carbon 45 (2007) 2253.

41. (a) P. Ayala, Jr. F.L. Freire, M.H. Ruemmeli, A. Grueneis, T. Pichler, Phys. Stat. Sol. B 244 (2007) 4051;

(b) H. Choi, J. Park, B. Kim, J. Phys. Chem. B 109 (2005) 4333;

(c) B.C. Satishkumar, A. Govindaraj, R. Sen, C.N.R. Rao, Chem. Phys. Lett. 293 (1998) 47;

(d) R. Andrews, D. Jacques, A.M. Rao, F. Derbyshire, D. Qian, X. Fan, E.C. Dickey, J. Chen, Chem. Phys. Lett. 303 (1999) 467.

42. X.Y. Tao, X.B. Zhang, F.Y. Sun, J.P. Cheng, F. Liu, Z.Q. Luo, Diam. Rel. Mat. 16 (2007) 425.

43 (a) B.C. Satishkumar, A. Govindaraj, C.N.R. Rao, Chem. Phys. Lett. 307 (1999) 158;

(b) M. Mayne, N. Grobert, M. Terrones, R. Kamalakaran, M. Rühle, H.W. Krato, D.R.M. Walton, Chem. Phys. Lett. 338 (2001) 101;
(c) B. Wei, R. Vajtai, Y.Y. Ajayan, P.M. Choi, Nano Lett. 2 (2002) 1105;
(d) C. Singh, M. Shaffer, I. Kinloch, A. Windle, Physica B 323 (2002) 339.
44. (a) P. Nikolaev, J. Bronikowski, R.K. Bradley, F. Rohmund, D.T. Colbert, K.A. Smith, R.E. Smalley, Chem. Phys. Lett. 313 (1999) 91;
(b) C.J. Lee, S.C. Lyu, H.W. Kim, C.Y. Park, C.W. Yang, Chem. Phys. Lett. 359 (2002) 109.

Chapter 2

[1]A review of shaped carbon nanomaterials: A personal perspective

2.1 Introduction

Carbon is a remarkable element and has been described as 'the key element of living substances' [1]. It is the ability of carbon to bond to itself to form oligomers and polymers that allows carbon to play this important role in life processes. This property can also be used to produce the myriad of structures that makes it such an important commodity element; for example, the element that leads to the basis of the Fischer-Tropsch process, used by Sasol in South Africa, to make fuels and chemicals. But its ability to form strong bonds to oxygen to generate CO_2 and lead to a carbon sink also reveals the 'dark side' of carbon. The control and understanding of the bonding properties of carbon thus becomes crucial if the chemistry of carbon is to be harnessed for the good of the world's peoples.

[1] N.J. Coville, S.D. Mhlanga, E.N. Nxumalo, A. Shaikjee, *S. Afr. J. Sci.* 107 (2011) 1

Carbon has four electrons that can be used for bonding and this determines the structural chemistry that is associated with the element. In the classical valence bond picture these four electrons (called sp^3 electrons) are used to form four bonds to other atoms. In the simplest case, when the bonds only occur between carbon atoms, C-C bonds are formed and the classical structure of diamond is produced (Fig. 2.1(a)). However, it is the ability of carbon to form multiple bonds between elements that gives carbon many of its unique features. In this way carbon can also link to another carbon atom to give C=C (found in graphite, Fig. 2.1(b)) and C≡C bonds (found in acetylene, Fig. 2.1(c)). The chemical and physical properties associated with the C-C, C=C and C≡C interactions are all different and the ability to controllably synthesize structures containing these units leads to an exploitation of the chemistry of carbon.

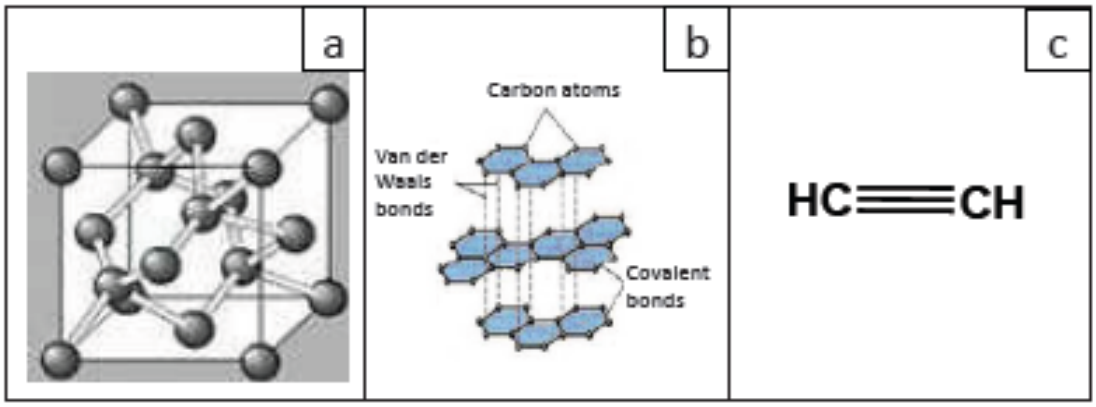


Fig. 2.1. Schematic diagrams of different carbon types: (a) diamond, (b) graphite and (c) acetylene.

This ability to make all-carbon containing nanomaterials, in particular those containing networks of C=C double bonds, has been one of the key events that has led to the current nanotechnology revolution. The discovery of fullerene in 1985 (Fig. 2.2(a)) [2] and the subsequent studies by Iijima [3] on carbon nanotubes in 1991 were key events that have spurred the study of nano structures in general and nano-carbon structures in particular. Through these discoveries a third

allotrope of carbon, following from the graphite (sp^2 hybridized carbon) and diamond (sp^3 hybridized carbon) allotropes, was recognized – this allotrope is based on a bent sp^2 hybridized carbon. These discoveries coincided with attempts to miniaturize devices (cell phones, computers, *etc*.) and the use and development of new characterization tools (scanning probe microscopes, electron microscopes) to visualize these new structures. The outcome has been the emergence of the field of Nanotechnology.

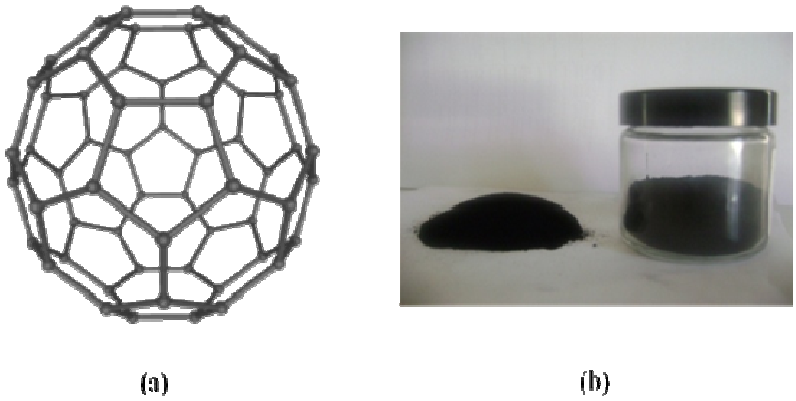


Fig. 2.2. Pictorial representation of: (a) a fullerene and (b) soot.

The most common form of oligomerized/polymerized carbon is soot (Fig. 2.2(b)). Soot, produced by burning carbonaceous materials, has an amorphous structure with little long range order. But, by controlled decomposition of carbon containing reactants under appropriate conditions it has been possible to make these carbons with long range order. Control of the experimental conditions permits morphology control (shape, length, diameter, *etc*.) of the carbon products at the nano level and this has generated a wide range of variously shaped carbon nanomaterials (SCNMs). The synthetic approach is based on templating and self-assembly principles, similar to the processes used to grow NaCl (salt) crystals from a salt solution, or rain-drops in clouds. Some of these SCNMs are shown in Fig. 2.3 and discussed in more detail below. As can be seen a wide range of structures can be made (tubes, spheres, helices, Y-junctions).

Each shape should influence the property of the carbon material and it is this carbon shape-property relationship that is the key to the manufacture of new devices. These new properties will also be influenced by the size of the SCNMs.

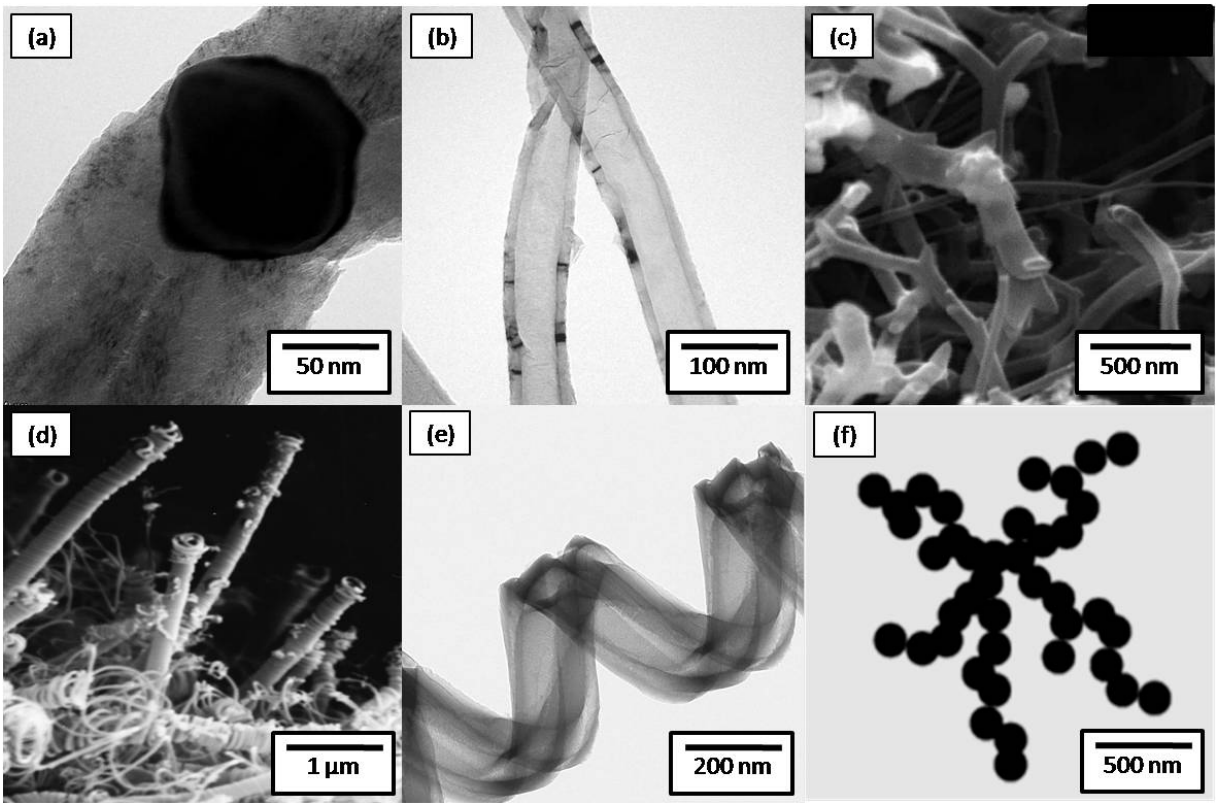


Fig. 2.3. Variety of shaped carbon materials: (a) solid fiber growing from catalyst particle, (b) tubular structure with hollow inner, (c) SEM image of branched carbon fibers, (d) SEM image of coiled carbon fibers, (e) TEM image of spring-like fiber and (f) Spherical carbon material.

The remarkable properties of nanocarbons include:

i) Carbon is a light element and structures made from carbon tend to be light weight (C is *ca* 6 x lighter than Fe).

ii) Carbon in tubular form has been shown to be the strongest material synthesized to date (Young's modulus for a single walled carbon nanotube (SWCNT) is *ca.*1 TPa) [4].

iii) Carbon can act as conductor, semi-conductor or insulator; this depends on the carbon-carbon bonding and the carbon structure.

iv) Carbon in the form of diamond or SWCNTs is the hardest material known.

v) The optical studies of carbon have shown that SWCNTs have absorbances of 0.98–0.99 over a wide range of wavelengths, making them a near perfect black body.

vi) The thermal conductivity of carbon is variable. In SWCNTs the thermal conductivity along the tube axis is 'ballistic' (10 x that of Cu) but perpendicular to the axis. A SWCNT is an insulator.

vii) The surface of carbon materials can be chemically modified (functionalized) leading to a new generation of reagents that can be used, for example, in composite materials.

Our own involvement in SCNMs dates back to the exploitation of using carbon as a catalyst support *i.e.* a material used to spread a metal catalyst and increase the number of metal atoms available at the surface for reaction. The finding that Au supported on carbon could be used to catalyze the reaction between ethyne (acetylene) and HCl to give CH_2=CHCl (vinyl chloride) as a monomer for polyvinylchloride synthesis [5] led us to investigate carbon nanotubes (CNTs) as Au supports in the mid 1990s. This required that we develop a programme for the synthesis of CNTs, studies that have since led us to investigate the synthesis of other shaped carbons as generic catalyst support materials.

A consideration of work on carbons in SA (and in Africa) has revealed little research in this area (with the exception of diamonds) prior to the mid 1990s. In SA, the company SA Carbide (operating out of Newcastle), has made carbon spheres for the battery market for decades. The carbon in pulp technology, for concentrating Au, has also been exploited in the mining industry since the 1990s [6]. More recently, the possibility of making C@U core-shell spheres for a

proposed Pebble Bed Modular Reactor (PBMR) to generate nuclear energy in SA has also seen an exploitation of the carbon market in the country [7].

Other than these examples the main development of carbons has been in the research arena, with activities focused in SA Chemistry and Physics Departments. For example, the CATOMAT research group based in the School of Chemistry at the University of the Witwatersrand is working on the synthesis of SCNMs and their application as strong materials in sensors, as catalyst supports, and in solar and fuel cells. Other groups at the University are working on new reactor designs for making SCNMs (Chemical Engineering), and studying their physical properties (*e.g.* mechanical, electronic properties; School of Physics) or their use as neuropharmaceuticals (Medical School). Research is also being performed on carbon nanotubes at many other SA Universities (University of Johannesburg, Tshwane University of Technology, University of KwaZulu Natal at Westville, Vaal University of Technology *etc.*) as well as at other SA research organizations (Centre for Nanostructured Materials, Council for Scientific and Industrial Research and MINTEK). The programmes range from pure synthesis to studies on the properties of carbon nanotubes.

Research in SA in this area is largely funded by the South African Department of Science and Technology while nanotechnology activities in SA are coordinated by the South African Nanotechnology Initaitive (SANi).

In the sections below a description of some of these new SCNMs that are being studied in our group is given. The coverage has been broken down according to the *shape* of the carbon material (tubes/fibers; spheres; helices; 'other' which includes graphene). Indeed all the SCNMs to be discussed can all be viewed as being generated from a single graphene sheet. For example Fig. 2.4 shows how a fullerene, a carbon nanotube or a graphite (layers) can be made from

grapheme sheet [8]. The review should thus provide an introduction to this new area of solid carbon chemistry.

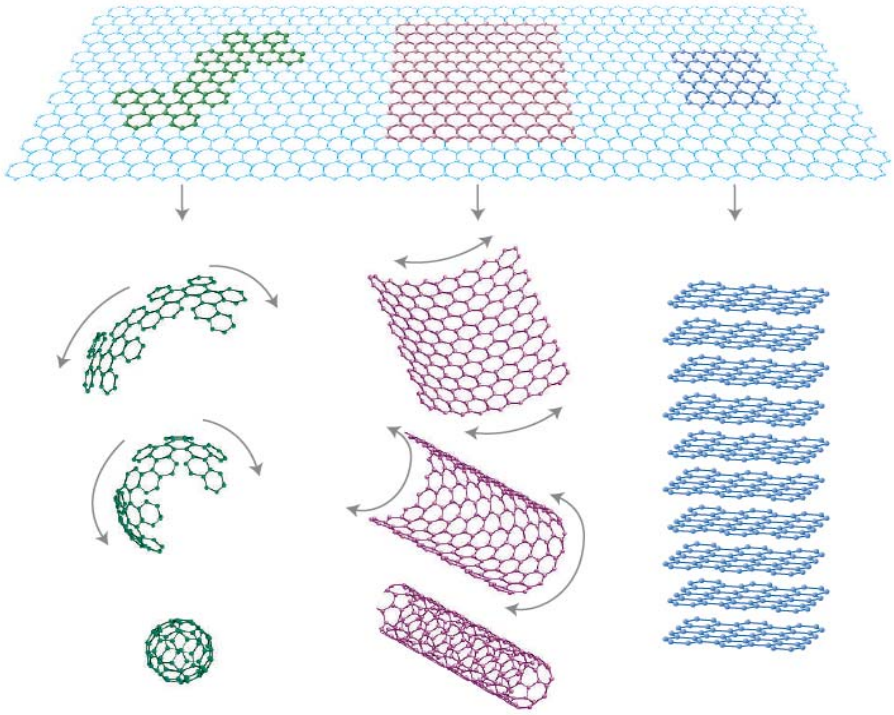


Fig. 2.4. Graphene is a 2D building material for carbon materials of all other dimensionalities. It can be wrapped up into 0D buckyballs, rolled into 1D nanotubes or stacked into 3D graphite [8].

2.2 Carbon nanotubes (CNTs) and carbon nanofibers (CNFs)

Carbon has the ability to form CNTs and CNFs in which the diameters are typically 1 - 100 nm while the lengths can range from 10 nm to a few cm's. Further, although typically represented as a material showing good alignment, CNTs and CNFs are generally synthesized with an appearance more like 'cooked spaghetti', made of interwoven strands of carbon as shown in Fig. 2.5. It is also possible to make carbon tubes that have Y- and T-junctions (Fig. 2.3(d)).

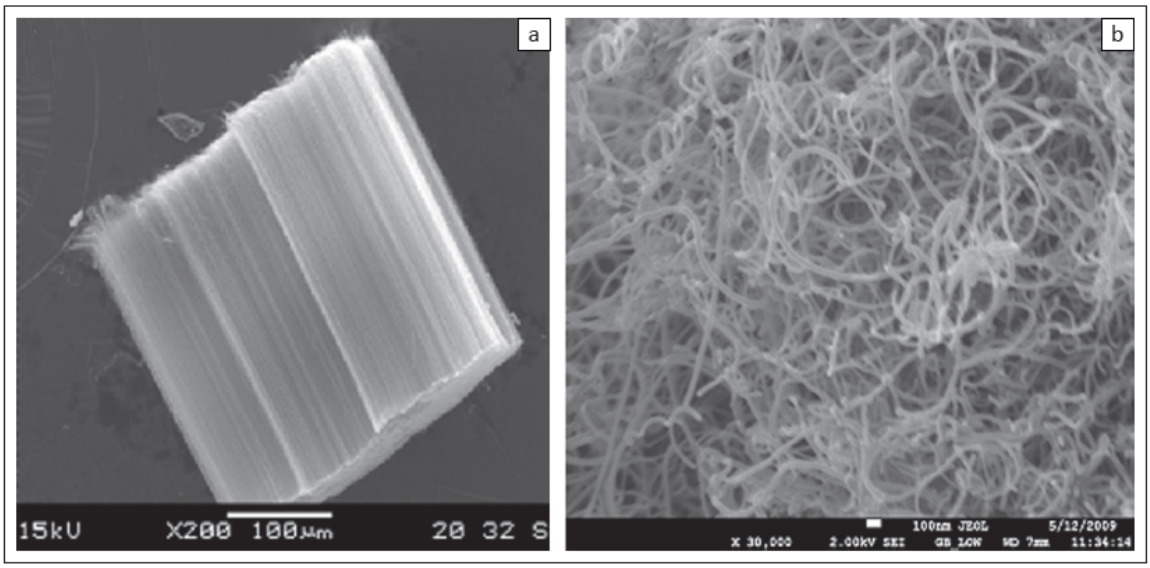


Fig. 2.5. SEM micrographs showing (a) aligned CNFs and (b) 'cooked spaghetti type' CNFs.

The difference between fibers and tubes relates to whether they are filled or hollow, but many variations of the filled and hollow tubes exist. Thus, the carbon tube/fiber can be made of V-shaped cups stacked on top of each other, or of flakes that generate a herring bone structure. Finally, the tubes can be partially layered in the tube hollow, generating a bamboo structure. (Fig. 2.6(c)). The ability to visualize the structures of carbon at the nano level has permitted the exploration of the synthesis and morphology of nanocarbons. Clearly, variations in the structural morphology must be related to the properties and uses of the tubes/fibers.

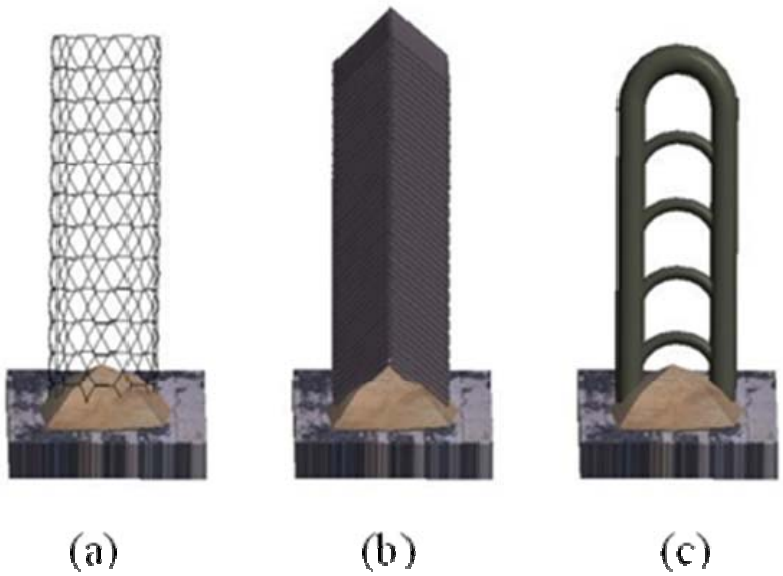


Fig. 2.6. Cartoon of (a) CNTs; (b) CNFs and (c) bamboo shapes.

CNTs can be described as seamless cylinders of rolled up graphene sheets of carbon atoms [9]. Depending on the number of rolled up graphene sheets, three types of CNTs have been observed, namely: single walled CNTs (SWCNTs), double walled CNTs (DWCNTs), and multi-walled CNTs (MWCNTs). On the other hand, CNFs are cylindrical nanostructures (Fig. 2.6(b)) with graphene layers arranged as stacked cones, cups or plates, as mentioned above. The history of CNFs dates back to 1889 [10] when CNFs were reported to be grown from carbon containing gases using a metallic crucible as the catalyst. In contrast, the history of CNTs dates to the 1950s [11] but with the explosive study of these materials only commencing in the 1990s [3]. In general, CNFs tend to be wider (> 100 nm) than CNTs (typically with internal diameters of < 50 nm) and can be synthesized at lower temperatures than required for CNT synthesis. Indeed fibers can be formed at T < 250 ^{O}C; these CNFs tend to be highly amorphous.

2.2.1 CNT and CNF synthesis

SCNMs are generally produced from the catalytic decomposition of hydrocarbon gases over selected metal nanoparticles. This process produces black 'soot', and when observed under an electron microscope, the tubular structures (tubes/fibers) can readily be detected. Generally, CNFs and CNTs are fabricated using similar synthetic approaches – heating a carbon source in the presence of a catalyst. However, changes in the reaction conditions, catalysts and precursors *etc*. determines whether CNFs or CNTs are produced. There are three conventional methods used to synthesize CNTs and CNFs: namely arc-discharge, laser ablation and catalytic chemical vapour deposition (CCVD). The CCVD process is the widely used technique to generate a relatively high yield of pure CNTs. Use of the CCVD method can produce aligned and ordered CNTs that can be grown in a controlled manner, which is not possible using the other conventional methods.

Typically, the CCVD approach requires a catalyst or template and a carbon source to produce SCNMs, in particular CNTs. The reaction is generally performed in a horizontal reactor such as that shown in Fig. 2.7. The reactor can also be arranged in a vertical geometry. The reactor system comprises of a quartz tube inserted into a hot oven. The carbon source is then passed through the quartz tube using an appropriate carrier gas at high temperature (typically 600 - 1100 ^{o}C) resulting in the decomposition of the reactants and production of the SCNMs. The reaction is usually performed in the presence of a catalyst. The catalyst can either be placed in the reactor (typically supported on an inert carrier to increase surface area) [12] or passed as a gas through the reactor (as a floating catalyst) [13]. While the supported catalyst method involves a catalyst dispersed on a support, the floating catalyst method normally uses volatile organometallic compounds as precursors, with $Fe(CO)_5$ and ferrocene typically being used in the catalytic synthesis procedure [14-15]. The latter method is advantageous because no support removal

procedures are required after the reaction and the catalyst can also be introduced into the CVD reactor as either a liquid or a gas.

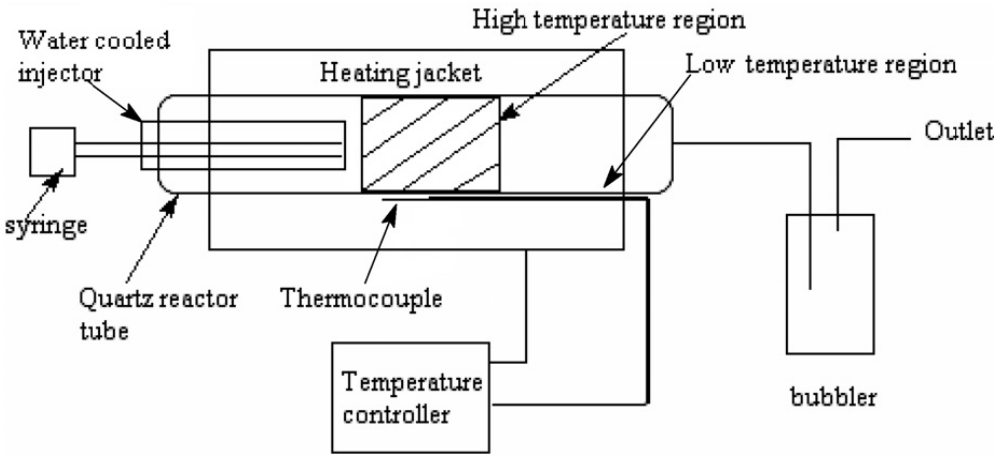


Fig. 2.7. Floating catalyst CVD reactor for the synthesis of SCNMs [14].

2.2.2 Modification of the CNT structure

CNTs are polymers of pure carbon that can be reacted and manipulated using the rich chemistry associated with carbon (sp^2 and sp^3 hybridisation states of C). This provides an opportunity to control the carbon nanostructure and also to optimise the solubility and dispersion characteristics of CNTs. Several strategies have been employed to modify the structure of the CNT both during and after synthesis. These methods include surface functionalization and substitutional doping.

2.2.3 Functionalization of CNTs

Many applications of CNTs require them to be dispersible in solvents (water, polar solvents) and to be compatible with polymer matrices. To achieve this, surface functionalization, especially of the outer wall of the CNT, is necessary. Functionalization modifies the physical and chemical

properties of the CNTs. CNT functionalization can be achieved by both covalent or non-covalent interactions and indeed, reviews have summarized functionalization strategies for CNTs [16]. Most of the methods reported require the synthesis and reactions of carboxylated CNTs, followed by covalent attachment of other functional groups to the CNTs [17].

Dispersion of CNTs can be achieved by sonication. The dispersion produced can be very stable and the CNTs can remain in solution for weeks or months. Functionalization methods such as oxidation of the CNTs can create more active bonding sites on the CNT surface. For biological uses, CNTs can be functionalized by attaching biological molecules, such as lipids and proteins, to surfaces. The CNT/biomolecule materials can be used to mimic biological processes, such as protein adsorption, the binding of DNA and drug molecules and the fixing of red blood cells. These reactions are very useful in medicine (and pharmaceutics), particularly in drug delivery systems.

2.2.4 Doping of CNTs

Doping is the intentional introduction of impurities into a material and the study of the doping of SCNMs with foreign atoms has attracted considerable interest. In the case of CNTs, this entails the inclusion of heteroatoms such as N and B into the all-carbon lattice. The heteroatom can be introduced into the CNT during the synthesis reaction (by using NH_3), or by adding N atoms to the carbon source or the catalyst ligand (if a floating catalyst is used).

The incorporation of heteroatoms (*e.g.* N) into a CNT modifies the tube characteristics. Microscopy studies reveal that the nitrogen doped CNTs (N-CNTs) are hollow inside with a likely occurrence of bamboo compartments [18] (Figs. 2.6 and 2.8). Incorporation of N atoms favors the formation of pentagons and heptagons and increases the reactivity of the neighboring C atoms resulting in a higher degree of disorder in a N-CNT relative to a ‘pure’ CNT. Thus,

considerable effort has been made to study the fabrication and the growth mechanism of the related carbon nanostructures with nitrogen as the dopant.

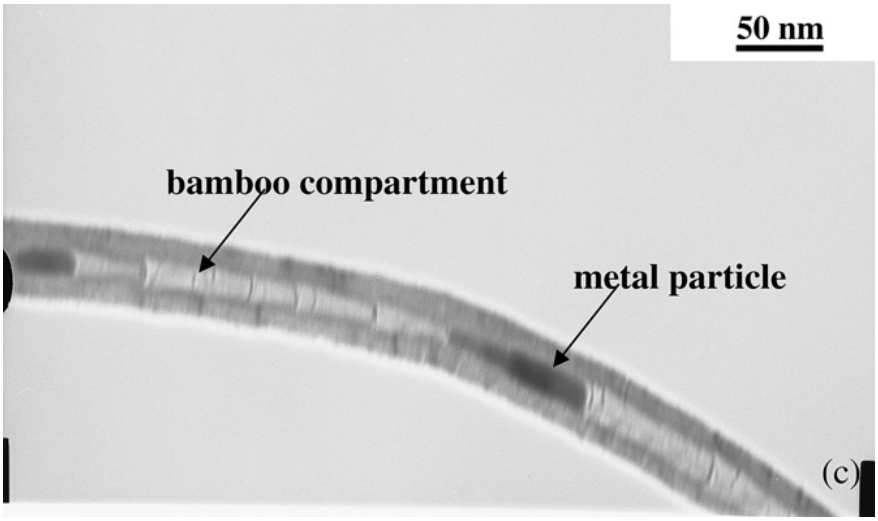


Fig. 2.8. TEM pictures of CNT grown from ferrocene/aniline mixtures. Note the bamboo compartments and metal catalyst particle trapped in the tube [18].

2.2.5 Growth mechanism

Many studies have reported the catalytic synthesis of CNTs and CNFs, in particular using metals such as Fe and Co as catalysts. There are two major mechanisms used to explain the catalytic growth of CNT or CNFs that depend on the position of the catalyst with respect to the substrate (Fig. 2.9). These are (i) the tip-growth mechanism (where the catalyst particle is located at the tip of a growing tube) and (ii) the root-growth mechanism (where the catalytic particle is found at the bottom of the tube) [13,19]. Thus, if the catalyst-support interaction is strong the base growth mechanism results but if the interaction is weak, the tip growth mechanism results. In both processes, the carbon reagent decomposes on the metal particle under the reaction conditions. The carbon deposited on the metal particle either dissolves in the metal and re-precipitates to

form a CNT (or CNF) or the carbon migrates over the metal particle to form the tube/fiber. If the catalyst particles are small, SWCNTs are formed and if they are larger, MWCNTS and CNFs are formed.

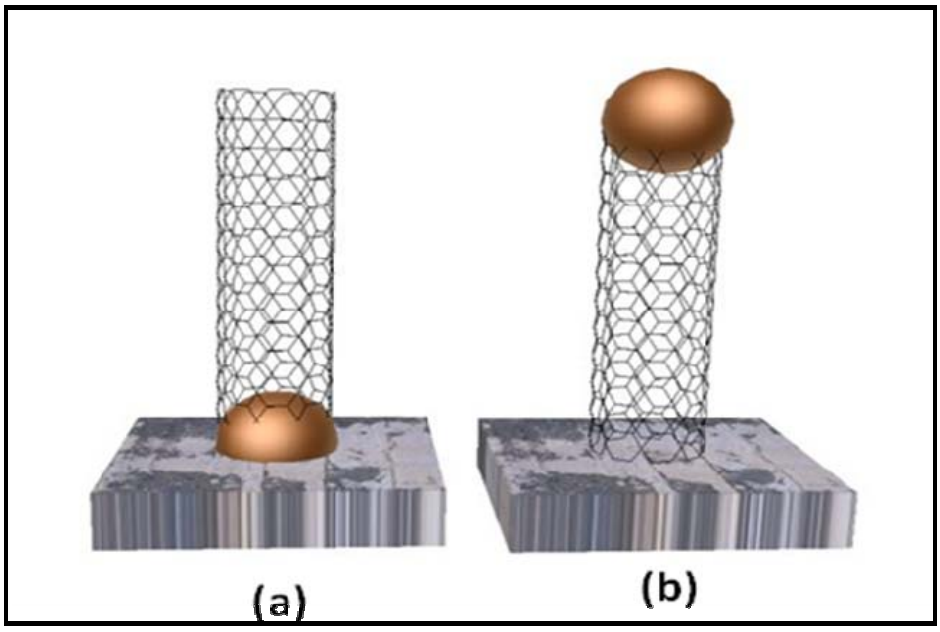


Fig. 2.9. CNT mechanistic models: (a) base growth and (b) tip growth mechanism

The use of a floating catalyst also generates metal particles leading to CNT (CNF) growth similar to that described above. The type of carbon formed will depend on the control of the catalyst particle morphology and catalyst particle size distribution during the reaction. To complicate mechanistic studies for carbon growth, carbon structures can also be formed *without* the use of a catalyst, although more typically carbon spheres (CSs) and amorphous carbon are produced in this instance.

2.2.6 Other types of tubular carbons

A few years after the discovery of straight tubular carbons, the synthesis of branched nanotubes was achieved [20]. These branched nanostructures (Fig. 2.2(c)) can form when non-hexagonal C rings are incorporated into the nanotube framework of the graphene sheet that builds the carbon nanostructure. Experimental studies on the production of branched MWCNTs, such as Y-branched CNTs (Y-CNTs), were first reported in 1995 using the arc-discharge method. These experiments were carried out under quite specific conditions, using a He atmosphere at 500 torr pressure and a hollow anode and Cu as a catalyst. Most methods to produce Y-CNTs usually take place at a relatively low growth temperature (typically 650 - 1000 °C; even at RT). In our own studies we have investigated the growth of branched CNTs using Cu as catalyst (arc-discharge method) and also observed that reaction conditions significantly affect the product obtained [21].

2.3 Properties and uses of tubular carbons

CNTs have been the focus of extensive studies because of their remarkable properties. However, CNFs also possess some of these special properties including among others: high electrical conductivity, high tensile strength, high elasticity, high thermal conductivity, low thermal expansion coefficient, good field emission properties and high aspect ratio [22]. Due to their extraordinary properties, tubular carbons provide a wide spectrum of applications in industry as well as in scientific research. Examples are field emission flat panel displays, field emission lamps, polymer fillers, hydrogen storage systems, gas sensors, X-ray sources, composite materials, electronics and gene or drug delivery [23]. CNTs and CNFs are also being used as catalyst supports for heterogeneous catalytic reactions. Due to their high surface area and diverse morphologies (sizes, shapes, *etc*.), tubular carbons have been used as supports in various catalytic reactions. For example, they have been explored as catalyst supports for Fischer-

Tropsch synthesis [24-25]. These metal/carbon materials display excellent activity and selectivity when compared to conventional catalyst supports such as alumina or silica.

Doping of CNTs with N or B induces novel electronic properties into the CNTs, and provides a means for tuning the field emission of CNT emitters. It has also been shown that N doping can enhance the mechanical, conducting, energy storage and electron transport properties of CNTs.

The branched CNTs have potential applications as building elements in nanoelectronic devices. For example, they can be used in a nanoscale three-terminal device or in other transistor applications.

2.4 Toxicity issues

Working at the nano level brings with it issues of health. Studies to investigate the toxicity of these new SCNMs is in its infancy with the impact of the materials on human cells being unknown. Studies are further complicated by the belief that effects will be influenced by the size, shape, agglomeration, as well as the concentration of the SCNMs. Care must thus be exercised by workers in this area of nanotechnology [26].

2.5 CNT market

The CNT market is growing rapidly and is estimated to exceed $1.9 billion by the end of 2010 [27]. Furthermore, governments, corporations and venture capitalists worldwide spent approximately $9.6 billion on nanotechnology research and development in 2005 [28]. The cost of CNTs varies from producer to producer. The variations in CNT prices are attributed to differences in production methods, locations, impurities, *etc.* The single-walled carbon nanotube (SWNT) market is projected to exceed $5 billion by 2012 [27,29]. In addition, advances in

nanotechnology have led to a drastic increase in publications and patents involving practical application of these materials in the past years [29]. Fig. 2.10 depicts a graph of the world's nanotechnology market in terms of application.

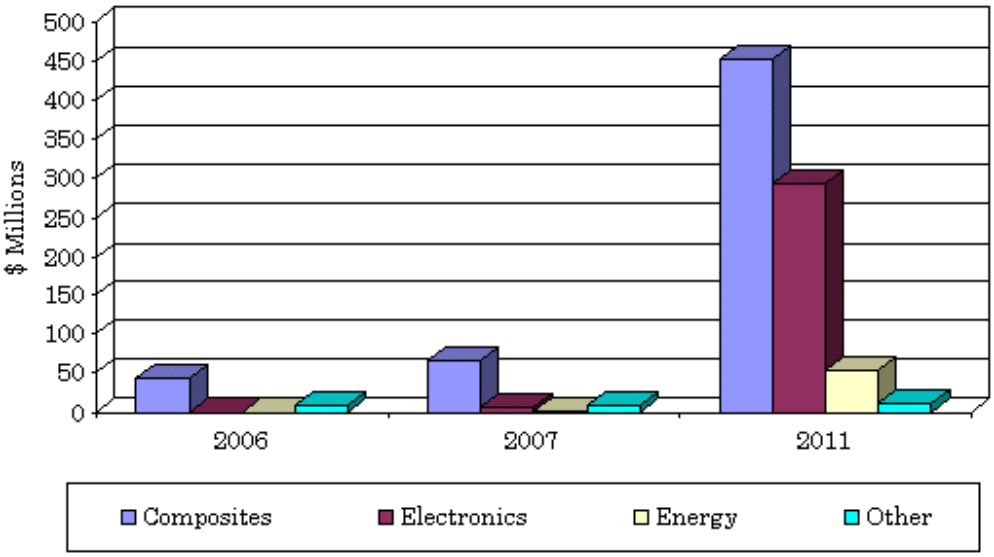


Fig. 2.10. Worldwide carbon nanotube market in terms of application [30].

CNTs have great potential to be used in a variety of applications such as composites, energy conversion, electronics, structural polymers, super capacitors, batteries, sensors, shielding, water, *etc.* [19,31-33]. With this wide range of applications it is important to understand the production costs for development of commercially viable CNT production. An understanding of the synthetic processes in the fabrication of CNTs is very important when estimating the cost involved in their production. The main method for large scale production of CNTs is the chemical vapor deposition (CVD) method and is considered as an inexpensive route when compared to other methods [34].

In the context of South Africa, however, very little has been done concerning commercializing the products of nanotechnology, especially CNTs. To date, only one manufacturing company is registered with the SA government to produce CNTs and other SCNMs in a large scale [35]. This company also seeks to supply industries and research institutions in SA and other African countries with information, consultation services and many products pertaining to nanoscience and nanotechnology. In the research and development department, the company focuses on methods and innovative processes of production as well as the development of the nanomaterials for use in specific applications [35].

References

1. P. Levi, The periodic table, New York: Shocken Books, 1984, p 227.
2. M.S. Dresselhaus, G. Dressalhaus, P.C. Eklund, Science of fullerenes and carbon nanotubes, New York: Academic Press, 1996.
3. S. Iijima, Nature 354 (1991) 56.
4. J.-P. Salvetat, G.A.D. Briggs, J-M. Bonard, *et al.,* Phys. Rev. Lett. 82 (1999) 944.
5. B.S. Nkosi, N.J. Coville, M.D. Adams, G.J. Hutchings, J. Catal. 128 (1991) 378.
6. M.D. Adams, J. South Afr. Inst. Min. Metall. (1994) Aug: 187.
7. C. McKune, S. Afr. J. Sci. 106 (2010) 1.
8. A.K. Geim, K.S. Novoselov, Nature Mater. 6 (2007) 183.
9. S. Iijima, T. Ichihashi, Nature 363 (1993) 603.
10. J. De, P. Krijn, J.W. Geus, Catal. Rev. Sci. Eng. 42(4) (2000) 481.
11. M. Monthioux, V.L. Kuznetsov, Carbon 44 (2006) 1621.
12. S.D. Mhlanga, K.C. Mondal, R. Carter, M.J. Witcomb, N.J. Coville, S. Afr. J. Chem. 62 (2009) 67.
13. V.O. Nyamori, S.D. Mhlanga, N.J. Coville, J. Organomet. Chem. 693 (2008) 2205.
14. V.O. Nyamori, E.N. Nxumalo, N.J. Coville, J. Organomet. Chem. 694(14) (2009) 2222.

15. M.S. Mohlala, X.Y. Liu, J.M. Robinson, N.J. Coville, Organometallics 24 (2005) 972.
16. K. Balasubramanian, M. Burghard, Small 1(2) (2005) 180.
17. R. Taylor, London Imperial College Press, 1999.
18. E.N. Nxumalo, V.O. Nyamori, N.J. Coville, J. Organomet. Chem. 693 (2008) 2942.
19. M. Endo, T. Hayashi, Y.A. Kim, M. Terrones, M.S. Dresselhaus, Phil. Trans. Roy. Soc. Lond. A 362 (2004) 2223.
20. Z. Osváth, A.A. Koós, Z.E. Horváth, *et al*., Chem. Phys. Lett. 365(3-4) (2002) 338.
21. S.H. Durbach, R.W. Krause, M.J. Witcomb, N.J. Coville, Carbon 43 (2009) 635.
22. T.W. Ebbesen, "Production and purification of carbon nanotubes," in Carbon Nanotubes: Preparation and Properties, T.W. Ebbesen, Ed., pp. 139–162, CRC Press, Boca Raton, Fla, USA, 1997.
23. M.S. Dresselhaus, M.A. Pimenta, K. Kneipp, S.D.M. Brown, P. Corio, A. Marucci, G. Dresselhaus. First and Second-Order Resonant Raman Spectra of Single-walled Carbon Nanotubes In Science and Applications of Nanotubes, D. Tomanek and R.J. Enbody (Eds.) Kluwer Academic, New York, 2000, p 255 – 76.
24. M.C. Bahome, L.L. Jewell, D. Hildebrandt, D. Glasser, N.J. Coville, Appl. Catal., A 287 (2005) 60.
25. M.C. Bahome, L.L. Jewell, K. Padayachy, *et al*., Appl. Catal., A 328 (2007) 243.
26. R.E. Hester, R.M. Harrison (Eds.), Nanotechnology - consequences for human health and the environment. Issues in Environmental Science and Technology, 2007, 24, Royal Society of Chemistry, Cambridge.
27. Lux Research (2006), The Nanotech Report, 4th edition, Lux Research Inc., New York, NY.
28. Report Code: NAN024C, Published: March 2007, Analyst: John Oliver.
29. J.A. Isaacs, A. Tanwani, M.L. Healy, L.J. Dahlben, J. Nanopart. Res. 12 (2010) 551.
30. New Report by Global Industry Analysts, Inc. http://www.strategyr.com/MCP-1507.asp (Accessed: 30 May 2010)
31. M. Paradise, T. Goswami, Mater. Des. 28 (2007) 1477.

32. M.J. Pitkethly, Nano Today (2004) 20.

33. http://www.nanoten.com/ntyp.html (Accessed on 20 May 2010).

34. A.C. Dupuis, Prog. Mater. Sci. 50 (2005) 929.

35. S.D. Mhlanga, E.N. Nxumalo, Sabinano Trading cc business plan, 2010.

Chapter 3
Experimental section

3.1 Introduction

Several methods exist for the synthesis of N-CNTs as reported in the literature [1-6]. These techniques include arc-discharge, laser ablation, chemical vapour deposition (CVD), autoclave systems, *etc.* In this study, three different procedures were used to make N-CNTs and other shaped carbon nanomaterials (SCNMs) namely (i) a CVD injection method, (ii) a spray pyrolysis method and (iii) an autoclave method. All the methods produced diverse SCNMs *i.e.* multiwall CNTs, carbon nanospheres, carbon nanofibers and amorphous materials. However, selectivity of the SCNMs produced was controlled by synthetic parameters *e.g.* synthetic precursors, temperature, flow rates, *etc.* For the production of N-CNTs, the methods require the use of a catalyst source, a carbon source and a nitrogen source to produce N-CNTs. In this work, several organometallic complexes (ferrocene and substituted ferrocenes) were studied as catalysts for N-CNT production and where appropriate the organometallic compounds were dissolved in an appropriate organic solvent such as toluene or benzene. In the sections below, the different methods are briefly described but more specific details for each method are given under the

experimental section of each chapter in this thesis. Characterization of the N-CNTs and other SCNMs was carried out using conventional characterization techniques as explained in section 3.3.

3.2 Production of SCNMs

3.2.1 CVD injection method

A quartz tube reactor (80 cm in length and 2.8 cm internal diameter) was inserted horizontally into an electrical furnace with the outlet of the tube connected to a gas bubbler as explained elsewhere [7-8]. The temperature inside the quartz tube was kept in the range of 800 – 1000 ^{o}C, under 5% H_2 in argon (*v/v*) at atmospheric pressure. The flow rate of H_2 in argon was varied between 100 and 200 ml/min. The organometallic precursors were dissolved in toluene (2.5 *wt.%* to 25 *wt.%*). In some instances, the catalyst loading in the solvent was limited by solubility constraints. The solutions were placed in a 10 ml or 20 ml syringe and injected into the heated tube by means of a SAGE syringe pump (0.2 to 1.0 ml/min injection rate). The solutions were injected into the tube reactor *via* a specially designed quartz tube (0.2 cm internal diameter and 20 cm in length) cooled by water. When solution injection was complete, the electrical furnace temperature was allowed to cool down to room temperature under 5% H_2 in argon (v/v), Ar or N_2.

3.2.2 Spray pyrolysis procedure

N-CNTs were also synthesized using the spray pyrolysis procedure (also referred to as the 'aerosol' procedure). In a typical synthesis, approximately 2.0 g of ferrocene was dissolved in a mixture of 50 ml of a nitrogen containing hydrocarbon and toluene. The precursors were nebulized using a 1.45 MHz oscillator [9-10] and carried into a 25 mm diameter quartz tube,

placed in a furnace which was maintained at a temperature of 850 ^{o}C. The average droplet size for the solvents is ~2.2 μm at 1.54 MHz frequency [9]. However, this frequency can be varied to yield different controlled droplet sizes. The nitrogen containing hydrocarbons were used as purchased (Sigma Aldrich and Fluka) and studied at concentrations of 1 - 8% in toluene. Ultra pure argon and hydrogen gases (and at times mixtures of gases) purchased at Afrox were used as the carrier gases and the gas flow rate was controlled using unit mass flow controllers. In a typical procedure, the carrier gas flow rate was kept at 400 ml (Ar) and 100 ml (H_2), respectively. The pyrolysis was carried out for 45 min. After the reaction, the argon flow rate was reduced to between 50 – 60 ml/min whilst the flow rate of hydrogen was switched off. The furnace was then allowed to cool to room temperature. The yields were determined by scraping the products from the reactor and weighing. Errors of < 10% can be expected in the yields, and trends are readily detected in the series of reactions performed.

3.2.3 Autoclave procedure

In this method, approximately 100 mg of the organometallic precursor compounds were sealed in a quartz tube (10 cm in length and 1.0 cm internal diameter) as explained previously [11-14]. The quartz tube was introduced into an electrical furnace and heated at a rate of 3 ^{o}C/min to reach a temperature of 500 ^{o}C *i.e.* above the precursor decomposition temperature. The tubes were held at this temperature for at least 30 min to ensure complete decomposition of reagents. The tube was then heated at a rate of 2 ^{o}C/minute to 800 ^{o}C (or 850 ^{o}C) and held at that temperature for 12 h before being gradually cooled to room temperature. In all instances, a black solid material was obtained and a small amount of the black carbonaceous material was transferred into a mortar and ground, using a pestle, to a fine material.

The samples obtained in each of the procedures were characterized by transmission electron microscopy (TEM), scanning electron microscopy (SEM), thermogravimetric analysis (TGA), Raman spectroscopy, CNH analysis, X-ray photoelectron spectroscopy (XPS), *etc.*

3.3 Characterization procedure

3.3.1 TEM analysis

Low magnification TEM analysis of the SCNMs was performed on a JEM 100S microscope and high magnification transmission electron microscopy was performed with a Philips CM200 microscope. Samples for TEM analysis were prepared by sonication of the SCNMs in methanol and a few drops of the resulting suspension were placed onto a holey copper TEM grid and viewed under several magnification. HRTEM was carried out on a Technai F20 X-twin FEG at 800 kV. The EFTEM image was constructed by recording with a 280 eV (carbon, green), 400 eV (nitrogen, blue), and 700 eV (iron, red) shift in the energy window and using 16 eV energy windows for background estimation.

3.3.2 SEM analysis

SEM results were performed on Jeol JSM 840 microscope. Samples for SEM analysis were mounted onto an aluminium stub using colloidal graphite and coated with carbon and gold-palladium.

3.3.3 TGA analysis

TGA data were collected from a Perkin Elmer TGA 7 analyzer. Samples (typically 5-10 mg) of SCNMs were loaded into platinum pans and heated to 1000°C in flowing air or N_2 at a heating rate of 10 ml/min.

3.3.4 Raman analysis

Raman spectra were measured using the single spectrograph stage of a Jobin-Yvon T64000 Raman spectrometer. The excitation source was 636.4 nm from a tunable Spectra-Physics dye laser. The laser beam was focused onto the sample using the 20x objective of an Olympus microscope. The backscattered light was dispersed using a 600 line/mm grating and detected using CCD detector.

3.3.5 XPS

XPS analysis was carried out on a Physical Electronics Quantum 2000 analyser with resolution of 0.1 at.%.

3.3.6 Other techniques

BET surface area analysis was carried out on a Micromeritics TriStar Surface Area and Porosity Analyzer and Powder X-ray diffractometry (PXRD) on a Bruker axs D8 Advance PXRD. The carbon, hydrogen and nitrogen (CHN) content was measured at the Institute for Soil, Climate and Water (Pretoria, South Africa). Infrared spectra were recorded in the range 400-4000 cm^{-1} using KBr pellets (Bruker Tensor 27 spectrometer). Electron spin resonance (ESR) spectroscopy measurements were carried out with a JEOL spectrometer with a modulation field of 0.4 mT, 0.9

mW microwave power and a microwave frequency of 9 GHz. A clean quartz sample tube was loaded with N-CNTs (200 mg) and inserted in the instrument. The measurements were carried out in the temperature range of 293 K to 400 K.

References

1. R. Sen, B. Satishkumar, A. Govindaraj, K.R. Harikumar, M. Renganathan, C.N.R. Rao, J. Mater. Chem. 7 (1997) 2335.

2. M. Glerup, M. Castignolles, M. Holzinger, G. Hug, A. Loiseau, P. Bernier, Chem. Comm. 20 (2003) 2542.

3. Y. Lee, N. Kim, S. Bae, J. Park, S. Yu, H. Ryu, *et al*., J. Phys. Chem. B 107 (2003) 12958.

4. A.A. Koos, M. Dowling, K. Jurkschat, A. Crossley, N. Grobert, Carbon 47 (2009) 30.

5. P. Ayala, A. Gruneis, C. Kramberger, M.H. Rummeli, Jr. F.L. Freire, I.G. Solorzano, *et al*., J. Chem. Phys. 127 (2007) 184709.

6. P. Ayala, A. Gruneis, T. Gemming, B. Buchner, M.H. Rummeli, D. Grimm, *et al*., Chem. Mat. 19 (2007) 6131.

7. B.C. Satishkumar, A. Govindaraj, R. Sen, C.N.R. Rao, Chem. Phys. Lett. 293 (1998) 47.

8. R. Andrews, D. Jacques, A.M. Rao, F. Derbyshire, D. Qian, X. Fan, E.C. Dickey, J. Chen, Chem. Phys. Lett. 303 (1999) 467.

9. S.R.C. Vivekchand, L.M. Cele, F.L. Deepak, A.R. Raju, A. Govindaraj, Chem. Phys. Lett. 386 (2004) 313.

10. L.M. Cele, Carbon nanotubes and nanospheres: Synthesis by nebulized spray pyrolysis and use in catalysis, PhD thesis, University of Johannesburg, 2008.

11. V.G. Pol, S.V. Pol, J.M.C. Moreno, A. Gedanken, Carbon 44 (2006) 3285.

12. C.P. Ewels, M. Glerup, J. Nanosci. Nanotechnol. 5 (2005) 1345.

13. T. Cheng, Z. Fang, G. Zou, Q. Hu, B. Hu, X. Yang, Y. Zhang, Bull. Mater. Sci. 29 (2006) 701.

14. J. Zhang, J. Li, J. Cao, Y. Qian, Mater. Lett. 62 (2008) 1839.

Chapter 4

[2]Nitrogen doped carbon nanotubes from organometallic compounds: A review

4.1 Overview

Carbon nanotubes (CNTs) and other shaped carbon nanomaterials (SCNMs) that include nanospheres, nanofibers, nanohorns, nanocages, *etc*. have been actively studied since the first reports on the synthesis of single-walled carbon nanotubes (SWCNTs) [1–2]. Since these reports, many different procedures have been used to make SCNMs. An analysis of the current literature reveals that the chemical vapor deposition (CVD) approach is the most common method used to make SCNMs and in particular CNTs on a large scale [3–4].

There are many variations of the CVD approach, but in all cases the procedure requires a catalyst [5–11] or template [12] and a carbon source to produce the SCNMs. A reaction is typically performed in a reactor such as that shown in Fig. 4.1 [8]. The reactor could also be arranged in a

[2] E.N. Nxumalo, N.J. Coville, *Materials*, 3 (2010) 2141

vertical geometry. The reactor system comprises of a quartz tube inserted into an oven. Passage of the reactants through the quartz tube at high temperature results in the decomposition of the reactants and production of SCNMs. From the perspective of organometallic chemistry, numerous organometallic complexes have been used in the catalytic synthesis procedure. These complexes can either be used to make a supported metal catalyst or can be added to the catalytic reactor, without addition of a support. The focus of this review is on the latter procedure where the organometallic complexes are decomposed *in situ* during CNT synthesis. In this approach the catalyst can be introduced as a liquid or gas.

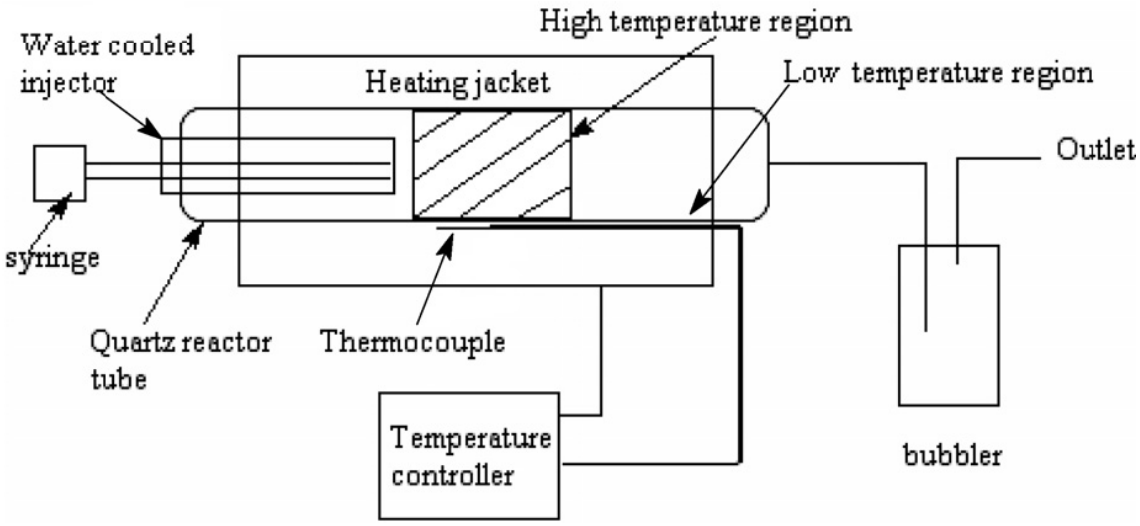


Fig. 4.1. Floating catalyst CVD reactor for the synthesis of SCNMs [8].

Liquid catalysts *e.g.*, iron pentacarbonyl ($Fe(CO)_5$), can be introduced by a syringe procedure either pure, or diluted in a solvent. However, most organometallic complexes that have been used are solids at room temperature. Alternative strategies are then needed. Introduction of ferrocene (FcH), for example, can be achieved in a process referred to as the injection CVD method by dissolving FcH in a suitable solvent, which is typically the carbon source used to make SCNMs and the solution introduced into the reactor by means of a syringe procedure. In a

second method, a variation of the above procedure, the FcH/solvent mixture can be introduced into the reactor by an aerosol process. In this instance, a mixture of FcH and solvent are sonicated and the aerosol produced is transferred to the reactor by means of a gas (Ar, N_2 or H_2). A third method used to introduce FcH into the reaction chamber is by means of sublimation. In this instance, a two zone reactor is used. Passage of an inert gas over the FcH situated in the first zone (T ~ 250 °C) carries the catalyst into the second zone (T ~ 700–1000 °C) where SCNM formation will occur. A fourth method that has been used is to introduce FcH and any other reactant/s into a closed environment (autoclave), which is then heated under autogenous conditions. All these techniques avoid the use of a catalyst support and the difficult and related expensive support removal procedures. To date, little work has been reported on the use of organometallic complexes for the production of *doped* SCNMs by the above procedures and in particular SCNMs doped with nitrogen atoms.

Heteroatom doping of a material is defined as the intentional introduction of impurities or foreign atoms into that material. In the case of SCNMs, this involves the replacement of a C atom in a SCNM by a dopant. Thus, doping of a CNT by N leads to a N-doped CNT (N-CNT). The introduction of foreign atoms into the walls of CNTs was first performed by Stephen *et al.* [13], who doped CNTs with nitrogen (and boron) using arc discharge procedures.

The presence of N in CNTs modifies the structure of a CNT leading to: (i) high surface areas [14], (ii) a high density of defects [14], (iii) chemically active impurity sites [15–16], (iv) unique inner closed shells in the CNT tube [14] and (v) narrow tubes (the numbers of walls decrease with N inclusion) [15–16].

This review will focus on the introduction of N into CNT structures, but mention will be made of studies involving other elements *e.g.*, B and P [17–19]. This review describes the synthetic strategies used to produce N doped SCNMs, in particular CNTs using organometallic complexes.

As will be seen, very few organometallic complexes have been used to make N-CNTs with most studies focused on ferrocene, substituted ferrocene and $Fe(CO)_5$. Characterization techniques used to establish the presence of N in the N-CNTs will be described. Why make N-CNTs and other N doped materials? To place this work in perspective, the properties and uses of N-CNTs will also be mentioned.

The introduction of a dopant atom into the SCNMs, in particular CNTs, can be achieved by adding the dopant atom as part of the catalyst or as part of the carbon source. Both these procedures will be discussed. A short review will also be given of the mechanistic models used to explain the formation of N-CNTs even though much of the information has been generated from doping studies that involve supported catalysts. The studies reported have involved the synthesis and evaluation of both singlewalled CNTs (SWCNTs) and multi-walled CNTs (MWCNTs).

4.2 Nitrogen doped CNTs (N-CNTs)

Much of section 2 relates to the properties and uses of N-CNTs either prepared from organometallic complexes or by other routes. Clearly, once synthesized the N-CNTs should have properties that are independent of the synthesis pathway. However, the method of preparation will play a key role in the actual formation materials; the expectation is that N-CNTs prepared from organometallic complexes *versus* those prepared by other routes will be different.

4.2.1 Properties of N-CNTs

The insertion of N into a CNT lattice changes the overall structure of the CNT and thus affects both the physical and chemical properties of the nanotubes.

4.2.1.1 N bonding in CNTs

N can be incorporated into the CNT lattice in several ways resulting in several bonding configurations. The three main bonding configurations (Fig. 4.2) that have been observed include: (i) pyridine-like: where the N atom is two-fold coordinated, (ii) pyrrole-like: where the N sits substitutionally in a five-membered ring and (iii) graphitic/substitutional: where N replaces a graphitic C atom in the CNT lattice.

According to Ewels *et al.* [20], the N atoms in (i) contribute p-electrons to the π system and the N is sp^2 coordinated to the C atoms. The pyridinic type of N atom has a localized electron pair which is active in base catalyzed reactions [21]. Thus the control of the amount of the pyridinic N is crucial for controlling catalytic reactions [22]. In (ii) N atoms with 2p-electrons contribute to the π system. Here the N is sp^3 coordinated. In (iii) the N sits in-plane, replacing a graphitic host C atom. The pyridinic configuration implies a two coordinated N atom upon the creation of a single C atom vacancy. According to Ayala *et al.* [23], this is responsible for the metallic behavior of N-CNTs. In the pyrollic type, the wall rearrangement leads to the formation of a five-fold ring system [24]. Pyridinic oxide structures can also be observed in N-CNTs [25] (see Fig. 2).

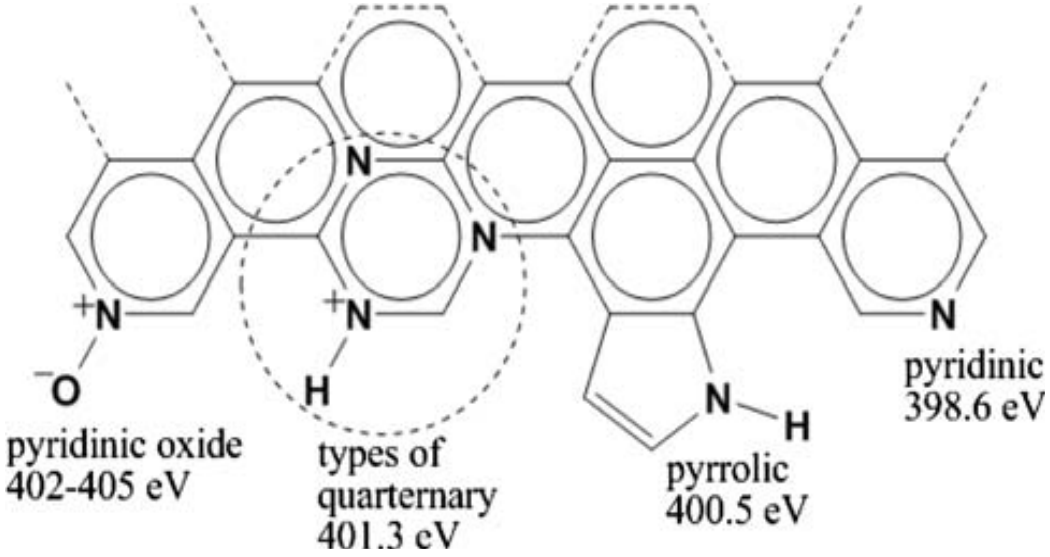


Fig. 4.2. Types of nitrogen species that can be incorporated into graphitic carbon and the XPS binding energies for each type [25].

4.2.1.2 N-CNT bamboo structures

One characteristic feature that is normally associated with the presence of N doping in a CNT is the formation of the so-called bamboo structure (Fig. 4.3) [15,26–29]. As can be seen in Fig. 4.3, the inner tube is not hollow, as found in a typical CNT but comprises of compartments. The bamboo structure can also be found in non-N doped structures, so this is not a unique feature of N-CNTs. Further, when Co or Ni is used to catalyze the formation of N-CNTs no compartments are observed [30]. However, there is at least one study where compartments were observed when Co was used (as a supported catalyst) to form N-CNTs [31]. Also, if the N content is low, compartments may not be detected even when Fe is used as a catalyst.

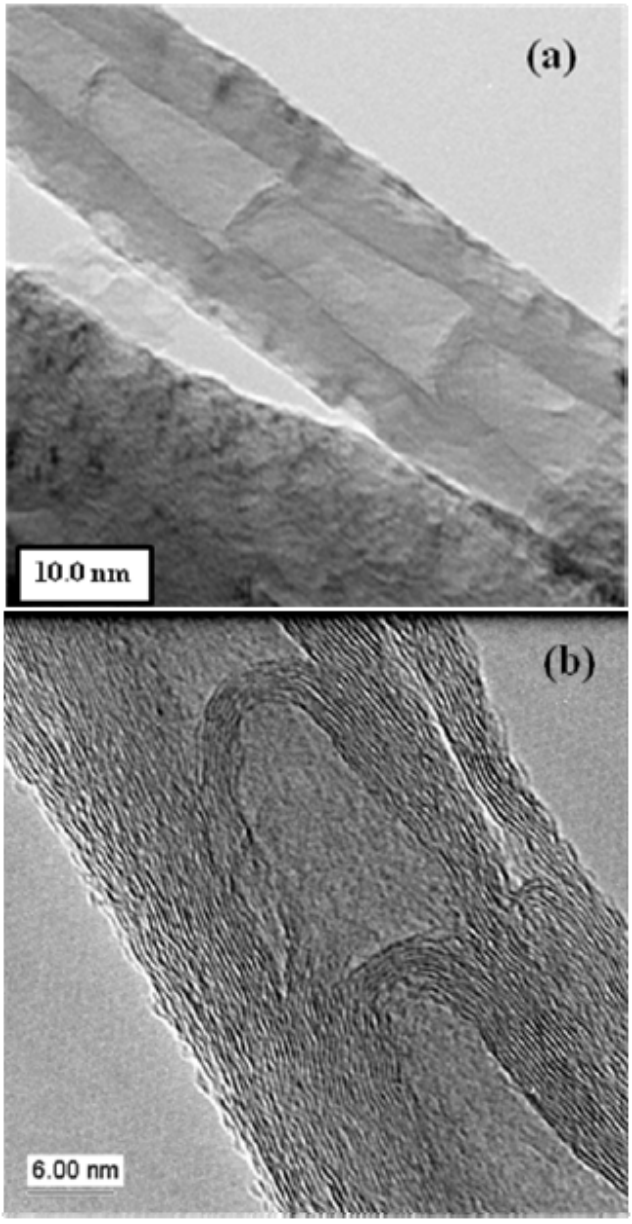


Fig. 4.3. TEM images at different magnifications (a, b) of CNTs obtained from the pyrolysis of toluene and ferrocene in the presence of 8% diethylamine [26].

Finally, it is not clear whether the use of pyridine and an organometallic complex results in the formation bamboo compartment. Literature reports do not indicate whether bamboo structures form [32]. This however could relate to the low N content in the CNT which was below detection levels by standard procedures, since our own studies show that bamboo structures are formed when 20% pyridine in toluene is used as reactant (FcH as a catalyst) [33]. The type of bamboo compartment is affected by the experimental conditions used. A wide range of compartment shapes have been observed (Fig. 4.4(a)) [34]. For example, the N-CNTs shown in Figs. 4.3 and 4.4a are quite different in terms of the wall thickness.

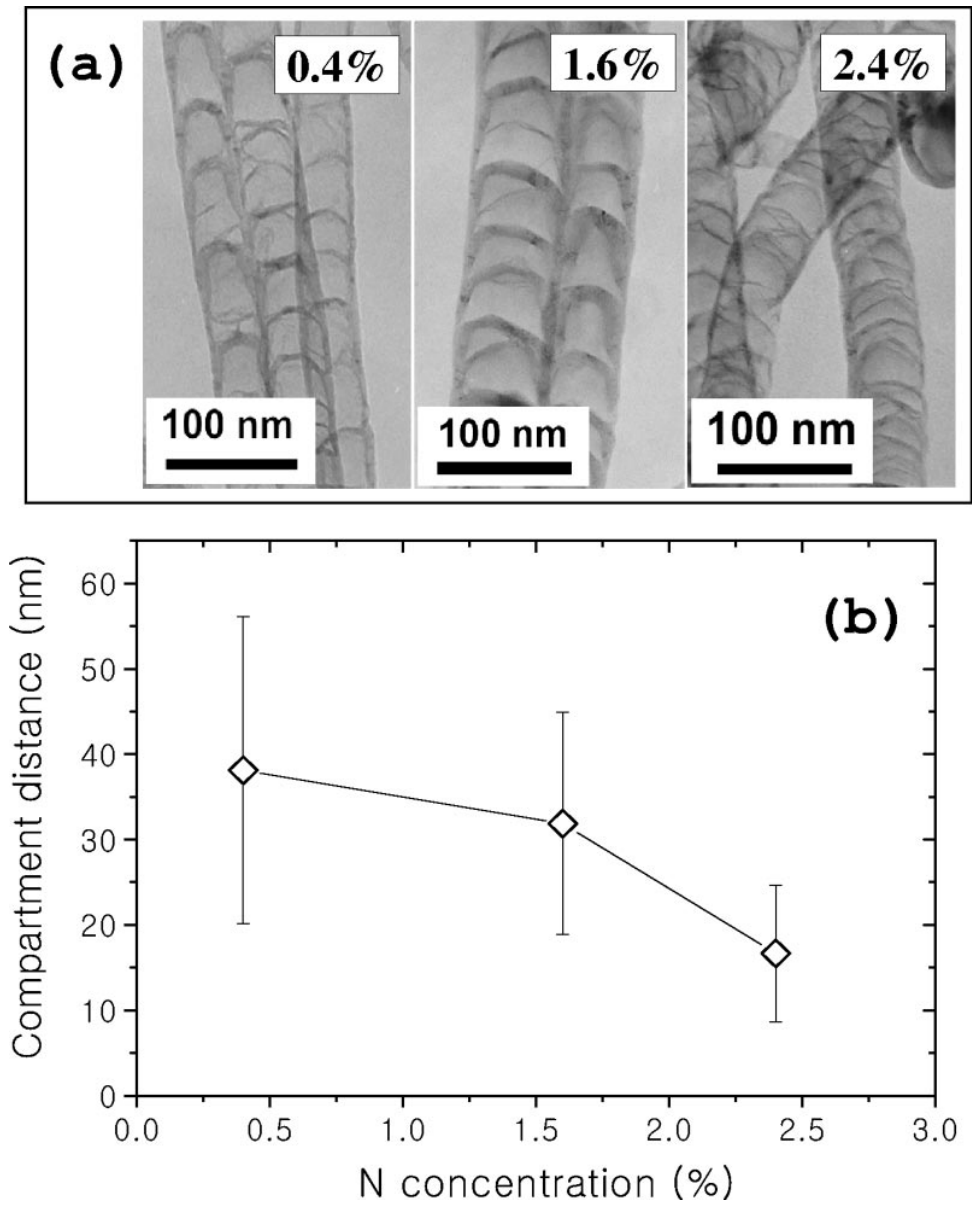


Fig. 4.4. The compartment structures for various nitrogen concentrations. (a) The TEM images of compartment layers of N doped tubes. (b) The compartment distance as a function of the nitrogen concentration. The NH_3 flow ratios of 30, 90, and 150 mL/min gave N-CNTs with N doping levels of 0.4%, 1.6%, and 2.4%. [34].

The separation between individual bamboo compartments is known to decrease with an increase in N concentration [15,35]. The separation between compartmentalized bamboo structures is thus influenced by the concentration of the N atom source used during growth. An example is shown in Fig. 4(b), where CNTs were grown on Fe catalyst deposited SiO_2 substrates using NH_3/C_2H_2 as N and C source, respectively [34]. Varying the NH_3 flow ratios to 30, 90, and 150 mL/min gave N content of 0.4, 1.6 and 2.4%, respectively. Currently, the CVD method is the main method for the production of bamboo-shaped CNTs [34].

The N-CNT bamboo compartment separation also increases with increase in the growth temperature [34]. As the temperature increases, the N content decreases and this results in the increased compartment separation [35]. Bamboo-like structures have also been observed in Y-junction CNTs [36]. In terms of a mechanistic model, both the base growth [22,37–38] and tip growth [39–40] mechanisms have been used to explain this bamboo morphology. The mechanistic model for bamboo morphology formation is discussed in section 4.2.4.

All the above discussions on the bamboo morphology relate to N-doping in MWCNTs. N-SWCNTs, as expected, do not exhibit these unique bamboo structures. Instead they are similar to their undoped counterparts exhibiting ‘straight unbuckled CNT walls’ [41–45].

4.2.1.3 Chemical properties of N-CNTs

Introduction of N into a CNT allows for a change in the chemical behavior of a CNT. This procedure provides an alternative method to the classical oxidation procedures, typically using HNO_3, that are used to functionalize a CNT surface. For example, the N sites in N-CNTs have been shown to bind strongly to metals leading to excellent metal dispersion in metal/N-CNT materials [46]. The surface modifications induced in CNTs by N doping can thus enhance the reactivity and the selectivity of carbon supported catalysts in many catalytic applications [47].

The chemical properties of N-CNTs will also be influenced by the type of N incorporated into the CNT, but to date, very little work on this issue has been reported.

4.2.1.4 Physical properties of N-CNTs

Doping of CNTs with heteroatoms results in a change in the CNT structure. Typical doping procedures have produced CNTs containing N and/or B [48–55] atoms. When N is inserted into the backbone of a CNT, the symmetry of the tube is modified and subsequently the structure and properties are altered [20,56]. Thus, doping of graphitic C lattices affects various physical properties associated with the sp^2 bonded carbon in SCNMs [23,57–60].

The substitutional doping of N has received much attention because major changes in hardness and electrical conductivity have been observed both theoretically and experimentally in N-CNTs [42]. N doping of CNTs has recently been considered as a feasible strategy to fine-tune the electronic properties of CNTs in a well defined manner [62–64]. Even small amounts of N incorporation can quite significantly alter the electronic transport properties within a CNT network [25,65]. Data suggested that N-CNTs are exclusively semiconducting [66].

4.2.2. Characterization techniques

N-CNTs have successfully been characterized by transmission electron microscopy (TEM), electron energy loss spectroscopy (EELS), Raman spectroscopy, X-ray photoelectron spectroscopy (XPS), thermogravimetric analysis (TGA), scanning electron microscopy (SEM), scanning tunneling microscopy (STM), *etc.* A major issue at the moment relates to the level of doping that can be measured. Typically, this is ~ 0.5%, using the methods listed above. Work using electron spin resonance (ESR) spectroscopy suggests that much lower concentration of N can be determined [67]. Fourier Transform infra-red (FT-IR) can also be used to investigate

small amounts of N incorporated into a CNT. The presence of the C-N peak implies doping of CNTs with the N substitution mode [68].

XPS analysis: The elemental composition of N-CNTs can be determined by XPS analysis. The XPS spectrum of a N-CNT can establish the presence of C, N and O. The O detected arises from exposure of the sample to the atmospheric air [69]. XPS analysis has the potential to give information about the hybridization state of the N in the N-CNTs [14,34,70]. According to Jang *et al.* [34], the type of N observed at high N concentrations in CNTs has been shown to be sp^3 hybridized; at lower N concentrations, a sp^2 signal for N was observed. These results were obtained using NH_3/C_2H_2 reactant mixtures over a Fe/SiO_2 catalyst. In a recent study using organometallic complexes, XPS data revealed that the use of the 15% FcH/aniline solution gave an XPS signal for N consistent only with sp^2 hybridized N while a 25% FcH/aniline solution gave two N XPS signals (50/50) consistent with both sp^2 and sp^3 nitrogen [15]. It is clear from the above examples that as the N content is increased the N hybridization converts from sp^2 to sp^3.

XPS data also shows that the % atomic N content present in the CNTs varies with the synthesis temperature. Yadav *et al.* [35] for instance have reported that N amounts of 8.29, 4.65, and 3.19% were obtained at 850, 900, and 950 °C, respectively for N-CNTs produced by the spray pyrolysis of FcH/acetonitrile. Van Dommele *et al.* [22] have reported similar findings on the influence of growth temperature on N content. These authors found that the C/N ratio increased with increasing temperature as a result of the thermodynamic stabilities of the metal carbides and nitrides formed [22]. XPS also revealed that the type of N present in the CNTs changed with increase in temperature from a pyridinic to a quaternary N [22–23].

EELS: Additional structural and electronic information of a N-CNT can be obtained from EELS. This technique gives information about the way the N and C atoms are bonded in the CNT

structure. With EELS, one can get information about the hybridization state of C and N in N-CNTs [71]. The main features of an EELS spectrum obtained from N-CNT are a prominent peak with a rounded shape at higher energies in the carbon K shell spectrum and a shoulder at 395 eV in the spectrum of the nitrogen K shell [45]. In recent studies, it was observed that the core-loss peaks (C and N; K-edge) reflected the density of unoccupied states above the Fermi level in the presence of a core hole [39,72–73]. EELS studies on CNTs showed extremely sharp edges centered at around 401 eV confirming the presence of N inside the CNT [61,72]. Elemental EELS mappings using Omega filtered microscopy has shown the presence of high concentrations of gaseous N_2 inside tube cores, but CNTs with open tips do not contain gaseous N_2 in their interior but only in the tube walls [39,70,72,74]. In another study, Golberg *et al.* [75] have shown using EELS that N-CNTs displayed undulated, ‘‘wavy’’ graphitic shells, with no specific chirality.

Raman spectroscopy: Raman spectroscopy has been applied to the identification and characterization of a wide variety of SCNMs [76–79], and the technique has been shown to be an excellent tool to investigate the graphitic nature of CNTs. Raman spectra of CNTs generally show a strong band around 1585 cm^{-1}, originating from the Raman active E_{2g} mode which is referred to as the G-band and a D-band at about 1350 cm^{-1} which is normally explained as a disorder-induced feature due to a finite particle size effect [60,80]. The D-band originates from defects in the curved graphene sheets [81].

In N-CNTs, the formation of pentagons and heptagons due to the doping of N atoms leads to a distortion in the graphite sheets. Thus, the intensity ratio of the D- to G-band in the N-CNTs will be affected by the number of defects originating from N incorporation [82–83]. As the concentration of the N atoms increases, the D-band becomes stronger and broader. The intensity ratio (I_D/I_G) is thus useful in estimating the defect concentration of N in the N-CNTs; as the I_D/I_G ratio decreases the CNTs will have a more ordered structure. For example, N-CNTs, produced

from ferrocenylaniline/toluene were found to be more disordered than CNTs produced from FcH/toluene alone [15]. The Raman analysis also revealed that as the concentration of aniline increased in FcH/aniline/toluene mixtures used to make N-CNTs, the degree of disorder also increased.

A shift in the G-band and D-band from 1578 to 1569 cm^{-1} and 1353 to 1344 cm^{-1} in N-CNTs, respectively, was observed when the temperature was increased from 850 to 950 °C [35]. However, almost negligible changes in the peak positions were observed in the I_D/I_G ratio for CVD grown NCNTs using pyridine and melamine as N sources [84]. Raman microscopy has also been used to assess quantitatively the compositional properties and bonding arrangements in N-CNTs [60]. Experimental evidence for a pyridinic N configuration can be seen in the intensity ratios of the D- and G-band in the Raman spectra of N-CNTs produced by the spray pyrolysis of a mixture of 4-tert-butylpyridine and FcH on silicon and quartz substrates in a nitrogen atmosphere [85]. Raman spectroscopy work on NCNTs obtained by the pyrolysis of polyvinyl pyrrolidine (Ppy) on an alumina template showed a peak at 1290 cm^{-1} (D-band) due to defects in the curved graphitic sheets and tube ends of the N-CNTs [12]. The D-band was found to be significantly stronger than the G-band indicating the amorphization of the graphite network is due to a much higher N content in the Ppy produced N-CNTs [12].

TGA studies: The thermal stabilities of many carbons have been evaluated by thermogravimetric analysis in air. TGA can indicate the presence of N in CNTs [15]. N-CNTs are found to be less stable than their undoped counterparts and this is attributed to the structural disorder introduced by the presence of N into the carbon lattice [86–87]. A recent study revealed that an increase in N concentration in a CNT correlated with the CNT stability. This is due to the enhanced defect and disorder achieved by the introduction of reactive sites in the N-CNTs [15,60,80].

SEM and TEM analysis: Key information that can be obtained from EM (electron microscopy) relates to the shape, length, diameter and morphology of doped CNTs. As mentioned in the introduction noticeable features of N-CNTs relate to the presence of the bamboo morphology, readily detected by EM.

Yadav *et al.* [35] reported tubes grown from a FcH/acetonitrile reactant mixture. SEM analysis of the N-CNTs revealed the formation of clean, well aligned N-CNT bundles that varied with the growth temperatures (850 – 950 °C). N-CNTs had lengths of about 430 μm. Further, SEM images showed that the tubes did not contain any impurities (*e.g.*, amorphous carbon).

A TEM study on the products produced from the synthesis of N-CNTs using FcH has revealed that as the toluene/benzylamine ratio was varied, the morphology of the tubes varied [88]. The CNTs had many kinks and their number, length and diameter decreased (the proportion of bamboo shaped NCNTs increased) as the benzylamine concentration increased [88]. TEM micrographs clearly illustrated that the N-CNTs had a bamboo shaped structure at all temperatures. The average diameters of the CNTs were about 55, 60, and 73 nm when prepared at 850, 900, and 950 °C, respectively. It is suggested that, as the growth temperature increased more sintering of the Fe catalyst occurred resulting in larger-sized catalyst nanoparticles and hence larger diameter nanotubes being formed. Similar observations on N-CNTs have been made using other precursors [89–90].

4.2.3 Applications of N-CNTs

Much work on the application of N-CNTs has been focused on catalysis. For instance, Ru catalysts have been shown to have a higher activity in NH_3 decomposition compared with other common metal catalysts such as Fe, Ni, Pd, Pt and Rh [91–96]. Further, studies have shown that Ru supported on CNTs exhibit higher activity than when supported on activated carbon, Al_2O_3

and TiO_2 [95–97]. Also, Chen *et al.* [96] have investigated the activity of Ru/CNTs in NH_3 decomposition. It was found that the pyridinic N atoms show a strong interaction with Ru particles. This high activity of N-containing CNTs also makes them ideal components in fast gas sensors [98].

Recently, well dispersed Pt nanoparticles with an average particle size of 2.63 nm were supported on N-CNTs by an impregnation procedure [99]. The Pt/N-CNT electrodes made from these nanoparticles showed a greater electrochemical surface area when compared to Pt/CNT electrodes and gave a higher performance in a H_2/O_2 fuel cell. These N-CNTs, with a C/N ratio of 6, were grown from the metal catalyst precursor, [Fe(acetylacetonate)$_3$], dissolved in a mixture of acetonitrile and tetrahydrofuran [99]. The development of catalysts with high activity and high durability is a key issue for proton exchange membrane fuel cells (PEMFCs). N doped SCNMs and their composites have demonstrated potential in PEMFC catalyst applications. Shao *et al.* [47] have reviewed N doping strategies to make SCNMs and their electrocatalytic aspects using N-containing carbons.

N-CNTs have also shown great potential as catalyst supports for Pt–Ru nanoparticles in the anodic oxidation of methanol in direct methanol fuel cells [100] and in environmental applications for use as adsorbents for organic and inorganic compounds (*e.g.* Cd^{2+} adsorption) in the aqueous phase [101]. N-CNTs treated at 800 °C showed improved electrocatalytic activity for oxygen reduction as compared with commercially available Pt/C catalysts [102]. N-CNTs have also been employed as a catalyst support in the liquid-phase hydrogenation of cinnamaldehyde using Pd as an active phase [103]. Du *et al.* [102] synthesized Pt nanoparticles and deposited them on N-CNTs which were grown on a carbon cloth electrode. The N-dopants in a CNT serve as the defect sites to enhance nucleation of Pt particles.

Functionalization of N-CNTs was found to be useful in chemical and biological applications that require sidewall substituents or polymer coatings [104–106]. A novel approach to produce N-CNTs is by treating oxidized CNTs with NH_3. In this post-doping process, the surface properties and oxygen reduction activities of the core/shell structures were modified and characterized by cyclic voltammetry and XPS [107]. Also, the use of N-CNTs in Li ion batteries has been proposed since high Li storage is favored by the defective sites formed upon N incorporation [108]. A major use for N-SWNTs is in the area of semiconductors where low doping levels can be attained successfully in a controlled manner [23].

The electrical conductivity of strands of N-CNTs obtained from the decomposition of FcH/ethanol/benzylamine solutions was found to increase with increasing N concentration [42]. Theoretical studies have revealed that doping affects the electronic transport of a CNT [20,109]. It has also been reported that N-SWCNTs synthesized in large scale using an electric arc discharge method show that the band gap of SWCNTs can be tuned by varying the degree of N insertion [109–111].

Literature reports have revealed that insertion of N into CNTs results in an enhancement in conductivity [55] and an improvement of transport and field emission properties of CNTs [56]. As highlighted earlier, this is due to the electron donor ability of the N atom that leads to the formation of a *n*-type semiconductor [112]. Field emission studies of the N-CNTs suggest that they are good emitters with a turn-on and threshold field of 1.8 V/μm and 2.53 V/μm, respectively [113]. This excellent field emission performance of N-CNTs is attributed to the presence of lone pairs of electrons on the N atom that supplies electrons to the conduction band [110].

4.2.4 N-CNT synthesis mechanism

The correlation between the morphology, crystallinity and properties of N-CNT structures is not completely understood [89]. To date a number of conflicting mechanistic models of N-CNT growth have been proposed, related to the role/influence of N on the growth mechanism of N-CNTs [114].

The base growth mechanism (where a catalyst is located at the bottom of the CNT) is commonly proposed as the mechanism that leads to the formation of bamboo shaped N-CNTs. In this method, catalyst particles dissociate reactant molecules resulting in the precipitation of N and C atoms. More C and N incorporation into or onto the catalyst results in the walls being pushed away from the catalyst nanoparticle to form a tubular structure [115]. The role of the nitrogen formed from precipitated C (and N) in bamboo compartment formation is suggested to be due to the generation of pentagons in addition to hexagons [31,116]. It is believed that the presence of N in the carbon deposit results in surface strain, leading to a 'pulsed' effect in which the C/N surface atoms detach from the metal particle intermittently, leading to the bamboo structure observed. The addition of N results in a structure that is more curved. The presence of nitrogen in the growth environment is a favourable condition for the formation of 'bamboo-like' CNTs obtained from Fe catalyzed reactions [31]. The formation of closed tips in the N-CNTs is consistent with a base growth mechanism.

The tip growth mechanism (where the catalyst sits at the tip of the CNT) has also been reported to explain the formation of CNTs. As shown in Fig. 4.5, during the CNT tip growth mechanism, intermediate reactions and processes take place on a catalyst nanoparticle. Typically, the precursor molecules absorb on the surface of the catalyst and dissociate [117]. Atomic C and N are released and then dissolve in or attach to the surface of the catalyst. The C and N atoms also

diffuse over the surface. The C and N atoms eventually precipitate on the opposite surface to form the N-CNT wall.

Both the above mechanisms relate to a catalyst that has been deposited on a support. Using the floating catalyst approach, nucleation of the Fe atoms to generate particles that will interact with the reactant should occur in the gas phase. Kuwana *et al.* [118] have developed a model to predict formation of Fe nanoparticles from FcH in a CVD reactor. The study revealed that the diameter of Fe particles varied throughout the reactor. The model explained the nucleation, surface growth and collision of nanoparticles. In this instance, N-CNT growth is similar to that found in the base or tip growth mechanism. However, as the particle is not attached to a support surface, both tip and base growth mechanisms are equivalent. The catalytic nanoparticle influences the N-CNT formation by modifying the (i) reactant and the (ii) reactant solubility [116,117].

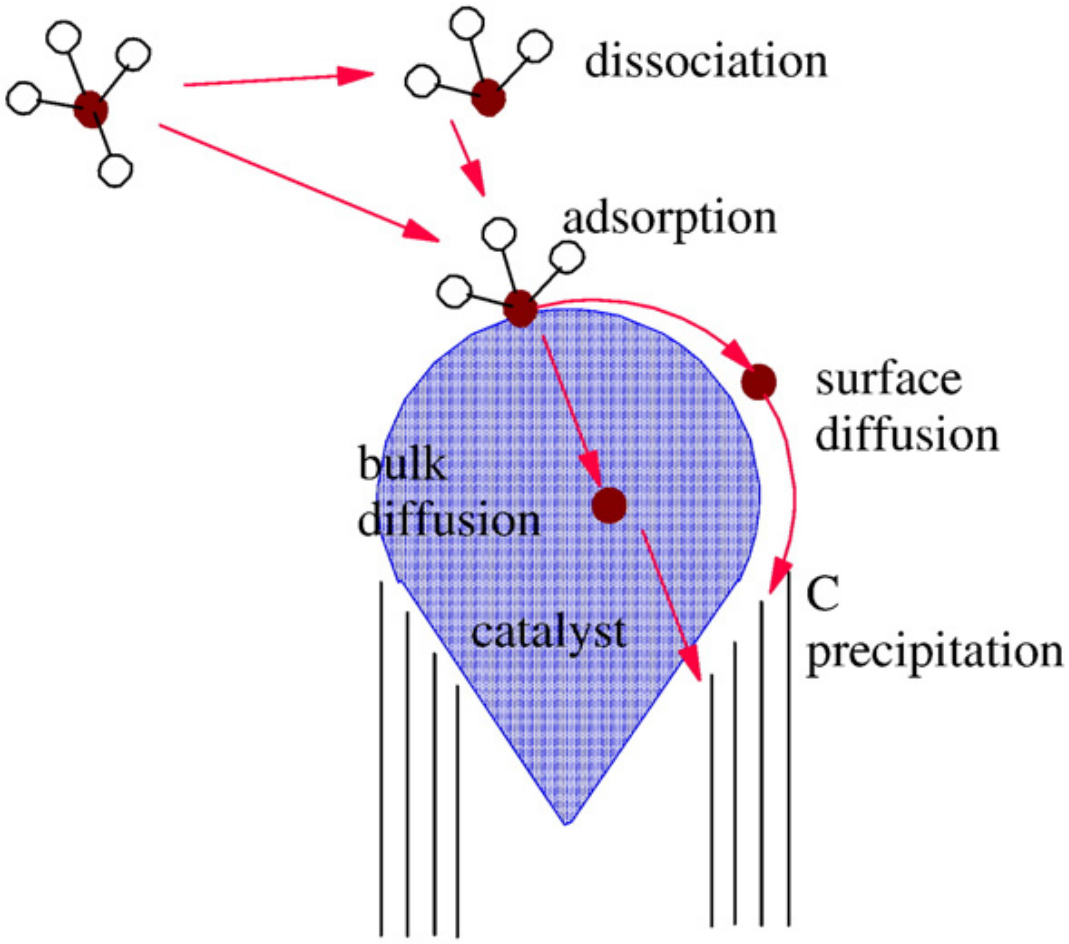


Fig. 4.5. Schematic of reactions and processes on a catalytic nano-particle during nanotube growth (tip growth illustrated) [117].

The increased complexity of having multiple catalyst particles adding to one tube and leading to growth has been described for CNTs. This is shown in Fig. 4.6. In this figure it can be seen that Fe particles generated in the gas phase lead to both tip and base growth [115]. Further, particles are then added to the growing tube over time leading to long CNTs. At each stage, when a new metal particle is added to the tube a mis-match occurs in the tube structure leading to CNTs with a disordered surface. This type of growth pattern should also hold for the production of SWCNTs and MWCNTs.

The specific influence of N on the growth mechanism of SCNMs has been investigated [31]. Kurt *et al.* [89] found that at high N content, the alignment of the CNT lattice is gradually lost. Contrary to this, Koos *et al.* [88] demonstrated that an increase in the amount of N decreased the number of kinks in a CNT resulting in the formation of more aligned N-CNTs. It has been proposed that the role of N was either (i) to enhance the formation of graphitic layers on the catalyst surface or (ii) to increase the separation of the graphitic layers from the catalyst [119]. It has been found that small concentrations of N (typically less that 2%) leads to the growth of straight cylindrical nanostructures containing nitrogen atoms bonded to three carbon atoms [31,120–122]. A possible growth mechanism for formation of Y-junction bamboo N-tubes has been suggested by Ghosh and co-workers [123].

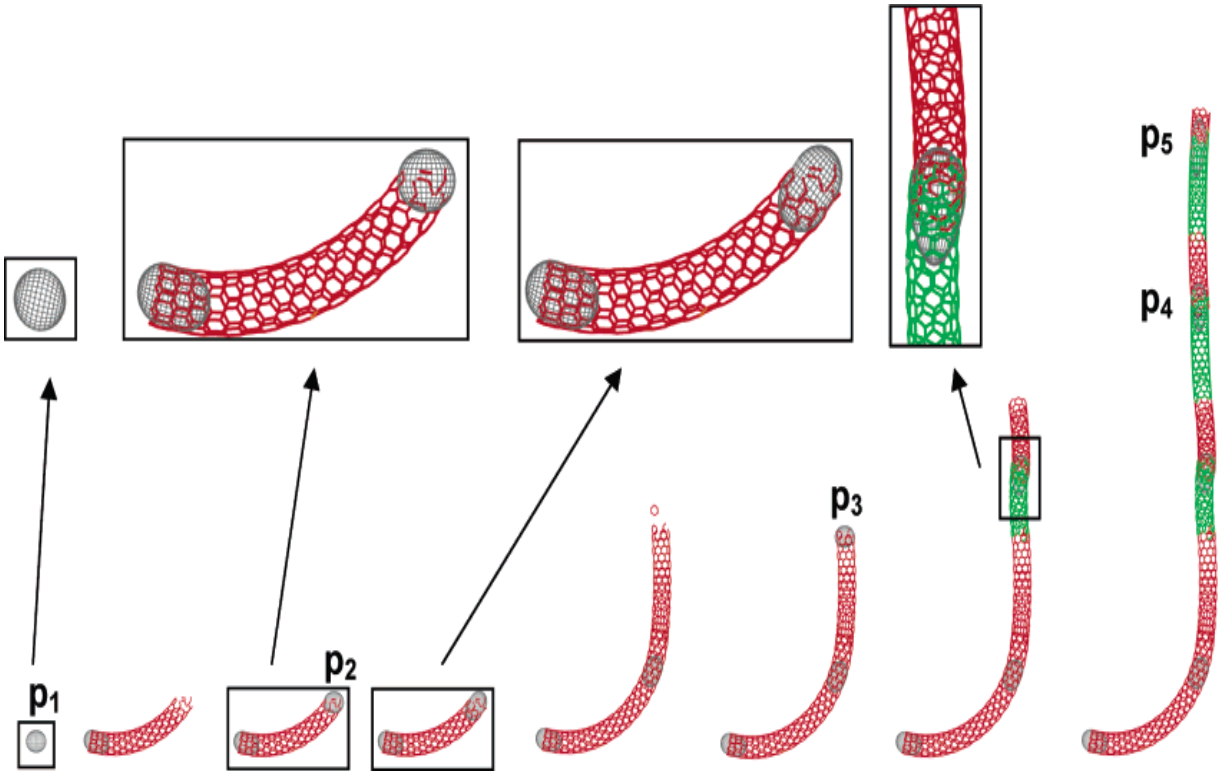


Fig. 4.6. Representation of the model of concurrent base and tip growth modes for consecutive catalyst particles [115].

4.3 N-CNT synthesis from organometallic complexes

While the synthesis of CNTs is generally performed by using a metal bound to a support, the use of support free catalyst is well known. Indeed, the HiPCo process is based on the use of $Fe(CO)_5$ under high pressure [124]. Surprisingly however, few studies have been reported on the gas phase reactions that produce CNTs generated from metal particles derived from organometallic complexes. This is also reflected in the content of previous reviews written on the topic [125,126].

Gas phase studies on either FcH or FcH and xylene decomposition have revealed complex reaction sequences [127–128]. Computational studies have been used to investigate the gas phase compositions generated from a catalyst and/or a reactant that lead to CNT growth [129–130]. The studies revealed that CNTs are formed through the interaction of the Fe particles and xylene and/or toluene at 700 °C [129–130]. The direct source of C for CNT growth could be xylene itself or the pyrolysis products of xylene (*e.g.*, toluene, benzene, methane, *etc.*).

The synthesis of N-SCNMs and, in particular, N-CNTs from organometallic complexes are at this stage limited. A summary of relevant papers is given in Table 1. Analysis of the data is given below. The first study on the use of FcH for the growth of CNTs was reported by Tibbets *et al.* in 1994 [131]. Many reports have since appeared in the literature using FcH as a catalyst for the growth of SCNMs and especially CNTs [125,132–135].

Thermal decomposition of FcH (used without an additional C or N source) can give SWCNTs. In a recent study, Barreiro *et al.* [136] used FcH as the sole source of both catalytic Fe particles and C feedstock for the production of CNTs. This study revealed that at a temperature of 500 °C, FcH decomposed completely to produce a range of fragments *viz.*: $Fe(C_5H_5)_2 \rightarrow Fe + H_2 + CH_4 + C_5H_5$ + other hydrocarbons. Fe clusters and reactive C species/atoms/radicals are also formed

in the gas phase. The SWCNTs then nucleated from the C species/atoms/radicals generated from FcH.

Investigations indicate that N insertion into CNTs strongly depends on the experimental conditions used (*e.g.*, reaction temperature and the gas flow rate), the precursor compounds and the catalysts. Most of the syntheses involved catalytic thermal decomposition of C or CN containing gas phase precursors, often under a nitrogen rich atmosphere [85–88]. When FcH was used together with a C source and a N source, the Fe/C ratio had a major impact on whether N-CNTs or N doped carbon nanospheres (N-CNSs) were formed [137–138]. Low N concentrations and low catalyst concentrations favor N-CNT production while the absence of a catalyst leads only to the formation of N-CNSs and other N-doped SCNMs (N-SCNMs) [137–138].

Table 4.1. Synthesis of N-CNTs using organometallic complexes.

N/C sources	Substrate	Catalyst	T (^oC)	N (*at.%*)	Method	Ref
Ethanol/toluene/ethylenediamine	-	FcH	850-950	-	CVD injection	14
Toluene/aniline, ferrocenylaniline	-	FcH, ferrocenyl-aniline	900	1.5	FC CVD	15
Triphenylphosphine/benzylamine	-	FcH	720-840	-	CVD aerosol	18
Toluene/hexamethylenediamine, benzylamine, quinoline	-	FcH	850		CVD aerosol	26
Pyridine	Quartz tube	$Fe(CO)_5$	900-1100	-	CVD	32
Benzene/CH_3CN	Quartz tube	FcH, $AgNO_3$	900	-	CVD aerosol	35
Ethanol/benzylamine	-	FcH	950	< 2	CVD	42
Benzylamine	-	FcH	850	-	CVD	50
Xylene/NH_3/pyridine	-	FcH	800	0-9.7	FC CVD	60
Thiophene/NiPc	-	Nickelocene, NiPc	900	-	CVD	64
Fullerene/NH_3	-	FcH	1050	> 0.1	CVD	73
Ethylenediamine	-	Co, FcH	780-1080	18.77-24.45	CVD injection	82
4-tert-butylpyridine	Quartz	FcH	700	1.6-2	CVD aerosol	85
Toluene/benzylamine	Quartz substrate	FcH	800-900	0 – 2.2	CVD aerosol	88
CH_3CN/THF	Carbon fiber paper	Fe acetylacetonate	850	0 – 2.2	CVD aerosol assisted	99

Table 4.1 continued

N/C sources	Substrate	Catalyst	T (^oC)	N (*at.%*)	Method	Ref
C_2H_2/NH_3	-	$Fe(CO)_5$	750-950	3.1-7.2	CVD	139
Monoethanolamine	Si	FcH	900	6.6	CVD	146
Monoethanolamine	GaAs	FcH	950	7.8	CVD	146
$C_3H_6N_6$	-	FcH	900-1000	2.3-11.5	FC CVD	147
Ethanol/ethylenediamine	Al_2O_3	FcH	900	1.2	CVD injection	148
NH_3/pyridine	Quartz tube	FcH	700-1000	4.8-8.8	CVD	149
FePc/thiophene/NH_3	-	FePc	900	< 9.0	CVD	156
CoPc/thiophene	-	CoPc	800-1000	1.9-2.9	CVD	158
CH_3CN/pyridine	-	FcH	650-900	-	FC CVD	165
Pyridine, methylpyrimidine, triazine	-	$Fe(CO)_5$	1100	2.3	CVD	166
Melamine		FcH	1050	2.0-7.0		167
$C_{18}H_{15}P$	Quartz tube	FcH	950	-	CVD	168
Pyridine, pyrimidine	-	FcH	750	1.0 – 3.2	CVD	169

*FC: floating catalyst

As mentioned in section 4.2.2, the N can be added to the CNT from either the catalyst or as a reactant. In these methods the N is added during the reaction that produces the CNT – an *in situ* procedure. It is also possible to add N to CNTs in a post-treatment synthesis procedure. For example, a CNT synthesized, then returned to the reactor to undergo a secondary reaction in which a nitrogen containing reactant decomposed to create a N/C layer on the CNT. In essence a type of core/shell structure is synthesized in which the core is pure carbon and the shell contains

N and C atoms. To our knowledge no reports on the use of post-synthesis procedures to add N to CNTs using organometallic complexes have been reported.

Synthetic procedures to produce N-CNTs from organometallic complexes can be divided into methods using a flow system or a closed environment.

4.3.1 Flow system

In a flow system, the catalyst and a reactant flow through a high temperature reactor. The catalyst is continually added to the system. Deposition of the N-CNTs occurs as the catalysts and the reactants decompose and the decomposed reactant atoms/molecules/ions/radicals then interact with each other. The synthetic conditions, particularly growth temperature, catalyst, gas flow rate, N/C sources and concentration, *etc.* all affect the physical and chemical properties of the resulting N-CNTs produced *i.e.,* by influencing the amount and type of N incorporated into the CNT.

N in the catalyst: In a recent comparative study [15], the use of organometallic precursors containing nitrogen (FcH/aniline solutions and 4-ferrocenylaniline) to synthesize N-CNTs and other species was reported. Molecular 4-ferrocenylaniline served as both the N source and catalyst to grow N-CNTs. In particular, the effect of varying the N source concentration (0 – 25 wt. %) on the types and yields of CNTs and other SCNMs produced was investigated. The proximity of N to Fe impacted on the formation of N-CNTs in the gaseous phase with the 4-ferrocenylaniline giving a higher degree of N doping than an equivalent FcH/aniline mixture [15].

N in the reactant: The *in situ* synthesis of N-CNTs is usually performed using the CVD method. NCNT synthesis has been achieved by using NH_3 [86,139] or by using a volatile C source that contains N. These N sources include pyridine [140], melamine [141], triazine [142], acetonitrile [143], metal phthalocyanines [114,144] benzylamine [26,42,89,145], ammonia [140–141], monoethanolamine [146], ethylenediamine [26,82], *etc.* (see Table 4.1). The reaction usually occurs in the presence of an organometallic catalyst that does not contain N.

In a recent study, N-CNTs were produced by a nebulised floating catalyst method at 850 °C using a mixture of toluene and 1–8% nitrogen containing reagents [26]. It was revealed that, in general, the amount of N in the nitrogen containing reagent is more important than the source and type of the N atoms used as revealed by trends in the morphology (diameter, length) of the N-CNTs produced. The average lengths and diameters of N-CNTs produced after addition of 1% N containing hydrocarbons (benzylamine and hexamethylenediamine) are longer and aligned than those synthesized using FcH/toluene (Fig. 4.7). However, the lengths shorten with increased N source concentration. As noted in our study, an increase in the nitrogen source decreases the CNT length and the study by Koos *et al.* [88] observed similar trends.

Several other synthesis methodologies and N sources used to form N-CNTs have been well documented in recent reviews [20,23].

Range of catalysts: Catalysts that have been used in the flow system method include: FcH, substituted FcH (with and without N substituents) and $Fe(CO)_5$. Bajpai *et al.* [32] synthesized aligned helical NCNTs by the co-pyrolysis of $Fe(CO)_5$ and pyridine on a quartz substrate at elevated temperature (900–1000 °C). Other catalysts used for the formation of N-CNTs are metallocenes such as nickelocene [126]. For example, the pyrolysis of nickelocene/thiophene mixtures gave N-CNTs with Y-junctions [64,126] (see Table 4.1).

Temperature effects: There are a number of experimental parameters that need to be taken into consideration when studying the controlled growth of N-CNTs. Growth temperature is a key parameter for the production of N-CNTs. Generally, a temperature range of 600 – 1100 °C is suitable for the growth of N-CNTs as the decomposition of the catalysts (FcH) and hydrocarbons occur at temperatures above 500 °C. In a recent study, Yadav *et al.* [35] revealed that N doped CNTs grown at the lower temperatures possess a higher degree of disorder and higher N incorporation. This was shown by using XPS and Raman spectroscopy studies. Koos *et al.* [88] reported that N-doping decreased by a factor of half when the temperature was increased from 800 to 900 °C. The N-CNTs were produced by spray pyrolysis of FcH in benzylamine/toluene mixtures under Ar.

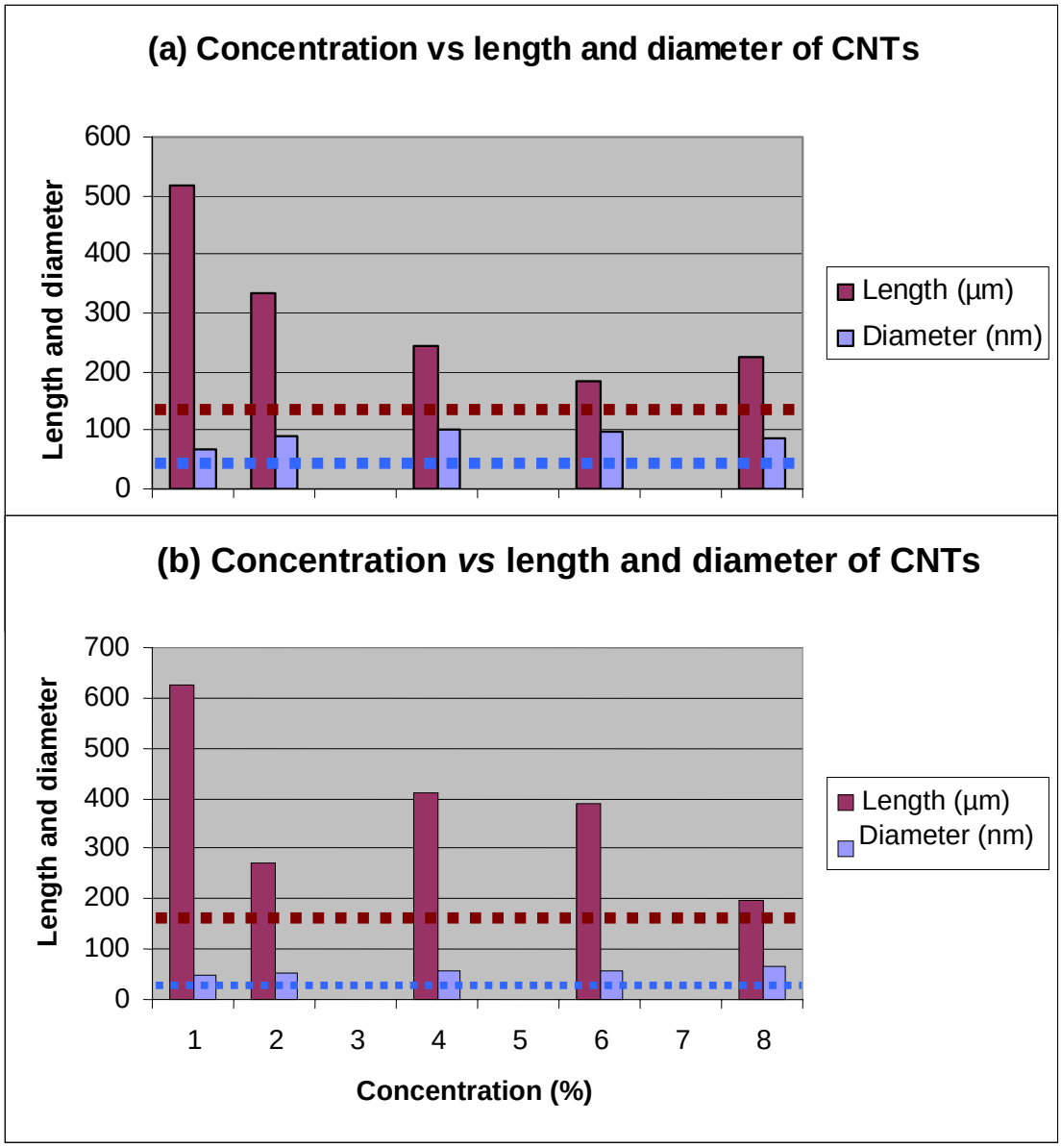


Fig. 4.7. Graph of concentration *versus* length and diameters of CNTs grown from (a) FcH/benzylamine; and (b) FcH/hexamethylenediamine mixtures. Horizontal dotted line indicates lengths and diameters of CNTs obtained from FcH/toluene [26].

Diameter and lengths: The concentration of the N containing reactant plays a major role in influencing the nature and size of N-CNTs. The N incorporated nanotubes made from FcH in benzylamine/toluene have smaller outer diameters but larger inner diameters when compared with undoped CNTs grown from a FcH/toluene solution under analogous experimental conditions [26]. The same observations were seen when FcH/aniline was used to form N-CNTs [15]. The lengths generally shorten with increased N incorporation.

Aligned N-CNTs: The synthesis of N-SWNTs that agglomerate in bundles and form long strands (< 10 cm), *via* the thermal decomposition of FcH/ethanol/benzylamine solutions in an Ar atmosphere at 950 °C have been reported [42]. Vertically aligned N-CNTs were prepared by the spray pyrolysis of turpentine oil, 4-tert-butylpyridine and FcH mixtures at 700 °C on silicon and quartz substrates using different amounts of N [85]. The length of the as-prepared material formed on silicon and quartz substrates was 12 μm and 9 μm, respectively [85]. In a separate study, films of vertically grown N-CNTs from different substrates were obtained from the pyrolysis of a mixture of FcH and melamine [147]. Li *et al.* [148] have grown high quality vertically oriented N-CNT arrays over an alumina substrate on a rough surface. This process is useful for commercial production of CNTs since this substrate is an inexpensive substrate. Synthesis of well-aligned N-MWCNT arrays over a large area, on quartz and silicon wafers, was achieved by use of a floating catalyst at fairly low temperatures (600 ºC) using FcH/pyridine mixtures [149]. Other workers have prepared vertically aligned N-CNTs possessing two different types of N atoms in the product (pyridinic and graphitic N) [85] *i.e.,* from FcH/4-tert-butylpyridine on silicon and quartz substrates.

N content: Maldonado *et al.* [60] doped CNTs with a range of N contents (0 – 10 at %) *via* the floating catalyst CVD method using FcH, NH_3, and xylene or pyridine. N1s XPS spectra showed three types of N bonding modes (pyridinic, pyrolic, and quaternary), with the pyridinic-like fraction selectively increasing from 0.0 to 4.5 at. % at a temperature of 900 °C. This work also

reported an iodimetric method to gauge the number of reducing sites on the N-CNTs, which is used to estimate the amount of N incorporated into the tubes. N-doped Y-junction bamboo shaped CNTs were synthesized from a FcH/monoethanolamine mixture over GaAs substrate at 950 °C [123]. The amount of N achieved from organometallic complexes using different N sources is presented in Table 1 (column 3).

The role of H_2: It is believed that the catalyzed synthesis of CNTs requires the use of a metal in the zero oxidation state. This is achieved by adding gaseous H_2 to the organometallic catalysts or using the H generated from the catalyst or C source *e.g.*, toluene, to reduce the Fe [150]. However, reactive H species generated in hydrocarbon based CNT growth have been shown to damage the formation of CNTs. To counteract this effect, O atoms from O_2 or oxygen containing molecules can be added to the reactants [151]. In this way, the H radical concentration can be controlled in the reactant mixture. The addition of O inhibits the process by attacking reactive H species/radicals. This provides a control over the C/H ratio that can lead to SWCNT growth or cleaner MWCNTs. Further, H_2 was found to significantly reduce the N content in N-CNTs [152]. These N-CNTs were obtained from the pyrolysis of MgO supported Fe catalysts.

Issues of using N_2 as carrier gas: A few reports exist where the reaction of N_2 gas with carbon radicals to produce CNTs has been suggested. However, it is not clear as to whether gaseous N_2 was incorporated into the CNT network to generate data suggestive of N incorporation into CNT structure. Indeed, many studies entailing CNT synthesis to make undoped CNTs are performed under N_2. While large amounts of N are not incorporated, small amounts, below the detection levels of the usual analytical techniques may indeed be doped into CNTs. Yang *et al.* [153] revealed that nitrogen could enhance CNT growth in CNTs grown over Ni by producing nickel nitride which in turn dissolves excess carbon to suppress the passivation of CNT growth. It has also been proposed that nitrogen combines with hydrogen to form NH_3 when $N_2/H_2/CH_4$ is used for the formation of CNTs [154]. The diameter of the CNTs decreased when a higher volume of

nitrogen gas was used as a carrier gas. Although N is not reportedly incorporated into the tubes, it is surprising that a similar effect is seen when N is incorporated into the tubes (*i.e.,* to form N-CNTs) [154]. The role of N_2 in the formation of N-CNTs needs further investigation.

4.3.2 Closed system

More recently there has been an increase in the number of reports on the synthesis of CNTs by the pyrolysis of organometallic complexes in a confined environment *e.g.*, stainless steel autoclaves or sealed glass vessels, at autogenous pressure [125,137]. Most of these methods have used Fe or Co catalysts.

In a recent study, it was reported that N-doping of CNTs in a confined space (sealed quartz vessels) using organometallic precursors (ferrocenylmethylimidazole, FcH/methylimidazole isomers) was possible [138]. An analysis of the SCNMs and the bamboo structures revealed that the three methylimidazoles structural isomers led to different products; in particular with N-CNTs that contained different amounts of N (as determined by bamboo compartment separation) and tube diameters.

4.3.3 Non-flow systems

An alternative to the use of a flow system is a CVD process entailing a metal dispersed on a support that is placed in a quartz reactor (Fig. 4.1). In this instance a typical metal/support catalyst is made by adding a catalyst precursor to a support. Organometallic complexes could be used to make these catalysts. However, most catalyst/support mixtures are made from cheaper metal salts. Issues of metal dispersion will be influenced by the metal (salt, organometallic complex) used but little has been described on the use of organometallic complexes in this context.

4.3.4 Alternative synthetic strategies

The advantages of using organometallic complexes as catalysts include solubility, volatility, cost, *etc.* However these advantages are not limited to organometallic complexes. Hence the use of other compounds to make N-CNTs is possible. These compounds include the use of metal phthalocyanines to produce N-CNTs.

For example, Liu and co-workers [155] synthesized pure aligned N-CNTs by the pyrolysis of Fe(II)phthalocyanine (FePc) and C_2H_2 using a double stage furnace system. These N-CNTs had the characteristic bamboo compartments and showed good crystallinity. N-CNTs were grown from a quartz plate using a vacuum technique using NiPc and FePc in a dual electric furnace (T = 350 and 700 °C) [156]. The diameters of these N-CNTs were in the range 20 – 40 nm while their lengths were 20 – 30 μm. Li *et al.* [157] have prepared honeycomb-like N-CNTs by the pyrolysis of FePc on a rough film surface.

The pyrolysis of metal (*e.g.*, Fe, Ni) phthalocyanines in the presence of thiophene is known to efficiently produce Y-junction CNTs [126]. More recently, N-CNTs with Y-junctions were prepared by the pyrolysis of NiPc–thiophene mixtures [144]. The electronic properties of junction CNTs were studied by scanning tunneling microscopy (STM) [64].

Liu *et al.* [155] produced large amounts of well-aligned bamboo shaped N-CNTs with open tips by pyrolysis of FePc. The aligned CNTs have an average length of about 10 μm and diameters ranging from 92 – 229 nm. Some of the CNTs showed Y-junction structures due to the self-joint growth of two neighboring CNTs. Wang and co-workers [158] synthesized bamboo-like N-CNTs by the pyrolysis of FePc under Ar/H at 1000 °C. Gago *et al.* [159] produced aligned coaxial nanowires of CNTs wrapped with conducting polymers under H_2/Ar using FePc in the temperature range 800–1000 °C.

High yields of N-CNTs were obtained by pyrolysis of FePc, either in a patterned or non-patterned manner under an Ar/H_2 atmosphere [144]. Zhi *et al.* [160] demonstrated that the pyrolysis of Ni(tetrakis(*tert*-butyl)-naphthalocyaninato) gave (i) CNTs with walls consisting of intact, well-aligned phthalocynanine disks; (ii) N-containing graphitic CNTs with well-ordered columnar wall structures, and (iii) graphitic CNTs with walls containing metallic Ni nanoparticles.

4.4 Other N doped shaped carbon nanomaterials

The focus of this review has been on studies relating to N-CNTs produced from organometallic complexes. CNTs are but one shape that carbon atoms can generate when they come together to form carbonaceous materials. The use of organometallic complexes to produce other SCNMs is still in its infancy. For instance, N-doped carbon nanospheres (N-CNSs) can be made with ease, but it is not clear whether catalysts are required to make these N-CNSs [161–163]. Wu and co-workers [164] synthesized N-doped horn-shaped CNTs by reducing pentachloropyridine with metallic sodium at relatively low temperatures (350 °C). TEM analysis indicated that the CNTs accounted for ~ 30% of the products, and the rest were solid and hollow N-CNSs with a diameter range of 50 – 290 nm.

4.5 Conclusions

We have reviewed the use of organometallic complexes for the synthesis of N doped carbon nanotubes. The organometallic catalysts employed to date to form the N-CNTs have been mainly limited to FcH, FcH containing substituents and $Fe(CO)_5$. Depending on the reaction conditions employed, the type of C and N source used and the growth temperature used, organometallic complexes can be used as catalysts to synthesize N-SWCNTs or N-MWCNTs or other SCNMs. The type of catalysts used during the N-CNT growth plays a role in the formation of the so-

called bamboo compartments. The information presented in the review indicates that the effect of N concentration on CNT growth is now known (high concentrations of N leads to shorter, thinner tubes with small compartments). But the shape of the compartment and the mechanism of N-CNT growth still need to be established. It is obvious from the review that much work still needs to be performed to generate N-CNTs with a specific morphology in high yields.

References

1. S. Iijima, Nature 354 (1991) 56.

2. D. Bethune, C-H. Kiang, M. de Vries, G. Gorman, R. Savoy, J. Vazquez, R. Beyers, Nature 363 (1993) 605.

3. P. Nikolaev, J. Bronikowski, R.K. Bradley, F. Rohmund, D.T. Colbert, K.A. Smith, R.E. Smalley, Chem. Phys. Lett. 313 (1999) 91.

4. O.A. Nerushev, M. Sveningsson, L.K.L. Falk, F.J. Rohmund, J. Mat. Chem. 11 (2001) 1122.

5. S. Amelinckx, X.B. Zhang, D. Bernaerts, X.F. Zhang, V. Ivanov, J.B. Nagy, Science 265 (1994) 635.

6. A.C. Dupuis, Prog. Mater. Sci. 50 (2005) 929.

7. J.B. Park, G.S. Choi, Y.S. Cho, S.Y. Hong, D. Kim, S.Y. Choi, J.H. Lee, K.I. Cho, Cryst. Growth 244 (2002) 211.

8. M.S. Mohlala, X.Y. Liu . J.M. Robinson, N.J. Coville, Organometallics 24 (2005) 972.

9. A.M. Cassell, J.A. Raymakers, J. Kong, H. Dai, J. Phys. Chem. B 103 (1999) 6484.

10. Q.W. Li, H. Yan, Y. Cheng, J. Zhang, Z.F. Liu, J. Mater. Chem. 12 (2002) 1179.

11. J.F. Colomer, C. Stephan, S. Lefrant, G. Van Tendeloo, I. Willems, Z. Konya, Ch. Laurent, J.B. Nagy, Chem. Phys. Lett. 317 (2000) 83.

12. T. Maiyalagan, B. Viswanathan, Mater. Chem. Phys. 93 (2005) 291.

13. O. Stephen, P.M. Ajayan, C. Colliex, Ph. Redlich, J.M. Lambert, P.Bernier, P.Letin, Science 266 (1994) 1683.

14. J. Feng, Y. Li, F. Hou, X. Zhong, Mater. Sci. Eng. A 473 (2008) 238.

15. E.N. Nxumalo, V.O. Nyamori, N.J. Coville, J. Organomet. Chem. 693 (2008) 2942.

16. X.Y. Tao, X.B. Zhang, F.Y. Sun, J.P. Cheng, F. Liu, Z.Q. Luo, Diamond Relat. Mater. 16 (2007) 425.

17. F. Lin, C. Hsu, T. Tang, P. Kang, F. Yang, Mater. Chem. Phys. 107 (2008) 115–121.

18. E. Cruz-Silva, D.A. Cullen, L. Gu, J.M. Romo-Herrera, E. Muñoz-Sandoval, F. López-Urías, B.G. Sumpter, V. Meunier, J.-C. Charlier, D.J. Smith, H. Terrones, M. Terrones, ACS Nano 2 (2008) 441.

19. K. Mondal, N.J. Coville, M.J. Witcomb, J. Havel, G. Tejral, Chem. Phys. Lett. 43 (2007) 787.

20. C.P. Ewels, M. J. Glerup, Nanosci. Nanotechnol. 5 (2005) 1345.

21. S. Van Dommele, K.P. Van de Jong, J.H. Bitter, Chem. Commun. (2006) 4859.

22. S. Van Dommele, A. Romero-Izquirdo, R. K.P. Brydson, de Jong, J.H. Bittera, Carbon 46 (2008) 138.

23. P. Ayala, R. Arenal, M. Rummeli, A. Rubio, T. Pichler, Carbon 48 (2010) 575.

24. J. Robertson, C.A. Davis, Diamond Relat. Mater. 4 (1995) 441.

25. E.J. Biddinger, D. von Deak. Ozkan, U.S. Top. Catal. 52 (2009) 1566.

26. E.N. Nxumalo, P.J. Letsoala, L.M. Cele, N.J. Coville, J. Organometal. Chem. 695 (2010) 2596.

27. P. Ghosh, M. Zamri, M. Subramanian, T. Soga, T. Jimbo, R. Katoh, M. Tanemura, J. Phys. D: Appl. Phys. 41 (2008) 155405.

28. X.X. Zhang, Z.Q. Li, G.H. Wen, K.K. Fung, J. Chen, Y. Li, Chem. Phys. Lett. 333 (2001) 509.

29. Y.Y. Wang, G.Y. Tang, F.A.M. Koeck, B. Brown, J.M. Garguilo, R.J. Nemanich, Diamond Relat. Mater. 13 (2004) 1287.

30. A.G.Kudashov, A.V. Okotrub, L.G. Bulusheva, I.P. Asanov, Yu.V. Shubin, N.F. Yudanov, L.I. Yudanova, V.S. Danilovich, O.G. Abrosimov, J. Phys. Chem. B 108 (2004) 9048.

31. C.H. Lin, H.L. Chang, C.M. Hsu, A.Y. Lo, C.T. Kuo, Diamond Relat. Mater. 12 (2003) 1851.

32. V. Bajpai, L. Dai, T.J. Ohashi, Am. Chem. Soc. 126 (2004) 5070.

33. M.A. Mamo, F.S. Freitasde, J.N. Freitas, W.A.L. van Otterlo, A.F. Nogueira, N.J. Coville, Application of 3-hexylthiophene functionalized CNTs in photovoltaic devices. *Submitted (2010).*

34. J.W. Jang, C.E. Lee, S.C. Lyu, T.J. Lee, C.J. Lee, Appl. Phys. Lett. 84 (2004) 2877.

35. R.M. Yadav, P.S. Dobal, T. Shripathi, R.S. Katiyar, O.N. Srivastava, Nanoscale Res. Lett. 4 (2009) 197.

36. R.M. Yadav, D.P. Singh, T. Shripathi, O.N. Srivastava, J. Nanopart. Res. 10 (2008) 1349.

37. J. Jiang, T. Feng, X. Cheng, L. Dai, G. Cao, B. Jiang, X. Wang, X. Liu, S. Zou, Nucl. Instrum. Meth. B 244 (2006) 327.

38. C.J. Lee, J. Park, Appl. Phys. Lett. 77 (2000) 339.

39. S. Trasobares, O. Stephan, C. Colliex, W.K. Hsu, H.W. Kroto, D.R.M. Walton, J. Chem. Phys. 116 (2002) 8966.

40. S.B. Sinnot, R. Andrews, D. Qian, A.M. Rao, Z. Mao, E.C. Dickey, F. Derbyshire. Chem. Phys. Lett. 315 (1999) 25.

41. M. Glerup, J. Steinmetz, D. Samaille, O. Stephan, S. Enouz, A. Loiseau, S. Roth, P. Bernier, Chem. Phys. Lett. 387 (2004) 193.

42. F. Villalpando-Paez, A. Zamudio, A.L. Elias, H. Son, E.B. Barros, S.G. Chou, Y.A. Kim, H. Muramatsu, T. Hayashi, J. Kong, H. Terrones, G. Dresselhaus, M. Endo, M. Terrones, M.S. Dresselhaus, Chem. Phys. Lett. 424 (2006) 345.

43. H. Lin, J. Lagoute, J. Chacon, R. Arenal, O. Stephan, V. Repain, Y. Girard, S. Enouz, L. Bresson, S. Rousset, A. Loiseau, Phys. Stat. Sol. B 245 (2008) 1986.

44. H. Lin, R. Arenal, S. Enouz-Vedrenne, O. Stephan, A. Loiseau, J. Phys. Chem. C 113 (2009) 9509.

45. R. Jr Droppa, P. Hammer, A.C.M. Carvalho, M.C. dos Santos, F. Alvarez, J. Non-Cryst. Solids 299–302 (2002) 874.

46. S.R. Stoyanov, A.V. Titov, P. Král, Chem. Rev. 253 (2009) 2852.

47. Y. Shao, J. Sui, G. Yin, Y. Gao, Appl. Catal. B Environ. 79 (2008) 89.

48. R. Czerw, M. Terrones, J.C. Charlier, X. Blase, B. Foley, R. Kamalakaran, N. Grobert, H. Terrones, D. Tekleab, P.M. Ajayan, W. Blau, M. Ruhle, D.L. Carroll, Nano Lett. 1 (2001) 457.

49. K. Xiao, Y.Q. Liu, P.A. Hu, G. Yu, Y.M. Sun, D.B. Zhu, J. Am. Chem. Soc. 127 (2005) 8614.

50. M. Terrones, N. Grobert, H. Terrones, Carbon 40 (2002) 1665.

51. J.J. Vela´zquez-Salazar, E. Munoz-Sandoval, J.M. Romo-Herrera, F. Lupo, M. Ruhle, H. Terrones, M. Terrones, Chem. Phys. Lett. 416 (2005) 342.

52. P.E. Lammert, V.H. Crespi. Phys. Rev. Lett. 87 (2001) 136402:1

53. B.Q. Wei, R. Spolenak, P.K. Redlich, M. Ruhle, E. Arzt, Appl. Phys. Lett. 74 (1999) 3149.

54. D.L. Carroll, P. Redlich, X. Blase, J.C. Charlier, S. Curran, P.M. Anaya, S. Roth, M. Ruhle, Phys. Rev. Lett. 81 (1998) 2332.

55. D. Golberg, Y. Bando, C.C. Tang, C.Y. Zhi, Adv. Mater. 19 (2007) 2413.

56. R.B. Sharma, D.J. Late, D.S. Joag, A. Govindaraj, C.N.R. Rao, Chem. Phys. Lett. 428 (2006) 102.

57. M. Endo, T. Hayashi, S.H. Hong, T. Enoki M.S. Dresselhaus, J. Appl. Phys. 90 (2001) 5670.

58. S. Glenis, A.J. Nelson, M.M. Labes, J. Appl. Phys. 86 (1999) 4464.

59. J.D. Wiggins-Camacho, K.J. Stevenson, J. Phys. Chem. C 113 (2009) 19082.

60. S. Maldonado, S. Morin, K.J. Stevenson, Carbon 44 (2006) 1429.

61. J. Robertson, Mat. Sci. Eng. Rep. 37 (2002) 129.

62. B. Wang, Y. Ma, Y. Wu, N. Li, Y. Huang. Y. Chen, Carbon 47 (2009) 2112.

63. J. Wei, H. Hu, H. Zeng, Z. Zhou, W. Yang, P. Peng, Physica E 40 (2008) 462.

64. F.L. Deepak, N.S. John, A. Govindaraj, G.U. Kulkarni, C.N.R. Rao. Chem. Phys. Lett. 411 (2005) 468.

65. S. Latil, F. Triozon, S. Roche, NATO Sci. II Math. Phys. Chem. 222 (2006) 143.

66. Q.-H. Yang, P.-X. Liu, M. Unno, S. Yamauchi, R. Saito, T. Kyotani, Nano Lett. 5 (2005) 2465.

67. S.D. Mhlanga, E.N. Nxumalo, N.J. Coville, S. Vallabhapurapu, Nitrogen doping of CVD multiwalled carbon nanotubes: Observation of a large g shift, *Submitted (2010).*

68. A. Misra, P.K. Tyagi, M.K. Singh, D.S. Misra, Diamond Relat. Mater. 15 (2006) 385.

69. C. Tang, Y. Bando, D. Golberg, F. Xu, Carbon 42 (2004) 2625.

70. M. Reyes-Reyes, N. Grobert, R. Kamalakaran, T. Seeger, D. Golberg, M. Rühle, Y. Bando, H. Terrones, M. Terrones, Chem. Phys. Lett. 396 (2004) 167.

71. M. Bongiorno, P. Blomqvist, P. Piseri, C. Milani, C. Lenardi, T. Ducati, P. Caruso, S. Rudolf, S. Wachtmeister, E. Csillag, G. Coronel, Carbon 43 (2005) 1460.

72. K.Suenaga, E. Sandre, C. Colliex, C.J. Pickard, H. Kataura, S. Iijima, Phys. Rev. B 63 (2001) 165404.

73. W. Han, P. Kohler-Redlich, T. Seeger, F. Ernst, M. Ruhle, N. Grobert, W.-K. Hsu, B.-H. Chang, Y.-Q. Zhu, H.W. Kroto, D.R.M. Walton, M. Terrones, H. Terrones, Appl. Phys. Lett. 77 (2000) 1807.

74. M. Terrones, R. Kamalakaran, T. Seeger, M. Rühle, Chem. Commun. 12 (2000) 2335.

75. D. Golberg, Y. Bando, M. Mitome, K. Kurashima, T. Sato, N. Grobert, M. Reyes-Reyes, H. Terrones, M. Terrones, Physica B: Condens. Mater. 323 (2002) 60.

76. M.S. Dresselhaus, F. Dresselhaus, R. Saito, A. Jorio. Phys. Rep. 409 (2005) 47.

77. Y. Li, B. Zhang, X.Y. Tao, J.M. Xu, W.Z. Huang, J.H. Luo, T. Li, Y. Bao, H.J. Geise, Carbon 43 (2005) 295.

78. P.Tan, L. An, L. Liu, Z. Guo, R. Czerw, D.L. Carroll, P.M. Ajayan, N. Zhang, H. Guo, Phys. Rev. B 66 (2002) 245410.

79. H.D. Zhao, Q. Wagner, Phil. Trans. R. Soc. Lond. A 362 (2004) 2407.

80. S. Choi, K.H. Park, S. Lee, K.H. Koh, J. Appl. Phys. 92 (2002) 4007.

81. L. Liu, Y. Qin, Z.X. Guo, D. Zhu, Carbon 41 (2003) 331.

82. E.J. Liang, P. Ding, H.R. Zhang, X.Y. Guo, Z.L. Du, Diamond Relat. Mater. 13 (2004) 69.

83. L.G. Bulusheva, A.V. Okotrub, I.A. Kinloch, I.P. Asanov, A.G. Kurenya, A.G. Kudashov, X. Chen, H. Song, Phys. Stat. Sol. 245 (2008) 1971.

84. S. Webster, J. Maultzsch, C. Thomsen, J. Liu, R. Czerw, M. Terrones, F. Adar, C. John, A. Whitley, D.L. Carroll, Mater. Res. Symp. Proc. 772 (2003) M7.8.1̃.

85. P. Ghosh, T. Soga, K. Ghosh, R.A. Afre, T. Jimbo, Y. Ando, J. Non-Cryst. Solids 354 (2008) 4101.

86. R. Kurt, A. Karimi, Chem. Phys. Chem. 2 (2001) 388.

87. X. Ma, E.G. Wang, Appl. Phys. Lett. 78 (2001) 978.

88. A.A. Koo´s, M. Dowling, K. Jurkschat, A. Crossley, N. Grobert, Carbon 47 (2009) 30.

89. R. Kurt, C. Klinke, J.M. Bonard, K. Klaus, A. Karimi, Carbon 39 (2001) 2163.

90. Y.T. Lee, N.S. Kim, S.Y. Bae, J. Park, S.C. Yu, H. Ryu, J.H. Lee, J. Phys. Chem. B 107 (2003) 12958.

91. X.K. Li, W.J. Ji, J. Zhao, S.J. Wang, C.T. Au, J. Catal. 236 (2005) 181.

92. T.V. Choudhary, C.D. Sivadinarayana, W. Goodman, Chem. Eng. J. 93 (2003) 69.

93. L. Li, Z.H. Zhu, G.Q. Lu, Z.F. Yan, S.Z. Qiao, Carbon 45 (2007) 11.

94. L. Li, Z.H. Zhu, Z.F. Yan, G.Q. Lu, L. Rintoul, Appl. Catal. A 320 (2007) 166.

95. S.F. Yin, B.Q. Xu, X.P. Zhou, C.T. Au, Appl. Catal. A 277 (2004) 1.

96. J. Chen, Z.H. Zhu, S. Wang, Q. Ma, V. Rudolph, G.Q. Lu, Chem. Eng. J. 156 (2010) 404.

97. S.F. Yin, B.O. Xu, C.F. Ng, C.T. Au, Appl. Catal. B Environ. 48 (2004) 237.

98. F. Villalpando-Paez, A. Romero, E. Munoz-Sandoval, L. Martinez, H. Terrones, M. Terrones, Chem. Phys. Lett. 386 (2004) 137.

99. M.S. Saha, R. Li, X. Sun, S. Ye, Electrochem. Commun. 11 (2009) 438.

100. R. Chetty, S. Kundu, W. Xia, M. Bron, W. Schuhmann, V. Chirila, W. Brandl, T. Reinecke, M. Muhler, Electrochim. Acta 54 (2009) 4208.

101. P.E. Diaz-Flores, F. López-Urı´as, M. Terrones, J.R. Rangel-Mendez, J. Colloid Interface Sci. 334 (2009) 124.

102. H.-Y. Du, C.-H. Wang, H.-C. Hsu, S.-T. Chang, U.-S. Chen, S.C. Yen, L.C. Chen, H.-C. Shih, K.H. Chen, Diamond Relat. Mater. 17 (2008) 5535.

103. J. Amadou, K. Chizari, M. Houllé, I. Janowska, O. Ersen, D. Bégin, C. Pham-Huu, Catal. Today 138 (2008) 62.

104. J.C. Carrero-Sanchez, A.L. Elias, R. Mancilla, G. Arrellin, H. Terrones, J.P. Laclette, M. Terrones, Nano Lett. 6 (2006) 1609.

105. A.L. Elias, J.C. Carrero-Sanchez, H. Terrones, M. Endo, J.P. Laclette, M. Terrones, Small 3 (2007) 1723.

106. B. Fragneaud, K. Masenelli-Varlot, A. Gonzalez-Montiel, M. Terrones, Cavaille, J. Chem. Phys. Lett. 419 (2006) 567.

107. T.C. Nagaiah, S. Kundu, M. Bron, M. Muhler, W. Schuhmann, Electrochem. Commun. 12 (2010) 338.

108. Z. Zhou, X. Gao, J. Yan, D. Song, M. Morinaga, Carbon 42 (2004) 2677.

109. J. Wei, H. Hu, H. Zeng, Z. Zhou, W. Yang, P. Peng, Physica E 40 (2008) 462.

110. M. Terrones, P.M. Ajayan, F. Banhart, X. Blase, D.L. Carroll, J.C. Charlier, R. Czerw, B. Foley, N. Grobert, R. Kamalakaran, P. Kohler-Redlich, M. Rühle, T. Seeger, H. Terrones, Appl. Phys. A Mater. 74 (2002) 355.

111. M.S. He, S. Zhou, J. Zhang, Z.F. Liu, C. Robinson, J. Phys. Chem. B 109 (2005) 9275.

112. N. Krainara, S. Nokbin, P. Khongpracha, Ph.A. Bopp, J. Limtrakul, Carbon 48 (2010) 176.

113. K. Ghosh, M. Kumar, T. Maruyama, Y. Ando, Carbon, 48 (2010) 191.

114. K. Suenaga, M. Yudasaka, C. Colliex, S. Iijima, Chem. Phys. Lett. 316 (2000) 365.

115. L.M. Dell'Acqua-Bellavitis, J.D. Ballard, R. Vajtai, P.M. Ajayan, R.W. Siegel, J. Phys. Chem. C 111 (2007) 2623.

116. X.F. Zhang, X.B. Zhang, G.V. Tendelloo, S. Amelinckx, M.O. de Beeck, J.V. Landuyt, J. Cryst. Growth 130 (1993) 368.

117. C.T. Wirth, S. Hofmann, J. Robertson, Diamond Relat. Mater. 18 (2009) 940.

118. K. Kuwana, K. Saito, Carbon 43 (2005) 2088.

119. M. Jung, K.Y. Eun, Y.J. Baik, K.-R. Lee, J.-K. Shin, S.-T. Kim, Thin Solid Films 398/399 (2001) 150.

120. H. Murakami, M. Hirakawa, C. Tanaka, H. Yamakawa, Appl. Phys. Lett. 76 (2000) 1776.

121. S.H. Tsai, C.W. Chao, C.L. Lee, H.C. Shih, Appl. Phys. Lett. 74 (1999) 3462.

122. A. Badzian, T. Badzian, E. Breval, A. Piotrowski, Thin Solid Films 398 (2001) 170.

123. P. Ghosh, M. Subramanian, R.A. Afre, M. Zamri, T. Soga, T. Jimbo, V. Filip, M. Tanemura, Appl. Surf. Sci. 255 (2009) 4611.

124. M.J. Bronikowski, P.A. Willis, D.T. Colbert, K.A. Smith, R.E. Smalley, J. Vac. Sci. Technol. A 19 (2001) 1800.

125. V.O. Nyamori, S.D. Mhlanga, N.J. Coville, J. Organomet. Chem. 693 (2008) 2205.

126. C.N.R. Rao, A. Govindaraj, Acc. Chem. Res. 35 (2002) 998.

127. N. Chopra, B. Hinds, Inorg. Chim. Acta 357 (2004) 3920.

128. M. Maghrebi, A.A. Khodadadi, Y. Mortazavi, S. Mhaisalkar, Appl. Surf. Sci. 255 (2009) 7243.

129. H. Endo, K. Kuwana, K. Saito, D. Qian, R. Andrews, E.A. Grulke, Chem. Phys. Lett. 387 (2004) 307.

130. K. Kuwana, T. Li, K. Saito, Chem. Eng. Sci. 61 (2006) 6718.

131. Y.G. Tibbetts, A. Carlos, D.W. Bernardo, L. Gorkiewicz, A. Robert, Carbon 32 (1994) 569.

132. A. Cao, L. Ci, G. Wu, B. Wei, C. Xu, J. Liang, D. Wu, Carbon 39 (2001) 152.

133. E.C. Dickey, C.A. Grimes, M.K. Jain, K.G. Ong, D. Qian, P.D. Kichambare, R. Andrews, D. Jacques, Appl. Phys. Lett. 79 (2001) 4022.

134. M. Mayne, N. Grobert, M. Terrones, R. Kamalakaran, R.M. Rühle, H.W. Krato, D.R.M. Walton, Chem. Phys. Lett. 338 (2001) 101.

135. C. Singh, M.S.P. Shaffer, A.H. Windle, Carbon 41 (2003) 359.

136. A. Barreiro, S. Hampel, M.H. Rümmeli, C. Kranberger, A. Grüneis, K. Biedermann, A. Leonhardt, T. Gemming, B. Buchner, A. Bachtold, T. Pichler, J. Phys. Chem. B 110 (2006) 20973.

137. V.O. Nyamori, N.J. Coville, Organometallics 26 (2007) 4083.

138. E.N. Nxumalo, V.P. Chabalala, V.O. Nyamori, M.J. Witcomb, N.J. Coville, J. Organomet. Chem. 695 (2010) 1451.

139. C.J. Lee, S.C. Lyu, H.-W. Kim, J.H. Lee, I.C. Cho, Chem. Phys. Lett. 359 (2002) 115.

140. M. Nath, B.C. Satishkumar, A. Govindaraj, C.P. Vinod, C.N.R. Rao, Chem. Phys. Lett. 322 (2000) 333.

141. N. Grobert, M. Terrones, S. Trasobares, K. Kordatos, H. Terrones, J. Olivares, J.P. Zhang, Ph. Redlich, W.K. Hsu, C.L. Reeves, D.J. Wallis, Y.Q. Zhu, J.P. Hare, A.J. Pidduck, H.W. Kroto, D.R.M. Walton, Appl. Phys. A 70 (2000) 175.

142. M. Terrones, N. Grobert, J. Olivares, J.P. Zhang, H. Terrones, K. Kordatos, W.K. Hsu, J.P. Hare, P.D. Townsend, K. Prassides, A.K. Cheetham, H.W. Kroto, D.R.M. Walton, Nature 388 (1997) 52.

143. R. Che, L.M. Peng, Q. Chen, X.F. Duan, Z.N. Gu, Appl. Phys. Lett. 82 (2003) 3319.

144. F.L. Deepak, A. Govindaraj, C.N.R. Rao, Chem. Phys. Lett. 345 (2001) 5.

145. Z. Osváth, A.A. Koós, N. Grobert, Z. Vértesy, Z.E. Horváth, L.P. Biró, J. Nanosci. Nanotechnol. 9 (2009) 6139.

146. P. Ghosh, M. Tanemura, T. Soga, M. Zamri, T. Jimbo, Solid State Commun. 147 (2008) 15.

147. H. Liu, Y. Zhang, R. Li, X. Sun, S. Désilets, H. Abou-Rachid, M. Jaidann, L.S. Lussier, Carbon 48 (2010) 1498.

148. Y.L. Li, F. Hou, Z.T. Yang, J.M. Feng, X.H. Zhong, J.Y. Li, Mat. Sci. Eng: B 158 (2009) 69.

149. J. Liu, S. Webster, D.L. Carroll, J. Phys. Chem. B 109 (2005) 15769.

150. W. Wasel, K. Kuwana, P.T.A. Reilly, K. Saito, Carbon 45 (2007) 833.

151. G. Zhang, D. Mann, L. Zhang, A. Javey, Y. Li, E. Yenilmez, Q. Wang, J.P. McVittie, Y. Nishi, J. Gibbons, H. Dai, Proc. Nat. Acad. Sci. USA 102 (2005) 16141.

152. Y. Hao, L. Qingwen, Z. Jin, L. Zhongfan, Chem. Phys. Lett. 380 (2003) 347.

153. D.J. Yang, Q. Zhang, S.F. Yoon, J. Ahn, S.G. Wang, Q. Zhou, Q. Wang, J.Q. Li, Surf. Coat. Technol. 167 (2003) 288.

154. S.-C. Chang, T.-S. Li, T.-C. Lin, Mater. Lett. 62 (2008) 1893.

155. B.C. Liu, T.J. Lee, S.H. Lee, C.Y. Park, C.J. Lee, Chem. Phys. Lett. 377 (2003) 55.

156. N.S. Kim, Y.T. Lee, J. Park, J.B. Han, Y.S. Choi, S.Y. Choi, J. Choo, G.H. Lee, J. Phys. Chem. B 107 (2003) 9249.

157. J. Li, C. Papadopoulos, J. Xu, Nature 402 (1999) 253.

158. X. Wang, W. Hu, Y. Liu, C. Long, Y. Xu, S. Zhou, D. Zhu, L. Dai, Carbon 39 (2001) 1533.

159. M. Gago, S. Yoshimura, L. Dai, G. Wallance, R. Gao, Z. Wang, Angew. Chem. Int. Ed. 39 (2000) 20.

160. L. Zhi, T. Gorelik, J. Wu, U. Kolb, K.J. Mullen, Am. Chem. Soc. 127 (2005) 12792.

161. A.A. Deshmukh, R.U. Islam, M.J. Witcomb, W.A.L. van Otterlo, N.J. Coville, Chem. Cat. Chem. 2 (2009) 51.

162. W. Li, D. Chen, Z. Li, Y. Shi, Y. Wan, G. Wang, Z. Jiang, D. Zhao, Carbon 45 (2007) 1757.

163. A. Nieto-Márquez, D. Toledano, P. Sánchez, A. Romero, J.L. Valverde, J. Catal. 269 (2010) 242.

164. X. Wu, Y. Tao, C. Mao, L. Wen, J. Zhu, Carbon 45 (2007) 2253.

165. I. Kunadian, S.M. Lipka, C.R. Swartz, Q. Dali, R. Adrews, J. Electrochem. Soc. 156 (2009) K110.

166. R. Sen, B.C. Satishkumar, A. Govindaraj, K.R. Harikumar, M.K. Renganathan, C.N.R. Rao, J. Mater. Chem. 7 (1997) 2335.

167. K. Jiang, A. Eitan, L.S. Schadler, P.M. Ajayan, R.W. Siegel, N. Grobert, M. Mayne, H. Terrones, M. Terrones, Nano Lett. 3 (2003) 275.

168. I.O. Maciel, J. Campos-Delgado, E. Cruz-Silva, M.A. Pimenta, B.G. Sumpter, V. Meunier, F. Lopez-Urı´as, E. Munoz-Sandoval, H. Terrones, M. Terrones, A. Jorio, Nano Lett. 9 (2009) 2267.

169. J. Liu, R. Czerw, D.L. Carroll, J. Mater. Res. 20 (2005) 538.

Chapter 5

[3]CVD synthesis of nitrogen doped carbon nanotubes using ferrocene/aniline mixtures

5.1 Introduction

Carbon nanotubes (CNTs) and related structured carbon nanomaterials (spheres, fibers, horns, cages *etc.*) have been actively studied since the synthesis and identification of single-walled carbon nanotubes (SWCNTs) [1]. Much of the subsequent work in this area has been driven by the possible uses of the carbon materials in polymer blends, as light weight and conducting materials, as catalyst supports *etc.* [2]. Indeed recent reports reveal that demand for these carbon materials is increasing and that the industrial production of CNTs in the ton scale is now underway [3].

An analysis of the current literature reveals that the chemical vapour deposition (CVD) floating catalyst approach is the common method used to make CNTs on a large scale [4,5]. In this process a carbon source and a catalyst are passed through a hot quartz tube where the carbon

[3] E.N. Nxumalo, V.O. Nyamori, N.J. Coville, *J. Organomet. Chem.* 693 (2008) 2942

source decomposes to form shaped carbon nanomaterials (SCNMs), in particular CNTs. This CVD methodology avoids the use of a catalyst support and the subsequent support removal procedures. The catalyst required to achieve this result is typically a volatile organometallic complex such as ferrocene (FcH) or $Fe(CO)_5$ [6]. Surprisingly, to date, little has been reported on the variation of the catalyst source on CNT synthesis procedures and a systematic approach using classical ligand effects has been little investigated [7]. In recent studies we and others have been using alternative organometallic complexes to ferrocene to synthesise CNTs by the floating catalyst method [8,9]. Interestingly most of these studies have focused on ferrocene derivatives as they provide a facile means of adding elements such as carbon and sulphur into the reactant stream. For example, a recent study reports a method of using a hetero atom (sulfur) to modify multi-walled carbon nanotube (MWCNT) synthesis using a modified sulfur containing ferrocene catalyst acting as both a catalyst and a carbon source [10].

When a hetero atom is inserted into the backbone of a CNT, the symmetry of the tube is modified and the structure and properties are altered [11]. Introduction of foreign atoms into the walls of CNTs was first performed by Stephen *et al*. [12], who doped CNTs with nitrogen (and boron) using arc discharge procedures. Incorporation of N into the CNT lattice can result in the enhancement of the electrical properties of the CNTs [13], which make them promising candidates for electronic devices [14]. Nitrogen doped carbon nanotubes (N-CNTs) are known to be exclusively conducting, showing n-type semiconducting characteristic [15]. Doping is also an important procedure to fine-tune the surface properties of CNTs. The doping of CNTs thus provides a unique entry into the chemistry of CNTs. In particular doping of CNTs with N permits the chemical reactivity of the CNT to be altered as would be expected by N insertion into any graphitic material, hence broadening the horizon of CNT chemistry.

N-Containing CNTs have been prepared by a template synthesis using a polyacrylonitrile precursor [16]. Recently, Point *et al*. [17], synthesized N-CNTs by electron cyclotron resonance

CVD. Long strands of N-CNTs that agglomerated into bundles have been prepared *via* thermal decomposition of a ferrocene/ethanol/benzylamine solution [18]. Whilst doping is a crucial process to alter the properties of CNTs, the challenge is to control the amount of N inserted into the tubes.

In this publication, we wish to report on the use of ferrocene (FcH)/aniline ($PhNH_2$) solutions to synthesize N-CNTs and other carbon species. We also report on the use of 4-ferrocenylaniline ($FcPhNH_2$) as both the N source and catalyst to grow N-CNTs. In particular, the effect of varying the N source concentration (0 – 25 *wt.%*) on the types and yield of CNTs and other SCNMs produced has been investigated. Characterization of the as-synthesized N-CNTs was achieved by conventional techniques. To the best of our knowledge, other than the use of metal porphyrin complexes [19], studies in which organometallic precursors containing nitrogen are used in the synthesis of N-CNTs have not been previously exploited.

5.2 Experimental methods

The precursor for 4-ferrocenylaniline *i.e.* 4-nitrophenyferrocene was prepared as described previously in 33% yield [20]. 4-Ferrocenylaniline was obtained by catalytic reduction of 4-nitrophenylferrocene in 66% yield and characterized by IR and NMR spectroscopy [21].

The crystal structure of 4-ferrocenylaniline was determined from single crystals grown from a mixture of dichloromethane and hexane. The 4-ferrocenylaniline crystals were obtained as orange needles with a melting point of 159 ^{o}C. Intensity data were collected on a Bruker APEX II CCD area detector diffractometer with graphite monochromated Mo Ka radiation (50 kV, 30 mA) using the APEX 2 [22] data collection software. The collection method involved x-scans of width 0.5^{o} and 512 X 512 bit data frames. Data reduction was carried out using the program SAINT+ and face indexed absorption corrections were made using XPREP [23]. The crystal

structure was solved by direct methods using SHELXTL [24]. Non-hydrogen atoms were first refined isotropically followed by anisotropic refinement by full matrix least-squares calculations based on F^2 using SHELXTL. Hydrogen atoms were first located in the difference map then positioned geometrically and allowed to ride on their respective parent atoms. Diagrams and publication material were generated using SHELXTL, PLATON [25] and ORTEP-3 [26].

The CVD floating catalyst method was used for the synthesis of N-CNTs. Growth of the CNTs was carried out in a tubular furnace in a horizontal quartz tube (with dimensions of 800 mm and 28 mm) at atmospheric pressure (Fig. A5.1; Appendices). The temperature inside the reactor was kept at 900 ^{o}C and this was determined by means of a thermocouple positioned in the middle of the furnace. Typically, the quartz tube was heated to the desired temperature in 5% H_2 in argon (v/v) (AFROX) at a constant rate to remove the air from the system. The gases were flowed through the reactor at a controlled flow rate of 100 ml/min using an injection method. Solutions of toluene and 4-ferrocenylaniline (or ferrocene/ aniline) were prepared and transferred to a 10 ml syringe driven by a SAGE pump. The ferrocenyl solutions were then injected into the high temperature zone of the furnace at an injection rate of 0.8 ml/min through a quartz water cooled system [27]. The reactor was then allowed to cool and the carbonaceous material was collected from the walls of the quartz tube. All reagents were used as commercially supplied.

Characterization of the carbonaceous materials was performed by transmission electron microscopy (TEM), thermal gravimetric analysis (TGA), Raman spectroscopy and X-ray photoelectron spectroscopy (XPS). BET was employed to establish the surface areas and pore volumes of the CNTs. TEM analysis were performed on a JEOL JEM-100S Electron Transmission Microscope at 80 kV and at varying magnifications. The TEM samples were dispersed in methanol using a sonicator and loaded onto a copper grid. The composition of the SCNMs formed was determined by counting at least 100 ‘shaped objects’ per sample. These were randomly chosen from different TEM images. The methodology thus provides a crude but

easy method of comparing the effect of reaction variables on the product distribution. Raman spectroscopy data was obtained from a Jobin-Yvon T6400 spectrometer. The excitation source was 636.4 nm from a tunable spectra Physics dye laser, while the backscattered light was dispersed using a 600 line/nm grating. TGA data were collected from a Perkin Elmer TGA analyzer in air at a heating rate of 10 ^{o}C/min. XPS analysis was carried out on a Physical Electronics Quantum 2000 analyser (CSIR, Pretoria) with resolution of 0.1 at.%.

5.3 Results and discussion

5.3.1 Crystal structure of 4-ferrocenylaniline

A single crystal of 4-ferrocenylaniline was grown by slow evaporation of a dichloromethane/hexane solution containing the compound. The crystal data was collected at 173 K and the least squares refinement of the structure gave a final R factor of 0.0221. The PLATON diagram of the molecule giving its numbering scheme is shown in Fig. 5.1. The summary of structural refinement data is provided in the Appendices (Tables A5.1 and A5.2). More refinement data and detailed crystal data (*cif file*) has been deposited with the Cambridge Data File # CCDC 680815.

4-Ferrocenylaniline was observed to crystallize in the orthorhombic crystal system showing four molecules per unit cell. The distance of the Fe atom from the centroids of the substituted (1.651 Å) and the unsubstituted cyclopentadienyl (Cp) (1.654 Å) ring for this compound were found to be generally longer than those for similar arylferrocene compounds such as 4-nitrophenylferrocene [28,29]. This could be due to the NH_2 group being an electron donating group, hence 'pumping' electrons to the metal center. This leaves the Fe center more negative causing repulsion of both the Cp rings leading to a lengthening of the Fe-centroid distances in an attempt to overcome the increasing electron cloud density induced by the NH_2 group. On the

contrary, NO_2 on 4-nitrophenylferrocene is an electron withdrawing group, and therefore has an opposite impact on the bond lengths. The short C6–C11 (1.478(2) Å) length on 4-ferrocenyaniline does suggest a partial double bond character. This suggests the enhanced conjugation between the NH_2 on the phenyl and the Cp ring. This is also supported by the torsion angles which indicate that the Cp ring and the phenyl ring are fairly co-planar allowing for good overlap of p-electrons for bonding. The ferrocenyl moiety of the 4-ferrocenyaniline was found to be in a staggered conformation which is also not unusual. The packing diagram of 4-ferrocenyaniline shows discrete molecules packed in an ordered fashion and the only interactions obtained are those *via* normal Van der Waals contacts.

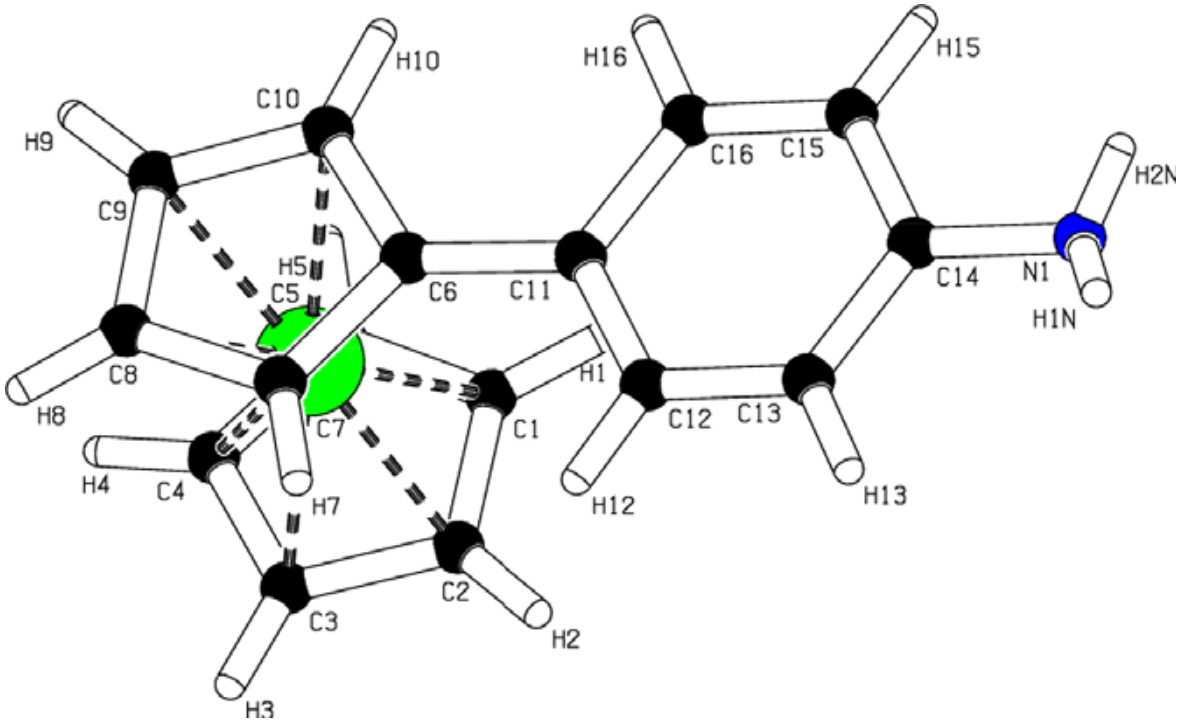


Fig. 5.1. Crystal structure for 4-ferrocenylaniline.

5.3.2 Synthesis and characterization of N-CNTs

N-doped carbon nanotubes were synthesized from solutions of 4-ferrocenylaniline in toluene (2.5 or 5.0 *wt.%* $FcPhNH_2$) or solutions of varying concentrations of aniline (0, 2.5, 5, 10, 15 or 25 *wt.%*) in toluene while keeping the concentration of ferrocene constant (2.5 *wt.%* FcH). Toluene, aniline and the cyclopentadienyl ligands provided the carbon for CNT growth. The catalysts used in this study are shown in Fig. 5.2.

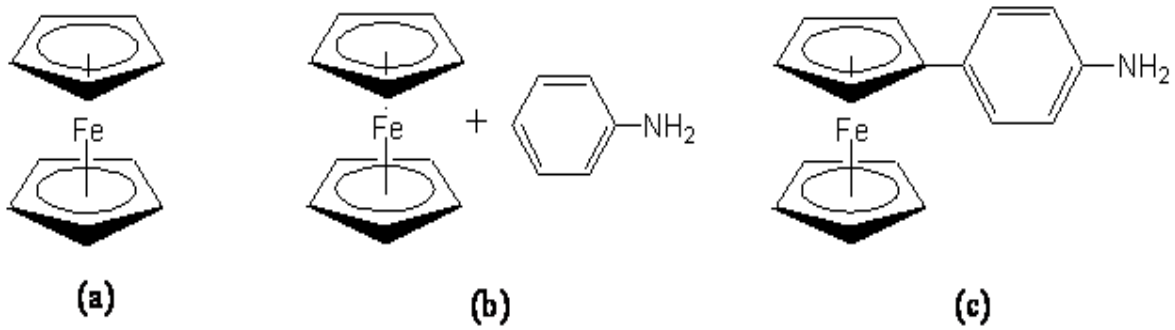


Fig. 5.2. The catalyst systems used with toluene as carbon source: (a) ferrocene (FcH); (b) ferrocene + aniline ($FcH/PhNH_2$) and (c) 4-ferrocenylaniline ($FcPhNH_2$).

5.3.2.1 TEM analysis

A reaction was recorded using FcH (2.5 *wt.%*) and toluene (no aniline) at 900 ^{o}C to provide base line data (Table 5.1). SEM images of the product obtained from both FcH and a FcH/aniline/toluene reaction are shown in Fig. 5.3. As can be seen, the product comprises mostly of CNTs. Further, whereas the FcH product shows good alignment of CNTs the sample made from the Fc/aniline mixture indicates alignment loss.

TEM analysis was used to examine the type, quality, size distribution and quantity (%) of the various SCNMs produced in the different synthesis reactions. In every instance MWCNTs were produced. TEM analysis allowed a facile measure of N doping to be determined. Nitrogen doping is known to significantly alter the morphological structure of CNTs, resulting in the formation of compartmentalized bamboo structures (Fig. 5.4). With FcH the SCNMs produced contain a modest yield of non-compartmentalized MWCNTs (Fig. 5.4a) together with nanofibers, nanospheres and amorphous carbon; with aniline, compartmentalized tubes are detected (Fig. 5.4b and c). At very low doping levels these bamboo structures may not be detected. The bamboo structures are produced by a base growth mechanism [30].

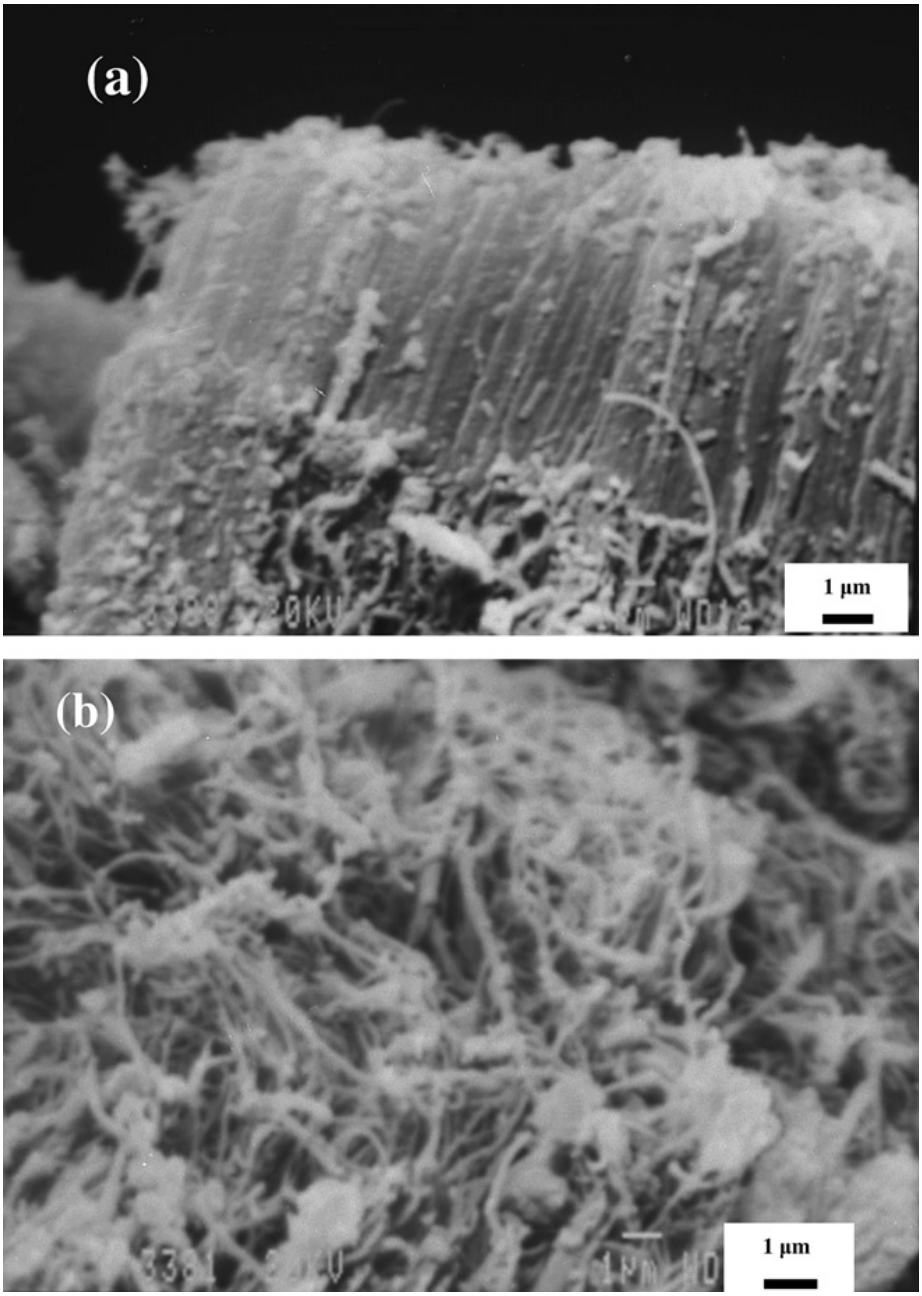


Fig. 5.3. SEM pictures of N-CNT bundles grown from; (a) FcH (2.5 *wt.%*) and FcH (2.5 *wt.%*)/$PhNH_2$ (15 *wt.%*).

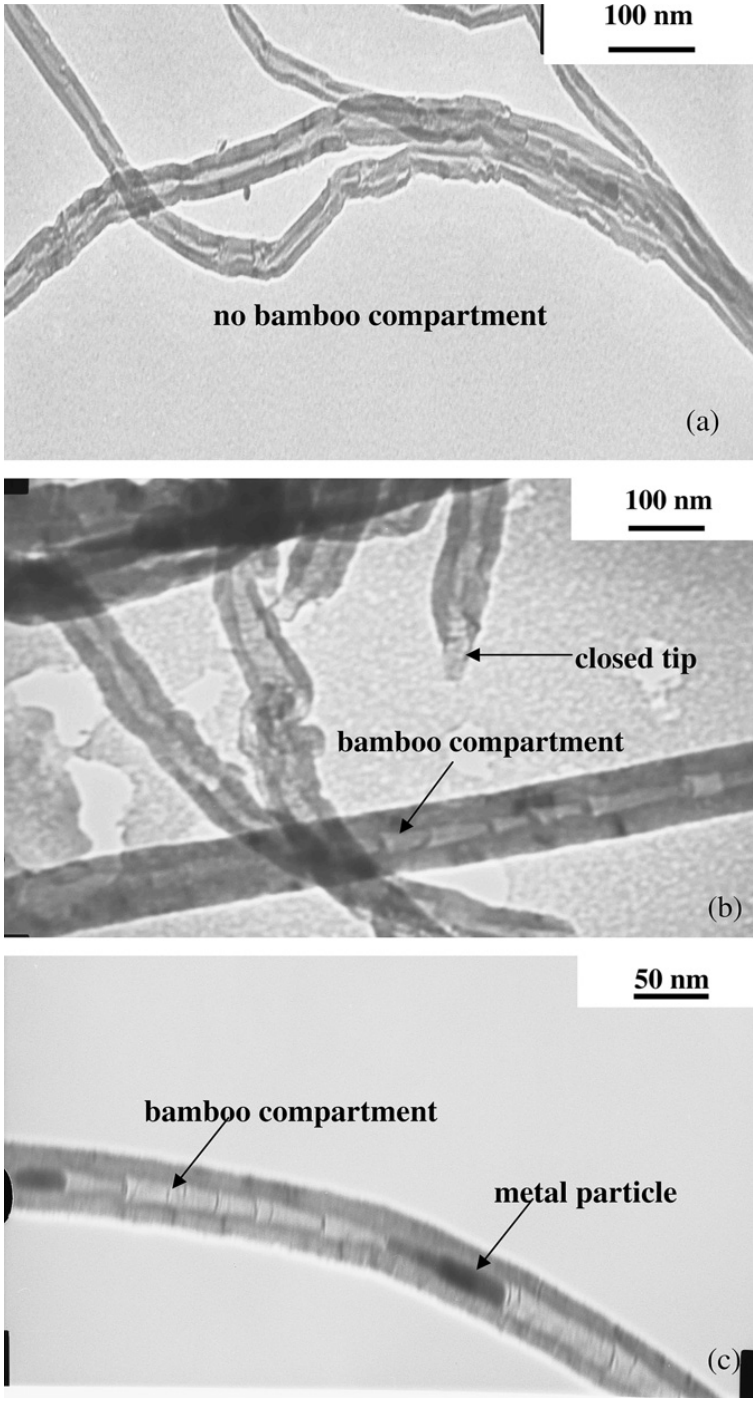


Fig. 5.4. TEM pictures of CNTs grown from (a) FcH (2.5 *wt.%*) (b) $FePhNH_2$ (2.5%) and (c) FcH (2.5 *wt.%*)/$PhNH_2$ (5 *wt.%*).

Replacement of FcH by either $FcPhNH_2$ or by $FcH/PhNH_2$ resulted in a substantial decrease in the total % of SCNMs formed, while the % CNTs formed increased. More importantly, N-CNTs were detected in both the above reactions and the degree of doping, determined by counting bamboo structured tubes is given in Table 5.1. The N-CNT diameters increased relative to the undoped CNTs. Fig. 5.4b and c provides low resolution TEM images of N-CNTs synthesized from the two different catalysts and reveals the bamboo compartments in both samples. Fig. 5.5 shows a high magnification TEM image of a N-CNT; the picture clearly reveals the tubular nature of the N-CNT as well as the compartment wall and the rough surface of the tube.

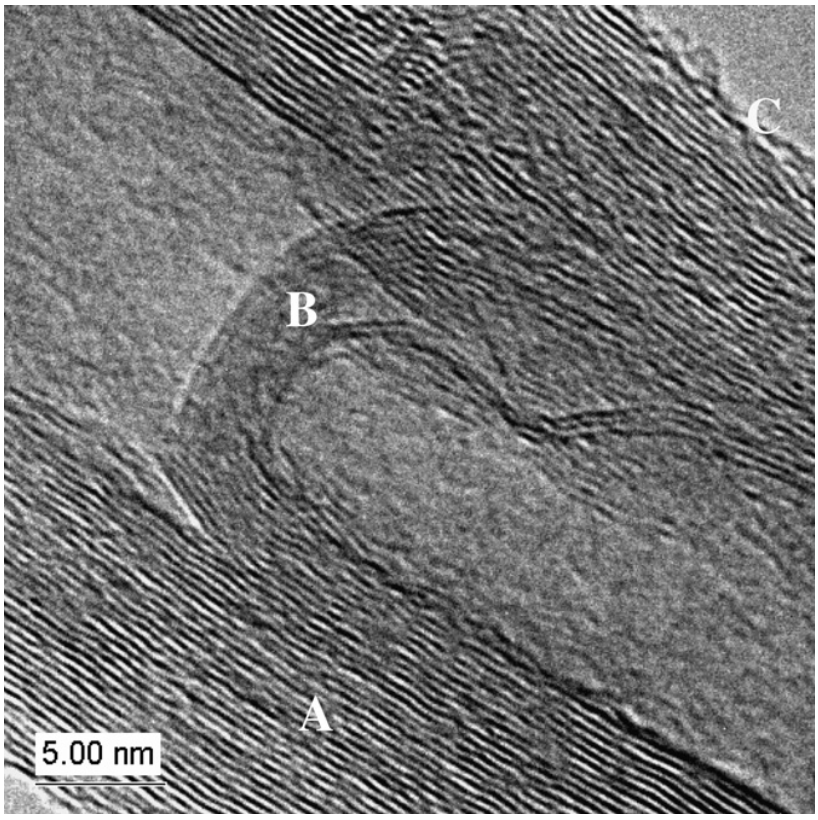


Fig. 5.5. High magnification TEM image of a N-CNT. The image clearly reveals the multi-walled nature of the tube (A), the compartment wall (B) and the rough CNT surface (C).

Doping reactions were performed with 5 *wt.%* catalyst solutions in which the Fe content and Fe/N ratio were kept constant. The TEM data for the SCNMs produced from FcH (3.33 *wt.%*)/$PhNH_2$ (1.67 *wt.%*) and from $FcPhNH_2$ (5 *wt.%*) have been compared, and the following differences have been noted:

(i) the total yield of SCNMs for $FcPhNH_2$ > $FcH/PhNH_2$;
(ii) the CNT yield for $FcH/PhNH_2$ < $FcPhNH_2$;
(iii) the CNT diameters for $FcPhNH_2$ > $FcH/PhNH_2$;
(iv) the % N doping for $FcPhNH_2$ > $FcH/PhNH_2$.

This indicates that the effect of the N hetero atom bound to the catalyst molecule can have a large impact on the size, type and distribution of SCNMs produced when compared to the case where the N hetero atom is not attached to the catalyst. The data obtained in the above reaction is consistent with the proximity of the N to the Fe playing a role in the formation of the N-CNTs. As will be described below, information from Raman spectroscopy is also consistent with this effect.

The data shown in Table 5.1 also allows for a comparison of the SCNMs produced at different concentrations viz. 2.5% and 5 *wt.%* $FcPhNH_2$ catalysts to be made (Table 5.1; and see below). Remarkable effects on tube formation and doping are to be noted.

Table 5.1. Summary of the yield and size distribution of SCNMs produced from different catalysts.

Concentration (*wt.%*)	Fe/N molar ratio	SCNMs (%)	CNTs diameters (nm)	Yield (mg)	Degree of doping (%)
FcH (2.5)	1:1	30T, 20F, 45aC, 5S	60T, 80F, 300S	560	0
$FcPhNH_2$ (2.5)	1.1	45T, 30F, 25aC	65T, 95F, 210S	342	7
$FcPhNH_2$ (5)	1.1	72T, 18F, 10aC	55T, 80F	340	90
FcH (3.33) + $PhNH_2$ (1.67)	1:1	80T, 18F, 5aC, 2S	40T, 75F, 320S	240	1
FcH (2.5) + $PhNH_2$ (1.25)	1:1	35T, 30F, 30aC, 5S	75T, 100F	431	3
FcH (2.5) + $PhNH_2$ (2.5)	1:2	45T, 40F, 15aC	65T, 100F	397	5
FcH (2.5) + $PhNH_2$ (5)	1:4	50T, 40F, 10aC	60T, 95F	495	26
FcH (2.5) + $PhNH_2$ (10)	1:8	70T, 15F, 15aC	40T, 80F	521	95
FcH (2.5) + $PhNH_2$ (15)	1:12	80T, 15F, 5aC	25T, 70F	510	>99
FcH (2.5) + $PhNH_2$ (25)	1:20	70T, 20F, 10aC	20T, 70F	436	90

T: Nanotubes, F: Nanofibers, aC: Amorphous carbon and S: Nanospheres

The effect of systematically varying the aniline concentration on the MWCNT yield was investigated. Thus, TEM studies on the products formed from 1.25 to 25 *wt.%* concentrations of aniline in toluene revealed the following:

(i) The N-CNT diameters decreased (75 – 20 nm) as the % aniline increased from 1.25% to 25% *i.e.* larger concentrations of the N-source yielded CNTs with smaller diameters (Fig. 5.4). Similar effects were observed in a recent study when benzylamine was used as a nitrogen source [31]. (ii) The total yield varied in a non-linear manner with aniline concentration. An increase in

aniline concentration favoured the production of more tubes. This is true until 25 *wt.%* aniline concentration was used; then a drop in N-CNT formation occurred.

(iii) The % doping increased with aniline concentration. It appears that a 15 *wt.%* aniline concentration is sufficient to produce close to 100% N-MWCNTs with a bamboo structure (Fig. 5.4b and c).

The distance between bamboo 'caps' was measured from TEM images (> 100 measurements per sample) for the different samples and the average distances are reported in Table 5.2. It appears that the distance between the bamboo 'caps' within a tube is affected by the concentrations of the N source. An increase in % N source decreases the compartment distance. This is not unexpected and is consistent with the mechanism proposed for N-CNT growth [14]. It was also noted from the TEM analysis that some of the tubes contained metal nanoparticles (see Fig. 5.4c). The presence of the Fe nanoparticles is consistent with the synthesis of N-CNTs *via* a tip or base growth mechanism.

Table 5.2. Distance between N-CNT bamboo compartments.

Concentration (*wt.%*)	Avg. Distance between individual bamboo compartments (nm)
FcH (2.5)	None
$FcPhNH_2$ (2.5)	40
$FcPhNH_2$ (5)	31
FcH (3.33) + $PhNH_2$ (1.67)	45
FcH (2.5) + $PhNH_2$ (1.25)	62
FcH (2.5) + $PhNH_2$ (2.5)	34
FcH (2.5) + $PhNH_2$ (5)	32
FcH (2.5) + $PhNH_2$ (10)	43
FcH (2.5) + $PhNH_2$ (15)	18
FcH (2.5) + $PhNH_2$ (25)	20

5.3.2.2 TGA studies

The thermal stabilities of the various products were evaluated by thermogravimetric analysis in air. Generally, decomposition of the SCNMs was observed from a temperature range of 500 – 610 ^{o}C. This accounts for most of the weight loss (*ca*. 90%). The thermal stability of the carbon nanostructures grown from FcH (2.5 *wt.%*)/$PhNH_2$(1.5 *wt.%*) and $FcPhNH_2$ (2.5 *wt.%*) are compared in Fig. 5.6. The weight loss for the $FcPhNH_2$ sample at T < 200 ^{o}C is attributed to the loss of moisture from the material (Fig. 5.5). The SCNMs grown from $FcPhNH_2$ (2.5 *wt.%*) are less stable than those of FcH (2.5 *wt.%*)/$PhNH_2$ (1.25 *wt.%*) and this is attributed to the structural disorder introduced by the presence of N into the carbon lattice [32]. (The N-CNTs are also less thermally stable than the CNTs synthesized from FcH (not shown)). The residual weight (5 – 10%) observed in the TGA profile is ascribed to FeOx residues formed in air from the catalyst.

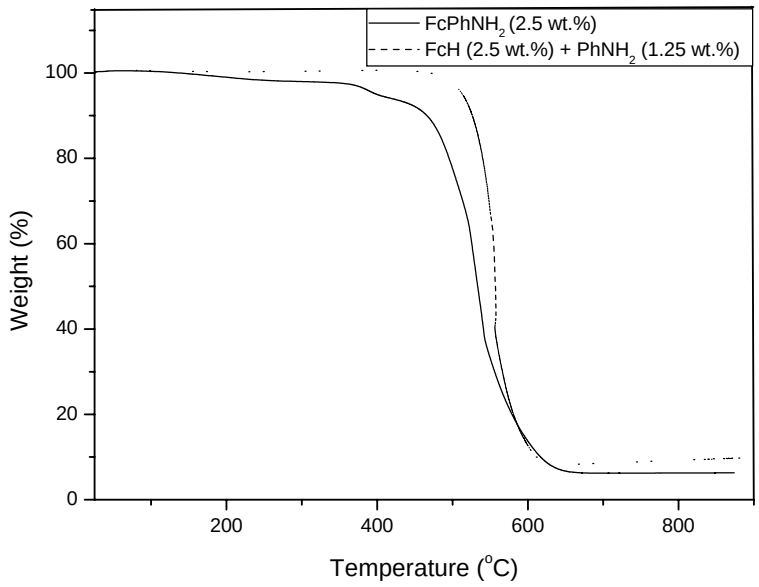


Fig. 5.6. TGA curves of CNTs grown from FcH (2.5 *wt.%*)/$PhNH_2$ (1.25 *wt.%*) and $FcPhNH_2$ (2.5 *wt.%*).

As expected, TGA profiles revealed that an increase in aniline concentration gave rise to the synthesis of less thermally stable N-CNTs (Figs. A5.2 and A5.3, Appendices). For example, CNTs synthesized from 15 *wt.%* aniline started decomposing at 510 ^{o}C while those grown from 5 *wt.%* aniline started losing mass at 560 ^{o}C. This is due to the defect and disorder achieved by the introduction of reactive sites in the N-CNTs [33].

5.3.2.3 Raman spectroscopy

Raman spectroscopy is an excellent tool for investigating the graphitic nature of carbon materials. The Raman spectra generally show two major peaks: a G-band at approximately 1590 cm^{-1} originating from the Raman active E2g mode and a D-band at about 1350 cm^{-1} which is normally explained as a disorder-induced feature due to a finite particle size effect [33]. The I_D/I_G ratio represents the extent of disorder in the graphitic carbon. Thus, as the ratio approaches 0 the carbon will have a more ordered structure. Doping leads to disorder. Table 5.3 shows the positioning of the G-and the D-bands, their intensities as well as the I_D/I_G ratio of the carbon grown from the different catalyst combinations.

Table 5.3. D- and G-band positions and I_D/I_G ratios of CNTs grown at different catalyst concentrations.

Catalyst conc. (*wt.%*)	**D-band (cm^{-1})**	**G-band (cm^{-1})**	**I_D/I_G Ratio**
FcH (2.5)	1356	1587	0.63
$FcPhNH_2$ (2.5)	1364	1587	0.97
$FcPhNH_2$ (5)	1351	1592	1.02
FcH (3.33) + $PhNH_2$ (1.67)			
FcH (2.5) + $PhNH_2$ (1.25)	1358	1589	0.67
FcH (2.5) + $PhNH_2$ (2.5)	1351	1587	0.86
FcH (2.5) + $PhNH_2$ (5)	1359	1591	0.87
FcH (2.5) + $PhNH_2$ (10)	1360	1597	1.05
FcH (2.5) + $PhNH_2$ (15)	1357	1596	1.06
FcH (2.5) + $PhNH_2$ (25)	1353	1596	0.99

As shown in Table 5.3, when N-CNTs are produced from solutions with equivalent Fe/N ratios $FcPhNH_2$ gave a higher I_D/I_G ratio of (0.97) as compared to that of the mixture FcH (2.5 *wt.%*) + $PhNH_2$ (1.25 *wt.%*) (0.67) which in turn was higher than that of the undoped CNTs (0.63) (see

also Fig. A5.4; Appendices). This implies that N-CNTs produced from $FcPhNH_2$ were more disordered than that produced from $FcH/PhNH_2$. In the case of the $FcH/PhNH_2$ mixtures, the I_D/I_G ratios (Table 5.2) suggest that, as the concentration of aniline increased, the degree of disorder also increased. Indeed, the products produced with 1.25 *wt.%*, 5 *wt.%* and 15 *wt.%*, aniline concentrations give rise to I_D/I_G ratios of 0.67, 0.87 and 1.06, respectively. Extrapolation of the graph of Raman ratios also suggests that $FcPhNH_2$ (2.5 *wt.%*) is similar to FcH + $PhNH_2$ when the $PhNH_2$ concentration is *ca.* = 7.5 *wt.%*. Thus the impact of having the aniline attached to or separate from the ferrocene leads to a comparative 2–5x increase in N doping.

5.3.2.4 XPS and CN analysis

XPS and CN elemental analyses were conducted on the as-synthesized SCNMs to investigate the N-content in the CNTs. These techniques demonstrate the presence of quantifiable amounts of N in the tubes. N concentrations for the tubes were approximately 1.00 at.% (Table 5.4). For example, XPS analysis of FcH (2.5 *wt.%*)/ $PhNH_2$ (> 15 *wt.%*) gave > 1% N content. The CN analysis similarly gave N atomic concentrations (%) of 1.07 and 1.05 for the $PhNH_2$ (15 *wt.%*) and $PhNH_2$ (25 *wt.%*) samples respectively. The C/N ratio of the N-CNTs produced by these two catalysts, were calculated to be 84 and 88. However, at lower concentrations of aniline (< 2.5 *wt.%*) no nitrogen was detected in any of the samples by the two techniques, indicating much larger C/N ratios.

Table 5.4. Nitrogen content for the N-CNTs synthesized from the various catalysts.

Precatalyst (*wt.%*)	**XPS (N at.%)**	**CN (N at.%)**
$FcPhNH_2$ (2.5)	ND	ND
FcH (2.5) + $PhNH_2$ (1.25)	ND	ND
FcH (2.5) + $PhNH_2$ (15)	1.50	1.07
FcH (2.5) + $PhNH_2$ (25)	1.00	1.05

ND: not detected

XPS analysis has the potential to give information about the hybridisation state of the N in the N-CNTs. According to Jang *et al.* [34], the type of N observed at high N concentrations in CNTs has been shown to be sp^3 hybridized; at lower N concentrations, a sp^2 signal for N was observed. The above results were obtained using NH_3/C_2H_2 reactant mixtures over a Fe/SiO_2 catalyst [34]. In this study the XPS data revealed that use of the 15% aniline solution gave an XPS signal for nitrogen consistent only with sp^2 hybridized N while a 25% aniline solution gave two nitrogen XPS signals (50/50) consistent with both sp^2 and sp^3 nitrogen. This suggests that chemical reactions that can be used to functionalize NCNTs will give different reactions for the N-CNTs produced with different N contents.

5.3.2.5. BET surface area and pore volume

The surface area and pore volume data for the as-synthesized NCNTs were obtained using the Brunauer Emmett Teller (BET) method (Table 5.5). As expected the surface area and the pore volumes of the N-CNTs increased significantly as the aniline concentration increased. For example, the surface area for FcH (2.5 *wt.%*)/$PhNH_2$ (5 *wt.%*) = 24.0 m^2/g while that for 25 *wt.%*

= 30.2 m^2/g. This is related to (i) the observed decrease in diameter of the N-CNTs and (ii) the more disordered CNT surface as the aniline concentration increased (Table 5.1).

Table 5.5. Surface areas and pore volumes of N-CNTs grown at different catalyst concentrations.

Catalyst conc. (*wt.%*)	**Surface area (m^2/g)**	**Pore volume (cm^3/g)**
FcH (2.5)	18.9	0.047
$FcPhNH_2$ (2.5)	25.6	0.088
$FcPhNH_2$ (5)	14.2	0.063
FcH (3.33) + $PhNH_2$ (1.67)	32.4	0.231
FcH (2.5) + $PhNH_2$ (1.25)	19.2	0.062
FcH (2.5) + $PhNH_2$ (2.5)	19.9	0.091
FcH (2.5) + $PhNH_2$ (5)	24.0	0.102
FcH (2.5) + $PhNH_2$ (10)	26.5	0.085
FcH (2.5) + $PhNH_2$ (15)	29.9	0.182
FcH (2.5) + $PhNH_2$ (25)	30.2	0.182

The surface area of the sample produced from $FcPhNH_2$ (2.5 *wt.%*) is similar to that of the sample produced from *ca.* = FcH (2.5 *wt.%*)/$PhNH_2$ (10 *wt.%*). This result is in agreement with the correlations observed from the Raman data presented in Table 5.3.

5.4 Conclusions

We have studied the effect of varying the N-source concentration on the production of N-doped CNTs and other SCNMs in a CVD reactor. Successful N-doping was evidenced by the presence of compartmentalized bamboo structures in the CNT walls. A ferrocene/ aniline catalyst (15

wt.%) produced predominantly pure NCNTs with only small amounts of amorphous carbon and other SCNMs. Generally, the Raman spectra of the as-synthesised N-CNTs showed a low degree of graphitization indicating the presence of defects and disorder in the CNT walls. XPS analysis demonstrated the presence of quantifiable amounts of N in the tubes. The study thus reveals that the diameters of the tubes can be controlled by systematically varying the N source concentration. More significantly a higher N content is achieved by using the aniline substituted ferrocene as a catalyst when compared to ferrocene/aniline mixtures. A *ca.* 2–5x increase was determined in N content using similar catalyst concentrations.

References

1. (a) S. Iijima, T. Ichihashi, Nature 363 (1993) 603;

(b) D.S. Bethune, C.H. Kiang, M.S. De Vries, G. Gorman, R. Savoy, J. Vazquez, R. Beyers, Nature 363 (1993) 605;

(c) H.P. Boehm, Carbon 35 (1997) 581.

2. (a) R. Saito, G. Dresselhaus, M.S. Dresselhaus, Physical properties of carbon nanotubes, Imperial College Press., London, 1998;

(b) G. Cao, Nanostructures and nanomaterials: Synthesis, properties and applications, Imperial College Press, London, 2004;

(c) M.S. Dresselhaus, G. Dresselhaus, P.C. Eklund, Science of fullerenes and carbon nanotubes, Academic Press, San Diego, 1996;

(d) M.J. O'Connell, Carbon nanotubes: Properties and applications, Taylor & Francis Group, LLC, Calirfonia, 2006.

3. (a) A.M. Thayer, Chem. Eng. News (2007) 29. November;

(b) J. Evans, Chem. World (2007) 17. November.

4. (a) P. Nikolaev, J. Bronikowski, R.K. Bradley, F. Rohmund, D.T. Colbert, K.A. Smith, R.E. Smalley, Chem. Phys. Lett. 313 (1999) 91;

(b) O.A. Nerushev, M. Sveningsson, L.K.L. Falk, F. Rohmund, J. Mater. Chem. 11 (2001) 1122.

5. (a) S. Amelinckx, X.B. Zhang, D. Bernaerts, X.F. Zhang, V. Ivanov, J.B. Nagy, Science 265 (1994) 635;

(b) A.C. Dupuis, Prog. Mater. Sci. 50 (2005) 929;

(c) J.B. Park, G.S. Choi, Y.S. Cho, S.Y. Hong, D. Kim, S.Y. Choi, J.H. Lee, K.I. Cho, J.Cryst. Growth 244 (2002) 211;

(d) H. Dai, Surf. Sci. 500 (2002) 218;

(e) A.M. Cassell, J.A. Raymakers, J. Kong, H. Dai, J. Phys. Chem. B 103 (1999) 6484;

(f) Q.W. Li, H. Yan, Y. Cheng, J. Zhang, Z.F. Liu, J. Mater. Chem. 12 (2002) 1179;

(g) J.F. Colomer, C. Stephan, S. Lefrant, G. Van, I. Willems, Z. Konya, C. Laurent, J.B. Nagy, Chem. Phys. Lett. 317 (2000) 83.

6. (a) K.C. Mondal, N.J. Coville, Encyclopedia of Nanoscience and Nanotechnology, American Scientific Publishers, California, USA, in press.;

(b) A. Govindaraj, C.N.R. Rao, Pure Appl. Chem. 74 (2002) 1571;

(c) V.O. Nyamori, S.D. Mhlanga, N.J. Coville, J Organometal. Chem. 693 (2008) 2205.

7. (a) T.M. Keller, S.B. Qadri, Chem. Mater. 16 (2004) 1091;

(b) M.S. Mohlala, X.Y. Liu, M.J. Witcomb, N.J. Coville, Appl. Organomet. Chem. 21 (2007) 275;

(c) X.Y. Liu, B. C Huang, N.J. Coville, Fullerenes Nanotubes Carbon Nanostruct. 10 (2002) 339.

8. M. Laskoski, T.M. Keller, S.B. Qadri, Carbon 45 (2007) 443.

9. (a) M.S. Mohlala, X.Y. Liu, J.M. Robinson, N.J. Coville, Organometallics 24 (2005) 972;

(b) V.O. Nyamori, N.J. Coville, Organometallics 26 (2007) 4083.

10. M.S. Mohlala, X.Y. Liu, N.J. Coville, J. Organomet. Chem. 691 (2006) 4768.

11. M. Reyes-Reyes, N. Grobert, R. Kamalakaran, T. Seeger, D. Golberg, M. Rühle, Y. Bando, H. Terrones, M. Terrones, Chem. Phys. Lett. 21 (2004) 67.

12. O. Stephen, P.M. Ajavan, C. Colliex, Ph. Redlich, J.M. Lambert, P. Bernier, P. Letin, Science 266 (1994) 1683.

13. R.B. Sharma, D.J. Late, D.S. Joag, A. Govindaraj, C.N.R. Rao, Chem. Phys. Lett. 428 (2006) 102.

14. C.P. Ewels, M. Glerup, J. Nanosci. Technol. 5 (2005) 1345.

15. Q.-H. Yang, P.-X. Liu, M. Unno, S. Yamauchi, R. Saito, T. Kyotani, Nano Lett. 5 (2005) 275.

16. R.V. Parthasarathy, K.L.N. Phani, C.R. Martin, Adv. Mater. 7 (1995) 896.

17. S. Point, T. Minea, B. Bouchet-Fabre, A. Granier, G. Turban, Diamond Relat. Mater. 14 (2005) 891.

18. F. Villalpando-Paez, A. Zamudio, A.L. Elias, H. Son, E.B. Barros, S.G. Chou, Y.A. Kim, H. Muramatsu, T. Hayashi, J. Kong, H. Terrones, G. Dresselhaus, D. Endo, M. Terrones, M.S. Dresselhaus, Chem. Phys. Lett. 424 (2006) 345.

19. (a) C.N.R. Rao, A. Govindaraj, G. Gundiah, S.R.C. Vivekchand, Chem. Eng. Sci. 59 (2004) 4665;

(b) F.L. Deepak, A. Govindaraj, C.N.R. Rao, Chem. Phys. Lett. 345 (2001) 5;

(c) C.N.R. Rao, A. Govindaraj, Acc. Chem. Res. 35 (2002) 998.

20. T. Lanez, P.L. Pauson, J. Chem. Soc., Perkin Trans. I (1990) 2437.

21. A.N. Nesmeyanov, E.G. Perevalova, R.V. Golovnya, L. Shilovtseva, Dokl. Akad. Nauk SSSR 102 (1955) 535.

22. Bruker, APEX2, Version 2.0-1, Bruker AXS Inc., Madison, WI, USA, 2005.

23. Bruker, SAINT-NT, Version 6.0 (includes XPREP and SADABS), Bruker AXS Inc., Madison, WI, USA, 2005.

24. Bruker, SHELXTL, Version 5.1 (includes XS, XL, XP, XSHELL), Bruker AXS Inc., Madison, WI, USA, 1999.

25. A.L. Spek, J. Appl. Crystallogr. 36 (2003) 7.

26. L.J. Farrugia, J. Appl. Crystallogr. 30 (1997) 565.

27. M.S. Mohlala, N.J. Coville, J. Organomet. Chem. 692 (2007) 2965.

28. J.F. Gallagher, G. Ferguson, S.Z. Ahmed, C. Glidewell, A. Lewis, Acta Crystallogr., Sect. C 53 (1997) 1772.

29. R.M.G. Roberts, J. Silver, B.M. Yamin, M.G.B. Drew, U. Eberhardt, J. Chem. Soc., Dalton Trans. (1988) 1549.

30. P.J. Harris, Carbon 45 (2007) 229.

31. X.Y. Tao, X.B. Zhang, F.Y. Sun, J.P. Cheng, F. Liu, Z.Q. Luo, Diamond Relat. Mater. 16 (2007) 425.

32. (a) R. Kurt, A. Karini, Chem. Phys. Chem. 2 (2001) 388;

(b) X. Ma, E.G. Wang, Appl. Phys. Lett. 78 (2001) 978.

33 (a) S. Maldonado, S. Morin, K.J. Stevenson, Carbon 44 (2006) 1429;

(b) S. Choi, K.H. Park, S. Lee, K.H. Koh, J. Appl. Phys. 92 (2002) 4007.

34. J.W. Jang, C.E. Lee, S.C. Lyu, T.J. Lee, C.J. Lee, Appl. Phys. Lett. 84 (2004) 2877.

Chapter 6

[4]Influence of methylimidazole isomers on ferrocene-catalysed nitrogen doped carbon nanotube synthesis

6.1 Introduction

Since the report on the synthesis of carbon nanotubes (CNTs) in 1991 by Iijima [1], many researchers have devoted much time and effort in developing new strategies for the synthesis of shaped carbon nanomaterials (SCNMs). Organometallic complexes have often been used in the synthesis of these SCNMs that include CNTs [2], carbon nanofibers (CNFs) [3], carbon nanospheres (CNSs) [4], carbon nanocoils [5], *etc.* The advantages of using organometallic compounds are that they do not need to have a counterion, they do not have to be used in the presence of a support and they act as both a catalyst and as a carbon source to form SCNMs. Initial reports using organometallic complexes such as ferrocene [6], cobaltocene [7] and

[4] E.N. Nxumalo, V.P. Chabalala, V.O. Nyamori, M.J. Witkomb, N.J. Coville, *J. Organomet. Chem.* 695 (2010), 1451

nickelocene [8], under reducing conditions revealed that the pyrolysis of the metallocenes generated CNTs.

When ferrocene is used together with a carbon source, the Fe/C ratio has a major impact on whether CNTs or CNSs are the major products formed in the reaction [9]. Low catalyst concentrations favour CNT production and the absence of a catalyst leads only to CNSs and amorphous materials [10]. Increasing the Fe/C ratio leads to an increase in the diameter of the nanotubes produced due to the formation of larger iron nanoparticles at higher metal concentration [9]. An increased Fe/C ratio also leads to a higher yield of iron filled CNTs [9a].

Doping of CNTs with heteroatoms leads to a change in the CNT structure. Nitrogen, for example, has profound effects on the nanotube morphology [11,12]. The presence of nitrogen in the growth environment is a favourable condition for the formation of 'bamboo- like' CNTs, but it is not a necessary condition [13–15]. N-doping of CNTs can be achieved by *in situ* N addition during CNT formation or post-synthesis doping of undoped CNTs. The doping of CNTs has been reported previously [16]. The routine method for the *in situ* synthesis of nitrogen doped CNTs (N-CNTs) is the chemical vapour deposition (CVD) method using nitrogen containing compounds [17]. Ammonia [18] or any volatile nitrogen-compound containing an organic component can be used as an N source. Most experiments performed using nitrogen gas or ammonia in a CVD process generates vertically aligned CNTs [19]. Films of vertically grown N-CNTs from different substrates have also been obtained by the pyrolysis of a mixture of ferrocene and melamine [20]. Li *et al.* [21] have shown that it is possible to grow high quality vertically oriented N-CNT arrays over an alumina substrate on a rough surface. Qian *et al.* [22] successfully synthesized well-aligned N-doped multi-walled carbon nanotube arrays over a large area, on quartz and silicon wafers, by a floating catalyst CVD method at fairly low temperature (600 °C) using pyridine–ferrocene mixtures. The nitrogen incorporated nanotubes have smaller

outer diameters but larger inner diameters compared with CNTs grown from a xylene–ferrocene mixture under similar conditions [22].

N-CNTs have recently shown great potential as catalyst supports for Pt–Ru nanoparticles in the anodic oxidation of methanol in direct methanol fuel cells [23]. They have also been used in environmental applications, in the aqueous phase, as adsorbents of organic and inorganic compounds and ions [24]. A recent review described theoretical studies involving carbon nanostructures that have been substitutionally doped with transition metals and nitrogen atoms [12]. Literature reports reveal that the incorporation of N into CNTs results in an enhancement in conductivity [25] and improvement of transport and field emission properties of CNTs [26]. N-doped single-walled CNTs (SWCNTs) synthesized in large scale using an electric arc discharge method show that the band gap of SWCNTs can be tuned by varying the degree of N insertion [27]. This is due to the electron donor ability of the nitrogen atom that leads to the formation of a *n*-type semiconductor [28].

More recently there has been an upsurge of interest in the synthesis of CNTs by the pyrolysis of organometallic complexes in a confined environment *e.g.* stainless steel autoclaves or sealed glass vessels, at autogenous pressure especially using Fe and Co metal catalysts [29]. Undoped CNTs can be produced in high yields by directly pyrolyzing ferrocene in an autoclave [30]. Zhang *et al*. [31] also synthesized larger diameter undoped CNTs through the catalytic decomposition of polypropylene and maleated polypropylene using Ni as a catalyst in an autoclave at 700 ^{o}C. The possible growth process for CNTs grown using this method was also described.

In this work, we report the N-doping of multi-walled CNTs in a confined space (sealed quartz vessels) using organometallic precursors. The use of ferrocenylmethylimidazole as a catalyst for the synthesis of N-CNTs as well as the use of different ratios of ferrocene/ i-methylimidazole (i =

1, 2 or 4) (Fig. 6.1) in a confined space yielded N-CNTs with different morphologies and several other SCNMs. Furthermore, we reveal that the growth of N-CNTs is determined by the fragments produced by decomposition of the reactants and that the different imidazoles yield N-CNTs with different nitrogen contents.

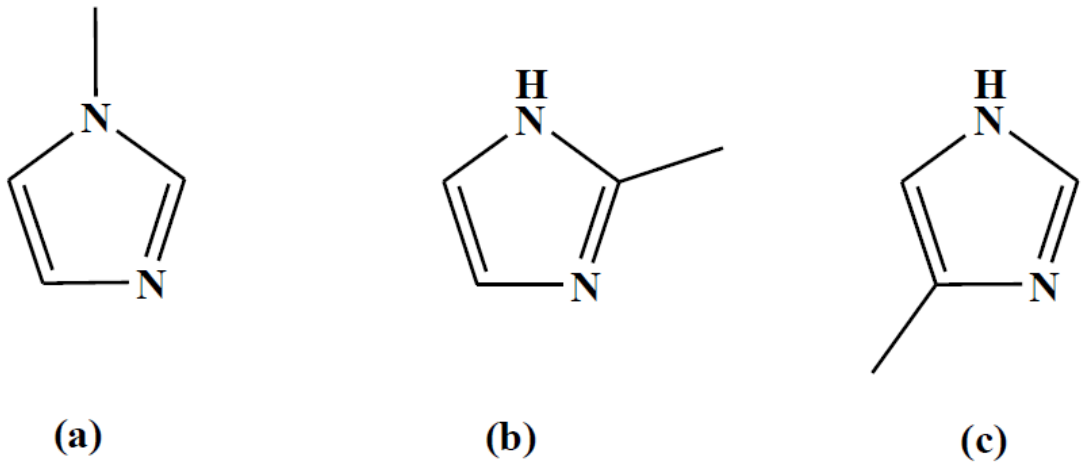


Fig. 6.1. Structures of the N sources used during the formation of SCNMs: (a) 1-methylimidazole; (b) 2-methylimidazole and (c) 4-methylimidazole.

6.2 Experimental

6.2.1 General procedure

The synthesis of ferrocenyl derivatives were performed under an inert atmosphere of pure argon. This was achieved by using standard Schlenk techniques. Silica Gel 60 was used for column chromatography. Commercial dichloromethane was initially dried over calcium chloride, and then distilled from calcium hydride. Preparation of anhydrous diethyl ether was achieved by drying over fresh sodium wire. Ferrocene and ferrocene carboxaldehyde were purchased from

Strem Chemicals, Inc. (USA). The three isomers (1-methylimidazole, 2-methylimidazole and 4-methylimidazole) were purchased from Sigma–Aldrich.

6.2.2 Instrumentation

Raman spectra were measured using the single spectrograph stage of a Jobin–Yvon T64000 Raman spectrometer. The excitation source was 636.4 nm from a tunable Spectra-Physics dye laser. The laser beam was focused onto the sample using the 20X objective of an Olympus microscope. The backscattered light was dispersed using a 600 line/mm grating and detected using a CCD detector. Thermogravimetric analysis (TGA) measurements were performed under air on a Perkin–Elmer TGA 7 at a heating rate of 10 ^{o}C/min. TEM analysis was performed on a JEOL JEM-100S Electron Transmission Microscope at 80 kV and on a Philips CM200 (Philips, Eindhoven, The Netherlands) equipped with a Gatan Imaging Filter. The TEM samples were dispersed in methanol using an automated sonicator and loaded onto a holey Cu grid.

6.2.3 Synthesis of ferrocene derivatives

6.2.3.1 Synthesis of ferrocenylmethylimidazole

Ferrocenylmethanol was obtained by the reduction of ferrocene carboxylaldehyde using an ethereal solution of lithium aluminium hydride. Ferrocenylmethylimidazole was achieved by reacting equimolar amounts of ferrocenylmethanol and N,N-carbonylimidazole in anhydrous dichloromethane in an inert atmosphere [32].

6.2.3.2 Synthesis of SCNMs in sealed tubes

Approximately 100 mg of precursor compounds (ferrocenylmethyimidazole or FcH/methylimidazole) were sealed in a quartz tube (10 cm in length and 1.0 cm internal diameter). The quartz tube (Fig. 6.2(a)) was introduced into an electrical furnace and heated at a rate of 3 ^{o}C/min to reach a temperature of 500 ^{o}C *i.e.* above the precursor decomposition temperature. The tubes were held at this temperature for at least 30 min to ensure complete decomposition of reagents. The tube was then heated at a rate of 2 ^{o}C/minute to 800 ^{o}C and held at that temperature for 12 h before being gradually cooled to room temperature. A black solid material was obtained (Fig. 6.2(b)). A small amount of the black carbonaceous material was transferred into a mortar and ground using a pestle to a fine material. The sample was then characterized by TEM, TGA and Raman spectroscopy.

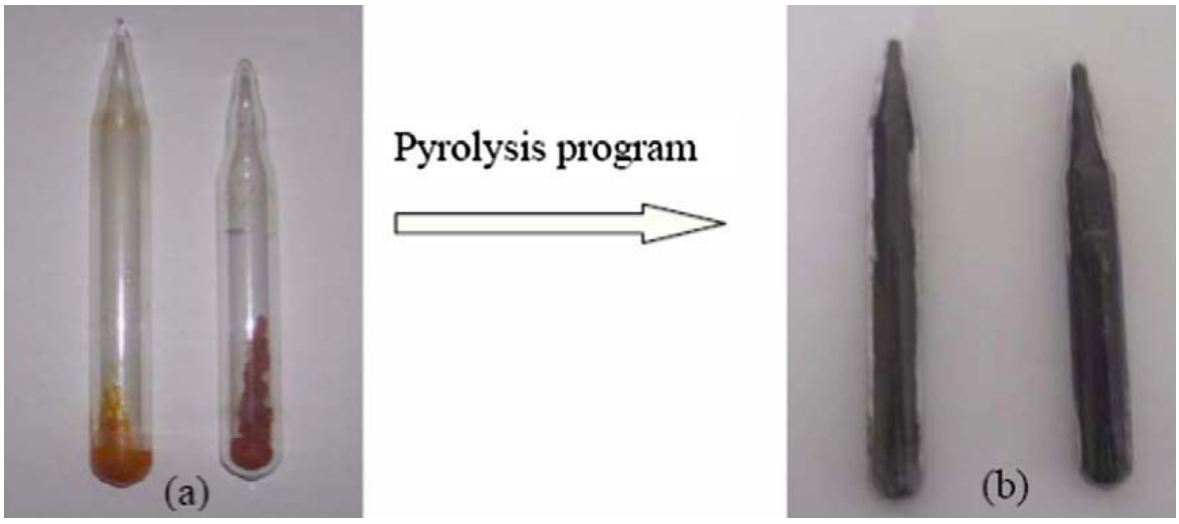


Fig. 6.2. Quartz tube reaction vessels (a) before and (b) after reaction.

6.3 Results and discussion

6.3.1 Synthesis of ferrocenylmethylimidazole

Ferrocenylmethylimidazole was synthesized from equimolar amounts of ferrocenylmethanol and N,N-carbonylimidazole in anhydrous dichloromethane as reported by Simenel *et al.* [32]. The chemical structures of these two compounds were confirmed by ^{1}H NMR, ^{13}C NMR and FTIR spectroscopies and XRD patterns.

6.3.2 Synthesis of carbon nanotubes

Carbonaceous materials were synthesized successfully by the solid state pyrolysis of ferrocenylmethylimidazole or varying ratios of mixtures of FcH and methylimidazole in sealed quartz tubes. The advantage of this procedure is that the effect of high pressure on product formation can be utilized. Methylimidazoles were chosen for study as they have a high N content (~ 30% by mass), are air-stable and exist as solids and liquids. Reaction conditions were chosen to ensure breakdown of the reactants by decomposition. In the closed environment the reactants will break down into C, H, N and Fe containing species [33]. The conditions will produce ionic species as well as radicals, molecular species and ions, and the type of reactant and the reactant ratio could thus impact on the products formed.

In this study the effect of the position of the methyl group in methylimidazole has been investigated in the synthesis of nitrogen doped CNTs. In particular, three different methylimidazoles (*i.e.* 1, 2 or 4-methylimidazole) were chosen for investigation. As these compounds all have the same elemental composition any differences in the products formed will relate to the position of the Me group on the ring backbone. In principle, if they all break down completely under the reaction conditions then all three isomers should generate similar ratios and

types of carbonaceous products. Indeed the current mechanism proposed for CNT growth involves carbon atoms dissolving in a catalyst and re-precipitating to give CNT growth [34]. The three methylimidazole isomers do, however, have different physical and chemical properties and hence we may expect decomposition products and rates to be different.

In this investigation, the pyrolysis reactions all gave black carbonaceous materials that were then analysed by TEM, TGA and Raman spectroscopy.

6.3.2.1 TEM analysis of CNTs

TEM analysis was used to evaluate the products generated in the pyrolysis reactions. TEM images showed that different products (amorphous carbon, spheres, fibers, hollow tubes and bamboo tubes) were obtained from the different reactions and the data is summarised in Table 6.1. All the tubes obtained in this study were of the multi-walled type and TEM images of typical N-CNT products are shown in Figs. 6.3 and 6.4. The product morphology distributions were estimated from the TEM photographs and while the error bar was *ca.* 5 – 10%, trends in the morphologies can still be noted. The product ratios indicate that the type of imidazole used did indeed impact on the product distribution detected.

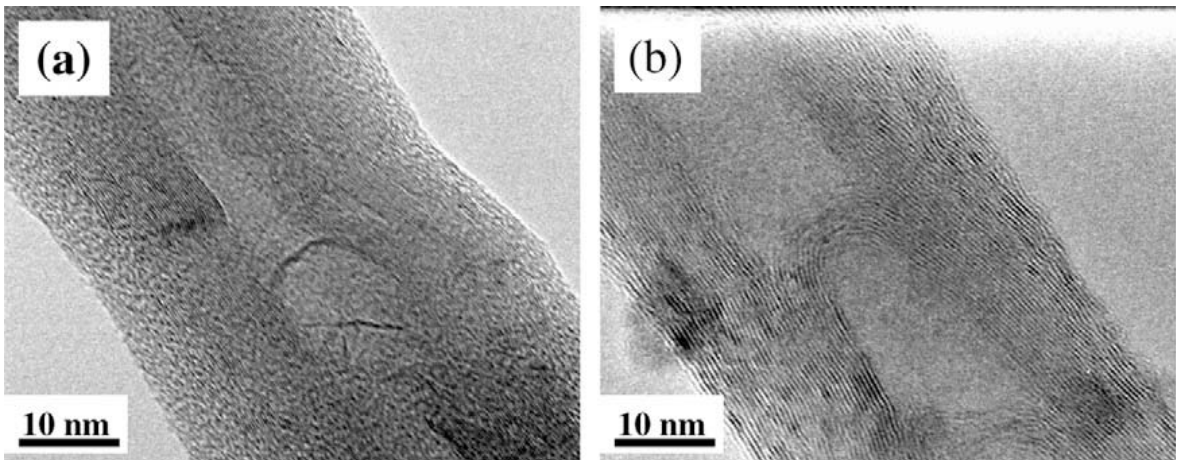


Fig. 6.3. HRTEM images of N-CNTs grown from the pyrolysis of (a) FcH/4-methylimidazole (50:50) and (b) ferrocenylmethylimidazole.

In these systems there is no flowing H_2 since the reactions are performed in sealed quartz tubes. Thus the formation of amorphous carbon is inevitable [35]. The molecules FcH and ferrocenylmethylimidazole generally give tubes which are cleaner compared to those obtained from the FcH/methylimidazole mixtures (*e.g.* the 50/50 mix) under analogous reaction conditions. Such an observation is also common for floating catalyst systems [17,36]. While the amorphous carbon and the spheres may have contained nitrogen, it is not possible to determine the nitrogen content in these materials. In contrast, CNTs that contain nitrogen can readily be detected by the bamboo morphology that is characteristic of the Fe catalysed synthesis of N-CNTs [37–39]. Thus analysis of this sub-set of products allows for an analysis of the effect of nitrogen on the CNT products generated.

6.3.2.2 Effect of FcH/imidazole ratio

The TEM images of CNTs grown from ferrocene (100%) show hollow tubes (outer diameter = 120 nm and inner diameter = 60 nm) that typically contain encapsulated iron nanoparticles (Fig.

A6.1, Appendices). The data shows that the products obtained are similar to those obtained in a typical floating catalyst flow system (except for the production of more amorphous material in the closed systems) [40].

The average outer diameters (ODs) of the multi-walled CNTs (MWCNTs) produced from ferrocenylmethylimidazole were 70 nm, whilst their average internal diameters (IDs) were 30 nm. These narrower tubes (relative to FcH) are expected [41]. Importantly, the presence of nitrogen has resulted in the expected formation of bamboo N-CNTs. Images of the bamboo morphology are shown in Fig. 6.4a.

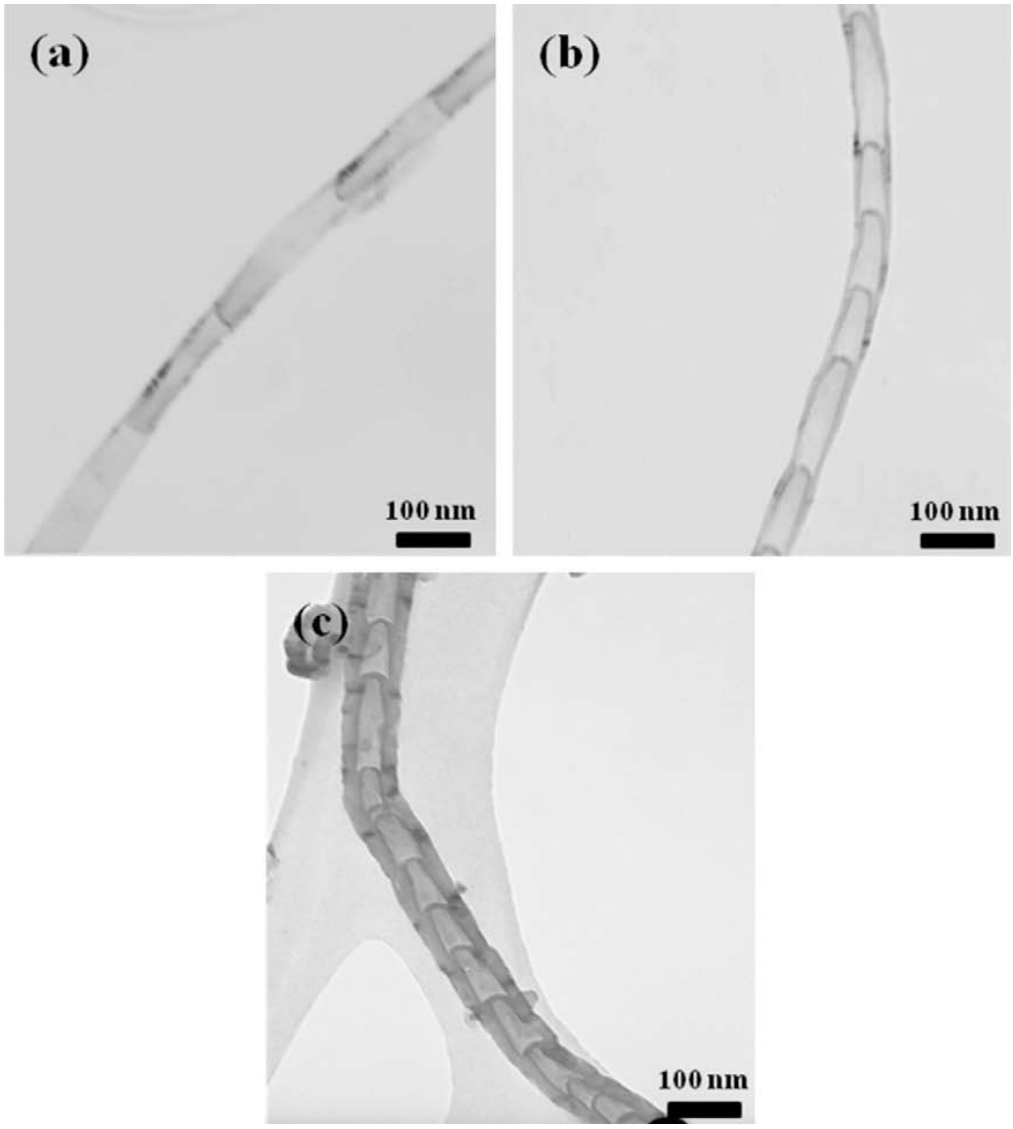


Fig. 6.4. TEM images of N-CNTs showing bamboo structures grown from the pyrolysis of (a) FcH/1-methylimidazole; (b) FcH/2-methylimidazole and (c) FcH/4-methylimidazole (50:50).

Of more interest is the impact of the mixtures of FcH and methylimidazoles on the products produced. Remarkably the position of the ring substituent impacts on both the product distribution (in particular N-CNT yield) and the product morphology (NCNT diameters) (see Table 6.1). Thus, for a FcH/i-methylimidazole (50:50) mixture the N-CNT yields decreased in

the order i =1 > 2 > 4. Further, the average tube inner and outer diameters generally became smaller, in the order i = 1 > 2 > 4. This decrease in diameter suggests a higher degree of N-doping of the CNTs (increase in N concentration) as has been suggested previously [42]. The product data for the FcH/methylimidazole mixture are most similar to the products obtained from ferrocenylmethylimidazole.

The degree of N-doping also could be calculated from the % of the CNTs that had a bamboo structure or an open structure. For example, the pyrolysis of FcH/1-methylimidazole gave a degree of doping of 15% while FcH/2-methylimidazole gave a degree of doping of 75% at a similar ratio (50:50). FcH/4-methylimidazole (50:50) and ferrocenylmethylimidazole gave higher degrees of doping (> 95%). This is consistent with the observed tube diameters as well as the bamboo compartment distances (Figs. 6.7 and 6.8).

Other FcH/i-methylimidazole ratios were also used to study the reaction (90:10; 80:20; 20:80; 10;90). The general trends noted were:
(i) The trends listed above for the 50:50 ratio hold (in general) for the other ratios.
(ii) The total yields of all products decreased with increasing imidazole content.
(iii) Increasing the Fe/C ratio results to an increase in the diameter of the CNTs. This is related to the formation of larger iron nanoparticles when a higher catalyst content is used.
(iv) These higher Fe/H ratios (0.100) favour the formation of more CNTs while at lower Fe/H ratios (0.0076) more amorphous material is generated (see Table 6.1). This is associated with the formation of more gaseous materials under a more reducing atmosphere.
(v) Most samples contained > 10% of Fe filled nanotubes.

Table 6.1. Relative % distribution of CNTs, CNFs, CNSs and a-C with the size distribution and the relative yields produced from the pyrolysis of FcH, ferrocenylmethylimidazole and FcH/*i*-methylimidazole at varying ratios.

Catalyst used to grow CNTs	Fe/H ratio	SCNMs (%)	Diameters (nm)	Yield (mg)
FcH (100%)	0.100	80T, 20a-C	120(OD), 60(ID)	78.2
Ferrocenylmethylimidazole (100%)	0.0714	50T, 20F, 30a-C	70(OD), 30(ID)	73.0
FcH/1-methylimidazole (90:10)	0.0833	40T, 60a-C	90(OD), 40(ID)	51.2
FcH/2-methylimidazole (90:10)	0.0833	30T, 5S, 65a-C	150(OD), 120(ID)	67.0
FcH/4-methylimidazole (90:10)	0.0833	30T, 5F, 65a-C	100(OD), 40(ID)	59.1
FcH/1-methylimidazole (80:20)	0.0769	45T, 5S, 50a-C	100(OD), 25(ID)	46.1
FcH/2-methylimidazole (80:20)	0.0769	45T, 5F, 55a-C	140(OD), 120(ID)	65.9
FcH/4-methylimidazole (80:20)	0.0769	35T, 15F, 50a-C	120(OD), 100(ID)	62.5
FcH/1-methylimidazole (50:50)	0.0435	50T, 10F, 40a-C	70(OD), 20(ID)	44.8
FcH/2-methylimidazole (50:50)	0.0435	30T, 10F, 60a-C	60(OD), 25(ID)	47.5
FcH/4-methylimidazole (50:50)	0.0435	5T, 35S, 60a-C	50(OD), 20(ID)	46.1
FcH/1-methylimidazole (20:80)	0.0156	70T, 20F, 10a-C	100(OD), 80(ID)	30.7
FcH/2-methylimidazole (20:80)	0.0156	80T, 10F, 10a-C	90(OD), 40(ID)	30.0
FcH/4-methylimidazole (20:80)	0.0156	10T, 5F, 85a-C	50(OD), 20(ID)	40.4
FcH/1-methylimidazole (10:90)	0.0076	30T, 30F, 40a-C	80(OD), 40(ID)	14.2
FcH/2-methylimidazole (10:90)	0.0076	10T, 40F, 50a-C	70(OD), 40(ID)	37.7
FcH/4-methylimidazole (10:90)	0.0076	5T, 45F, 50a-C	35(OD), 10(ID)	40.2

T = Tubes, F = CNFs, S = CNSs, a-C = amorphous carbon.

The products obtained from the three imidazoles are thus different in terms of yields and morphologies. This could be due to breakdown products produced in the reaction. Clearly the manner in which decomposition occurs varies with the imidazole used. The three imidazoles are structural isomers; hence, they have different physical and chemical properties. The difference in their physical properties should affect the rate and nature of their decomposition.

6.3.2.3 Analysis of the bamboo structures

In a previous study, we have quantified the N content of CNTs, using XPS and CHN analysis. In this study this is not possible due to the large amount of non-CNT products formed. However the amount of N added to a CNT can be correlated to the distance between individual bamboo compartments [17]. The larger the bamboo compartments the lower the nitrogen content of the N-CNTs produced when similar reaction conditions are used [43].

The N-CNTs produced from the FcH/i-imidazole 50:50 mixtures were analysed for their nitrogen content using the procedure described above. The distance between bamboo compartments (Fig. 6.4) was measured from TEM images (> 200 measurements per sample) for each of the imidazole samples produced. The distance between the bamboo 'caps' within a N-CNT is clearly seen to vary with the positioning of the methyl group in the imidazole (Figs. 6.5 and 6.6 and Figs. A6.2 and A6.3 (Appendices)). Tubes grown from 1-methylimidazole have a larger compartment distance (avg value = 210 nm) followed by those obtained from 2-methylimidazole (avg = 95 nm) and those obtained from 4-methylimidazole (avg = 40 nm). These results indicate that the N-CNTs produced from 4-methylimidazole have a higher N content; a result consistent with the tube diameter analysis described above.

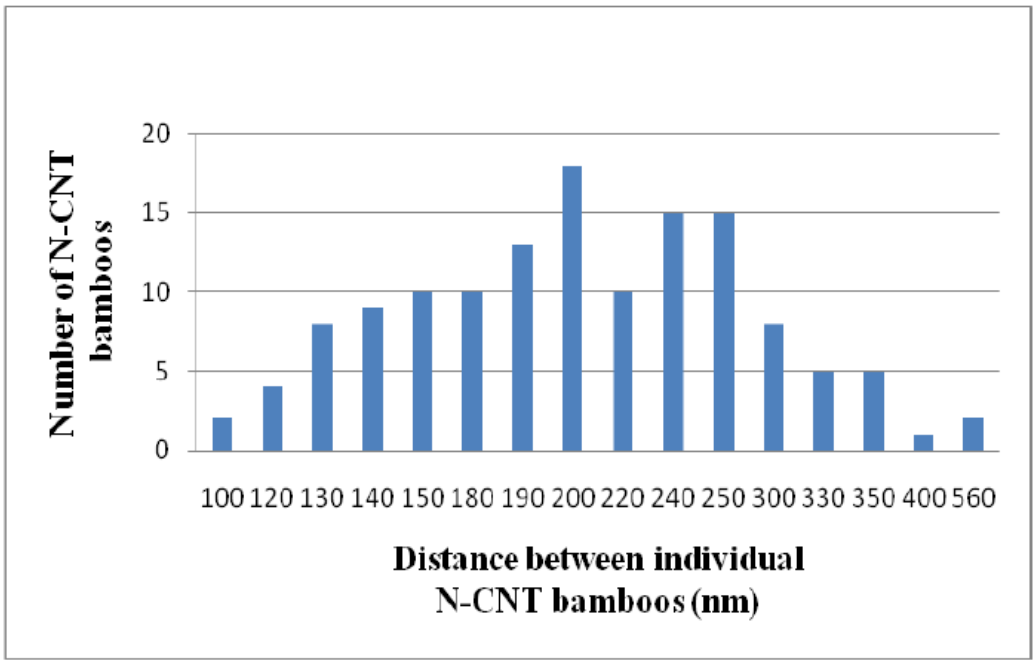


Fig. 6.5. Distance between individual bamboo compartments obtained from the pyrolysis of 1-methylimidazole (50:50).

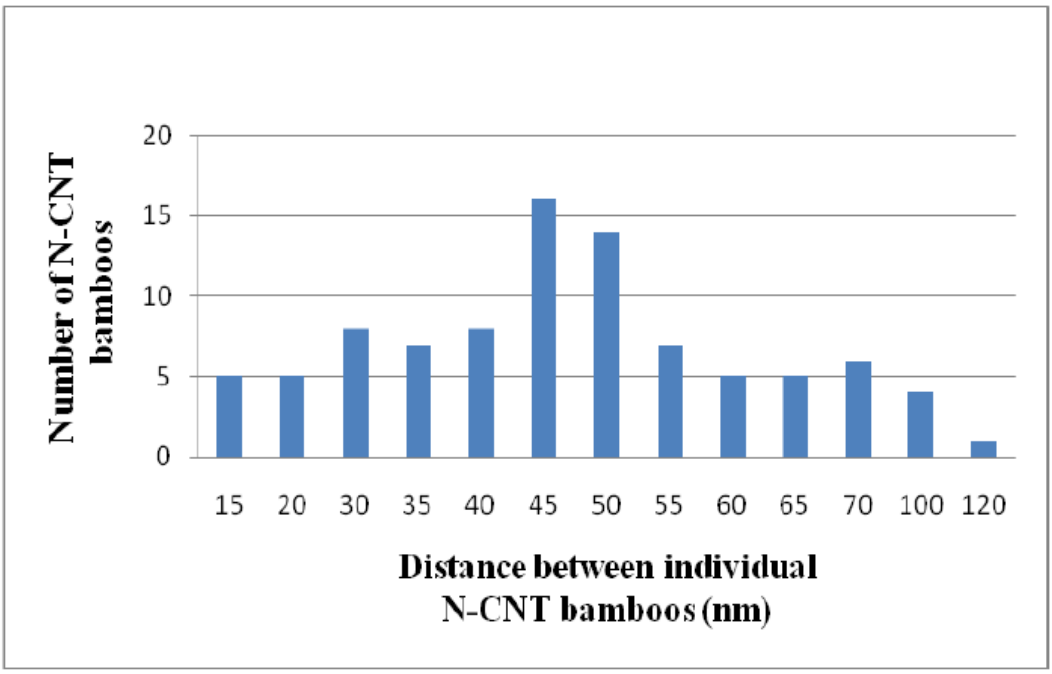


Fig. 6.6. Distance between individual bamboo compartments obtained from the pyrolysis of ferrocenylimidazole.

The average distance between individual bamboo compartments obtained from the pyrolysis of ferrocenylmethylimidazole was found to be 45 nm, close to the N-CNT values obtained from 4-methylimidazole (Fig. 6.6). High N values are expected for the CNTs produced from ferrocenylmethylimidazole due to the proximity of N group to the Fe catalyst in the reaction [14].

6.3.3 TGA analysis

Thermogravimetric analysis (TGA) of nanotubes under O_2 is a useful technique for studying the thermal stability of carbonaceous samples. The shape of the TGA curve can give information about the presence of carbon by-products, such as amorphous carbon [44,45].

All samples prepared in this study showed similar oxidation behaviour in TGA experiments and typical TGA profiles are shown in Fig. 6.7. A slight weight loss at ~ 200 ^{o}C is due to the loss of water and organic volatiles. Decomposition of the CNTs was observed from 450 to 610 ^{o}C. Generally, this accounts for most of the weight loss (60%). It has been observed that the N-CNTs are generally less stable than the undoped CNTs (prepared from FcH) and hence should decompose at lower temperatures [46]. This is reportedly caused by the presence of a higher defect content in their walls [47]. Most of the tubes have 5 – 20% residual weight after oxidation (Fig. 6.7). This is attributed to the metal residue (FeOx) that remains after carbon has been oxidized. This residual weight varies with the amount of FcH used in the synthesis of the CNTs (Table 6.1) [48,49]. Of note is the slight weight gain around 400 ^{o}C, due to oxidation of the residual Fe catalyst trapped in the tubes.

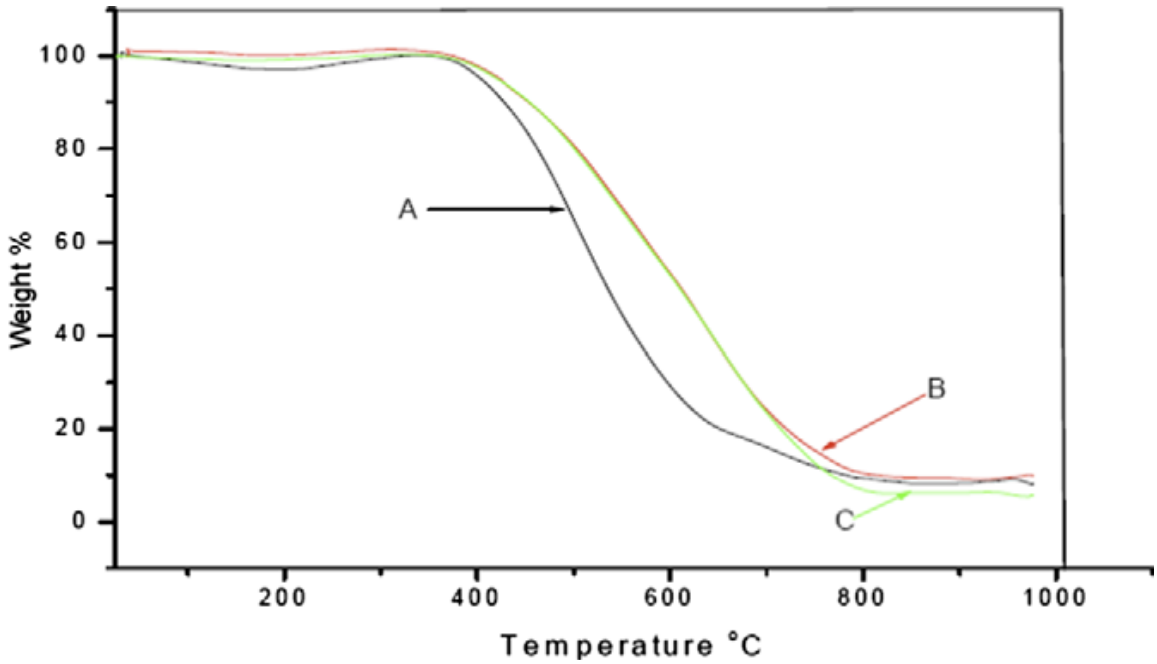


Fig. 6.7. TGA curves of CNTs grown from (A) FcH/1-methylimidazole (10:90); (B) FcH/2-methylimidazole (10:90) and (C) FcH/4-methylimidazole (10:90).

6.3.4 Raman analysis

Raman spectroscopy was used to obtain information about disorder in the carbon materials. For most spectra, three peaks are observed: a peak around 1350 cm^{-1} (the D-band), a peak around 1580 cm^{-1} (the G-band) and a small shoulder at around 1615 cm^{-1}. The Raman D-band is associated with disorder and is a manifestation of an in plane vibrational mode. The G-band originates from the symmetric vibrations of the Raman active E2g mode [50]. The small shoulder at around 1615 cm^{-1} is also induced by disorder.

The intensity ratio (I_D/I_G) indicates the degree of disorder of the SCNMs. When samples are compared the I_D/I_G ratio can establish which sample contains the most graphitic (most ordered) structure. Disorder can arise from the range of structures produced as well as the degree of N-

doping of the CNTs. The ratios are displayed in the Appendices (Table A6.1). Fig. 6.8 shows the Raman spectra for samples grown at a similar reactant ratio (50:50). Generally, a dramatic broadening of the D- and G-band is seen in these crude samples (compared with the undoped CNT) [43]. Further, the I_D/I_G ratio of the samples varied with the FcH/imidazole ratio. This observation can be correlated to the products obtained from the three different imidazole isomers. It appears that, in general (and as expected), reactions with 4-methylimidazole give the largest I_D/I_G ratios.

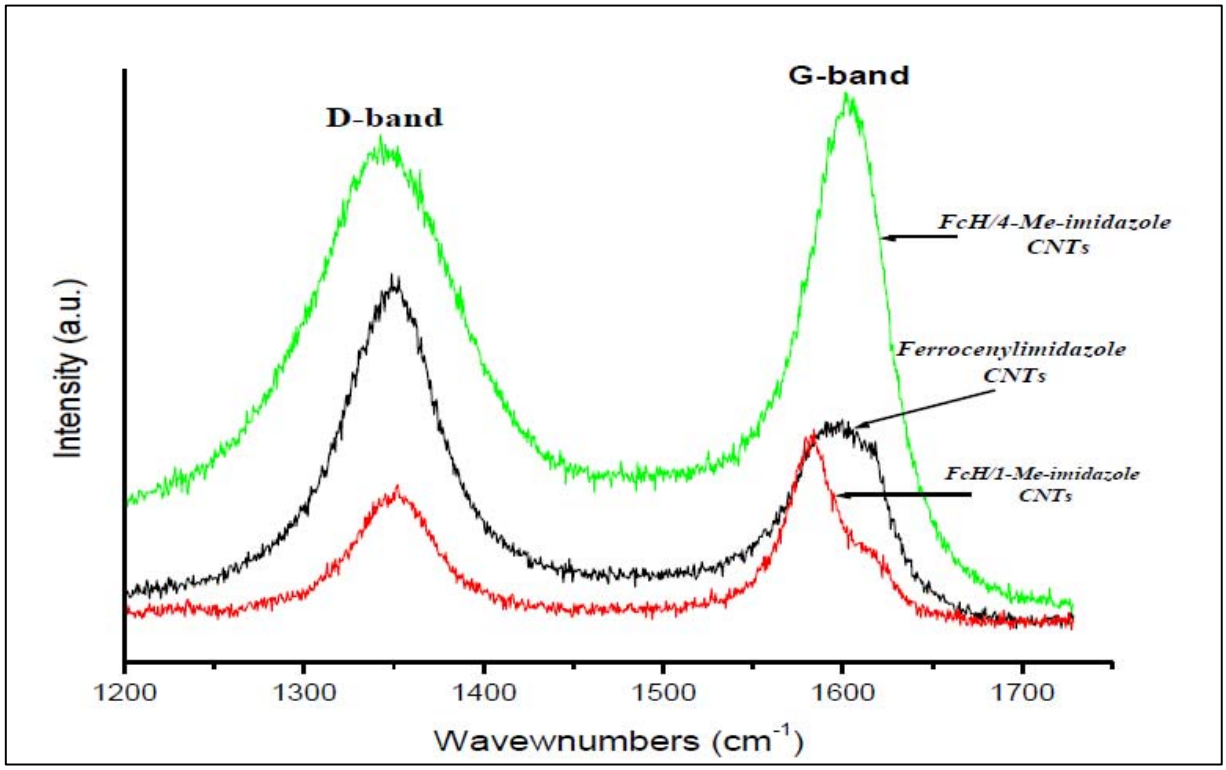


Fig. 6.8. Raman spectra of CNTs grown from ferrocenylmethylimidazole, FcH/1-methylimidazole (50:50) and FcH/4-methylimidazole (50:50).

6.3.5 Mechanism

A mechanism that leads to the formation of N-CNTs with different morphologies generated from the pyrolysis of imidazole isomers can be proposed (Fig. 6.9). When heated to elevated temperatures, imidazoles decompose to form radicals, ions and molecular species (Fig. 6.9, step 1). Under suitable conditions these decomposition products will break down further to C and N atoms (step 2), which then interact with Fe nanoparticles to form N-CNTs and other carbon species *via* the classical CNT growth mechanism [34].

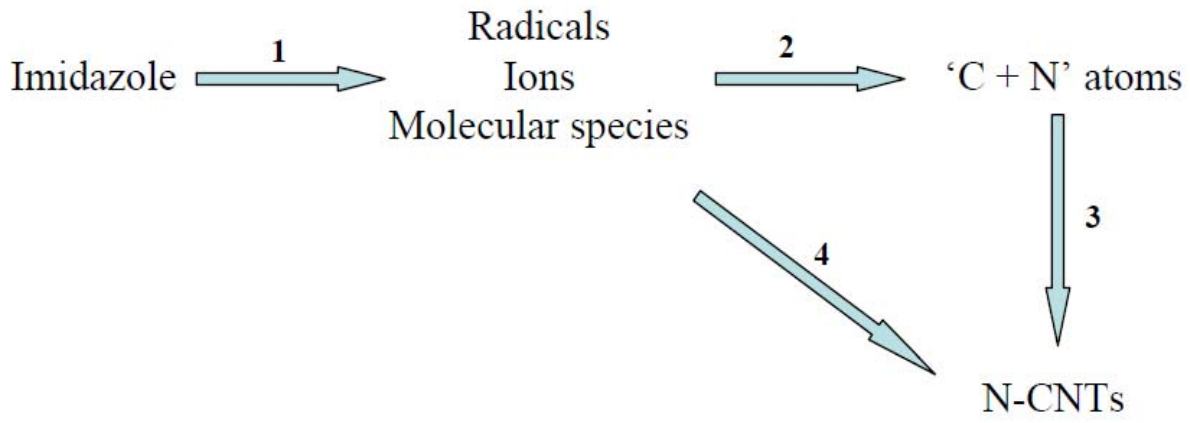


Fig. 6.9. A model for the formation of N-CNTs from the methylimidazole decomposition.

The mechanism above does not however fully account for the different products and product ratios that are formed from the different imidazole isomers and that could lead to the different product yields and morphologies. The three imidazole isomers decompose to give different breakdown products. This is associated with the different physical and chemical properties and different methyl group and C=N positions in the different isomers and that lead to the formation of the different decomposition products. This suggests that the radicals, ions and molecular

species formed can interact directly with the Fe nanoparticles (step 4). Presumably these radicals, ions and molecular species then decompose to C and N atoms that eventually lead to the N-CNT growth. This would suggest control (*via* the breakdown products) of CNT morphology by chemical procedures is possible. This proposal indicates that CNT growth can be controlled by the choice of reactants, as has been suggested by others [14,33]. Thus a key finding from our experiments is that control of species formed in the reaction can be controlled by the chemical nature of the reactants. Experiments to further probe the above proposal are currently underway.

6.4. Conclusion

A method for the N-doping of CNTs based on the pyrolysis of ferrocenes and imidazoles in a confined environment has been described. We have shown that the position of the methyl group attached to the imidazole can influence the size distribution and the type of SCNMs produced in the 'autoclave' system. An analysis of the SCNMs and the bamboos structures reveals that the three structural isomers of methylimidazoles lead to different products; in particular with N-CNTs that contain different amounts of N as determined by measurements of bamboo compartments and tube diameters. The results show that the control of N-CNTs is determined by fragments produced by decomposition of reactants at high temperature.

References

1. S. Iijima, Nature 354 (1991) 56.

2. (a) A. Govindaraj, C.N.R. Rao, Pure Appl. Chem. 74 (2002) 1571;

(b) R. Sen, A. Govindaraj, C.N.R. Rao, Chem. Phys. Lett. 267 (1997) 276;

(c) C.N.R. Rao, R. Sen, B.C. Satishkumar, A. Govindaraj, Chem. Commun. (1998) 1525.

3. (a) R. Andrews, D. Jacques, A.M. Rao, F. Derbyshire, D. Qian, X. Fan, E.C. Dickey, J. Chen, Chem. Phys. Lett. 303 (1999) 467;

(b) R. Kamalakaran, M. Terrones, T. Seeger, P. Kohler-Redlich, M. Ruhle, Y.A. Kim, M. Endo, Appl. Phys. Lett. 77 (2002) 3385;

(c) A. Cao, L. Ci, G. Wu, B. Wei, C. Xu, J. Liang, D. Wu, Carbon 39 (2001) 152;

(d) E.C. Dickey, C.A. Grimes, M.K. Jain, K.G. Ong, D. Qian, P.D. Kichambare, R. Andrews, D. Jacques, Appl. Phys. Lett. 79 (2001) 4022;

(e) M. Mayne, N. Grobert, M. Terrones, R. Kamalakaran, M. Ruhle, H.W. Krato, D.R.M. Walton, Chem. Phys. Lett. 338 (2001) 101.

4. (a) F. Rohmund, L.K.L. Falk, E.E.B. Campell, Chem. Phys. Lett. 328 (2000) 369;

(b) X.Y. Liu, B.C. Huang, N.J. Coville, Carbon 40 (2002) 2791.

5. (a) S. Amelinckx, X.B. Zhang, D. Bernaerts, X.F. Zhang, V. Ivanov, J.B. Nagy, Science 265 (1994) 635;

(b) M. Zhang, Y. Nakayama, L. Pan Japan, J. Appl. Phys. 39 (2000) L1242;

(c) L. Pan, T. Hayashida, Y. Nakayama, J. Mater. Res. 17 (2001) 45;

(d) C. Kuzuya, W. Hwang, S. Hirako, Y. Hishikawa, S. Motojima, Chem. Vapor Deposition 8 (2002) 57;

(e) V.K. Varadan, J. Xie, Smart Mater. Struct. 11 (2002) 728.

6. (a) X. Zhang, A. Cao, B. Wei, Y. Li, J. Wei, C. Xu, D. Wu, Chem. Phys. Lett. 362 (2002) 285;

(b) C. Singh, M. Schaffer, I. Kinloch, Physica B 323 (2002) 339;

(c) B. Wei, R. Vajtai, Y.Y. Choi, P.M. Ajayan, Nano Lett. 2 (2002) 1105;

(d) C. Singh, M.S.P. Schaffer, A. H Windle, Carbon 41 (2003) 59.

7. C. Singh, T. Quest, C.B. Boothroyd, P. Thomas, I.A. Kinloch, A.I. Abou-Kandil, A.H. Windle, J. Phys. Chem. B 106 (2002) 10915.

8. C.N.R. Rao, A. Govindaraj, Acc. Chem. Res. 35 (2002) 998.

9. (a) V.O. Nyamori, N.J. Coville, Organomet. 26 (2007) 4083;

(b) M.S. Mohlala, X.-Y. Liu, J.M. Robinson, N.J. Coville, Organomet. 24 (2005) 972;

(c) J. Cheng, X.P. Zou, G. Zhu, M.F. Wang, Y. Su, G.Q. Yang, X.M. Lu, Solid State Commun. 149 (2009) 1619.

10. S. Bai, F. Li, Q-H. Yang, H-M. Cheng, J-B. Bai, Chem. Phys. Lett. 376 (2003) 83.

11. (a) M. Terrones, P.M. Ajayan, F. Banhart, X. Blase, D.L. Carroll, J.C. Charlier, *et al*., Appl. Phys. A 74 (2002) 355;

(b) P. Redlich, J. Loeffler, P.M. Ajayan, J. Bill, F. Aldinger, M. Ruhle, Chem. Phys. Lett. 260 (1996) 465;

c) Z. Weng-Sieh, K. Cherrey, N.G. Chopra, X. Blase, *et al*., Phys Rev. 51 (1995) 11229.

12. J.W. Jang, C.E. Lee, S.C. Lyu, T.J. Lee, C.J. Lee, Appl. Phys. Lett. 84 (2004) 2877.

13. C.H. Lin, H.L. Chang, C.M. Hsu, A.Y. Lo, C.T. Kuo, Diamond Relat. Mater. 12 (2003) 1851.

14. M. Jung, K.Y. Eun, J.-K. Lee, Y.-J. Baik, K.-R. Lee, J.W. Park, Diamond Relat. Mater. 10 (2001) 1235.

15. L.M. Cao, X.Y. Zhang, C.X. Gao, W.K. Wang, Z.L. Zhang, Z. Zhang, Nanotechnology 14 (2003) 931.

16. (a) R. Sen, B.C. Satishkumar, A. Govindaraj, K.R. Harikumar, M.K. Renganathan, C.N.R Rao, J. Mater. Chem. 7 (1997) 2335;

(b) R. Sen, B.C. Satishkumar, A. Govindaraj, K.R. Harikumar, G. Raina, J.-P. Zhang, A.K. Cheetham, C.N. R Rao, Chem. Phys. Lett. 287 (1998) 671;

(c) M. Nath, B.C. Satishkumar, A. Govindaraj, C.P. Vinod, C.N.R. Rao, Chem. Phys. Lett. 322 (2000) 333;

(d) L.S. Panchakarla, A. Govindaraj, C.N.R. Rao, ACS Nano 1 (2007) 494.

17. (a) E.N. Nxumalo, V.O. Nyamori, N.J. Coville, J. Organomet. Chem. 693 (2008) 2942;

(b) T.-Y. Kim, K.-R. Lee, K.Y. Eun, K.-H. Oh, Chem. Phys. Lett. 372 (2003) 603.

18. C.J. Lee, S.C. Lyu, H.-W. Kim, J.H. Lee, K.L. Cho, Chem. Phys. Lett. 359 (2002) 115.

19. (a) N.H. Quang, M.V. Trinh, B.-H. Lee, J.-S. Huh, Sens. Actuators, B 113 (2006) 341;

(b) C. Tang, Y. Bando, T. Sato, Chem. Phys. Lett. 362 (2002) 185.

20. Y. Chai, Q.F. Zhang, J.L. Wu, Carbon 44 (2006) 687.

21. Y.-L. Li, F. Hou, Z.-T. Yang, J.-M. Feng, X.-H. Zhong, J.-Y. Li, Mater. Sci. Eng., B 158

(2009) 69.

22. L.C. Qin, X. Zhao, K. Hirahara, Y. Miyamoto, Y. Ando, S. Iijima, Nature 408 (2000) 50.

23. R. Chetty, S. Kundu, W. Xia, M. Brona, W. Schuhmann, V. Chirila, W. Brandl, T. Reinecke, M. Muhler, Electrochim. Acta 54 (2009) 4208.

24. P.E. Diaz-Flores, F. Lopez-Urı´as, M. Terrones, J.R. Rangel-Mendez, J. Colloid Interf. Sci. 334 (2009) 124.

25. D.-P. Kim, C.L. Lim, T. Mihalisin, P. Heiney, M.M. Labes, Chem. Mater. 3 (1991) 686.

26. K.-Y. Chun, H.S. Lee, C.J. Lee, Carbon 47 (2009) 169.

27. B. Wang, Y. Ma, Y. Wu, N. Li, Y. Huang, Y. Chen, Carbon 47 (2009) 2112.

28. V. Krstic´, G.L.J.A. Rikken, P. Bernier, S. Roth, M. Glerup, Europhys. Lett. 77 (2007) 37001.

29. (a) V.G. Pol, S.V. Pol, J.M.C. Moreno, A. Gedanken, Carbon 44 (2006) 3285;

(b) C.P. Ewels, M. Glerup, J. Nanosci. Nanotechnol. 5 (2005) 1345.

30. T. Cheng, Z. Fang, G. Zou, Q. Hu, B. Hu, X. Yang, Y. Zhang, Bull. Mater. Sci. 29 (2006) 701.

31. J. Zhang, J. Li, J. Cao, Y. Qian, Mater. Lett. 62 (2008) 1839.

32. A.A. Simenel, E.A. Morozova, Y.V. Kuzmenko, L.V. Snegur, J. Organomet. Chem. 665 (2003) 13.

33. (a) P.T.A. Reilly, W.B. Whitten, Carbon 44 (2006) 1653;

(b) E.G. Wang, Z.G. Guo, J. Ma, M.M. Zhou, Y.K. Pu, S. Liu, G.Y. Zhang, D.Y. Zhong, Carbon 41 (2003) 1827.

34. (a) T. Watanabe, T. Notoya, T. Ishigaki, H. Kuwano, H. Tanaka, Y. Moriyoshi, Thin Solid Films 506–507 (2006) 263;

(b) Y. Shiratori, H. Hiraoka, M. Yamamoto, Mater. Chem. Phys. 87 (2004) 31.

35. (a) N. Sano, H. Akazawa, T. Kikuchi, T. Kanki, Carbon 41 (2003) 2159;

(b) W. Wasel, K. Kuwana, P.T.A. Reilly, K. Saito, Carbon 45 (2007) 833.

36. V.O. Nyamori, E.N. Nxumalo, N.J. Coville, J. Organomet. Chem. 694 (2009) 2222.

37. R. Andrew, D. Jacque, A. Rao, F. Derbyshire, D. Qian, X. Fan, E. Dickey, J. Chen. Chem. Phys. Lett. 303 (1999) 467.

38. C. Lee, C. Luy, W. Kin, H. Lee, I. Cho, Chem. Phys. Lett. 359 (2002) 115.

39. C. Tang, B. Yoshio, D. Golbert, F. Xu, Carbon 42 (2004) 2625.

40. Y.-Y. Fan, A. Kaufmann, A. Mukasyan, A. Varma, Carbon 14 (2006) 2160.

41. X.Y. Tao, X.B. Zhang, F.Y. Sun, J.P. Cheng, F. Liu, Z.Q. Luo, Diamond Relat. Mater. 16 (2007) 425.

42. F. Villalpando-Paez, A. Zamudio, A.L. Elias, H. Son, E.B. Barros, *et al*., Chem. Phys. Lett. 424 (2006) 345.

43. S. Maldonado, S. Morin, K.J. Stevenson, Carbon 44 (2006) 1429.

44. A.M.F. Lima, A.W. Musumeci, H.-W. Liu, E.R. Waclawik, G.G. Silva, J. Therm. Anal. Calorim. 97 (2009) 257.

45. D. Bom, R. Andrews, D. Jacques, J. Anthony, B. Chen, M.S. Meier, J.P. Selegue, Nano Lett. 2 (2002) 615.

46. G. Kudashov, V. Okotrub, G. Bulusheva, P. Asanov, V. Shubin, F. Yudanov, L. Yadanova, S. Danilovich, G. Abrosimor, J. Phys. Chem. B 108 (2004) 9048.

47. F. Villalpando-Paez, A. Zamudio, A.L. Elias, H. Son, E.B. Barros, *et al*., Chem. Phys. Lett. 424 (2006) 345.

48. M. Laskoski, T.M. Keller, S.B. Qadri, Carbon 45 (2007) 443.

49. T.M. Keller, S.B. Qadri, Chem. Mater. 16 (2004) 1091.

50. J. Kaufman, S. Melin, Phys. Rev. B: Condens. Matter 39 (1989) 13053.

Chapter 7

[5]The influence of nitrogen sources on nitrogen doped multi-walled carbon nanotubes

7.1 Introduction

The synthesis and characterization of nitrogen doped carbon nanotubes (N-CNTs) have been extensively investigated over the last decade [1-2]. This is due to the enhancement in particular of the electronic structure of carbon nanotubes (CNTs) upon the insertion of N into the CNT lattice [3-4]. N-doping has been proven to be a feasible strategy to tailor the electronic properties of CNTs in a well defined manner [5-6].

Several workers have reported on the growth of N-CNTs using chemical vapour deposition (CVD) approaches. This is demonstrated by the considerable number of literature reviews that exist in this field [7-10]. Investigations indicate that N incorporation into CNTs strongly depends on the synthesis conditions used, such as the precursor, catalyst, reaction temperature as well as the gas flow rate. Several nitrogen containing reagents have been used to make N-CNTs [11-20].

[5] E.N. Nxumalo, P.J. Letsoala, L.M. Cele, N.J. Coville, *J. Organomet. Chem.* 695 (2010), 2596

Floating catalyst CVD methods are normally preferred for these reactions and ferrocene and $Fe(CO)_5$ have been usually employed as catalysts [12,21-22]. The choice of the catalyst and N source are highly dependent on ease of use, availability, cost and volatility.

It is now well known that N-CNTs demonstrate characteristic morphological features normally referred to as compartmentalized bamboo structures [23-25]. Indeed, doping with N also leads to more disorder in a tube through an increase in the number of defects created [26]. Furthermore, the number of walls in a CNT decreases when N is incorporated into CNTs. However, the correlation between the morphology and the type of N source used is not fully understood. Reports reveal that the pyrolysis of a carbon source and a nitrogen source in the CVD reactor (under appropriate experimental conditions) leads to the formation of N-CNTs. While the role of different types of carbon sources has been investigated, the role of the source and type of N has not been described.

To explore the role of using different N types and sources we report here a *systematic study* of N-CNTs, synthesized with a wide range of N containing reactants using a range of reagent concentrations (1 – 8%) to evaluate the effect of the N source and concentration on the new N-CNT materials. The range of nitrogen containing complexes studied includes amines and amides attached to a range of carbon functionalities (*i.e*. alkyl groups, aryl groups, *etc*.).

7.2 Experimental

7.2.1 Synthesis of doped carbon nanotubes

Carbon nanotubes were synthesized using the experimental setup shown in Fig. A7.1 (Appendices). In a typical synthesis, approximately 2.0 g of ferrocene ($Fe(C_5H_5)_2$), was dissolved in a mixture of 50 ml of a nitrogen containing hydrocarbon and toluene. The solution, nebulized

using a 1.45 MHz oscillator, was carried into a 25 mm diameter quartz tube, placed in a furnace which was maintained at a temperature of 850 ^{o}C. The average droplet size for the solvents is ~ 2.2 μm at 1.54 MHz frequency [27]. The nitrogen containing hydrocarbons (diethylamine, butylamine, iso-propylamine, benzylamine, *N*-benzylmethylamine, aniline, 1-methylpiperazine, hexamethylenediamine, trimethylenediamine, *N*-methylenediamine pyridine, quinoline, formamide, *N*,*N*dimethylformamide, *N*,*N*-dimethylacetamide) were used as purchased (Sigma Aldrich and Fluka) and studied at concentrations of 1%, 2%, 4%, 6% and 8% in toluene. Ultra pure argon and hydrogen gases purchased at Afrox were used as the carrier gases and the gas flow rate was controlled using unit mass flow controllers.

In a typical procedure, the carrier gas flow rate was kept at 400 sccm (argon) and 100 sccm (hydrogen) respectively. The pyrolysis was carried out for 45 min. After the reaction, the argon flow rate was reduced to between 50 – 60 sccm whilst the flow rate of hydrogen was switched off. The furnace was then allowed to cool to room temperature. The products were collected after the reaction tube has cooled to room temperature. The yields were determined by scraping the products from the reactor and weighing. Errors of < 10% can be expected in the yields, and trends are readily detected in the series of reactions performed.

7.2.2 Carbon nanotube analysis

Transmission electron microscopy (TEM) was performed on a JEM – 100S TEM instrument operating at 80 keV. Sample preparation for TEM studies involved sonicating approximately 0.09 g of sample in 10 cm^3 of methanol for approximately 10 min. A few drops of the resulting suspension were placed on a holey carbon TEM grid, after which TEM images were recorded. A scanning electron microscope (SEM) (JOEL- JSM-5600 operated at 15 keV) was used to observe the morphology of the carbon nanotube arrays and to measure the average MWCNT length that was determined from the thickness of the nanotube arrays. The thermogravimetric analysis

(TGA) was performed using a Perkin Elmer Pyris Thermogravimetric Analyzer 1 TGA under air at a flow rate of 25 ml/min. The samples were ramped from room temperature to 800 ^{o}C at a heating rate of 10 ^{o}C/min for the dynamic analysis. The sample weight used was approximately 5 mg. The laser Raman spectra were obtained from a Jobin Yvon T6400 laser Raman spectrometer operated in single spectrograph mode with a 600 line/nm grating. The 514.5 nm line of an argon ion laser was used as an excitation source. The laser power of the sample was kept at 1.2 mW or less to minimize local heating. Spectra were collected using a liquid nitrogen-cooled CCD detector (accumulation time varied from 120 to 180 sec).

7.2.3 Acid washing of the N-CNTs

Reaction of the nanotube samples (about 50 mg) with concentrated nitric acid (5 ml) was accomplished by placing the samples in a closed vessel inside a microwave oven (CEM Microwave Technology). An oven power of 100 W was used for 30 min. Carbon nanotubes prepared from the pyrolysis of toluene and ferrocene and from the pyrolysis of toluene and ferrocene in the presence of diethylamine (1%, 8%), quinoline (8%), hexamethylenediamine (1%) and *N*,*N*-dimethylacetamide (1%, 8%) were studied. After microwave treatment, the mixtures were washed with de-ionized water. The purified carbon nanotubes were then dried in a thermal oven at temperatures of about 100 ^{o}C. The morphologies of the purified N-CNTs were characterized by SEM, TEM, TGA and Raman spectroscopy.

7.3 Results and discussion

7.3.1 N-CNT yields

N-doped carbon nanotubes were synthesized by nebulized spray pyrolysis using approximately 2.0 g of ferrocene dissolved in 50 ml of toluene and nitrogen containing organic compounds at

concentrations of 1%, 2%, 4%, 6% and 8%. Standard reaction conditions were chosen so that a comparison of the effect of the different nitrogen donors on the yield and morphology of the CNTs could be made. The yield of carbon nanotubes synthesized in toluene without the addition of nitrogen containing organic compounds (0.70 g) provided a standard to evaluate the effect of the nitrogen on the reaction. The yield of CNTs obtained using the different reactants are given in Table 7.1. In addition, two graphical examples of the yield data are shown in Fig. 7.1. (see Appendices (Fig. 7.2 (a – d)) for other examples) which enables the data to be readily visualized.

Table 7.1. Yield of CNTs obtained from pyrolysis of toluene and ferrocene in the presence of various N containing reagents at different concentrations.[1]

Reagent	Mass (g)				
	1%	**2%**	**4%**	**6%**	**8%**
Diethylamine	1.26	1.02	0.89	0.56	0.58
Butylamine	1.28	0.69	0.58	0.61	0.53
Isopropylamine	0.97	0.83	0.55	0.56	0.36
Benzylamine	1.47	1.29	0.94	0.93	0.85
Pyridine	1.67	0.46	0.43	0.43	0.23
Aniline	-	1.09	0.88	0.87	0.81
Quinoline	1.86	1.19	1.28	0.76	0.69
N-benzylmethylamine	0.99	1.27	0.74	0.75	0.63
1-methylpiperazine	1.37	1.10	0.74	0.57	0.42
Hexamethylenediamine	1.07	1.23	1.15	1.32	-
N-methylethylenediamine	1.07	0.74	0.61	0.72	0.33
Trimethylenediamine	1.52	1.16	1.11	0.65	0.53
Formamide	1.53	1.07	0.95	0.68	0.99
N,*N*-dimethylformamide	1.82	0.97	0.57	0.52	0.49
N,*N*-dimethylacetamide	0.94	0.88	0.75	0.46	0.35

[1] Ferrocene/toluene with no added N containing reagent; yield = 0.70 g

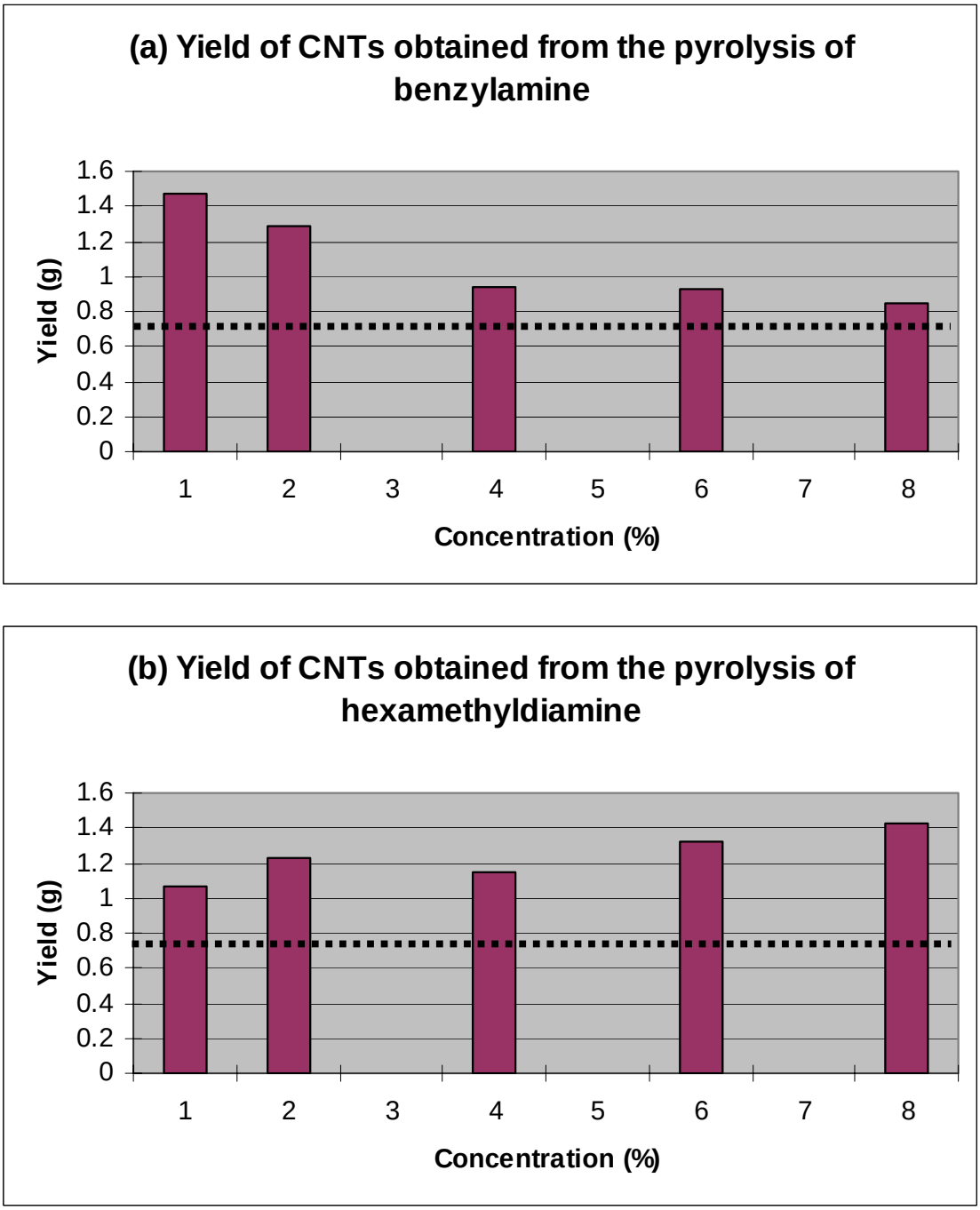


Fig. 7.1. Graphical representation of CNT yields grown from (a) benzylamine; and (b) hexamethylenediamine. Horizontal dotted line indicates yield of CNTs obtained from ferrocene/toluene.

An initial increase in mass relative to ferrocene/toluene (0.70 g) reagents is observed *in every case* when 1% of nitrogen containing hydrocarbons was added during the synthesis of the CNTs. The effect of increasing the concentration of the nitrogen containing reagent however varies with the reagent. Observations derived from information contained in Table 7.1 are listed below:

(i) For the amines (diethylamine, isopropylamine, butylamine, benzylamine) the yield of carbon nanotubes generally decreases with increase in amine concentration eventually producing yields close to or below that of the reaction containing only ferrocene (Fig. 7.1, Table 7.1).
(ii) Similar results were found for the aromatic reagents (pyridine, quinoline) and the amides.
(iii) While small amounts of pyridine and quinoline (N embedded in the aromatic ring) give very high yields of products at low concentrations, the effect falls off with increased concentration.
(iv) In general, at *high reagent concentrations* if the N is in the ring (quinoline, pyridine) yields are lower than if the N is external to an aromatic ring (aniline, benzylamine).
(v) Addition of methyl groups to a carbon chain appears to give reduced CNT yields at 1% reagent addition (compare butylamine and isopropylamine; dimethylformamide and dimethylacetamide; benzylamine with *N*-benzylmethylamine). This result is consistent with the reduced yields formed when Fe alone was used *i.e.* as the C/N ratio increases the yield decreases.
(vi) Butylamine and diethylamine that have the same molecular mass, but different structures, give very similar results.
(vii) The one anomalous result relates to the use of the hexamethylenediamine (Fig. 7.1) where a steady increase in yield was observed with increase in reagent content. This could relate either to the coordination ability of the amine or to the chain length linking the two amine moieties.

Samples sent for CHN analysis indicated an N content of < 0.5% N even when the highest concentrations of N containing reagents were used (8% amine). This is consistent with recently reported data for toluene/ferrocene/benzylamine mixtures [28]. It was not possible to quantify the N content of the CNTs by X-ray photoelectron spectroscopy.

In summary: with the exception of hexamethylenediamine, all the samples showed similar trends. This indicated that the source of the N is not as significant as the content of N in the reagent used to make the N-CNTs.

7.3.1.1 N-CNT morphology: SEM analysis

Information on the N-CNT lengths (Table 7.2) was obtained from SEM images and examples of the N-CNTs produced are shown in Fig. 7.2. The figure shows SEM micrographs of the CNTs grown by the pyrolysis of toluene and ferrocene in the presence of 2%, 4%, 6% and 8% formamide. All other N-CNTs synthesized in this study showed the same morphological features (data not shown).

Some general comments can be made from the results obtained from the range of reactants performed.

(i) The average length of carbon nanotubes obtained from the pyrolysis of ferrocene and toluene are 130 μm. This data provided a basis for comparison.

(ii) The N-CNTs grown are aligned [29-30]. The synthesized nanotubes have uniform lengths, but the lengths vary depending on the N source.

(iii) The images reveal that the CNTs are not all straight.

(iv) The average lengths of all synthesized nanotubes after addition of 1% of nitrogen containing hydrocarbons are *longer* that those synthesized using toluene and ferrocene (Table 7.2). They are also better aligned and more even in distribution. This is to be contrasted with a recent study using benzylamine to produce N-CNTs [28]. As noted in our study, an increase in the nitrogen source decreases the CNT length and the study by Koos *et al.* reveals that if the benzylamine concentration is increased further, the tubes become even shorter. The two studies thus complement each other.

(v) The lengths shorten with increased reagent concentration. Fig. 7.3 shows a graphical representation of the data for benzylamine and hexamethylenediamine (see also Figs. A7.5 and A7.6 (Appendices) for other N containing reagents).

(vi) Growth rates of the CNTs were calculated from the lengths of the carbon nanotubes made after 45 min. While the ferrocene/toluene mixture gave a growth rate of 2.88 μm/min the growth rate when 1% nitrogen containing mixtures were used varied between 6.47 – 6.91 μm/min.

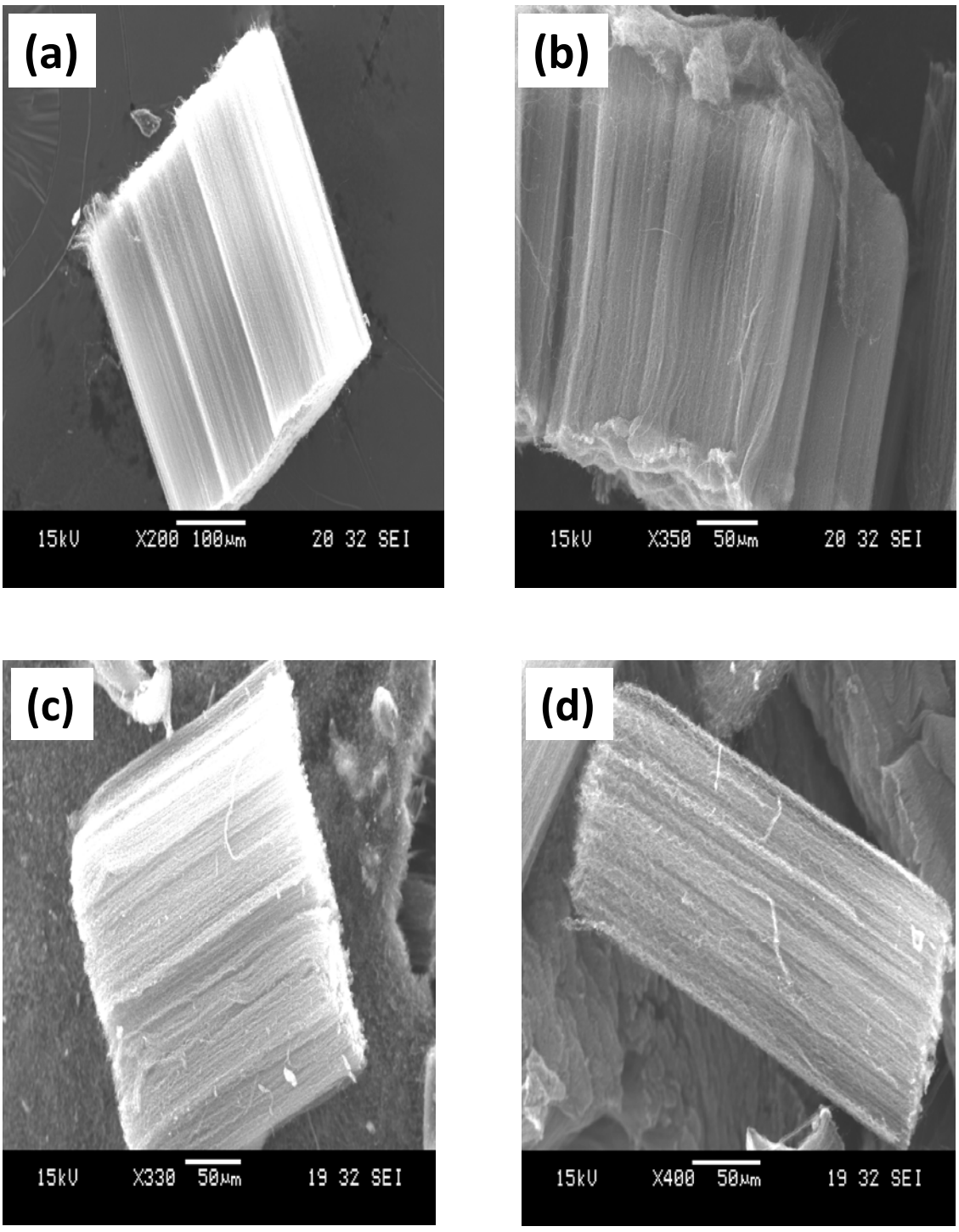


Fig. 7.2. SEM micrographs of CNT obtained from the pyrolysis of toluene and ferrocene in the presence of (a) 2%; (b) 4%; (c) 6%; and (d) 8% formamide.

Table 7.2. Average diameters and length of CNT obtained from the pyrolysis of toluene and ferrocene in the presence of various N containing reagents.

Reagent		1%	2%	4%	6%	8%
Diethylamine	length (μm)	393	300	241	270	184
	diameter (nm)	58	88	49	68	54
Butylamine	length (μm)	444	182	172	65	111
	diameter (nm)	78	65	73	63	61
Isopropylamine	Length (μm)	338	104	200	212	113
	diameter (nm)	71	86	85	68	78
Pyridine	length (μm)	393	237	175	137	111
	diameter (nm)	54	67	48	43	37
Benzylamine	length (μm)	518	333	245	184	226
	diameter (nm)	66	89	100	98	85
Aniline	length (μm)	393	325	209	205	270
	diameter (nm)	72	107	121	90	70
N-Benzylmethylamine	length (μm)	240	350	423	400	294
	diameter (nm)	73	90	88	86	84
Quinoline	length (μm)	229	306	450	278	290
	Diameter (nm)	59	95	63	52	62
1-Methylpiperazine	length (μm)	154	182	80	96	115
	diameter (nm)	58	79	43	50	53
Hexamethylenediamine	length (μm)	-	271	412	388	197
	diameter (nm)	49	51	55	59	65
N-methyethylenediamine	length (μm)	375	92	131	86	111
	diameter (nm)	47	52	43	56	45
Trimethylenediamine	length (μm)	307	162	111	164	245
	diameter (nm)	66	71	56	44	62
Formamide	length (μm)	340	311	291	222	292
	diameter (nm)	65	79	64	73	61
N,*N*-dimethylformamide	length (μm)	300	250	323	188	153
	diameter (nm)	51	49	62	68	65
N,*N*-dimethylacetamide	length (μm)	557	235	293	354	340
	diameter (nm)	57	52	59	66	62

[1] Ferrocene/toluene – no added N containing reagents: Length = 130 μm, diameter = 45 nm

The rate of N-CNT growth appears to be much slower than that reported by others; reactants/conditions used in this study are however quite different from that used in earlier reported studies. For example, Ren *et al.* [31] synthesized large arrays of well aligned carbon nanotubes on glass using acetylene as a carbon source and ammonia gas as a catalyst and dilution gas at 700 ^{o}C. It was estimated from the TEM and SEM micrographs that the nanotubes were about 100 nm in diameter and 20 mm in length with a growth rate that was calculated to be 2 mm/min. This is about 100 times faster than the growth rates noted in this study. Kayastha *et al.* [32] have also synthesized N-CNTs by addition of N_2 gas to C_2H_2. These samples were grown for 15 min with an estimated length of 200 mm: A remarkable growth rate of 13 mm/min was reported.

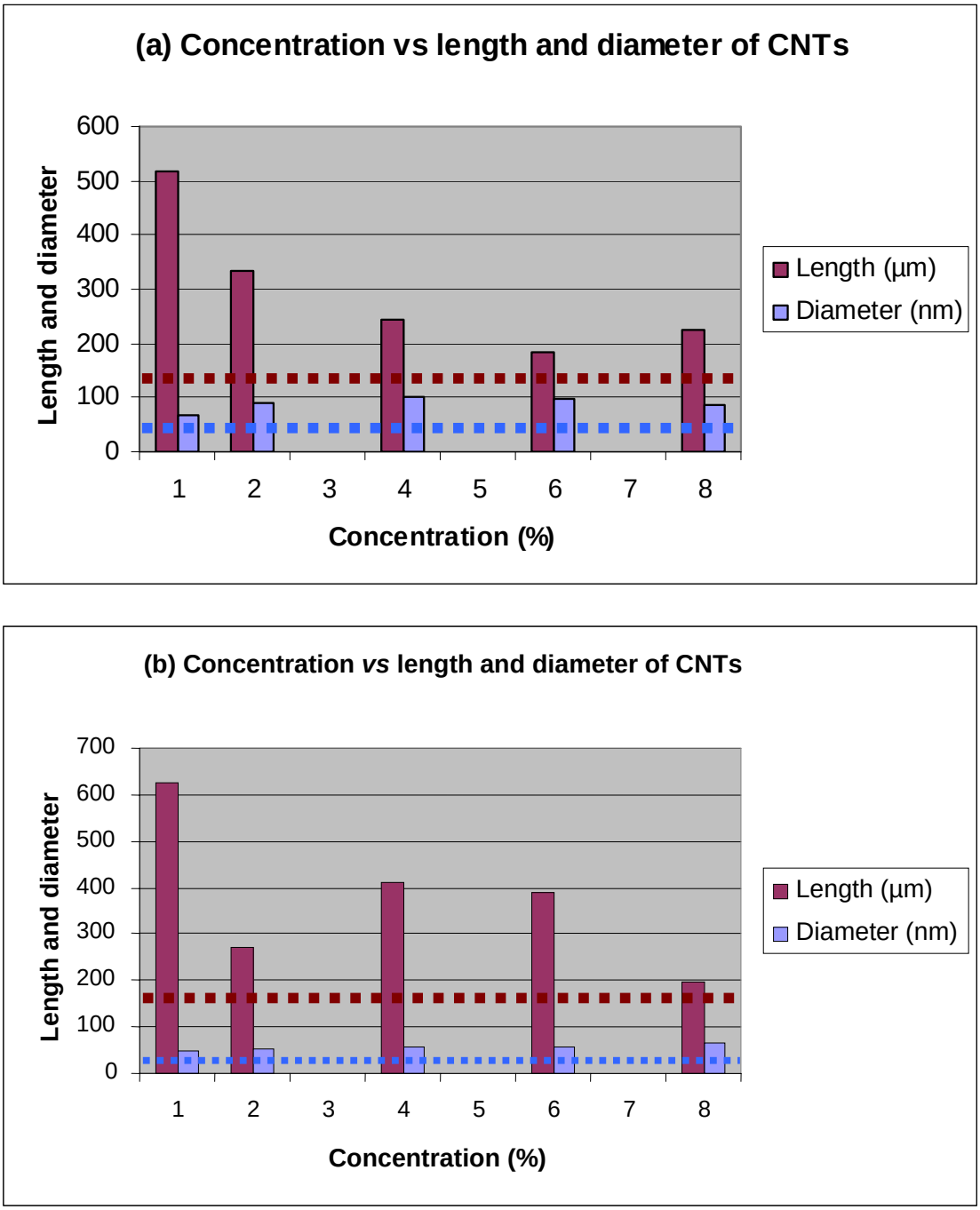


Fig. 7.3. Graph of concentration versus length and diameters of CNTs grown from (a) benzylamine; and (b) hexamethylenediamine. Horizontal dotted line indicates lengths and diameters of CNTs obtained from ferrocene/toluene.

7.3.1.2 N-CNT morphology: TEM analysis

The formation of MWCNTs is confirmed by TEM micrographs. A TEM image of carbon nanotubes prepared in the absence of nitrogen containing additives showed that the average outer diameter of the tubes is 55 nm. Table 7.2 gives the average outer diameters and average lengths of CNTs obtained from the pyrolysis of the nitrogen containing reagents at various concentrations. The outer diameters of N-CNTs were obtained by using the average measurement of about 50 nanotubes from at least 3 different TEM micrographs. Large tubes with diameters ranging from 40 nm to 88 nm were prepared from all the N containing reagents. Two sets of data (for benzylamine and hexamethylenediamine) are shown in Fig. 7.3. In every case the outer diameter was larger than that found for CNTs produced from ferrocene and toluene.

Fig. 7.4 (a) shows TEM images of N-CNTs obtained by the pyrolysis of toluene and ferrocene in the presence of 8% diethylamine. Fig. 7.4 (b) shows a typical TEM micrograph of a N-CNT taken at high magnification and demonstrates that indeed the tubes are of the multi-walled type. The image shows a CNT with an average diameter of approximately 49 nm. The image also reveals that the nanotubes synthesized have an expected bamboo-like structure [23,24,33]. The "bamboo-like" structure is also evident in *most* the N-MWCNTs synthesized in this study.

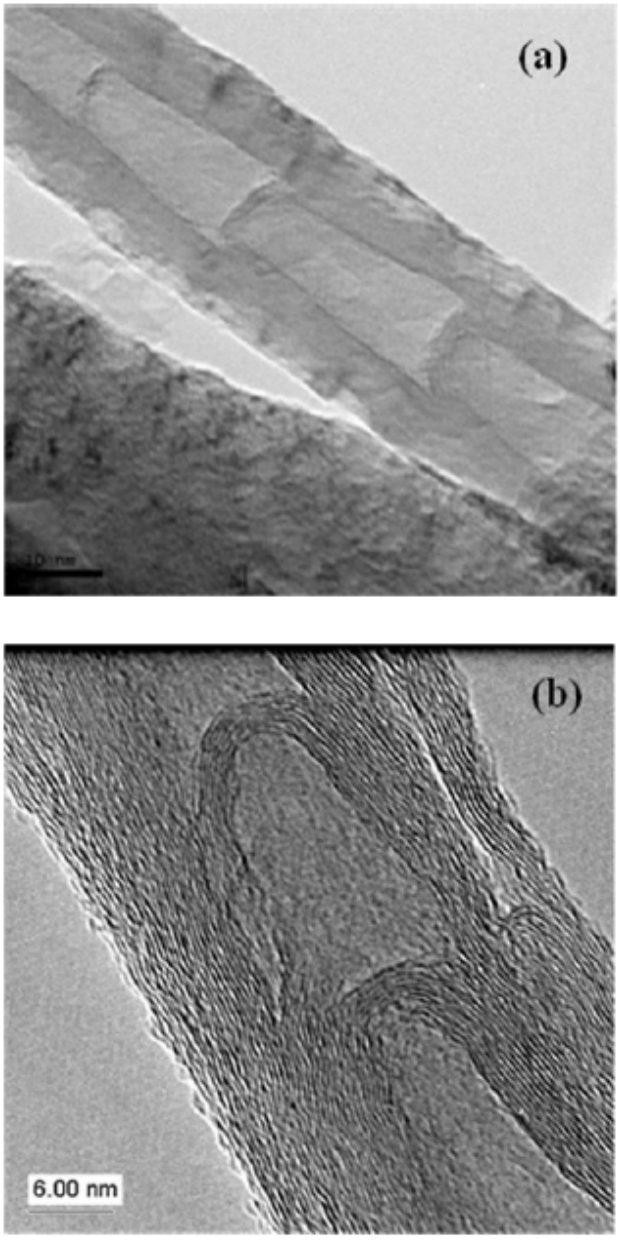


Fig. 7.4. TEM images of CNTs obtained from the pyrolysis of toluene and ferrocene in the presence of 8% diethylamine.

7.3.1.3 Thermal analysis and Raman studies of the N-CNTs

The thermal stabilities of the various MWCNTs were evaluated by TGA analysis in air. Fig. 7.5 (a) shows a TGA plot for CNTs obtained from the pyrolysis of toluene and ferrocene. The percentage residual mass, detected at T > 700 ^{o}C, is due to the oxidized catalyst. The CNTs did not degrade below 500 ^{o}C. The TGA plot of the CNTs prepared from ferrocene/toluene/8% hexamethylenediamine is depicted in Fig. 7.5 (b) and shows that the thermal degradation commences at a temperature of 500 ^{o}C. The residual weight of nearly 7% is again attributed to oxidized catalyst nanoparticles. The CNTs are completely oxidized by 800 °C.

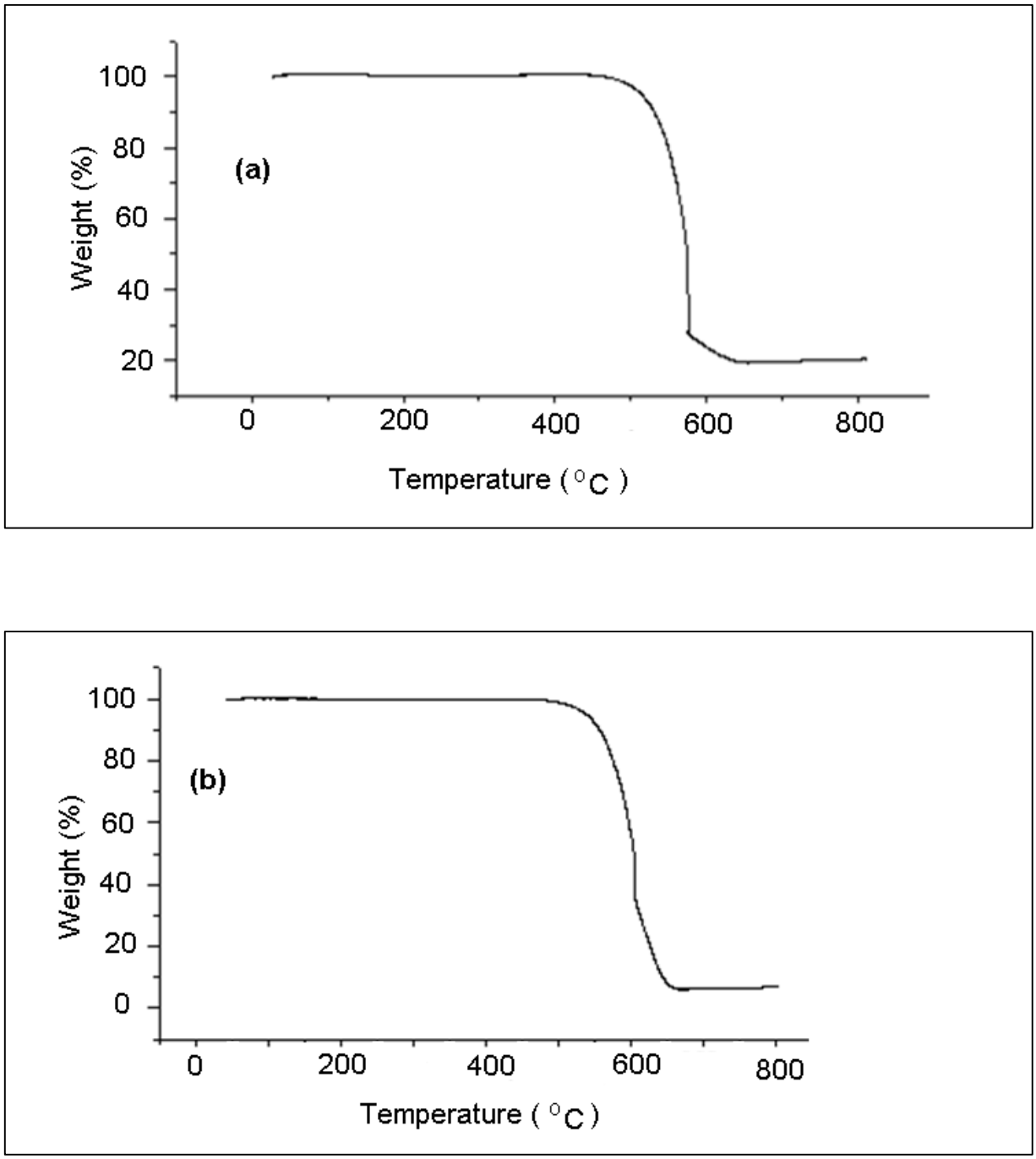


Fig. 7.5. TGA curve of CNTs obtained from the pyrolysis of (a) toluene and ferrocene; (b) toluene and ferrocene in the presence of 8% hexamethylenediamine.

The differential TGA (DTGA) graphs showed sharp oxidation peaks between 620 and 670 °C (not shown), which are lower than the oxidative temperature for pure MWCNTs. This suggests that the N-doped CNTs are easier to oxidize than the pure MWCNTs. The mass loss maxima (obtained from the DTGA profiles) decreased from 670 to 620 °C with increasing nitrogen content in the synthesis procedure. The shift in the mass loss maxima suggests more defects and disorder in the N-CNTs.

To further investigate the graphitic nature as well as the disorder of the CNTs, Raman spectroscopy studies were performed. Fig. 7.6 depicts the Raman spectrum obtained from the pyrolysis of toluene and ferrocene in the presence of 8% diethylamine (Table 7.3). It shows two peaks at 1356 cm^{-1} and 1585 cm^{-1}. The peak at 1585 cm^{-1} (G-band) corresponds to the high frequency E2g first order mode while the D-band occurs at 1356 cm^{-1} [34].

The intensity ratios of the G-band and D-band, measured by the integration of the spectral peaks are given in Table 3. The D-band and the G-band ratio (I_D/I_G) give a measure of the graphitic nature of CNTs. A lower I_D/I_G ratio indicates a higher graphitic content of CNTs. It is clear from the data that as the concentration of diethylamine increases from 2% to 8%, the intensity ratio increases from 0.55 to 0.81 and this is attributed to an increase in the presence of defects in the CNT lattice. The intensity of the Raman spectral absorptions of tubes synthesized by pyrolysis of 2%, 4% and 8% benzylamine and isopropylamine were also recorded and their I_D/I_G ratio are shown in Table 7.3. In all these samples, an increase in the N source concentration results in an increase in the Raman ratio indicating an increase in the CNT disorder. There is however no straightforward correlation between the N type and N source with the Raman ratio of the CNTs.

Table 7.3. I_D/I_G of CNTs obtained from the pyrolysis of toluene, ferrocene and N containing reagents.

Reagent	**D_{band}**	**G_{band}**	I_D/I_G
Pure (0%)	683.1	1582	0.43
Diethylamine 2%	571.9	1036.0	0.55
Diethylamine 4%	904.9	1157.6	0.78
Diethylamine 8%	1137.9	1403.1	0.81
Benzylamine 2%	740.0	1223.5	0.60
Benzylamine 4%	377.8	637.0	0.59
Benzylamine 8%	875.7	1146.9	0.76
Isopropylamine 2%	761.6	798.3	0.95
Isopropylamine 4%	609.8	735.9	0.82
Isopropylamine 8%	631.4	742.2	0.85
Isopropylamine 8%	631.4	742.2	0.85

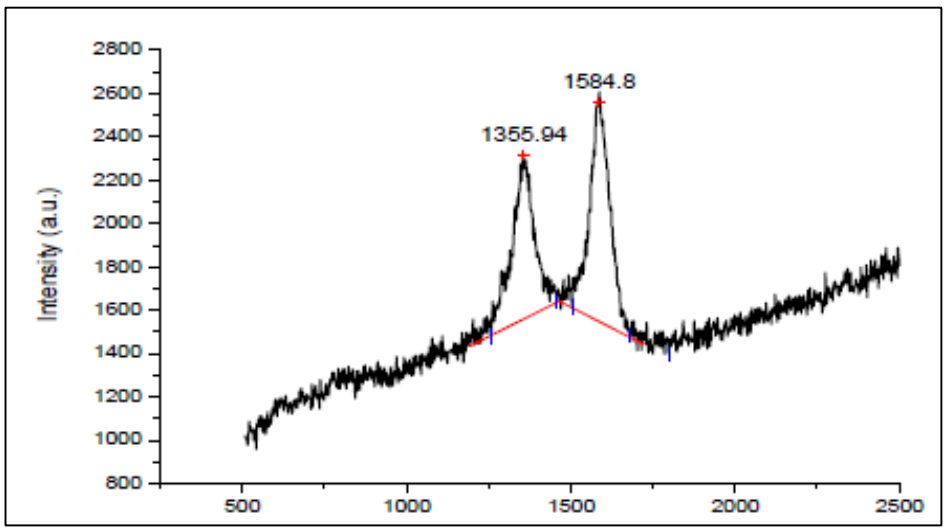


Fig. 7.6. Raman spectrum of CNTs obtained from the pyrolysis of toluene and ferrocene in the presence of 8% diethylamine.

7.3.2 Oxidation of N-CNTs

The effect of acid treatment on the N-CNT samples was investigated by TEM. Table 7.4 gives the data on the average diameter of untreated and nitric acid treated CNTs obtained by the pyrolysis of toluene and ferrocene. The acid treated CNTs from ferrocene/toluene have an average diameter of 44 nm. The diameters of the oxidised CNTs obtained from the pyrolysis of toluene and ferrocene in the presence of 1% and 8% diethylamine; 1% and 8% quinoline; 1% and 8% hexamethylenediamine; and 1% and 8% *N*,*N*-dimethylacetamide are also given in Table 7.4. It is apparent that the diameters of the treated CNTs obtained from the pyrolysis of diethylamine, hexamethylenediamine and *N*,*N*-dimethylacetamide generally *decrease* with an increase in concentration of the aforementioned nitrogen containing hydrocarbons.

Table 7.4. Average diameters of acid treated CNTs obtained from the pyrolysis of toluene and ferrocene, in the presence of various nitrogen containing hydrocarbons.[1,2]

Nitrogen containing hydrocarbons	Diameter (nm)	
	1%	8%
Diethylamine	48 (58)	42 (54)
Quinoline	43 (59)	49 (62)
Hexamethylenediamine	50 (49)	48 (65)
N,*N*-dimethylacetamide	44 (57)	36 (62)

[1] Toluene/ferrocene CNTs length = 130 μm (136 μm); diameter = 44 (45) (untreated data in brackets)

[2] Untreated CNT diameters given in brackets

The SEM image of acid treated CNTs obtained from the pyrolysis of ferrocene and toluene is shown in Fig. 7.7. The image shows aligned CNTs with uniform length. The CNTs have an average length of 136 μm, similar to that of the untreated ferrocene CNTs (Table 7.4). Fig. 7.8 (a) and (b) shows the SEM images of acid treated CNTs obtained from the pyrolysis of toluene and ferrocene in the presence of 1% and 8% diethylamine, while Fig. 7.8 (c) and (d) depicts SEM images of acid treated CNTs obtained from the pyrolysis of toluene and ferrocene in the presence of 1% and 8% hexamethylenediamine, respectively. It is evident from the images that the CNTs have lost their alignment and that the overall effect is to generate products that have a "fused/melted" look compared to untreated CNTs synthesized under similar conditions. Tubes grown from 1% and 8% quinoline (Fig. A7.7, Appendices) show similar features.

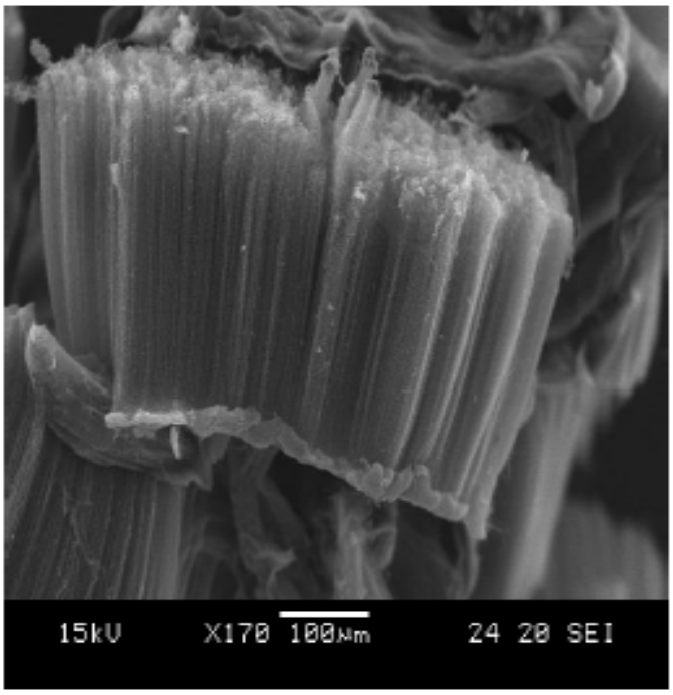


Fig. 7.7. SEM image of acid treated CNTs obtained from the pyrolysis of toluene and ferrocene.

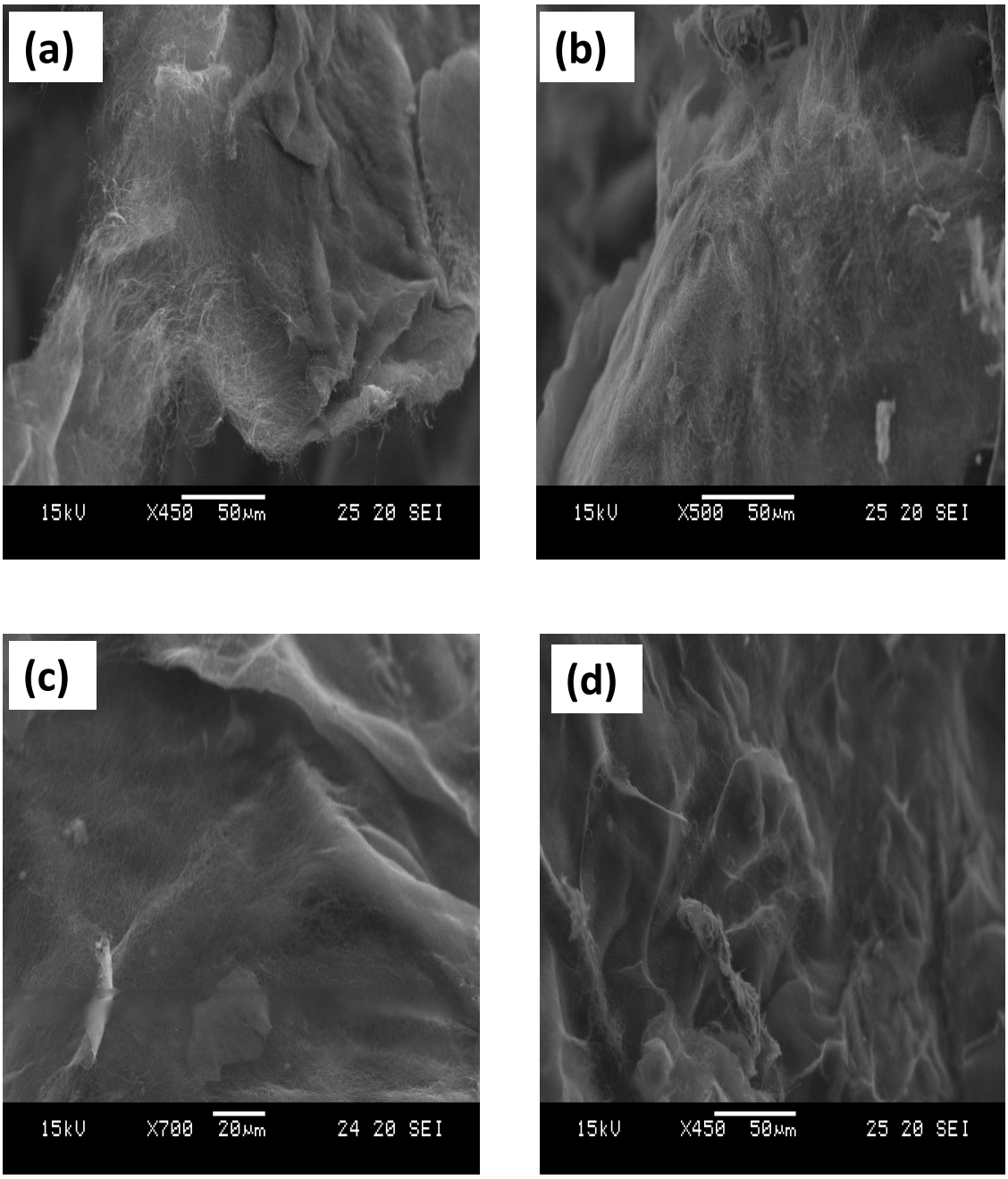


Fig. 7.8. SEM images of acid treated CNTs obtained from the pyrolysis of toluene and ferrocene in the presence of (a) 1%; and (b) 8% diethylamine; and (c) 1%; and (d) 8% hexamethylenediamine.

The TGA and DTGA curves of the acid treated samples obtained under flowing air show major differences between the toluene/ferrocene CNTs and those synthesized by the addition of N containing reagents to the ferrocene/toluene solution. Decomposition occurs in the temperature range of 300 – 620 ^{o}C for the treated standard CNTs. It can be seen from Fig. 7.9 (a) (for hexamethylenediamine) that the acid treated CNTs have a percentage weight loss of 94% at 620 ^{o}C, indicating increased purity after washing/oxidation (compare with Fig. 7.5). A two step degradation process for the treated CNTs obtained from the pyrolysis of toluene and ferrocene in the presence of 1% and 8% hexamethylenediamine between 300 and 610 ^{o}C is noted.

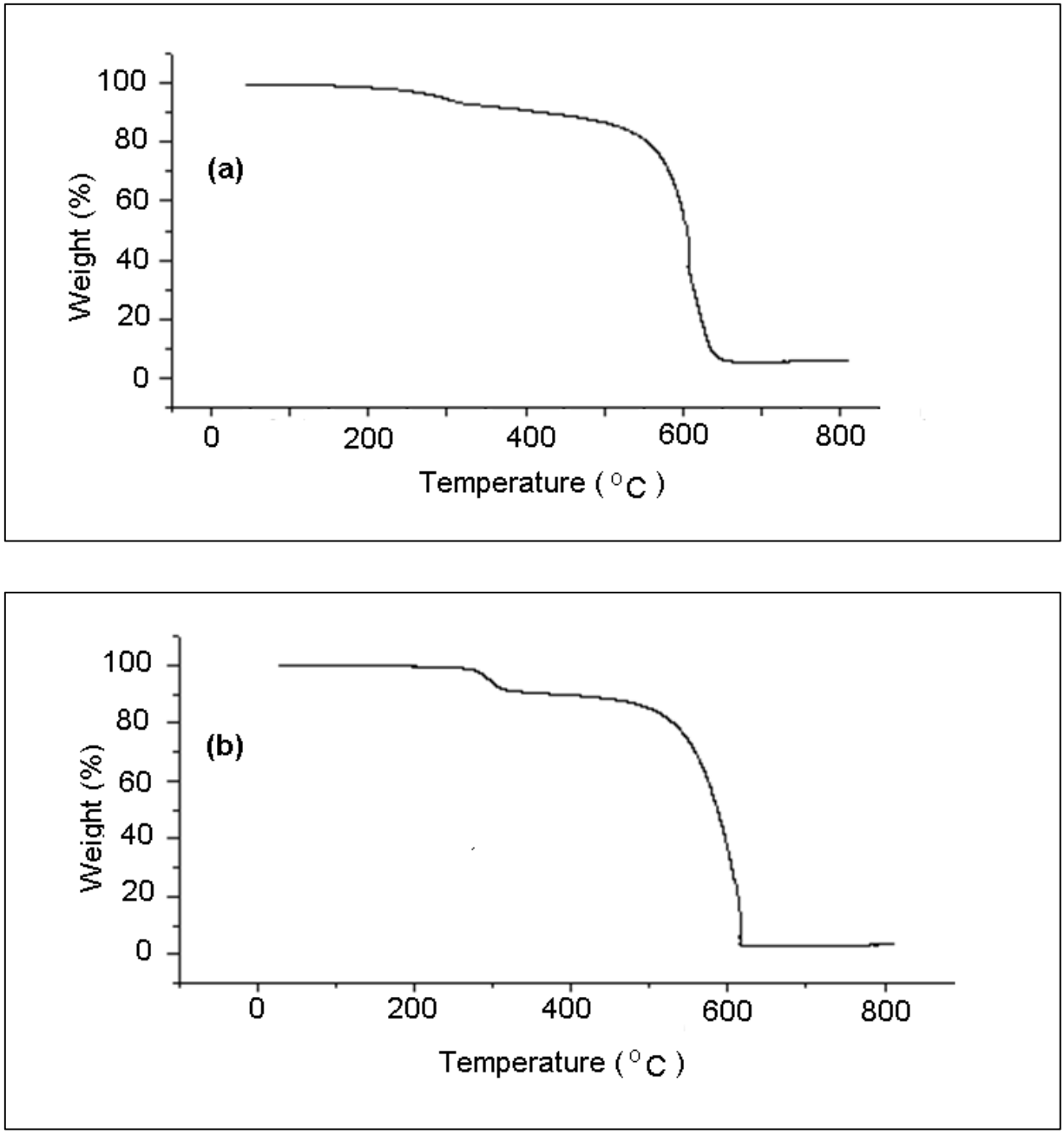


Fig. 7.9. TGA spectra of acid treated CNTs obtained from the pyrolysis of toluene and ferrocene in the presence of (a) 1%; and (b) 8% hexamethylenediamine.

The I_D/I_G band ratio obtained from the Raman spectra of acid treated 1% and 8% diethylamine CNTs was found to be 0.52 and 0.91, respectively. These observations were related to the oxidation of the CNTs by HNO_3, which resulted in an increase in the amount of disordered carbon caused by the partial destruction of CNTs. This result suggests that the graphitization of acid treated N-CNTs prepared at low concentration of the N source is better than those prepared at higher concentrations of the N source. Thus, the data again reveals that the oxidation of N-CNTs is influenced by the N content and that the type of N source is less important in the reaction.

7.4 Reaction mechanism

Bamboo shaped N-CNTs are proposed to form through a mechanism entailing interaction of iron clusters and C and N containing ions/radicals/atoms/clusters ('fragments') in the gas phase. At the high temperatures used, the ferrocene decomposes to form Fe atoms which cluster to form particles. At the same time, the different C and N containing reactants used to make the N-CNTs also decompose. The interaction between the Fe clusters and the C/N fragments lead to the formation of the N-CNTs.

A mechanism for the growth of bamboo N-CNTs has been proposed [36] and this mechanism can rationalize our findings. In this mechanism, the C/N fragments can either dissolve in the metal or diffuse over the metal surface. In either instance, they form a layer on the Fe particle containing C and N atoms. In the model, the C/N graphite-like layer takes the shape of the Fe particle. The presence of N in the layer is proposed to lead to stresses in the surface. This is released by a 'pulsed' effect [7,37] in which the C/N surface layer detaches from the Fe. This process is repeated over and over again leading to the bamboo shape.

In the gas phase, the type of 'fragment' formed will be influenced by the differences in the precursor used. These differences include (i) the C/N ratio of the reactant, (ii) the physical/chemical properties of the precursor and (iii) the concentration of the precursor. All of these factors will impact on the formed product. From our earlier studies on imidazoles as a source of N-CNTs [38], we also found that the structural configuration of the reactant influenced the final product.

A major conclusion from this study then is that the amount of N used is more important than the source of N used in determining the bulk yield and morphology of N-CNTs. Further analysis may still reveal subtle differences in the N-CNT structures that are due to the different N sources, but clearly these will be small effects relative to the role of the N content used to make CNTs.

7.5 Conclusion

We have successfully synthesized N-CNTs by a nebulised floating catalyst method using toluene and nitrogen containing reactants (1 - 8% mixtures) and shown the effect of employing different N containing reagent on the synthesis reactor. From the data and the discussions provided above, it is apparent that the increase in concentration of nitrogen containing hydrocarbons during the synthesis of N-CNTs results in an increase in the average outer diameter and an increase in the length of carbon nanotubes at low N concentration (< 5%). The data shows that the growth rate of CNTs from the pyrolysis of toluene and ferrocene in the presence of nitrogen containing hydrocarbons *decreases* with an increase in the addition of nitrogen containing species. Increasing N content in the reactant mixture gives shorter doped tubes and tubes with more disorder. Treatment of the N-CNTs with nitric acid results in chemically modified/oxidized nanotubes with loss of alignment, decreased stability and an increased number of defects. The

general conclusion is that the effects of N concentration are more important than the nature of the N source in determining the morphology and the yields of the synthesized N-CNTs.

References

1. (a) O. Stephen, P.M. Ajayan, C. Colliex, Ph. Redlich, J.M. Lambert, P. Bernier, P. Letin, Science 266 (1994) 1683;

(b) K. Suenaga, M. Yudasaka, C. Colliex, S. Iijima, Chem. Phys. Lett. 316 (2000) 365. 2. L. Carroll, P. Redlich, X. Blase, J.C. Charlier, S. Curran, P.M. Ajayan, S. Roth, M. Ruhle, Phys. Rev. Lett. 81 (1998) 2332.

3. B. Wang, Y. Ma, Y. Wu, N. Li, Y. Huang, Y. Chen, Carbon 47 (2009) 2112.

4. J. Wei, H. Hu, H. Zeng, Z. Zhou, W. Yang, P. Peng, Physica E 40 (2008) 462.

5. F.L. Deepak, N.S. John, A. Govindaraj, G.U. Kulkarni, C.N.R. Rao, Chem. Phys. Lett. 411 (2005) 468.

6. S. Latil, F. Triozon, S. Roche, NATO Sci. II Math. Phys. Chem. 222 (2006) 143.

7. E.N. Nxumalo, N.J. Coville, Materials 3 (2010) 2141.

8. C.P. Ewels, M. Glerup, J. Nanosci. Nanotechnol. 5 (2005) 1345.

9. P. Ayala, R. Arenal, M. Rummeli, A. Rubio, T. Pichler, Carbon 48 (2010) 575.

10. C.N.R. Rao, A. Govindaraj, Acc. Chem. Res. 35 (2002) 998.

11. F. Villalpando-Paez, A. Zamudio, A.L. Elias, H. Son, E.B. Barros, S.G. Chou, Y.A. Kim, H. Muramatsu, T. Hayashi, J. Kong, H. Terrones, G. Dresselhaus, M. Endo, M. Terrones, M.S. Dresselhaus, Chem. Phys. Lett., 424 (2006) 345.

12. E.J. Liang, P. Ding, H.R. Zhang, X.Y. Guo, Z.L. Du, Diamond Relat. Mater. 13 (2004) 69.

13. R. Kurt, A. Karimi, Chem. Phys. Chem. 2 (2001) 388.

14. C.J. Lee, S.C. Lyu, H.-W. Kim, J.H. Lee, I.C. Cho, Chem. Phys. Lett. 359 (2002) 115.

15. M. Nath, B.C. Satishkumar, A. Govindaraj, C.P. Vinod, C.N.R. Rao, Chem. Phys. Lett. 322 (2000) 333.

16. N. Grobert, M. Terrones, S. Trasobares, K. Kordatos, H. Terrones, J. Olivares, J.P. Zhang, Ph. Redlich, W.K. Hsu, C.L. Reeves, D.J. Wallis, Y.Q. Zhu, J.P. Hare, A.J. Pidduck, H.W. Kroto, D.R.M. Walton, Appl. Phys. A 70 (2000) 175.

17. M. Terrones, N. Grobert, J. Olivares, J.P. Zhang, H. Terrones, K. Kordatos, W.K. Hsu, J.P. Hare, P.D. Townsend, K. Prassides, A.K. Cheetham, H.W. Kroto, D.R.M. Walton, Nature 388 (1997) 52.

18. (a) R. Che, L.M. Peng, Q. Chen, X.F. Duan, Z.N. Gu, Appl. Phys. Lett. 82 (2003) 3319;

(b) F.L. Deepak, A. Govindaraj, C.N.R. Rao, Chem. Phys. Lett 345 (2001) 5.

19. Z. Osváth, A.A. Koós, N. Grobert, Z. Vértesy, Z.E. Horváth, L.P. Biró, J. Nanosci. Nanotechnol. 9 (2009) 6139.

20. P. Ghosh, M. Tanemura, T. Soga, M. Zamri, T. Jimbo, Solid State Commun. 147 (2008) 15.

21. (a) V. Bajpai, L. Dai, T. Ohashi, J. Am. Chem. Soc. 126 (2004) 5070;

(b) R. Sen, B.C. Satishkumar, A. Govindaraj, K.R. Harikumar, M.K. Renganathan, C.N.R. Rao, J. Mater. Chem. 7 (1997) 2335.

22. (a) P. Ghosh, T. Soga, K. Ghosh, R.A. Afre, T. Jimbo, Y. Ando, J. Non-Cryst. Solids 354 (2008) 4101;

(b) S. Maldonado, S. Morin, K.J. Stevenson, Carbon 44 (2006) 1429.

(c) J. Feng, Y. Li, F. Hou, X. Zhong, Mater. Sci. Eng. A 473 (2008) 238.

23. (a) R.M. Yadav, P.S. Dobal, T. Shripathi, R.S. Katiyar, O.N. Srivastava, Nanoscale Res. Lett. 4 (2009) 197;

(b) R.M. Yadav, D.P. Singh, T. Shripathi, O.N. Srivastava, J. Nanopart. Res. 10 (2008) 1349.

24. (a) J. Jiang, T. Feng, X. Cheng, L. Dai, G. Cao, B. Jiang, X. Wang, X. Liu, S. Zou, Nucl. Instrum. Meth. B 244 (2006) 327;

(b) C.J. Lee, J. Park, Appl. Phys. Lett. 77 (2000) 3397.

25. S. Trasobares, O. Stephan, C. Colliex, W.K. Hsu, H.W. Kroto, D.R.M. Walton, J. Chem. Phys. 116 (2002) 8966.

26. E.N. Nxumalo, V.O. Nyamori, N.J. Coville, J. Organomet. Chem. 693 (2008) 2942.

27. S.R.C. Vivekchand, L.M. Cele, F.L. Deepak, A.R. Raju, A. Govindaraj, Chem. Phys. Lett. 386 (2004) 313.

28. A.A. Koós, M. Dowling, K. Jurkschat, A. Crossley, N. Grobert, Carbon 47 (2009) 30.

29. D.Y. Zhong, S. Liu, G.Y. Zhang, E.G. Wang, J. Appl. Phys. 89 (2001) 5939.

30. C.J. Lee, J. Park, Appl. Phys. Lett. 77 (2000) 3397.

31. Z.F. Ren, Z.P. Huang, J.W. Xu, J.H. Wang, P. Bush, M.P. Siegal, P.N. Provencio, Science 282 (1998) 1105.

32. V. Kayastha, Y. Yapa, K.S. Dimovski, Y. Gogotsi, Appl. Phys. Lett. 85 (2004) 3265.

33. H. Liu, Y. Zhang, R. Li, X. Sun, S. Desilets, H. Abou-Rachid, M. Jaidann, L.-S. Lussier, Carbon 48 (2010) 1498.

34. M. Kohno, T. Orii, M. Hirasawa, T. Seto, Y. Murakami, S. Chiashi, Y. Miyauchi, S. Maruyama, Appl. Phys. A 79 (2004) 787.

35. K. Kuwana, K. Saito, Carbon 43 (2005) 2088.

36. M. Terrones, A.M. Benito, C. Manteca-Diego, W.K. Hsu, O.I. Osman, J.P. Hare, D.G. Reid, H. Terrones, A.K. Cheetham, K. Prassides, H.W. Kroto, D.R.M. Walton, Chem. Phys. Lett. 257 (1996) 576.

37. C.T. Wirth, S. Hofmann, J. Robertson, Diamond Relat. Mater. 18 (2009) 940.

38. E.N. Nxumalo, V.P. Chabalala, V.O. Nyamori, M.J. Witcomb, N.J. Coville, J. Organomet. Chem. 695 (2010) 1451.

Chapter 8

[6]The effect of arylferrocene ring substituents on the synthesis of multi-walled carbon nanotubes

8.1 Introduction

The synthesis of shaped carbon nanomaterials (SCNMs) such as carbon spheres (CNSs), carbon fibers (CNFs), nanohorns, nanocoils and in particular carbon nanotubes (CNTs) have become an increasingly important subject area in the field of nanostructured materials. Although the existence of filamentous carbon nanomaterials [1] has been known for decades, it is only since the 1990s that they have become a material type that has attracted considerable attention. This is due to their unique chemical and physical (electrical [2,3], magnetic [4,5] and mechanical [6,7]) properties. These properties have implications for industrial and technological applications [8–10], especially in nanoelectronics [11], energy storage [12] and in catalysis [13].

SCNMs have been synthesised using various vapour phase methods including laser vapourization [14,15], arc discharge [16,17] and chemical vapour deposition (CVD) [18,19]. The

[6] V.O. Nyamori, E.N. Nxumalo, N.J. Coville, J. Organomet. Chem. 694 (2009) 2222

CVD method is one of the most promising methods for the large scale production of SCNMs and the method has in particular been shown to produce high yields of CNTs in good purity, as well as aligned CNTs, even at low temperatures [20,21]. More recently another type of CNT synthesis methodology which utilizes a closed container (*e.g.* sealed quartz tubes or autoclaves) has also been developed [22].

Organometallic compounds such as ferrocene ($Fe(C_5H_5)_2$) [23] and $Fe(CO)_5$ [24] have been widely reported to produce good yields of CNTs and other SCNMs. These compounds do not have a counterion and they also contain both the metal and some carbon within their structure. Hence, they act both as a catalyst and as a carbon source in SCNM production. In general, a carbon source such as CH_4 [25], C_6H_6 [26], CO [27], *etc.* is also added to the catalyst to provide the major source of carbon to produce the SCNMs. The choice of this added carbon source also affects the kind and shape of SCNMs obtained. Toluene has proven to be a good carbon source for the synthesis of CNTs in the CVD reaction in the temperature range 800 – 1000 ^oC [28].

Currently only a limited number of studies have appeared in the literature describing the effect of ferrocene (FcH) substituents on SCNM product formation using the CVD floating catalyst method [29–31]. Furthermore, no information has been reported on the use of arylferrocenyl derivatives in the synthesis of SCNMs. A study of the effect of various *para*-substituted arylferrocenes, on the influence on SCNMs synthesis is thus reported in this study. A comparative study on the effect of mixing ferrocene with substituted benzenes, on SCNM synthesis relative to that of arylferrocenes, is also reported (Fig. 8.1).

8.2 Experimental procedures

Ferrocene was purchased from Strem Chemicals while toluene (analytical grade) was obtained from Sigma Aldrich Chemical Company and was used as the carbon source. Both were used as

received. Phenylferrocene (FcPhH), 4-hydroxyphenylferrocene (FcPhOH), 4-bromophenylferrocene (FcH) and 4-nitrophenylferrocene ($FcNO_2$) were prepared by the diazonium salt method [32] while 4-ferrocenylacetophenone ($FcPhCOCH_3$) was prepared by a modified Suzuki cross-coupling reaction [33]. 4-Ferrocenylaniline ($FcPhNH_2$) was obtained by the catalytic reduction of 4-nitrophenylferrocene ($FcPhNO_2$) [34].

A quartz tube reactor, 80 cm in length and 2.8 cm internal diameter, was inserted horizontally into an electrical furnace with the outlet of the tube connected to a gas bubbler (Appendices; material; Fig. A5.1). The temperature inside the quartz tube was determined by means of a thermocouple placed in the middle of the furnace. Synthesis of CNTs was carried out in the temperature range 800 – 1000 ^{o}C, under 5% H_2 in argon (v/v) at atmospheric pressure. The flow rate of H_2 in argon was kept constant at 100 ml/min. The substituted arylferrocenes were dissolved in toluene (2.5 *wt.%* or 5 *wt.%*); the catalyst loading in toluene was limited by solubility constraints. The solutions were placed in a 10 ml syringe and injected into the heated tube by means of a SAGE syringe pump (at 0.8 and 0.2 ml/min injection rate). The solutions were injected into the tube reactor *via* a specially designed quartz tube 0.2 cm internal diameter and 20 cm in length, cooled by water. The solutions were injected directly into the high temperature zone of the large quartz tube reactor. When solution injection was complete the electrical furnace temperature was allowed to cool down to room temperature under 5% H_2 in argon (v/v).

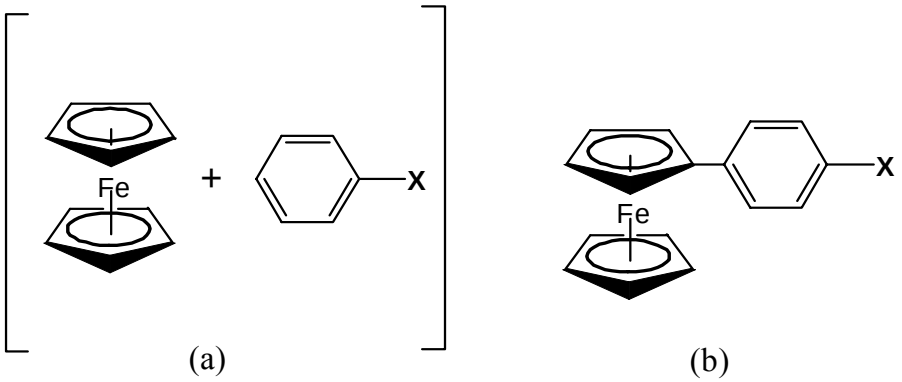
The carbon deposited materials that formed were scraped from the walls of the quartz tube. These materials were characterized by low resolution transmission electron microscopy (TEM; JEOL JEM 100 S). The samples for TEM analysis were prepared by sonication of the carbonaceous materials in methanol or ethanol. A few drops of the resulting dispersed suspension were placed onto a holey TEM copper grid for analysis at 80 kV and at varying magnifications. The distribution, number and size of the various nanoparticles materials were

obtained from the TEM photographs by counting procedures (counting at least 100 ‘carbon shaped objects’ per sample). These were randomly chosen from different TEM images and represent average values.

Raman spectra were measured using the single spectrograph stage of a Jobin-Yvon T64000 Raman spectrometer. The excitation source was 636.4 nm from a tuneable Spectra-Physics dye laser. The laser beam was focused onto the sample using the 20X objective of an Olympus microscope. The backscattered light was dispersed using a 600 line/mm grating and detected using a liquid nitrogen cooled CCD detector. Thermal gravimetric analysis (TGA) measurements were performed under flowing air on a Perkin– Elmer TGA 7 at a heating rate of 10 ^{o}C/min.

8.3 Results and discussion

The SCNMs were synthesised from solutions of FcH, FcPhH, FcPhOH, FcPhBr, $FcPhCOCH_3$ and $FcPhNH_2$ in toluene. They were also synthesised from mixtures of solutions of FcH and substituted benzenes in toluene (2.5 *wt.%*). Toluene, *para*-substituted phenyl rings and the cyclopentadienyl ligands provided the carbon for the CNT growth. The catalysts used in this study are shown in Fig. 8.1.



X = H, $COCH_3$, OH, Br

Fig. 8.1. The precursors used for synthesis of SCNMs in toluene: (a) ferrocene (FcH) and *para*-substituted benzenes; (b) arylferrocenes (FcPhX).

8.3.1 Analysis of SCNMs

Generally four types of SCNMs were made using the above catalysts, namely; (i) CNTs, (ii) carbon fibers (CNFs), (iii) carbon spheres (CNSs) and (iv) amorphous carbon (a-C). Reactions with FcH and FcPhH were performed to provide reference data for the effect of the substituted benzenes and arylferrocenes on the reaction products formed.

Good yields of well structured MWCNTs were obtained at 800 ^{o}C (Fig. 8.2) and 900 ^{o}C with 2.5 *wt.%* of FcH in toluene, while no CNTs were found at 1000 ^{o}C (Table 8.1). Generally, the pyrolysis of hydrocarbons at high temperatures (*e.g.* 1000 ^{o}C) favours the production of CSs and amorphous carbon. Transmission electron microscopy (TEM) studies revealed that the mean internal diameter of the CNTs produced at 800 ^{o}C was 35 nm with a mean external diameter of 55 nm while at 900 ^{o}C the CNT diameters were found to be 30 nm and 40 nm, respectively. This observation of narrower tube formation as the temperature is increased is not unexpected. The average tube length (obtained from TEM pictures) at 800 ^{o}C and 900 ^{o}C were 5.5 μm and 6.0

μm, respectively. The mean diameter of the nanofibers was found to be 125 nm at 900 ^{o}C and 100 nm at 1000 ^{o}C.

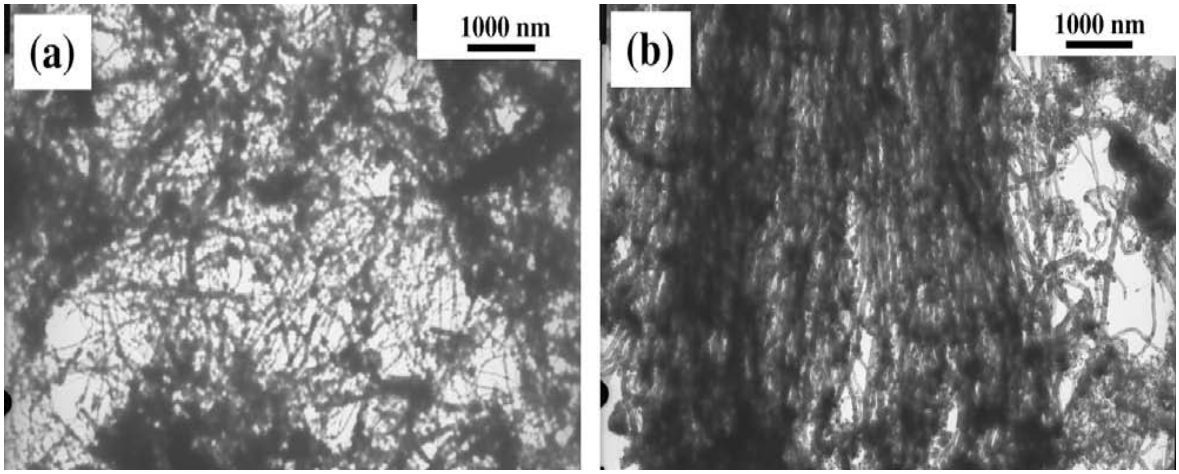


Fig. 8.2. CNTs formed from pyrolysis of (a) 2.5 *wt.%* FcH and (b) 2.5 *wt.%* FcPhH in toluene with a flow rate of 0.8 ml/min and at temperature of 800 ^{o}C.

FcPhH in toluene (2.5 *wt.%* and 5 *wt.%*, Table 8.1) was used as a catalyst to synthesise the CNTs at 800 ^{o}C, 900 ^{o}C and 1000 ^{o}C. At all the temperatures used, MWCNTs were formed with T = 1000 ^{o}C providing very low percentages of CNTs at both catalyst concentrations. The 2.5 *wt.%* catalyst concentration gave CNTs with a mean length of 13.0 μm while that of 5.0 *wt.%* catalyst was found to give slightly shorter tubes (11.0 μm). At higher concentration (5.0 *wt.%*) and higher temperature (> 1000 ^{o}C) a significant increase in amorphous material (85%) was noted.

In general, the phenyl ring appears to have a very modest effect on the SCNM yield and morphology when compared to ferrocene. Even the addition of more catalyst (compare 2.5% and 5% results) has only a minor effect on the product yield/dimensions.

Due to solubility constraints 2.5 *wt.%* catalyst concentrations were used in all studies involving the *para*-substituted arylferrocenes, FcPhX (X = OH, $COCH_3$, Br). For comparative purposes, the experiments were conducted at three different temperatures (800 ^oC, 900 ^oC and 1000 ^oC). These conditions allowed for a comparison with the FcPhX (X = H) catalyst described above.

The reactions with FcPhX (X = OH) at 800 ^oC were performed at two different flow rates, 0.8 and 0.2 ml/min (Table 8.1). Although higher yields of SCNMS were formed at the lower flow rate (0.2 ml/min) the product was mainly comprised of amorphous carbon. Again at the highest temperature, CNT formation was at a minimum (both flow rates). A comparison of the morphological data with X = H indicates that the tubes prepared with X = OH tend to have narrower outer diameters. The outer tube diameter was larger at the lower flow rate. The CFs showed a larger mean diameter than those observed using ferrocene (Table 8.1). The tube lengths could not be easily measured since they were not well aligned but were estimated to be in the micro length range of 2.0 – 2.2 μm.

Table 8.1. Summary of the yield and size distribution of SCNMs produced from different catalysts under a constant flow rate of 100 ml/min of 5% H_2 in argon (v/v) at different temperatures.

Catalyst	Temp. (ºC)	Injection flow rate (ml/min)	Yield (g)	SCNMs formed (%)	Mean CNTs and CFs diameters (nm)
FcH (2.5 *wt.%*)	800	0.8	0.210	80T, 20a-C	35 T(ID), 55T(OD)
	900	0.8	0.375	70T, 10F, 20a-C	30T(ID), 40T(OD), 125F
	1000	0.8	4.200	25F, 5S, 70a-C	100F
FcPhH (2.5 *wt.%*)	800	0.8	0.300	85T, 10F, 5a-C	20T(ID), 50T(OD), 120F
	900	0.8	1.254	40T, 50F, 10a-C	15T(ID), 60T(OD), 160F
	1000	0.8	2.605	5T, 5F, 10S, 80a-C	55T(ID), 85T(OD), 170F
FcPhH (5.0 *wt.%*)	800	0.8	0.305	80T, 20a-C	25T(ID), 45T(OD)
	900	0.8	1.264	30T, 50F, 20a-C	10T(ID), 40T(OD), 120F
	1000	0.8	2.701	5T, 5F, 5S, 85a-C	10T(ID), 35T(OD), 110F
FcPhOH (2.5 *wt.%*)	800	0.8	0.050	70T, 10F, 10S, 10a-C	20T(ID), 40T(OD), 125F
		0.2	0.210	20T, 50F, 30a-C	15T(ID), 50T(OD), 135F
	900	0.8	0.250	50T, 50a-C	25T(ID), 35T(OD)
		0.2	1.300	15T, 50F, 5S, 30a-C	15T(ID), 40T(OD), 140F
	1000	0.8	0.260	40F, 40S, 20a-C	135F
		0.2	1.670	20F, 30S, 50a-C	140F

Table 8.1 continued

Catalyst	Temp. (°C)	Injection flow rate (ml/min)	Yield (g)	SCNMs formed (%)	Mean CNTs and CFs diameters (nm)
$FcPhCOCH_3$ (2.5 *wt.%*)	800	0.8	0.015	10T, 40F, 30S, 20a-C	15T(ID), 65T(0D) 100F
	900	0.8	0.926	20F, 30S, 50a-C	110F
	1000	0.8	3.065	10F, 10S, 80a-C	120F
FcPhBr (2.5 *wt.%*)	900	0.8	0.260	10T, 5F, 80S, 5a-C	15T(ID), 30(OD), 60F
	800	0.8	0.390	2T, 5F, 90S, 2T	20T(ID), 45(OD), 80F

T = CNTs, F = CFs, S = CSs, a-C = Amorphous carbon; T(ID) = Mean tube inner diameter; T(OD) = Mean tube outer diameter.

The use of $FcPhCOCH_3$ (2.5 *wt.%*) as catalyst gave MWCNTs at 800 °C in very low yield (Table 8.1). The mean internal diameter of 15 nm and outer diameter of 65 nm were similar to those found when FcH was used as catalyst. Fig. 8.3a depicts TEM micrographs of the MWCNTs observed. The mean length of the tubes was observed to be 2.5 – 3.0 μm. A large amount of amorphous carbon and fused CSs with typical diameters in the range of 0.8 μm to 1.50 μm were obtained at 1000 °C (Fig. 8.3b).

The use of FcPhBr (2.5 *wt.%*) in the synthesis of CNTs resulted in the production of 90% spheres and < 2% small diameter tubes even at a temperature of 800 °C. Thus the presence of the Br leads to sphere formation rather than CNT or amorphous carbon production.

Reactions were also attempted in which FcH and PhX (X = OH, OMe, Br) were used in a 1:1 molar ratio (Table 8.2). A comparison of the data in Table 8.1 with this data (Table 8.2) permits an evaluation of the effect of proximity of the Fe catalyst to the heteroatom substituent to be

established [35]. Comparative reactions were carried out at 900 ^{o}C at a flow rate of 0.8 ml/min. In every instance, yields for the FcH/PhX mixture were lower. However, the type of SCNM formed varied - more tubes were formed using the FcH/PhX mixture than with FcPhX (see Fig. 8.3).

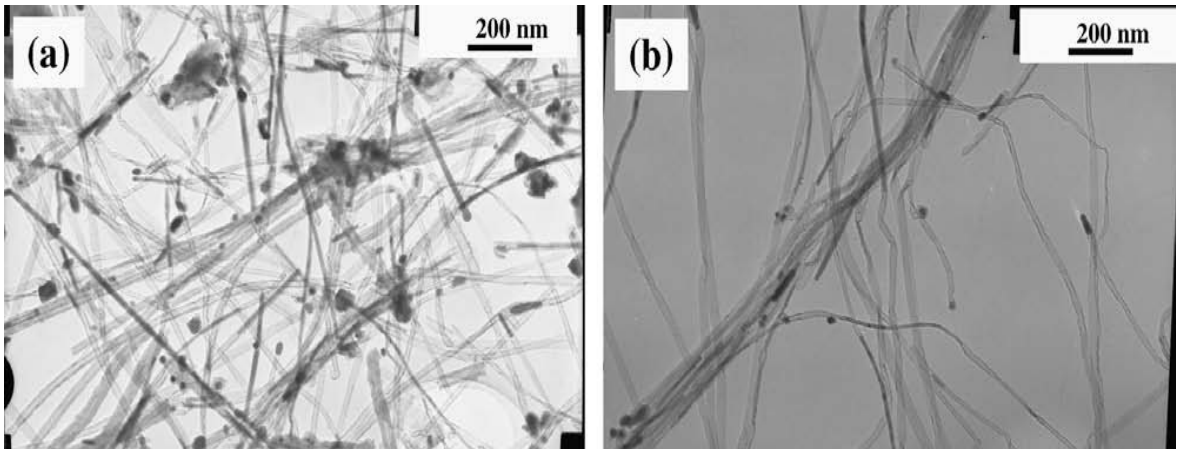


Fig. 8.3. TEM pictures of CNTs produced from the pyrolysis of FcPhBr (2.5 *wt.%*) at 900 ^{o}C.

Table 8.2. Summary of the yield and size distribution of SCNMs produced from mixtures of ferrocene and *para*-substituted phenyls in toluene under a constant flow rate of 100 ml/min of 5% H_2 in argon (v/v) at 900 ^oC.

Catalyst	Temp. (^oC)	Injection flow rate (ml/min)	Yield (g)	SCNMs formed (%)	Mean CNTs and CFs diameters (nm)
FcH (2.5 *wt.%*)	900	0.8	0.375	70T, 10F, 20a-C	30T(ID), 40T(OD), 125F
FcH/Ph (2.5 *wt.%*)	900	0.8	0.125	98S, 2T	30T(ID), 50(OD)
FcH/$PhCOCH_3$ (2.5 *wt.%*)	900	0.8	0.315	70T, 25F, 5a-C	35T(ID), 50T(OD), 110F
FcH/PhBr (2.5 *wt.%*)	800	0.8	0.295	95S, 5a-C	-

T = CNTs, F = CFs, S = CSs, a-C = Amorphous carbon; T(ID) = Mean tube inner diameter; T(OD) = Mean tube outer diameter. Fc/PhX Molar Ratio = 1:1.

8.3.2 TGA analysis

TGA studies were carried out to study the thermal stability of the unpurified SCNM mixtures produced by heating the samples at elevated temperatures in air at a constant rate. In all cases the TGA profiles showed that the products commenced decomposition at T > 500 ^oC. In every instance about 5 – 10% residue was observed in the TGA profile at T > 700 ^oC; due to the presence of iron oxide (Fig. 8.4). The TGA data for reactions performed at 900 ^oC are shown in Fig. 8.4. The TGA curves reveal that SCNMs grown from $FcPhCOCH_3$ are thermally more stable than those grown from all the other organometallic complexes (FcH, FcPhOH, $FcPhNH_2$) decomposing at 590 ^oC (*e.g.* compared to 550 ^oC for SCNMs produced from FcH). The SCNMs

obtained from FcPhOH gave the thermally least stable materials that commenced decomposing at lower temperatures (500 ^{o}C). This effect is attributed to the nature of the carbon products in the mixture. Generally, samples containing more amorphous carbon and CSs tend to lose weight at much lower temperatures than those containing more CNTs and CNFs.

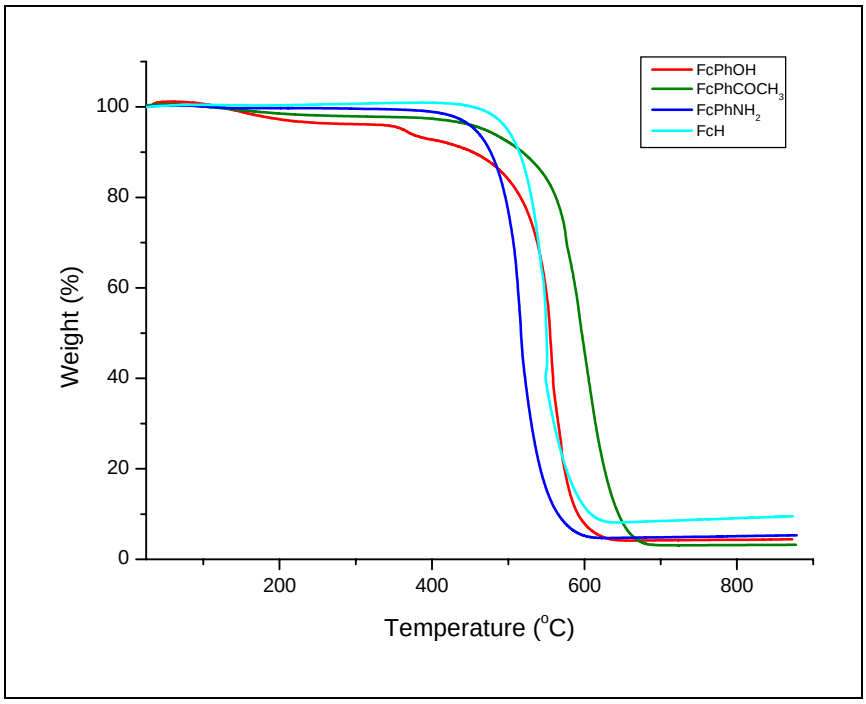


Fig. 8.4. TGA curves of CNTs grown from different arylferrocenes (2.5 *wt.%*) at 900 ^{o}C.

8.3.3 Raman spectroscopy studies

The Raman spectra for all the unpurified samples showed the presence of two major peaks: a G-band at approximately 1590 cm^{-1} originating from the Raman active E2g mode and a D-band at around 1350 cm^{-1} known as the disorder-induced band. The Raman spectra of SCNMs produced from a range of catalysts at 900 ^{o}C is depicted in Fig. 8.5. The I_D/I_G ratio gives a measure of the extent of disorder in the nanomaterials. For example, a higher I_D/I_G ratio implies more disorder within the CNTs, while lower ratios imply less disorder.

Table 8.3. D-and G-band positions and I_D/I_G ratios of SCNMs grown from different aryl ferrocenes.

Entry	Catalyst (2.5 *wt.%*)	D-band (cm^{-1})	G-and (cm^{-1})	I_D/I_G Ratio
1	FcH	1356	1587	0.63
2	$FcPhCOCH_3$	1334	1590	0.69
3	FcPhOH	1367	1602	0.83
4	FcPhBr	1349	1600	0.89
5	$FcPhNH_2$[1]	1364	1587	0.97

[1] ref. 35

The SCNMs grown from both FcH and $FcPhCOCH_3$ demonstrate low I_D/I_G ratios (0.63 and 0.69, respectively) while FcPhOH synthesised SCNMs show more disorder (0.83; Table 8.3). This data corresponds with the TGA data since CNTs derived from FcH and $FcPhCOCH_3$ are more stable (*i.e.* graphitic) than those produced from FcPhOH. Interestingly the Raman data obtained for SCNMs produced from FcPhX with X = NH_2 [35] gave an even higher I_D/I_G ratio; this is readily explained by the doping of C by N in the SCNMs.

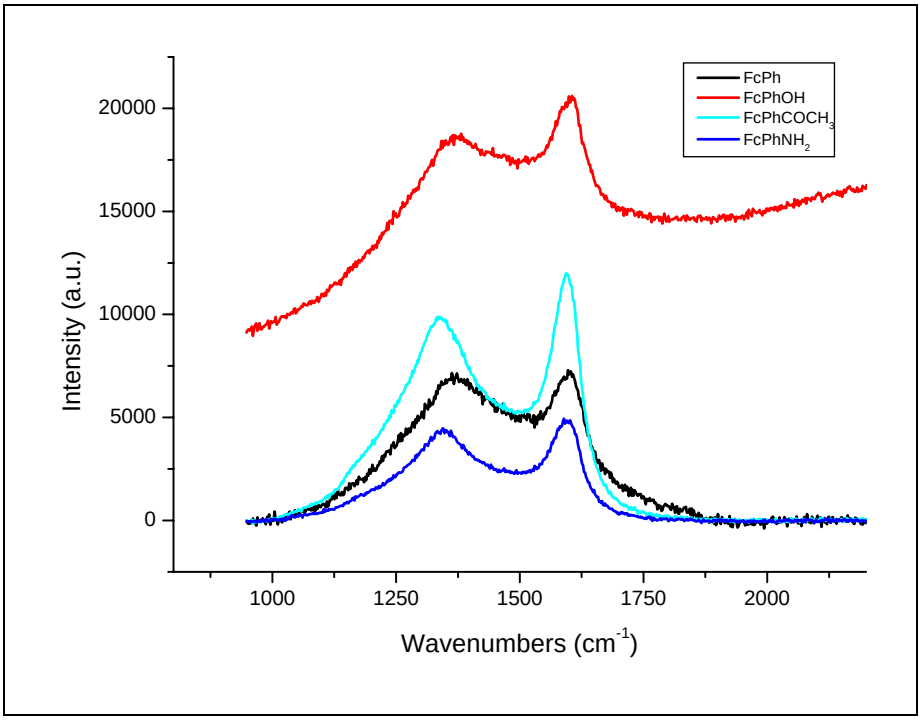


Fig. 8.5. Raman spectra of CNTs grown from different arylferrocenes (2.5 *wt.%*) at 900 ^{o}C.

8.3.4 Mechanism of catalyst deactivation

The mechanism by which CFs, CNTs and CSs are produced in the presence of ferrocene has been well documented [30]. The Fe acts as a catalyst for C growth to form CNTs (or CNFs if the Fe particles are big) while the FcH plays little or no role in CNS growth [28]. This information provides the basis for establishing the impact of ferrocene ring substituents on SCNM yield and morphology. The effect of varying the arylferrocenes on the production of SCNMs in this study revealed the following:

(i) The total yield of carbonaceous material for all catalysts increased with temperature.

(ii) As the temperature increased the CNT product yield decreased while either the CNS or amorphous carbon content increased.

(iii) The presence of 'O' containing *para*-substituents (-OH, -$COCH_3$) gave lower yields of all SCNMs compared to the other arylferrocenes.
(iv) The presence of Br generates more spheres than are generated from the other aryl substituted ferrocene catalysts. The CNTs produced from the X = Br catalyst had very narrow diameters.
(v) The proximity of the heteroatom substituent to the iron catalyst impacts on the SCNMs produced (compare results in Tables 8.1 and 8.2).

Points (i) and (ii) are expected results and are consistent with the behaviour of Fe catalyst systems. Points (iii) and (iv) reveal that the ability of Fe to act as a catalyst is modified by the presence of O and Br.

8.3.4.1 Effect of 'O'

In both studies the yield of SCNMs is reduced, relative to FcH. This indicates that the O poisons the catalyst. This is unexpected as there are many studies that indicate that O assists in cleaning CNTs. This is achieved by reaction of reactive (non graphitic) carbon with oxygen [36]. It is also clear that the experiments using FcPhX (X = OH and $COCH_3$) give different results. The presence of the OH results in the production of very low yields of all SCNMS at all temperatures. Further, much less amorphous carbon is produced when OH is present (relative to the other catalysts).

8.3.4.2 Effect of 'Br'

The Br has a dramatic effect on the formation of SCNMs. Poor yields are noted and a predominance of spheres are to be seen. This is reminiscent of studies with ferrocene at high temperatures. The data suggest that the Br destroys the catalytic activity of the Fe. Similar effects

have been observed when $CpFe(CO)_2I$ was used as a catalyst [37]. In these reactions the I poisoned the catalyst.

Point (v) is consistent with some related studies from our group [35]. In this study the influence of NH_2 groups was investigated – FcPhX and FcH/PhX mixtures were compared. It was observed that the Fe catalyst atoms interacted with both carbon and heteroatoms in the gas phase. Further, the closer the Fe and the heteroatom were to each other in the gas phase, the larger the impact of the heteroatom. A similar result was observed here for both O and Br atoms.

This information can be explained by the following mechanism. At the high temperatures used the catalysts and reagents decompose into radicals, atoms and ions. The type and concentration of these gas phase species will vary depending on the catalysts used. The Fe catalyst interacts with these species to generate the SCNMs that are produced. The data suggest that Br ions/radicals react with Fe to form 'FeBr' species that are not catalytically active and thus CSs are preferentially produced. In contrast Fe reacts with O containing ions/radicals to form 'FeO' species. These species react differently to the 'FeBr' species and generate more amorphous carbon. Both the 'Br' and 'O' produced in this study poison CNT growth.

8.4 Conclusions

In this study we have shown that the role of *para*-substituted ferrocene complexes is to provide a source of metal, carbon and heteroatom (O or Br) radicals/atoms/ions. The toluene also provides an extra source of carbon. This mixture of radicals/atoms/ ions can act as a precursor for the production of SCNMs. Not unexpectedly, the heteroatoms impact on the catalyst activity and selectivity and thus influence the yields and morphologies of the resulting SCNMs. The overall finding is that the presence of Br and O in these studies significantly reduces CNT growth.

References

1. I. Martin-Gullon, J. Vera, J.A. Conesa, J.L. Gonza´lez, C. Merino, Carbon 44 (2006) 1572.

2. J.I. Pascual, J. Me´ndez, J. Go´mezHerrero, A.M. Baro, N. Garcia, U. Landman, W.D. Luedtke, E.N. Bogachek, H.P. Cheng, Science 267 (1995) 1793.

3. P.G. Collins, A. Zettl, H. Bando, A. Thess, R.E. Smalley, Science 278 (1997) 100.

4. X.L. Dong, Z.D. Zhang, S.R. Jin, W.M. Sun, X.G. Zhao, Z.J. Li, Y.C. Chuang, J. Mater. Res. 14 (1999) 1782.

5. Z.D. Zhang, J.G. Zheng, I. Skorvanek, G.H. Wen, J. Kovac, F.W. Wang, J.L. Yu, Z.J. Li, X.L. Dong, S.R. Jin, W. Liu, X.X. Zhang, J. Phys.: Condens. Mat. 13 (2001) 1921.

6. P. Calvert, Nature 399 (1999) 210.

7. P.M. Ajayan, L.S. Schadler, C. Giannaris, A. Rubio, Adv. Mater. 12 (2000) 750.

8. P.M. Ajayan, Chem. Rev. 99 (1999) 1787.

9. R.H. Baughman, A.A. Zakhidov, W.A. De Heer, Science 297 (2002) 797.

10. V.N. Popov, Mater. Sci. Eng. R 43 (2004) 61.

11. (a) S.J. Trans, A.R.M. Verschueren, C. Dekker, Nature 393 (1998) 49;

(b) T. Rueckes, K. Kim, E. Joselevich, G.Y. Tseng, C.-L. Cheung, C.M. Lieber, Science 289 (2000) 94;

(c) A. Bachtold, P. Hadley, T. Nakanishi, C. Dekker, Science 294 (2001) 1317;

(d) W. Liang, M. Bockrath, D. Bozovic, J.H. Hafner, M. Trinkham, H. Park, Nature 411 (2001) 665.

12. (a) H.-M. Cheng, Q.-H. Yang, C. Liu, Carbon 39 (2001) 1447;

(b) A. Chambers, C. Park, R.T.K. Baker, N.M. Rodriguez, J. Phys. Chem. B 102

(1998) 4253;

(c) C. Park, P.E. Anderson, A. Chambers, C.D. Tan, R.J. Hidalgo, N.M. Rodriguez, J. Phys. Chem. B 103 (1999) 10572.

13. M.C. Bahome, L.L. Jewell, D. Hildebrandt, D. Glasser, N.J. Coville, Appl. Catal. A 287 (2005) 60.

14. T. Guo, P. Nikolaev, A. Thess, D.T. Colbert, R.E. Smalley, Chem. Phys. Lett. 243 (1995) 49.

15. W.K. Maser, E. Munoz, A.M. Benito, M.T. Martnez, G.F. de la Fuente, Y. Maniette, E. Anglaret, J.L. Sauvajol, Chem. Phys. Lett. 292 (1998) 587.

16. S. Iijima, T. Ichihashi, Nature 363 (1993) 603.

17. D.S. Bethune, C.H. Kiang, M.S. de Vries, G. Gorman, R. Savoy, J. Vazquez, R. Beyers, Nature 363 (1993) 605.

18. J.H. Hafner, M.J. Bronikowski, B.R. Azamiam, P. Nikolaev, A.G. Rinxler, D.T. Colbert, R.E. Smalley, Chem. Phys. Lett. 296 (1998) 195.

19. B. Kitiyanan, W.E. Alvarez, J.H. Harwell, D.E. Resasco, Chem. Phys. Lett. 317 (2000) 497.

20. W. Z Li, S.S. Xie, L.X. Qian, B.H. Chang, B.S. Zou, W.Y. Zhou, R.A. Zhao, G. Wang, Science 274 (1996) 1701.

21. (a) R. Andrews, D. Jacques, A.M. Rao, F. Derbyshire, D. Qian, X. Fan, E.C. Dickey, J. Chen, Chem. Phys. Lett. 303 (1999) 467;

(b) C.J. Lee, K.H. Son, J. Park, J.E. Yoo, Y. Huh, J.Y. Lee, Chem. Phys. Lett. 338 (2001) 113.

22. (a) V.O. Nyamori, N.J. Coville, Organometallics 26 (2007) 4083;

(b) D. Jain, A. Winkelm, R. Wilhelm, Small 2 (2006) 752;

(c) J. Liu, M. Shao, Q. Xie, L. Kong, W. Yu, Y. Qian, Carbon 41 (2003) 2101;

(d) M. Laskoski, W. Steffen, J.G.M. Morton, M.D. Smith, U.H.F. Bunz, J. Am. Chem. Soc. 124 (2002) 13814;

(e) B. El Hamaoui, L. Zhi, J. Wu, U. Kolb, K. Müllen, Adv. Mater 17 (2005) 2957;

(f) L. Zhi, T. Gorelik, R. Friedlein, J. Wu, U. Kolb, W.R. Salaneck, K. Müllen, Small 1 (2005) 798;

(g) J. Wu, B. El Hamaoui, J. Li, L. Zhi, U. Kolb, K. Müllen, Small 1 (2005) 210;

(h) S. Liu, X. Tang, Y. Mastai, I. Felner, A. Gedanken, J. Mater. Chem. 10 (2000) 2502;

(i) C. Wu, X. Zhu, L. Ye, C. OuYang, S. Hu, L. Lei, Y. Xie, Inorg. Chem. 45 (2006) 8543;

(j) P.I. Dosa, C. Erben, V.S. Iyer, K.P.C. Vollhardt, I.M. Wasse, J. Am. Chem. Soc. 121 (1999) 10430;

(k) V.S. Iyer, K.P.C. Vollhardt, R. Wilhelm, Angew. Chem., Int. Ed. 42 (2003) 4379.

23. (a) R. Kamalakaran, M. Terrones, T. Seeger, P. Kohler-Redlich, M. Rühle, Y.A. Kim, M. Endo, Appl. Phys. Lett. 77 (2002) 3385;

(b) A. Cao, L. Ci, G. Wu, B. Wei, C. Xu, J. Liang, D. Wu, Carbon 39 (2001) 152;

(c) E.C. Dickey, C.A. Grimes, M.K. Jain, K.G. Ong, D. Qian, P.D. Kichambare, R. Andrews, D. Jacques, Appl. Phys. Lett. 79 (2001) 4022;

(d) M. Mayne, N. Grobert, M. Terrones, R. Kamalakaran, M. Rühle, H.W. Krato, D.R.M. Walton, Chem. Phys. Lett. 338 (2001) 101;

(e) C. Singh, M. Shaffer, I. Kinloch, A. Windle, Physica B 323 (2002) 339;

(f) B. Wei, R. Vajtai, Y.Y. Choi, P.M. Ajayan, Nano Lett. 2 (2002) 1105;

(g) C. Singh, M.S.P. Shaffer, A.H. Windle, Carbon 41 (2003) 359.

24. (a) H. Hou, Z. Jun, F. Weller, A. Greiner, Chem. Mater. 15 (2003) 3170;

(b) J. Liu, M. Shao, Q. Xie, L. Kong, W. Yu, Y. Qian, Carbon 41 (2003) 2101;

(c) F. Rohmund, L.K.L. Falk, E.E.B. Campell, Chem. Phys. Lett. 328 (2000) 369.

25. (a) K. Awasthi, A.K. Singh, O.N. Srivastava, J. Nanosci. Nanotechnol. 3 (2003) 540;

(b) J.H. Hafner, M.J. Bronikowski, B.R. Azamian, P. Nikolaev, A.G. Rinzler, D.T. Colbert, K.A. Smith, R.E. Smalley, Chem. Phys. Lett. 296 (1998) 195.

26. (a) K.M. Samant, S.K. Haram, S. Kapoor, Pramana-J. Phys. 68 (2007) 51;

(b) Y.-Y. Fan, F. Li, H.-M. Cheng, G. Su, Y.-D. Yu, Z.-H. Shen, J. Mater. Res. 13 (1998) 2342;

(c) S. Bai, F. Li, Q.H. Yang, H.-M. Cheng, J.B. Bai, Chem. Phys. Lett. 376 (2003) 83;

(d) M. Mayne, N. Grobert, M. Terrones, R. Kamalakaran, M. Rühle, H.W. Kroto, D.R.M. Walton, Chem. Phys. Lett. 338 (2001) 101.

27. (a) S. Huang, X. Cai, C. Du, J. Liu, J. Phys. Chem. 107 (2003) 13251;

(b) P. Nikolaev, M.J. Bronikowski, R.K. Bradley, F. Rohmund, D.T. Colbert, K.A. Smith, R.E. Smalley, Chem. Phys. Lett. 313 (1999) 91.

28. X.Y. Liu, B.C. Huang, N.J. Coville, Carbon 40 (2002) 2791.

29. M.S. Mohlala, X.-Y. Liu, N.J. Coville, J. Organomet. Chem. 691 (2006) 4768.

30. V.O. Nyamori, S.D. Mhlanga, N.J. Coville, J. Organomet. Chem. 693 (2008) 2205.

31 (a) T.M. Keller, M. Laskoski, S.B. Qadri, J. Phys. Chem. C 111 (2007) 2514;

(b) M. Laskoski, T.M. Keller, S.B. Qadri, Carbon 45 (2007) 443;

(c) T.M. Keller, S.B. Qadri, Chem. Mater. 16 (2004) 1091;

(d) M.S. Mohlala, X.-Y. Liu, J.M. Robinson, N.J. Coville, Organometallics 24 (2005) 972;

(e) M.S. Mohlala, X.-Y. Liu, M.J. Witcomb, N.J. Coville, Appl. Organometal. Chem. 21 (2007) 275.

32. (a) T. Lanez, P.L. Pauson, J. Chem. Soc., Perkin Trans. 1 (1990) 2417;

(b) G.D. Broadhead, P.L. Pauson, J. Chem. Soc. (1955) 367.

33. C. Imrie, C. Louber, P. Engelbrecht, C.W. McCleland, J. Chem. Soc., Perkin Trans. 1 (1999) 2513.

34. A.N. Nesmeyanov, E.G. Perevalova, R.V. Golovnya, L. Shilovtseva, Dokl. Akad. Nauk SSSR 102 (1955) 535.

35. E.N. Nxumalo, V.O. Nyamori, N.J. Coville, J. Organomet. Chem. 693 (2008) 2942.

36. L.F. Su, J.N. Wang, F. Yu, Z.M. Sheng, H. Chang, C. Pak, Chem. Phys. Lett. 420 (2006) 421.

37. M.S. Mohlala, N.J. Coville, J. Organomet. Chem. 692 (2007) 2965.

Chapter 9

[7]Nitrogen doping of CVD multi-walled carbon nanotubes: Observation of a large *g*-shift

9.1 Introduction

Doping of carbon nanotubes (CNTs) with a heteroatom (*e.g.* nitrogen, boron) has been shown to result in enhanced electronic properties, chemical reactivity, and mechanical properties of the CNTs [1-8]. Nitrogen doped CNTs (N-CNTs) have in recent times received considerable attention due to the superior properties they exhibit over their undoped counterparts (pristine CNTs). They have been exploited for possible use in electronic devices [8-9], as catalyst supports [10-11], for chemical and biological applications that require complex functional groups on the surface of the CNTs [12-14], as components for gas sensors [15-16], and in field emission devices [8,17].

[7] S.D. Mhlanga, E.N. Nxumalo, N.J. Coville, S.V. Vallabhapurapu, *Materials Chemistry and Physics* (2010), *submitted*

Many reports have shown that the N-CNTs are generally characterized by bamboo-like compartments in their wall structure as shown by transmission electron microscopy (TEM) and Raman spectroscopy studies [18-19] and they are readily functionalized compared to pristine CNTs [4,20]. N-CNTs are usually synthesized using the catalytic chemical vapour deposition (CCVD) process, which involves the molecular decomposition of a carbon- and nitrogen-containing hydrocarbon in the presence of a desirable metal catalyst [4]. Other methods that have been used to synthesize N-CNTs include plasma enhanced CVD [21], laser ablation [22], arc discharge [23] and autoclave reactions [22] but those methods have been used less frequently.

There is now overwhelming evidence that N doping in CNTs can effect both electronic and magnetic properties of the doped carbons [17,25,26]. Ma *et al.* [25] studied the atomic, electronic, and magnetic properties of N impurities in graphite and CNTs. They observed that substitutional N atoms (graphitic N) in both graphite and CNTs do not support a magnetic moment. They also concluded that N atoms on the surface of the graphite and CNTs (molecular N) produced localized magnetic moments [25]. It was reported that nitrogen addition into CNTs changed the energy levels of localized states, with a shift towards the Fermi level [17]. Further, coupled states were created with mixed properties of localized and extended states [17]. The role of N adatoms in graphite and CNTs has been well studied by Ma *et al.* [25]. N adatoms form bridge-like structures, giving rise to sp^3 hybridization of C-atoms and the structures are reported to have magnetic moments in graphite [25]. In the case of CNTs the magnetic moment was attributed to the p-orbital of the N adatom [25]. Also, substitutional N impurities create magnetic defect complexes [25].

With this kind of rich physics involving electronic and magnetic property modifications in N-doped CNTs, N-CNT system has become a very attractive system to probe with electron spin resonance (ESR) spectroscopy. ESR spectroscopy is a powerful tool to study and probe the electronic properties and defects in CNTs [27-35]. ESR studies have often been conducted to

identify conduction electrons in CNTs and also to predict whether metallic or narrow gap semiconducting tubes are present in samples [36]. ESR signals have also been identified in oxidized CNTs upon chemical treatment because of the presence of conducting electrons [37]. It has been reported that the use of inert gases (He and Ar) give variations in ESR spectral line shape, line widths and *g*-values [38]. In this communication, we report on the ESR measurements in N-doped MWCNTs. In particular we report on the observation of a large *g*-factor shift in N-doped MWCNTs.

9.2 Experimental

9.2.1 Synthesis and characterization of MWCNTs and N-CNTs

Both N-CNTs and MWCNTs were synthesized using a modified CVD floating catalyst setup [4]. The N-CNTs were synthesized by the decomposition of a ferrocene (FcH)/triethylamine/(TEA)/toluene solution mixture that contained 10 *wt.%* FcH, and 2, 3, 5, or 10 *wt.%* TEA in toluene. TEA was the N source while the FcH acted as the catalyst and toluene as the main carbon source. In another experiment, 10 *wt.%* acetonitrile (CH_3CN) or 5% dimethylamine (DMA) was used as a nitrogen source with FcH and toluene. The MWCNTs were also synthesized using the same experimental setup and conditions as the CNTs produces in the absence of a nitrogen containing solvent.

Typically the solution, placed in a 20 ml syringe, was injected into the quartz tube reactor heated to 900 °C through a quartz water cooled system, using an electronically controlled SAGE pump at a flow rate of 0.8 ml/min. Nitrogen gas (99.9%) or 5% H_2/Ar (AFROX; 100 ml/min) was used to remove air from the quartz tube reactor and was also used to transport the decomposed vapours through the reactor to an exhaust outlet. Once all of the solution had been injected into the furnace, which took about 25 min, the reactor was then allowed to cool and the carbonaceous

material was collected from the walls of the quartz tube. All reagents were used as commercially supplied (Sigma Aldrich).

The microstructure of the as synthesized samples were studied using a JEOL JEM-2100 high resolution transmission electron microscope (HRTEM), scanning electron microscopy (SEM) using a JEOL JSM-7500F field emission SEM and Raman spectroscopy (Horiba Jobin-Yvon HR800 UV micro-Raman spectrometer equipped with a liquid nitrogen cooled charge coupled device detector). Samples were measured after excitation with a laser wavelength of 514.5 nm.

9.2.2 ESR measurements

The ESR measurements were carried out with a JEOL spectrometer. The system was well calibrated. The measurements were carried out with a modulation field of 0.4 mT, 0.9 mW microwave power and a microwave frequency of 9 GHz. A clean quartz sample tube was used for these measurements of an appropriate amount of N-doped MWCNTs (200 mg). The measurements were carried out in the temperature range of 293 K to 400 K.

9.3 Results and discussion

9.3.1 Structural characterization of N-CNTs and MWCNTs

The SEM images of the N-CNTs and MWCNTs are shown in Fig. 9.1 (a) and 9.1 (b). The TEM images of the corresponding samples are shown in the figure inset. The TEM images showed that the N-CNTs possess ‘bamboo-like compartments’ in the wall structure. The presence of CNTs with compartments varied with the amount of N used in the starting solution. When less than 5% TEA was used, the resulting materials contained a mixture of MWCNTs (~ 90% rel. abundance) and N-CNTs (~ 10% rel. abundance) as determined by the presence of the bamboo structures.

When 10% TEA was used, the majority of the CNTs were N-CNTs with a bamboo structure (> 95).

The CNTs were obtained in high yields of up to 1.5 g per 20 ml injected solution and they possessed a narrow size distribution with outer diameter (OD), 30 - 50 nm. The undoped MWCNTs, were not as aligned as the N-CNTs. Rather, these were randomly oriented in a spaghetti-like fashion, with a more larger OD size range (30 – 80 nm). It was also observed that the MWCNTs contained some amorphous carbon (< 5%), which was not observed in the N-CNTs samples.

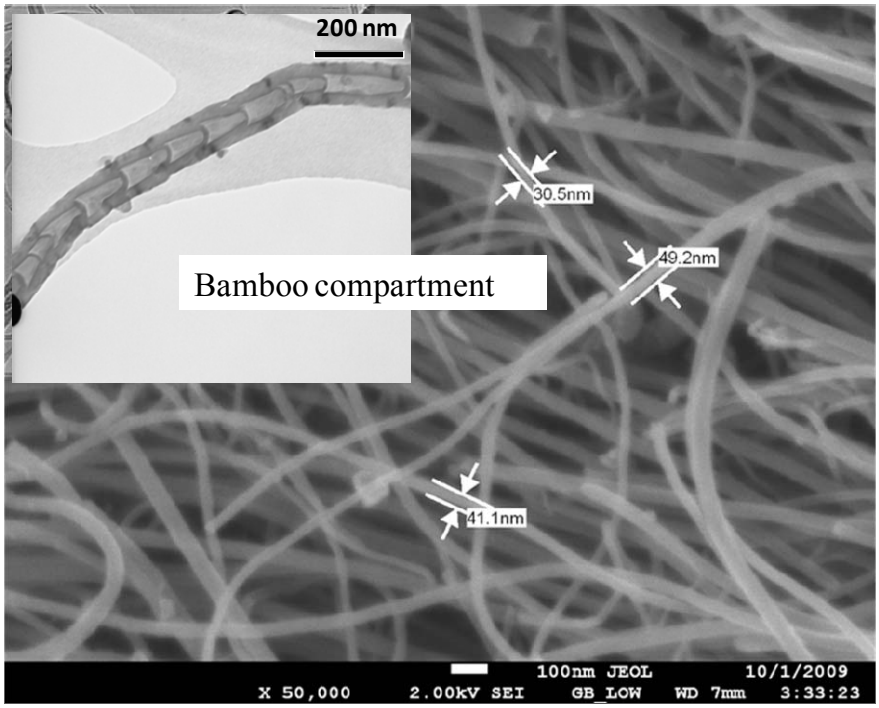


Fig. 9.1 (a). A SEM and TEM image (inset) of N-CNTs synthesized using a mixture of 10% FcH and 10% TEA in toluene.



Fig. 9.1 (b). A SEM and TEM image (inset) of MWCNTs synthesized using a mixture of 10% FcH in toluene.

The graphitic nature of the bulk samples of the MWCNTs and N-CNTs was studied using Raman spectroscopy (Fig. 9.2). The effect of nitrogen doping on the Raman spectra of multi-walled CNTs was recently studied by Bulusheva *et al.* [20]. Our observations differ with those of Bulusheva *et al.* [20]; the ratios between the D- and G- bands, suggest that the N-CNTs have more structural defects MWCNTs (0.85-0.96). Indeed, characterization of the CNTs using HRTEM supports this explanation. The graphite layers of the pristine CNTs are more ordered and have fewer defects. This is expected, since our own work shows the positive of this observation (more N lead to shorter, more disordered tubes with more defects) [4]. The surface of the N-CNTs is smoother while the MWCNTs possessed a high amount of detects on the wall structure.

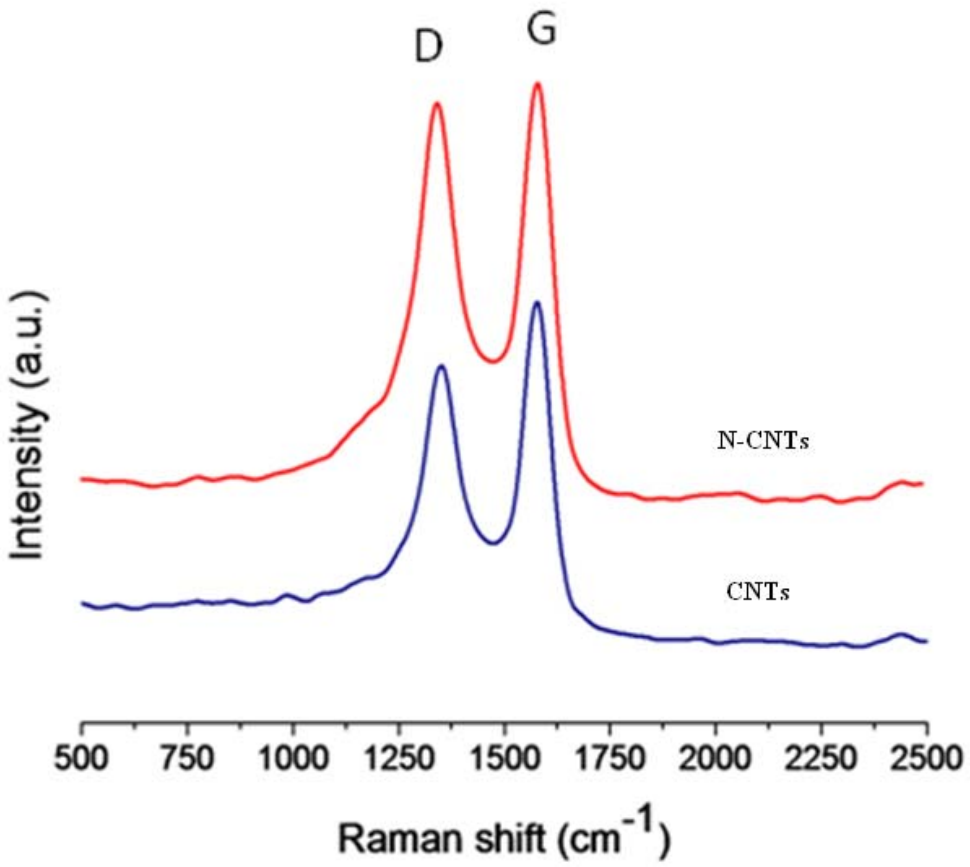


Fig. 9.2. Raman spectra of MWCNTs and N-CNTs showing the D- and G- bands (laser excitation 514 nm).

9.3.2 ESR analysis

In Fig. 9.3 we show ESR spectra of MWCNTs with different levels of N-doping. The relatively broad line spectrum obtained for the N-CNT samples is generally similar to that obtained for pristine CNTs and many other shaped carbon nanomaterials and is attributed to conduction electrons [39]. N-CNTs have a large paramagnetic peak superimposed on a broad background [40]. The strong paramagnetic signal is ascribed to the presence of substitutional N in the CNTs and an increase in N content resulted in a stronger paramagnetic signal [40]. In Fig. 9.4 the measured *g*-factor shifts (defined as measured *g*-factor – free electron g-factor) of N-doped MWCNTs and undoped MWCNTs are shown. The *g*-factor shift (or simply *g*-shift, Δg) is almost temperature independent for the (a) undoped MWCNTs and (b) N-CNTs synthesized using 10% TEA and 10% CH_3CN. The *g*-factor for the undoped MWCNT is closer to the free electron value. However, one can see a very large shift of *g*-factor for the N-CNTs tubes grown from 3% , 5% TEA , and 5% DMA. At room temperature the shifts are 0.22741, 0.30461 and 0.14644 for N-CNTs grown from 5% DMA and 3% TEA precusors, respectively. The *g*-shift rises beyond a characteristic temperature T^* in the 2%, 3%, 5% TEA and the 5% DMA samples. However a further increase of N-doping, for example 10% doping, brings the *g*-factor back closer to the undoped MWCNT values. This is the first report of such a large shift of *g*-factor in doped CNTs and the high temperature rise of the values beyond a characteristic temperature.

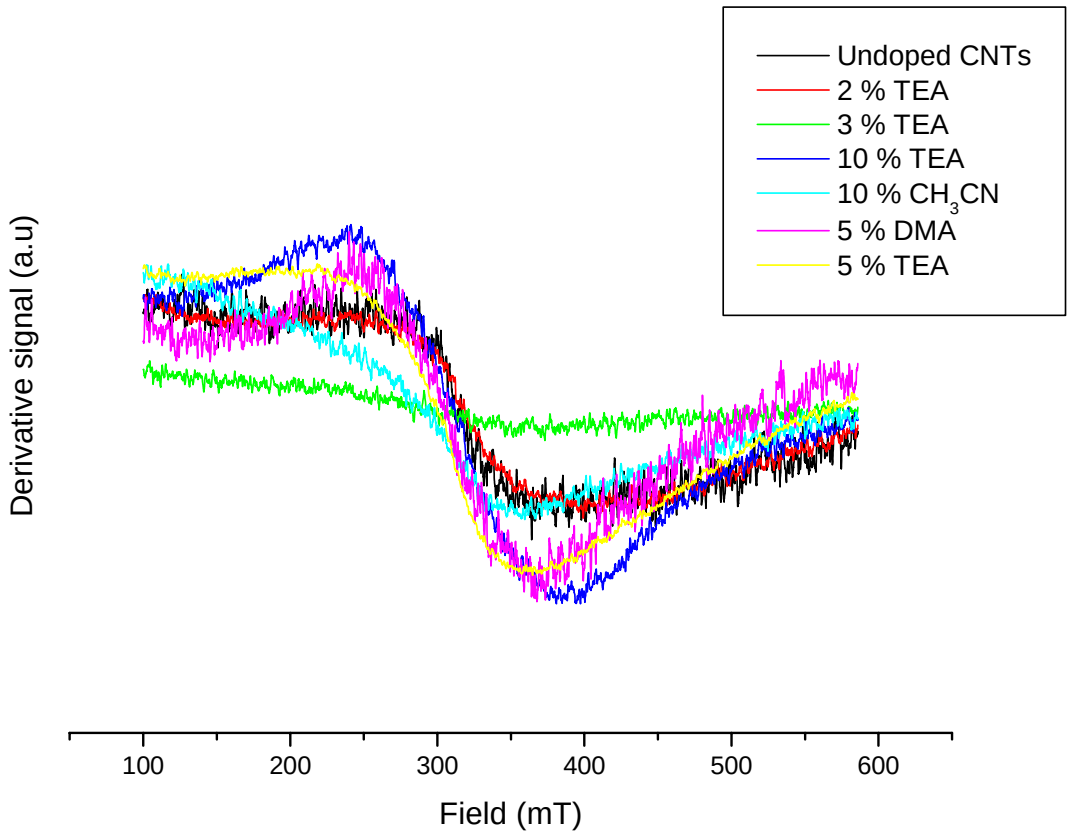


Fig. 9.3. ESR spectra of undoped and N-CNTs at 293 K. TEA = triethylamine, CH_3CN = acetonitrile, DMA = dimethylamine.

9.3.2.1 Models for the *g* factor

To fully investigate the role of N on the magnetic properties of CNTs the *g*-factor data was analysed in our N-CNT and CNT samples. Two approaches to model the *g*-factor shift were used.

(i) Elliott-Wagoner model

The magnitude of *g* shift from the free electron value has the general form

$$\Delta g \sim \lambda/\Delta E \qquad (1)$$

where Δg is the g shift, λ is the spin orbit coupling and ΔE is the energy separation of the states being mixed in by the L.S coupling [41].

If one neglects the shape of the bands, the g shift can be expressed in terms of the Fermi energy (ξ) measured relative to the band edge [41] since $\Delta g \sim \lambda/\xi$. In the case of graphite, with $\lambda \sim 0.0037$ eV and $\xi \sim 0.017$ eV Wagoner [41] has estimated the g shift to be ~ 0.2. This is a large value for a g shift. In fact the modification of the g-factor in graphite and graphite-like materials is particularly significant, since it is sensitive to the band structure details at the Fermi level [27]. In the case of pure CNTs the g-factor is close to the free electron value and is temperature independent. However, nitrogen doping can shift the Fermi level [17]. For example the Fermi level evaluated from the vacuum level is about -4.36 eV for the N-CNTs as compared to that of their undoped counterparts, which is about -4.53 eV [3]. Thus, there is a significant change in the Fermi level upon nitrogen doping. It is very tempting to attribute the observed large g-factor shift in our N-CNT samples to this possible Fermi level shift. However, the temperature dependence of the g shift in the Elliott-Wagoner model [41], is given by

$$\Delta g = (T_F/T)\,(\Delta g)_F \qquad (2)$$

where T_F is the degeneracy temperature as defined by Wagoner *et al.* [41] and $(\Delta g)_F$ is the value of Δg measured well below T_F. The g shift is thus inversely proportional to the temperature. However, our experimentally measured g shifts in all the N-CNT samples actually increase with increasing temperature in the range 293 K to 400 K. It is to be noticed that the temperatures are much higher than the typical T_F value ~ 200 K in graphite [41] and we assume that the value will

be similar in the CNTs. The linewidths observed for the N-CNTs are also much larger than the very narrow linewidths reported for pure graphite [41] and highly pure CNTs where linewidths do not exceed a few mT [30,33]. Therefore, the origin of the large *g* shifts in our N-CNT samples do not correlate with the Elliott-Wagoner model (spin-orbit coupling).

Another approach in which *g* shifts and their temperature dependence have been successfully treated in graphite is by an improved version of McClure-Fayet's theory [42,43] given by Stankowskii *et al.* [44]. In this approach, the temperature dependence of the α coefficient which is the 3d function with the π bond is considered. In this model, the *g* shift decreases with increasing temperature, again the opposite behaviour as compared to our g shift *vs* temperature values.

(ii) Exchange coupling and the Bottleneck model

In this model, the localized and itinerant spins are strongly coupled and a bottleneck regime is achieved when one of the spin systems dominates the overall behaviour. In the high temperature regime, conduction electron spins dominate while the localized spins dominate at low temperatures. In this regime, one can express the *g* factor as

$$g = (g_1 c/x_2 + g_2 T)/(c/x_2 + T) \qquad (3)$$

where g_1,g_2 are the *g* factors for localized spins and conduction spins respectively and x_1,x_2 are the corresponding susceptabilities.

This model gives the right temperature dependence for our N-CNTs samples. In the CNTs synthesized using 2%, 3% and 5% TEA, the *g*-shift shows a systematic decrease with

temperature. The shift is constant up to a certain characteristic temperature (T^*) and then beyond this temperature the *g*-shift increases with increasing temperature (see Fig. 5). A simulation study using equation (3) showed that an increasing *g*-shift with increasing temperature occurs when $g_2 > g_1$ and that the *g*-shift is independent of temperature when $g_2 = g_1$. A cross over temperature occurs when ($g_2 > g_1$) changes ($g_2 = g_1$). This temperature (T^*) should be characteristic of each doped sample and depends on doping levels. In some samples, the *g*-shift is independent of temperature in the measured range of temperatures (for example, N-CNTs grown from 10% TEA and 10% CH_3CN, and undoped CNTs). Within the above model, even when $g_2 = g_1$ the temperature beyond the characteristic temperature T^*. In the case of DMA sample the T^* could be much lower than room temperature. Such a characteristic temperature has been observed and is shown in Fig. 9.4. This is possible in our samples because the *g* shift measurements are in the high temperature range (293 K to 400 K). When $g_2 = g_1$ then *g* value does not change with temperature and the *g*-shift is also independent of temperature. It is suggested that at T^* these samples cross over from a regime where $g_2 = g_1$ to a regime $g_2 > g_1$.

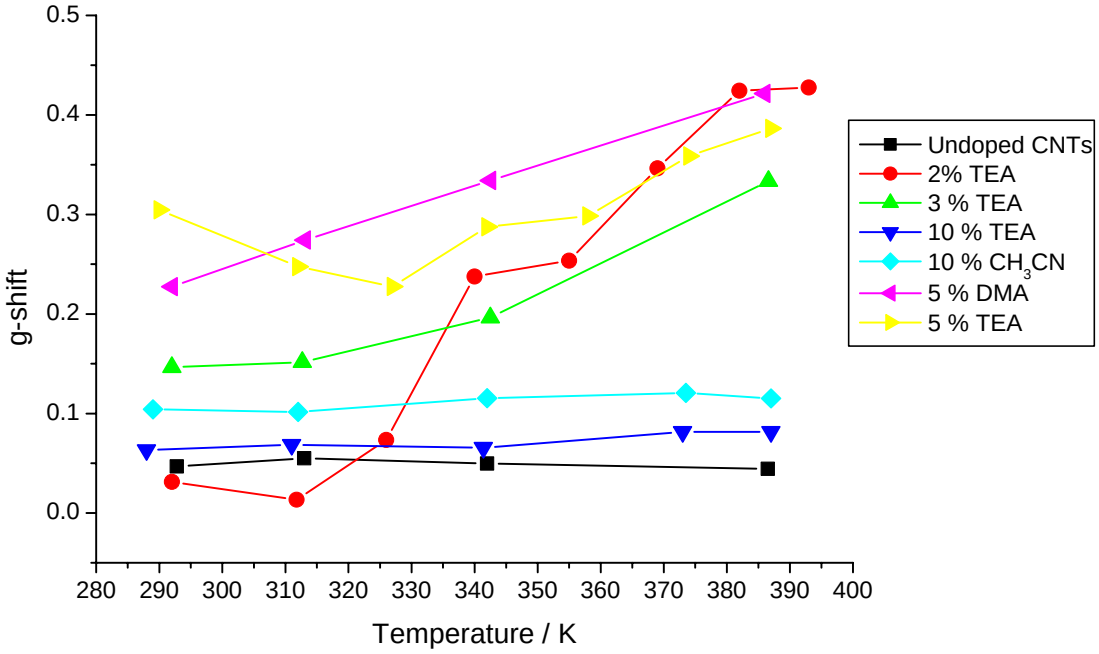


Fig. 9.4. *g*-shift values *vs* temperature of undoped and N-CNTs. TEA = triethylamine, CH_3CN = acetonitrile, DMA = dimethylamine.

9.3.2.2 Line widths

In Fig. 9.5 we show the measured line widths for our N-CNT samples. The linewidths are in general very large for both undoped CNT and N-CNT samples and they are of the order of kOe. These large linewidths indicate inhomogenieties in our CNT and N-CNT samples. Linewidths in CNTs have different temperature dependences arising from different origins. For example, Bando [32] reported that the line width temperature dependence changes from $T^{-1/2}$ to T^3 for CNTs before and after annealing respectively. The $T^{-1/2}$ dependence is due to scattering effects coming from lattice defects and impurities [33]. T^3 dependence is due to the scattering effect from the lattice vibration [33]. The linewidths in our undoped CNT and N-CNTs show temperature dependence (Fig. 9.5). The 5% DMA sample which shows a large *g*-shift and strong temperature dependence has a weak linewidth dependence on temperature. The undoped CNTs

also show weak linewidth temperature dependence. For the TEA samples the linewidths do increase with temperature. However, as the linewidths are very large, we can only conclude that the large linewidths of the order of kOe imply inhomogenieties in the samples. Further studies are currently underway to fully ascertain the mechanism behind this observation.

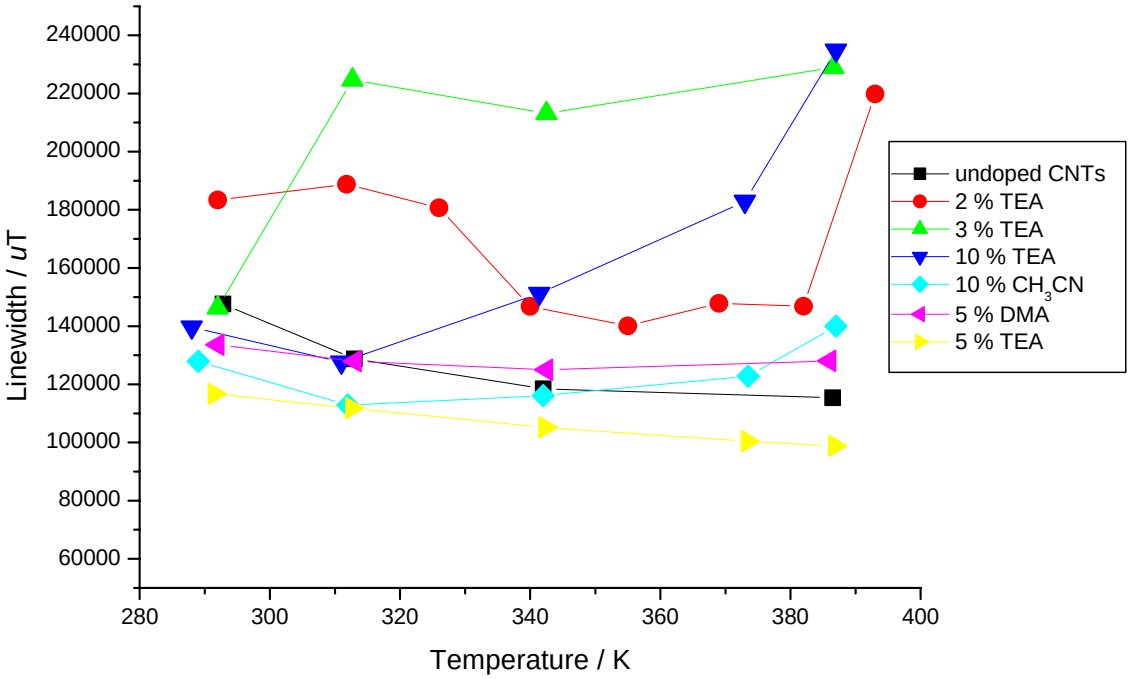


Fig. 9.5. Line width graphs for N-CNTs and MWCNTs at different temperatures. TEA = triethylamine, CH_3CN = acetonitrile, DMA = dimethylamine.

9.4 Conclusion

We have synthesized a range of N doped and undoped CNTs by the CVD method using common precursors. Variations in the CNT ESR spectral line shape, the *g*-factor shift and the line width at different temperatures were observed and are attributed to the presence of varying amounts of N in the CNTs. Generally, the undoped CNTs show a weak temperature dependence for their line

widths. A significantly large *g*-factor shift for the N-CNT tubes was observed and that can be explained by the Exchange coupling and Bottleneck models.

References

1. O. Stephen, P.M. Ajavan, C. Colliex, Ph. Redlich, J.M. Lambert, P. Bernier, P. Letin, Science 266 (1994) 1683.
2. R.B. Sharma, D.J. Late, D.S. Joag, A. Govindaraj, C.N.R. Rao, Chem. Phys. Lett. 428 (2006) 102.
3. C.P. Ewels, M. Glerup, J. Nanosci. Technol. 5 (2005) 1345.
4. E.N. Nxumalo, V.O. Nyamori, N.J. Coville, J. Organometal. Chem. 693 (2008) 2942.
5. V.O. Nyamori, S.D. Mhlanga, N.J. Coville, J. Organometal. Chem. 693 (2008) 2205.
6. L.S. Panchakarla, K.S. Subrahmanyam, S.K. Saha, A. Govindaraj, H.R. Krishnamurthy, U.V. Waghmare, C.N.R. Rao, Adv. Mater. 21 (2009) 4726.
7. J.Y. Yi, J. Bernholc, Phys. Rev. B. 47 (1993) 1708.
8. P. Ayala, R. Arenal, M. Rümmeli, A. Rubio, T. Pichler, Carbon 48 (2010) 575.
9. S.H. Lim, H.I. Elim, X.Y. Gao, A.T.S. Wee, W. Ji, J.Y. Lee, J. Lin, Phys. Review B. 73 (2006) 045402.
10. R. Chetty, S. Kundu, W. Xia, M. Brona, W. Schuhmann, V. Chirila, W. Brandl, T. Reinecke, M. Muhler, Electrochim. Acta 54 (2009) 4208.
11. F.R. García-García, J. Álvarez-Rodríguez, I. Rodríguez-Ramos, A. Guerrero-Ruiz, Carbon 48 (2010) 267.
12. J.C. Carrero-Sanchez, A.L. Elias, R. Mancilla, G. Arrellin, H. Terrones, J.P. Laclette, Nano. Lett. 6 (2006) 1609.
13. A.L. Elias, J.C. Carrero-Sanchez, H. Terrones, M. Endo, J.P. Laclette, M. Terrones, Small 3 (2007) 1723.

14. B. Fragneaud, K. Masenelli-Varlot, A. Gonzalez-Montiel, M. Terrones, J. Cavaille, Chem. Phys. Lett. 419 (2006) 567.
15. S. Peng, K. Cho, Nano Lett. 3 (2003) 513.
16. F. Villalpando-Paez, A. Romero, E. Munoz-Sandoval, L. Martinez, H. Terrones, M. Terrones, Chem. Phys. Lett. 386 (2004) 137.
17. H.-S. Ahn, K.-R. Lee, D.-Y. Kim, S. Han, Appl. Phys. Lett. 88 (2006) 093122L.
18. R. Droppa Jr., C.T.M. Ribeiro, A.R. Zanatta, M.C. dos Santos, F. Alvarez, Phys. Rev. B. 69 (2004) 045405.
19. J.W. Jang, C.E. Lee, S.C. Lyu, T.J. Lee, C.J. Lee, Appl. Phys. Lett. 84 (2004) 2877.
20. G. Bulusheva, A.V. Okotrub, I.A. Kinloch, I.P. Asanov, A.G. Kurenya, A.G. Kudashov, X. Chen, H. Song, Phys. Stat. Sol. (b) 245 (2008) 1971.
21. J.H. Yang, D.H. Lee, M.H. Yum, Y.S. Shin, E.J. Kim, C.-Y. Park, M.H. Kwon, C.W. Yang, J.-B. Yoo, H.-J. Song, H.-J. Shin, Y.-W. Jin, J.-M. Kim, Carbon 44 (2006) 2219.
22. D. Golberg, Y. Bando, L. Bourgeois, K. Kurashima, T. Sato, Carbon 38 (2000) 2017.
23. B. Wang, Y. Ma, Y. Wu, N. Li, Y. Huang, Y. Chen, Carbon 47 (2009) 2112.
24. X. Wu, Y. Tao, C. Mao, L. Wen, J. Zhu, Carbon 45 (2007) 2253.
25. Y. Ma, A.S. Foster, A.V. Krasheninnikov, R.M. Nieminen, Phys. Rev. B. 72 (2005) 205416.
26. J.R. Soto, J. Austrich, R.M. Valladares, A. Valladares, M.L. Marquina, R. Espejel, A. Calles, Rev. Mex. Fis. S53 (2007) 34.
27. F. Beuneu, C.L. Huillier, J.P. Salvetat, J. M. Bonard, L. Forro, Phys. Rev. B. 59 (1999) 5945.
28. A.K. Dhami, S. Bhat, A. Sharma, S.V. Bhat, Spectrochim. Acta, Part A 69 (2008) 1178.
29. H. Zhang, S. Lin, A. Wei, Y. He, X. Tang, X. Xue, L. Liang, C. Wu, J. Phys. Chem. Solids 61 (2000) 1123.
30. J. Giraudet, M. Dubois, D. Claves, J.P. Pinheiro, M.C. Schouler, P. Gadelle, A. Hamwi, Chem. Phys. Lett. 381 (2003) 306.
31. K. Shen, D.L. Tierney, T. Pietra, Phys. Rev. B. 68 (2003) 165418.
32. S. Bando, J. Appl Phys. 80 (1996) 1020.

33. H. Yokomichi, Vacuum 74 (2004) 677.
34. M. Chipara, J.M. Zaleski, D. Hui, C. Du, N. Pan, J. Poly. Sci. Part B: 43 (2005) 3406.
35. O. Chauvet, G. Baumgartner, M. Carrard, W. Bacsa, D. Ugarte, W.A. de Heer, L. Forro, Phys. Rev. B 53 (1996) 13996.
36. K. Tanaka, T. Sato, T. Yamabe, K. Okahara, K. Uchida, M. Yumura, H. Niino, S. Ohshima, Y. Kuriki, K. Yase, F. Ikazaki, Chem. Phys. Lett. 223 (1994) 65.
37. M. Kosaka, T.W. Ebbesen, H. Hiura, K. Tanigaki, Chem. Phys. Lett. 225 **(**1994) 161.
38. H. Zhang, S. Liu, A. Weic, Y. He, X. Tang, X. Xue, L. Liang, C. Wu, J. Phys. Chem. Solids 61 (2000) 1123.
39. M. Chipara, F. Iacomi, J.M. Zaleski, J.B. Bai, J. Optoelec, Adv. Mat. 8 (2006) 820.
40. N. Kunjuzwa, The synthesis of nitrogen doped carbon nanospheres and polythiophene/carbon sphere composites, M.Sc. Dissertation, University of the Witwatersrand, 2009.
41. G. Wagoner, Phys. Rev. 118 (1960) 647.
42. J.W. McClure, Y. Fayet, University Park Pennsylvania Pergamon (1962) 22.
43. K. Matsubara, T. Tsuzuka, K. Sugihara, Phys. Rev. B. 44 (1991) 11845.
44. J. Stankowski, S. Waplak, W. Bednarski, Solid State Commn. 115 (2000) 489.

Chapter 10

[8]Facile method towards the fabrication of gold/nitrogen doped carbon nanotube hybrids

10.1. Introduction

Carbon nanotubes (CNTs) have been considered for many applications because of their remarkable chemical and physical properties. To broaden these applications, researchers are investigating the possibility of attaching metal nanoparticles onto CNT surfaces for applications in catalysis, water treatment, solar cells and data storage. Metal/CNT hybrid nanostructures are fascinating structures because they combine the properties of both the metal nanoparticles (NPs) and CNTs to provide attractive hybrids with novel properties.

A wide range of metal/CNT hybrids have been synthesized over the past years. These include metals such as Pd, Pt, Rh, and Ru with the purpose of using them as catalysts or gas sensors [1]. For example, Pt/CNT catalysts have been synthesized in supercritical carbon dioxide using Pt(II)

[8] E.N. Nxumalo, A. Shaikjee, M. Mamo, N.J. Coville, Facile method towards the fabrication of gold/nitrogen doped carbon nanotube hybrids, *submitted (2010)*

acetylacetonate as metal precursor [2]. Further, Pt decorated CNTs for highly sensitive amperometric glucose sensing have also been fabricated [3]. Recently, Pt/CNT and Pt/carbon composites were prepared as electrocatalysts for oxygen reduction reaction in proton exchange membrane fuel cells [4]. CNTs decorated with Pd nanoparticles (Pd-NPs) were successfully tested for use in catalysis [5]. Ru-NPs supported on CNTs have been used as efficient catalysts for selective conversion of synthesis gas to diesel fuel [6]. Preparation of Pt-Ru bimetallic catalysts supported on CNTs has also been reported [7]. Reports on the production of Au/CNT nanohybrid materials have been presented [8-10].

Among all the metal NPs discussed above, Au-NPs are of great interest due to their high catalytic activity and their remarkable electronic and optical properties. Au is particularly important in the field of nanotechnology because it is a noble metal. Further, Au nanoparticles anchored in CNTs can be used in applications ranging from catalysis to electronic devices [11]. However, practical production of Au/CNTs requires the use of facile inexpensive methods.

A major difficulty associated with Au attachment onto CNTs relates to the sintering of the Au. This arises from the weak interaction between the Au and the CNT. This can be overcame by functionalizing the CNT or doping the CNT e.g. with nitrogen. Much research has been conducted on methods to produce Au/CNT hybrid materials [12-15] by first functionalizing the CNTs. However, there is a paucity of data on the attachment of Au-NPs onto nitrogen doped CNTs (N-CNTs). The methodology followed in the production of those Au/N-CNTs was not straightforward. The procedure either involved an N-CNT suspension mixed with a cationic polyelectrolyte and Au colloids [16] or sonicating N-CNT cups in DMF and reacting the suspension with an ester, followed by mixing with coated Au-NPs in a buffered aqueous glycerol solution [17].

In the present study, a facile method to attach gold nanoparticles to the surface N-CNTs is discussed. The procedure involved two steps: the surface functionalization of the N-CNTs using the 'Prato' reaction [18] followed by the formation of the Au/N-CNT hybrid nanostructures by means of sonication and characterization of Au/N-CNTs by transmission electron microscopy (TEM) and energy disperse X-ray (EDX) spectroscopy.

10.2. Experimental Section

10.2.1 Growth and purification of N-CNTs

A typical procedure for the preparation of N-doped CNTs entailed pyrolyzing ferrocene/pyridine mixtures (in toluene) at 800 ^{o}C, under a constant flow of 5% H_2/Ar (AFROX, v/v) [19]. The mixtures were injected into the chemical vapour deposition reactor to form N-doped CNTs (10 *wt.%* with respect to pyridine). Our previous work reveals that the N content for CNTs synthesized using this method ranges between 1 - 2 *at.%* [20]. Undoped CNTs were synthesized under the same conditions using ferrocene and toluene as precursors. The synthesized N-CNTs and undoped CNTs were then purified by refluxing in HCl (35%) at 80 ^{o}C for 24 h. Filtering and washing the resulting material with acetone and water (5 x 300 ml) and drying at 400 ^{o}C for 30 min yielded pure N-CNTs and CNTs.

10.2.2 Functionalization of N-CNTs

The Prato reaction was performed on the oxidized N-CNTs [19]. Typically, N-CNTs (100 mg) were suspended in 1,2-dichlorobenzene (50 ml) and sonicated for 30 min. To the suspension was added 2-thiophenecarboxyaldehyde (0.120 g, 0.98 mmol) with stirring. N-methylglycine (0.158 g, 1.9 mmol) was added to the reaction mixture in small portions over 5 days at 160 ^{o}C. After cooling, N-CNTs were filtered-off using 1 μm pore size membrane filter papers (Sigma Aldrich).

A black solid product was obtained after successive washing (with DMF, ethanol and acetone) and drying in vacuum for 48 h at 45 ^{o}C. The undoped CNTs were functionalized using a similar approach. The yields obtained were 0.152 g (42 %) (for undoped CNTs) and 0.170 g (46%) (for N-CNTs).

10.2.3 Synthesis of gold/CNT nanostructures

In a typical synthetic procedure, Prato functionalized N-CNTs (f-N-CNTs) (100 mg) were suspended in acetone (10 ml) and sonicated for 30 min in a beaker (solution A). In a separate beaker, $HAuCl_4$ (5 mg) were suspended in acetone for 15 min (solution B). Solution B was then added dropwise to solution A while stirring. The resulting mixture was sonicated for a further 30 min to yield Au/N-CNT hybrid nanostructures (Fig. 10.1). The CNT material obtained was dried in a rotatory evaporator to yield 180 mg of the product. Visualization of the solid materials obtained (both reactants and final products) was performed by TEM. All reagents were used as obtained commercially (Sigma Aldrich).

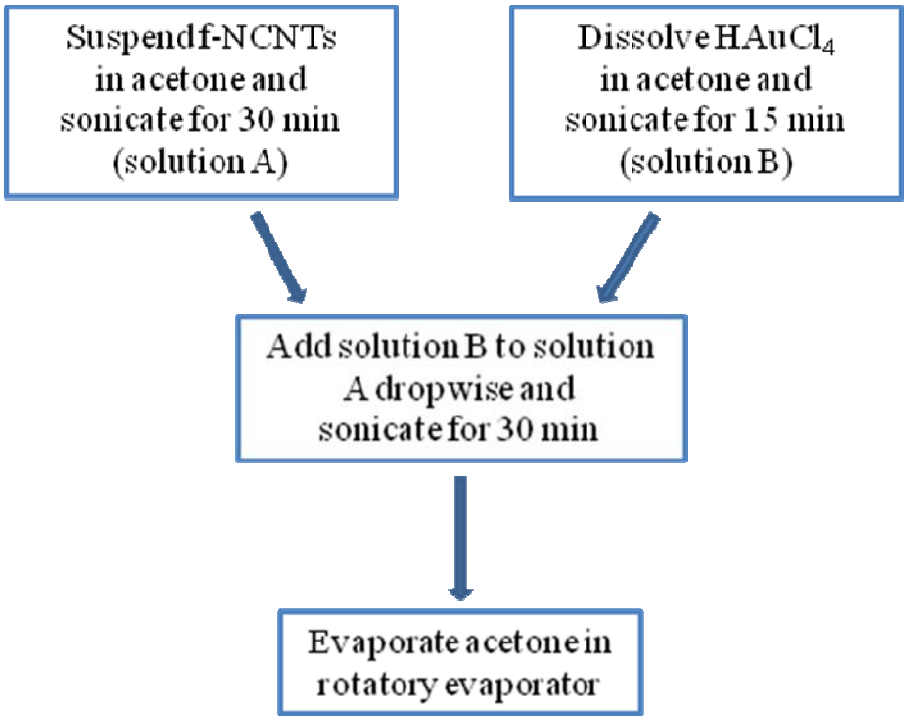


Fig. 10.1: Method for the synthesis of Au/N-CNT hybrid nanostructures.

10.2.4 Characterization of N-CNTs and Au/N-CNT nanostructures

Low magnification TEM analysis of the f-N-CNTs and Au/N-CNT was performed on a JEM 100S microscope and high magnification TEM was performed with a Spirit Technai FG microscope. EDX spectrometry was carried out with a spectroscope attached to the TEM. Samples for TEM analysis were prepared by sonication of the f-N-CNTs (or Au/N-CNTs) in methanol and a few drops of the resulting suspension were placed onto a holey Cu TEM grid and viewed at several magnifications. Thermogravimetric analysis (TGA) data on the f-N-CNTs were collected from a Perkin Elmer TGA 7 analyzer. Samples (typically 5 - 10 mg) of f-N-CNTs were loaded into platinum pans and heated to 1000 °C in flowing air at a heating rate of 10 ml/min.

10.3 Results and discussion

10.3.1 Synthesis and characterization of N-CNTs

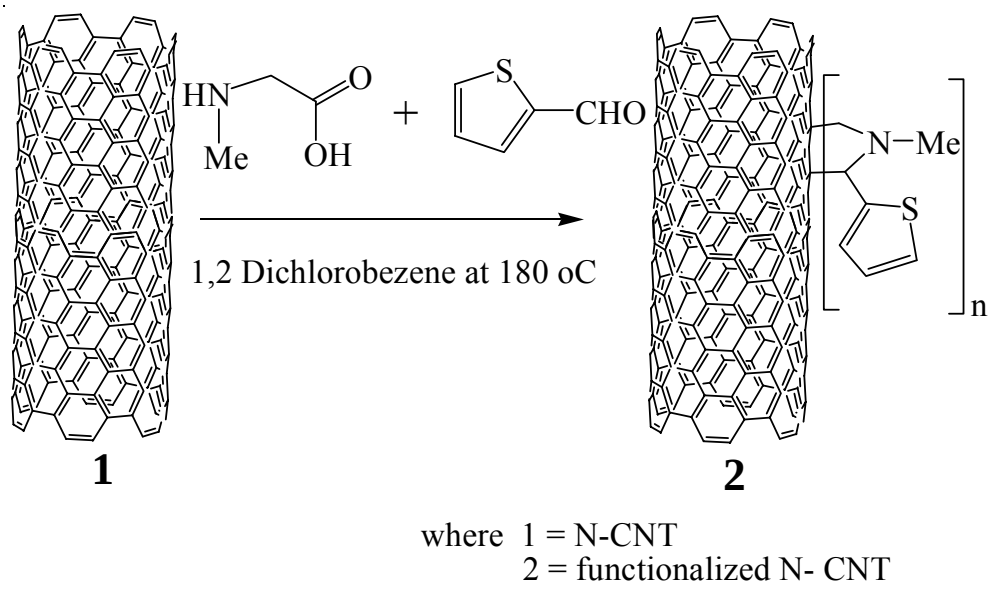
TEM analysis was used to investigate the morphology (size, shape) of the N-CNTs synthesised. TEM images clearly revealed that the as-prepared N-CNTs mostly exhibited bamboo-like structure with clearly separated compartments (*ca* 95 %). The closeness of the bamboo compartment reveals that the N-CNTs were highly doped with N with a compartment range of 25 - 130 nm [21].

10.3.2 Functionalization reactions of N-CNTs

In a recent study, we have shown using FT-IR spectroscopy, that functionalization of N-CNTs using acid treatment generates different functional groups on the N-CNTs (namely; -COOH, -OH, -CO) [19]. While, these functional groups create sites for attachment of nanoparticles in the N-CNTs, they can also be further reacted to produce other chemical groups.

In this study, the functionalization of N-doped and undoped CNTs, by 2-thiophenecarboxaldehyde and *N*-methylglycine was studied. Functionalization of the CNTs using azomethine ylides was first reported by Georgakilas *et al.* [22]. The reagent has been successfully added to graphitic surfaces *via* a 1,3-dipolar cycloaddition reaction, forming pyrrolidine fused rings on the side wall of the CNTs. The 1,3-dipolar cycloaddition reaction of azomethine ylides with alkene or alkyne is a very effective method for the construction of pyrrolidine- and pyrrole-rings in the synthesis of pyrrolidine- and pyrrole-containing molecules. This procedure initially was developed to modify C_{60} fullerenes and has been termed the “Prato reaction” [18].

The Prato functionalized CNTs were obtained as a gray dark product for both the N-doped and undoped CNTs (see Scheme 10.1). The increase in mass (between 5 and 10%) after the reaction indicated that the side walls of the CNTs had been functionalized. Furthermore, the TGA scan after functionalization indicated that the decomposition temperatures were lower than the pristine CNTs [23].



Scheme 10.1. Functionalization of N-CNTs with Prato reaction [23].

10.3.3 Analysis of Au/N-CNT nanostructures

After functionalization, the N-CNTs were dispersed in acetone together with a $HAuCl_4$ solution to yield Au/N-CNT hybrid nanostructures and visualized under TEM. Several loadings of gold were prepared (1, 3 and 5 *wt.%*).

TEM studies confirmed the successful attachment of Au nanoparticles to N-CNTs (Fig. 10.2). Well dispersed Au nanoparticles appeared along the N-CNTs and were found to decorate the

functionalized CNT surfaces in a uniform fashion. This is line with earlier studies that decorating CNTs can be used to identify the location of functional groups on the tubes [16,24]. However, very small amounts of Au-NPs were found on the surfaces of undoped and unfunctionalized CNTs (Fig. 10.2a) and clustered Au-NPs were observed in the doped CNTs (Fig. 10.2c). For the undoped/unfunctionalized CNTs the insertion can happen in two ways: (i) through sonication which could enhance insertion of particles by possibly weakening the CNT structure and (ii) through tubes with open ends. This indicates that functionaliozation plays a key role in the attachment which acts as a bridge to connect Au-NPs with N-CNTs. The attachment is enhanced by the high affinity of sulphur to Au.

It is also noteworthy that the overall bamboo structure of the N-CNT was not lost after both functionalization of N-CNTs and attachment of the Au-NPs (Fig. 10.2). This preservation of the bamboo structure justifies that indeed the particles are located within the CNTs (see section 3.4).

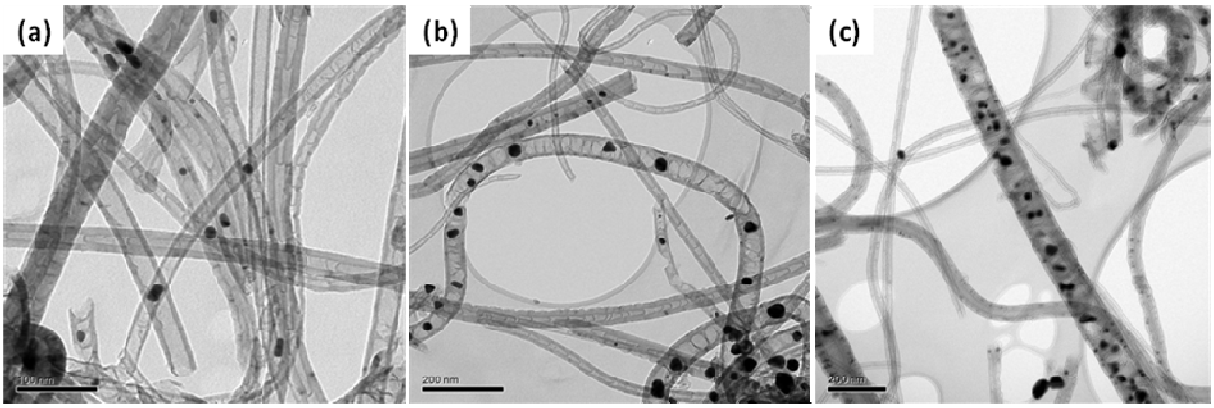


Fig. 10.2. TEM images of (a) Au/CNT; (b) 1 *wt.%* Au/N-CNT and (c) 3 *wt.%* Au/N-CNT hybrids.

To vary the diameters of attached gold nanoparticles, we selected three different dosages of $HAuCl_4$ (1, 3 and 5 *wt.%*). Fig. 10.2 shows TEM images of synthesized N-CNT/Au

nanostructures with different gold nanoparticle size. When 1 *wt.%* of $HAuCl_4$ was used, the size of Au-NPs in the N-CNTs were 10 - 15 nm. When 2 *wt.%* was used, the Au-NPs sizes were 20 – 30 nm and when 5 wt. % was used the diameters were 25 - 35 nm. Similar sizes have been obtained recently in another study [25,26].

10.3.4 Location of Au-NPs on the N-CNT structure

In order to verify the location of Au-NPs within the N-CNT, TEM tilting experiments were performed. Tubes were selected and tilted through an angle of ~100°. TEM images (Fig. 10.3) indicate that when tilted, Au particles appear consistently within the surfaces of the nanotube walls.

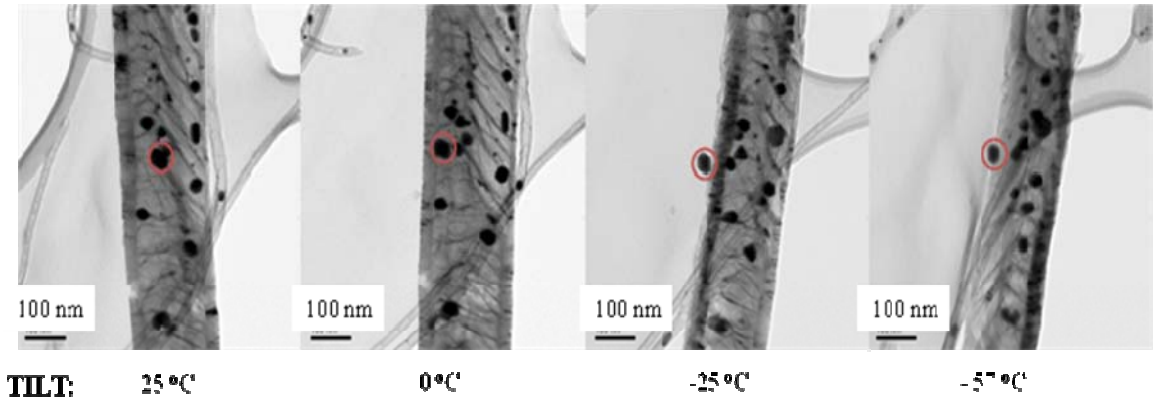


Fig. 10.3. TEM images of Au particles located on the surface of the N-CNT as the nanotube and particles are rotated through a combined orientation of ~ 82°. As the nanotube is tilted, it is revealed that particles (circled) are in fact located on the surface of the nanotube.

Various shapes of Au-NPs were found in the walls of and inside the CNT *i.e.* rod-like, triangular, flat shapes, spherical as reported by others [26,27]. Under what reaction conditions does each

particle shape results, is still under investigation. Also noteworthy is that concentration of Au-NPs on the CNT materials was not homogenous especially at low dosages (1 *wt.%*).

The Au/N-CNT nanostructures were further analyzed using an energy-dispersive X-ray (EDX) spectrometer attached to a transmission electron microscope to gather information on the elemental composition. The EDX spectrum (Fig. 10.4) of Au/N-CNT hybrids demonstrates the presence of Au, carbon, Cu and Fe (not shown). The Cu peak is caused by the copper grid on which the sample was mounted. The carbon comes from the CNT and Fe nanoparticles are also expected as they were not completely removed during purification or functionalization of the N-CNTs (embedded in the tubes).

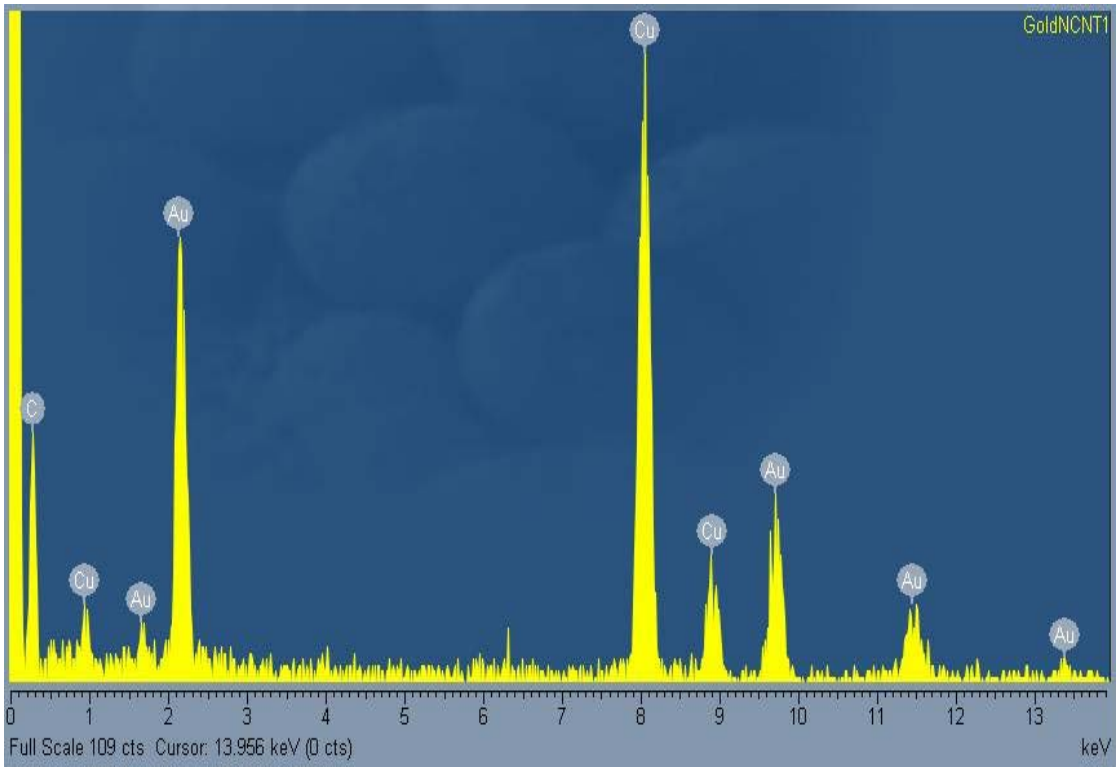


Fig. 10.4. EDX spectrum of Au/N-CNT nanostructures.

In summary, Au-NPs were anchored to the N-CNT surfaces by a facile and inexpensive method. The Au nanoparticles found on the N-CNTs have large diameters. However, this can be controlled by using a high dosage of $HAuCl_4$ with respect to the amount of N-CNTs used. Further studies are underway to fully characterize these nanostructures, investigate the Au/N-CNT interaction and to probe their use as novel gold nanocatalysts e.g. in the oxidation of styrene.

10.4 Conclusion

The present study describes a facile method to attach/incorporate gold nanoparticles into the N-CNT structure. As the N-CNTs are tilted under different orientations the particles are shown to be on the CNT surface. The Au nanoparticles attached have a wide range of diameters (10 – 35 nm) and possess different shapes. The method offers certain advantages, such as providing Au nanoparticles in good yields and ease of use. More work is still in process to fully investigate the use of these materials in catalysis.

References

1. S.F. Yin, B.Q. Xu, X.P. Zhou, C.T. Au, Appl. Catal. A 277 (2004) 1.

2. Y. Lin, X. Cui, C. Yen, C.M. Wai, J. Phys. Chem. B 109 (2005) 14410.

3. J. Xie, S. Wang, L. Aryasomayajula, V.K. Varadan, Nanotechnology 18 (2007) 065503.

4. M.M. Shaijumon, S. Ramaprabhua, N. Rajalakshmi, Appl. Phys. Lett. 88 (2006) 253105.

5. N. Karousis, G.-E. Tsotsou, F. Evangelista, P. Rudolf, N. Ragoussis, N. Tagmatarchis, J. Phys. Chem. C 112 (2008) 13463.

6. J. Kang, S. Zhang, Q. Zhang, Y.Wang, Angew. Chem. Int. Ed. 48 (2009), 2565.

7. B. Rajesh, K. Ravindranathan Thampi, J.M. Bonard, B. Viswanathan, Bull. Mater. Sci. 23 (5) (200) 341.

8. S. Fullam, D. Cottell, H. Rensmo, D. Fitzmaurice, Adv. Mater. 12 (2000) 1430.

9. L. Jiang, L. Gao, Carbon 41 (2003) 2923.

10. A.V. Ellis, K. Vijayamohanan, R. Goswami, N. Chakrapani, L.S. Ramanathan, P.M. Ajayan, *et al*., Nano Lett. 3 (2003) 279.

11. A. Tello, G. Cardenas, P. Haberle, R.A. Segura, Carbon 46 (2008) 884.

12. T. Sainsbury, J. Stolarczyk, D. Fitzmaurice, J. Phys. Chem. B 109 (2005) 16310.

13. J. Hu, J. Shi, S. Li, Y. Qin, Z.X. Guo, Y. Song, *et al*., Chem. Phys. Lett. 401 (2005) 352.

14. B. Kim, W.M. Sigmund, Langmuir 20 (2004) 8239.

15. X. Li, Y. Liu, L. Fu, L. Cao, D. Wei, G. Yu, *et al*., Carbon 44 (2006) 3139.

16. K. Jiang, A. Eitan, L.S. Schadler, P.M. Ajayan, R.W. Siegel, Nano Lett 3 (2003) 275.

17. B.L. Allen, P.D. Kichambare, A. Star, ACS Nano 2 (2008) 1914.

18. M. Maggini, G. Scorrano, M. Prato, J. Am. Chem. Soc. 115 (1993) 9798.

19. M.A. Mamo, F.S. Freitas, J.N. de Freitas, W.A.L van Otterlo, A.F. Nogueira, N.J. Coville, Application of 3-hexylthiophene functionalized CNTs in photovoltaic devices, ***Submitted (2010).***

20. E.N. Nxumalo, V.O. Nyamori, N.J. Coville. J. Organomet. Chem. 693 (2008) 2942.

21. E.N. Nxumalo, V.P. Chabalala, V.O. Nyamori, M.J. Witcomb, N.J. Coville, J. Organomet. Chem. 695 (2010) 1451.

22. V. Georgakilas, K. Kordatos, M. Prato, D. M. Guldi, M. Holzinger, A. Hirsch, J. Am. Chem. Soc. 124 (2002) 760.

23. M.A. Mamo, Functionalization of carbonaceous materials for photovoltaic cells, PhD thesis, University of the Witwatersrand, 2010.

24. M.M. Oliveira, A.J.G. Zarbin, J. Phys. Chem. C 112 (2008) 18783.

25. R. Zhang, M. Hummelgård, H. Olin, Mater. Sci. Eng., B 158 (2009) 48.

26. R. Zhang, Q. Wang, L. Zhang, S. Yang, Z. Yang, B. Ding, A: Physicochem. Eng. Aspects 312 (2008) 136.

27. K.-N. Lin, T.-Y. Yang, H.-M. Lin, Y.-K. Hwu, S.-H. Wu, C.-K. Lin, China Particuology 5 (2007) 237.

Chapter 11
[9]HRTEM studies of nitrogen doped carbon nanotubes

11.1 Introduction

Heterostructures have become a topic of increased importance in the study of shaped carbon nanostructures [1]. This arises from the physical and chemical properties that are created when a heteroatom is incorporated into a carbon structure such as a carbon nanotube (CNT). In particular, nitrogen doped carbon nanotubes (N-CNTs) have been synthesized because they exhibit enhanced chemical reactivity and modified conductivity, mechanical and magnetic properties caused by changes in the structural morphology of the CNTs upon N insertion [2]. The advantage of N-CNTs is that their electronic properties are primarily influenced by the nitrogen content and their syntheses are relatively easy to control. These N-CNTs can be synthesised under controlled conditions using a range of synthetic methodologies [3]. As a result, many research groups around the world have reported facile syntheses of N-CNTs [5-9]. The challenge

[9] E.N. Nxumalo, P. Frankylin, N.J. Coville, HRTEM studies of nitrogen doped carbon nanotubes, *submitted (2011)*

however, lies in choosing the methods or techniques for characterization that will enable structure/property relationship to be understood.

Previously, electrical and optical properties of CNTs were generally studied using microscopic and spectroscopic techniques and/or a combination of these techniques [10-12]. However, this has proved difficult, in particular when isolated CNTs are to be studied. In a recent study, we demonstrated that high-purity N-CNTs can be achieved by using chemical vapour deposition (CVD) floating catalyst methods under controlled conditions. The products can be characterized satisfactorily by scanning electron microscopy (SEM) and transmission electron microscopy (TEM) to determine their structural morphologies [13]. The individual N-CNTs produced exhibited bamboo-like structures with small diameters (10 – 80 nm) as evidenced by TEM studies. Further, we and others have attempted to explain the growth of the N-CNTs by models [14-16]. However, the growth mechanism itself is very complex and requires precise analytical techniques for analysis since N-CNT structural properties are different from those of pristine CNTs. One such technique is high resolution transmission electron microscopy (HRTEM).

Several researchers have probed N-CNTs using HRTEM. For example, a method that combines atomic force microscopy (AFM) measurements with an independent determination of the CNT structure by HRTEM has been developed. This technique is used to obtain information regarding the number of layers and the interlayer distance in the CNT walls [17]. This method uses a thin carbon grid membrane to allow samples to be easily transferred between AFM and HRTEM systems [18]. A recent HRTEM study looked at structural systematics in boron doped CNTs [19]. A handful of publications described studies on doped carbon systems probed by HRTEM [20-24]. In addition, in a recent study, HRTEM has been shown to provide an atomic image not only of the surface layer but also of the underlying structure of CNTs [25].

We present here some results from our current HRTEM investigations of surface and interior imaging of N-CNTs. The N-CNTs were synthesized by the thermal decomposition of ferrocene/diethylenetriamine mixtures at elevated temperatures and the structural/morphological changes in the tubes formed with change in concentration were noted. In order to refine the understanding of the role of N in the formation of bamboo structures, we employed the use of HRTEM to investigate the surfaces of the N-CNTs as well as the state of iron nanoparticles (size and morphology) embedded in the tubes. Energy filtered TEM (EFTEM) was used to establish the location of N in the tubes. In addition, we studied the structural properties of N-CNTs (*i.e.* diameters, number of layers, interlayer spacing and disorders/defect sites) at a range of N concentrations.

11.2 Experimental section

11.2.1 Synthesis of N-CNTs

The CVD floating catalyst method was used for the synthesis of N-CNTs. The synthesis was carried out in a horizontal furnace using a tubular quartz tube (with dimensions of 800 mm and 28 mm) at a temperature of 900 ^{o}C. The carrier gas (5% H_2/Ar, Afrox) was flowed through the CVD reactor at a controlled flow rate of 100 ml/min using a syringe process as reported before [13]. Solutions of toluene and ferrocene/diethylenetriamine (10 ml) (1 – 5 *wt.%*) were prepared and injected into the high temperature zone of the reactor at an injection rate of 1.0 ml/min. When injection was complete, the reactor was allowed to cool to RT and N-CNT products were collected as black ‘soot’. All reagents were used as commercially available (Sigma Aldrich).

11.2.2 TEM techniques

Characterization of the nanostructured materials was performed by low and high resolution TEM. Samples used for study by TEM and HRTEM were dispersed in methanol using a sonicator and loaded onto a copper grid. Low resolution TEM analysis of the N-CNTs was performed on a Spirit Technai FG microscope at 80 kV. HRTEM was carried out on a Technai F20 X-twin FEG at 800 kV. Work was done at low dosage where possible. However, some sections were also exposed to high dosages. Aside from some carbon contamination on the outside of the tubes, no changes were observed in the interior structure of the tubes with time. Our TEM studies also included EFTEM elemental mapping of carbon, nitrogen and iron distribution in the tubes.

11.3. Results and discussion

Nitrogen doped CNTs were synthesized by the thermal decomposition of ferrocene/diethylenetriamine mixtures at varying concentrations (1 – 5 *wt.%*) using the CVD injection technique. The as-synthesized N-CNTs were dispersed in methanol and a drop of suspension was put onto the holey carbon grid and viewed under TEM. Detailed structures of the N-CNTs are given by HRTEM and TEM images as discussed below.

11.3.1 Structural effects of the N-CNTs

We first performed low magnification TEM on the N-CNTs to determine the general trends in size and product distribution of doped nanotubes. TEM images confirmed that the CNTs obtained were doped with N owing to the presence of a unique structural morphology (*so called* bamboo compartments - in which the tube inside is separated into a series of partitions). The images revealed that most of the tubes were doped with N (*e.g.* < 95% for CNTs grown from 5

wt.%). In addition, N-CNTs showed these bamboo compartments even at very low concentrations of N (*e.g.* > 80% doped structures for CNTs grown from 1 *wt.%* of N-source) (Fig. 11.1). HRTEM studies to further investigate the morphology of N-CNTs as well as the Fe nanoparticles embedded to the N-CNTs were perfomed. It has been shown that the structural morphology (e.g. sizes, shapes, *etc*.) of these tubes can be controlled by systematically varying the concentrations of the N source as discussed in section 11.3.2.

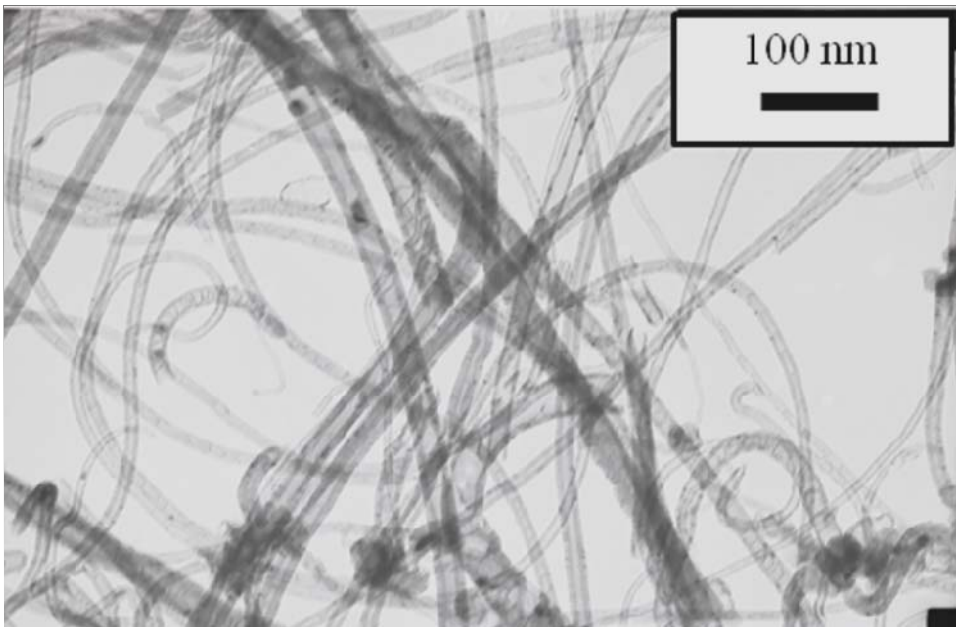


Fig. 11.1. Densely populated N-CNTs grown from 1 *wt.%* of N-source.

11.3.2 Effects of concentration: observation of HRTEM

The diameters of the N-CNTs appear to depend on the concentration of the N source used during the growth. As the concentration increases, the average diameter of CNTs decreases and the diameter distribution becomes broader. Further, HRTEM images show that the N-CNTs possess smaller diameters than their undoped counterparts. This observation has been made before [16].

The N-CNTs synthesized from 1 *wt.%* of the N-source demonstrate a broad distribution of diameters, ranging from 40 - 120 nm. The walls of these tubes are constructed from 20 – 45 graphene layers with inner diameters of 20 – 100 nm. Fig. 11.2 shows the bamboo links and lattice fringes observed in N-CNTs grown from 1 *wt.%* N-source. Meanwhile, there was availability of amorphous material attached to the CNT surface. The N-CNTs grown from 2 *wt.%* of N-source have a smaller diameter range (25 - 100 nm) compared to 1 *wt.%* samples and have less roughness in the CNT walls.

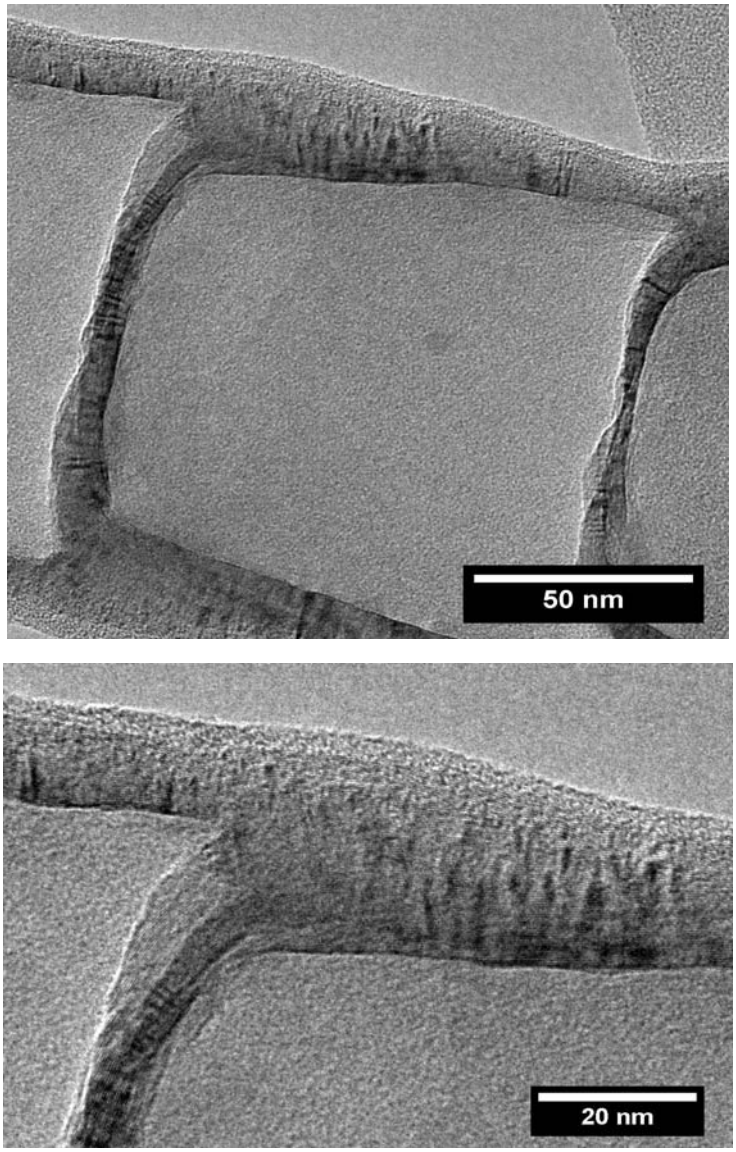


Fig. 11.2. HRTEM images for N-CNTs grown from 1 *wt.%* of ferrocene/diethylenetriamine mixtures. The top image shows a tube with bamboo link while the lower image is a zoomed region where lattice fringes are visible.

The outer tube diameters of the N-CNTs grown from 5 *wt.%* of N source range from 10 - 80 nm, and the inner tube diameters are in the 5 – 40 nm range. The surface of the walls appears to be rough and corrugated and the outer graphitic sheets of the wall have fringes/wrinkles. Typical

patterns of N-CNT with well graphitized structure with 10 – 25 graphitic layers were observed (Fig. 11.3). The formation of N-CNTs with corrugated walls (observed in the 5 *wt.%* samples) is attributed to the presence of N in the graphitic network. The incorporation of N atoms in the hexagonal network results in N hybridized pentagons that lead to the curving of the graphite sheet [26]. It was observed that the graphitic layers are stacked in a thimble type shape that terminates at the surface of the tube. This is important because undoped nanotubes are normally constructed from parallel graphitic layers. The terminating structure will have implications on the electronic properties of these tubes.

The atomically resolved image of the wall reveals well-separated graphitic sheets with inter-layer spacing of 0.34 nm while the bamboo linking generally had spacings of around 0.30 nm (Fig. 11.3). Therefore the N is compressing the layers, which is strange as N would be expected to push the layers further apart. So, the strain in keeping the sheet together with the bending added from the N. The strain may be sufficiently bigger, such that it overcomes the simple forces that hold graphitic sheets at a certain separation.

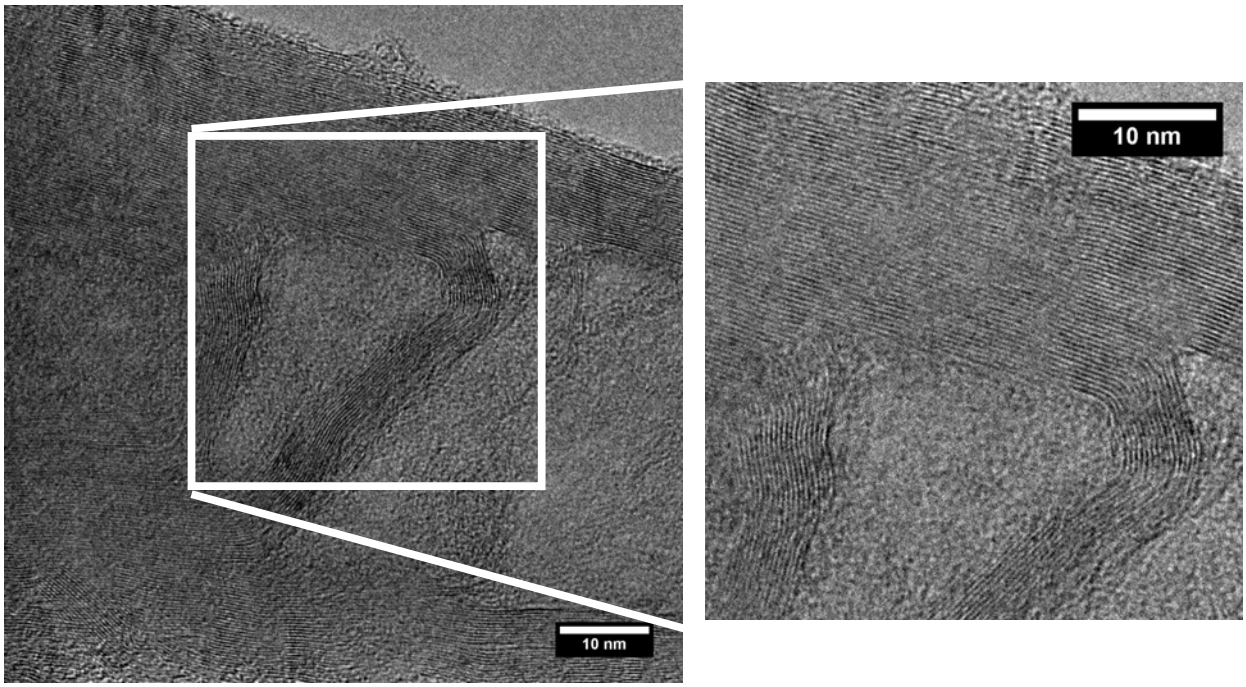


Fig. 11.3. Image showing well separated graphitic sheets in *5 wt.%* N-CNTs.

The graphitic sheets separating the tube inside are formed more randomly as the N-source concentration increases. The outer surface of the wall is not straight due to the randomly stacked compartment layers and shows disorder in the tubes. This observation is particularly associated with the 5 *wt.%* samples.

However, at low concentrations (1 *wt.%*), the compartment layers are smoothly curved to connect with the CNT wall without distortion. Thus, the walls become straight and thicker in diameter. The defects found in the tubes, more particularly at high concentrations, are attributed to the presence of N atoms by formation of pyridine-like bonds with carbon atom as observed by others [27]. The HRTEM image (Fig. 11.3) also indicates the presence of amorphous carbon coating the outer surface of the CNTs.

As the N content increases, more curved compartment layers appear more regularly. HRTEM reveal that as the N content increases the degree of crystalline perfection decreases. Thus, N doping is a promising way to control the crystallinity and structure of CNTs.

Our observation is that N doping significantly modifies:

(i) the interior structure of N-CNTs

(ii) the degree of crystalline perfection in the CNTs

(iii) the growth rate of N-CNTs [16]

(iv) the wall thickness of N-CNTs [13] and

(v) the graphitic wall arrangement and interlayer spacing

The properties mentioned above are influenced by the growth mechanism path followed (explained before [16]); as determined by the diffusion rate of C and N atoms. The presence of N in the layer generally leads to a strain in the surface. As more N atoms are added, the compartment layers are curved and connect with the wall under less strain.

11.3.3 EFTEM analysis

EFTEM is a technique used in TEM where electrons of certain kinetic energies can be used to form images or diffraction patterns and is a valuable tool for measuring elemental composition of materials [28, 29]. Elemental mapping of carbon, nitrogen and iron distribution in the tubes were analyzed by EFTEM [30].

Fig. 11.4 depicts (a) the bright field, (b) zero-loss and (c) false colour energy filtered TEM images of a 5 *wt.%* N-CNT sample. The EFTEM image was constructed by recording with a 280 eV (carbon, green), 400 eV (nitrogen, blue), and 700 eV (iron, red) shift in the energy window

and using 16 eV energy windows for background estimation. It was noted from these studies that the nitrogen concentration was highest in the thicker bamboo linking structures.

More importantly, it was noted that it was only in the well defined linking structures that N was contained. A second class of linking structure was observed where the bamboo links were wavy and irregular and generally thin (less than 5 graphitic layers). In these areas no N could be detected. A previous paper has indicated this could be due to beam damage [31]. However in this case the beam was kept spread and the work was done at a smaller spot size to limit the dosage to the nanotubes. Further, over a period of time the structure of the tubes did not vary significantly as bright field images were taken both before and after and there was no change to the geometry of the interior structures [30]. It would be expected that if beam damage was significant, it would continue and that the end result would be a continued removal of the nitrogen linking structures. During EELS characterization in STEM mode, it was observed that damage was done to the interior structure. Therefore, EELS mapping was excluded as a valid analytical technique [30].

It is clear that the N is not present in the same concentration in all the tubes. Further, EELS work also showed less nitrogen (blue) in the bamboo walls (Fig. 11.4). The nitrogen apparently at the edge of the nanotube is an artefact from an image correlation due to the very small amount of nitrogen present. This meant that the overall intensity range in the nitrogen map was small and so in the cross correlation between the background and spectral image there was some residual intensity left at the edges of the tubes. The dark lines in the Fe nanoparticles are from phase scattering.

In addition, it may be possible to examine the thickness of the linking wall to estimate the amount of nitrogen. Work to determine the structural relationship of the bamboo link geometry to the nitrogen content and to quantify the nitrogen content in the linking structure is currently underway.

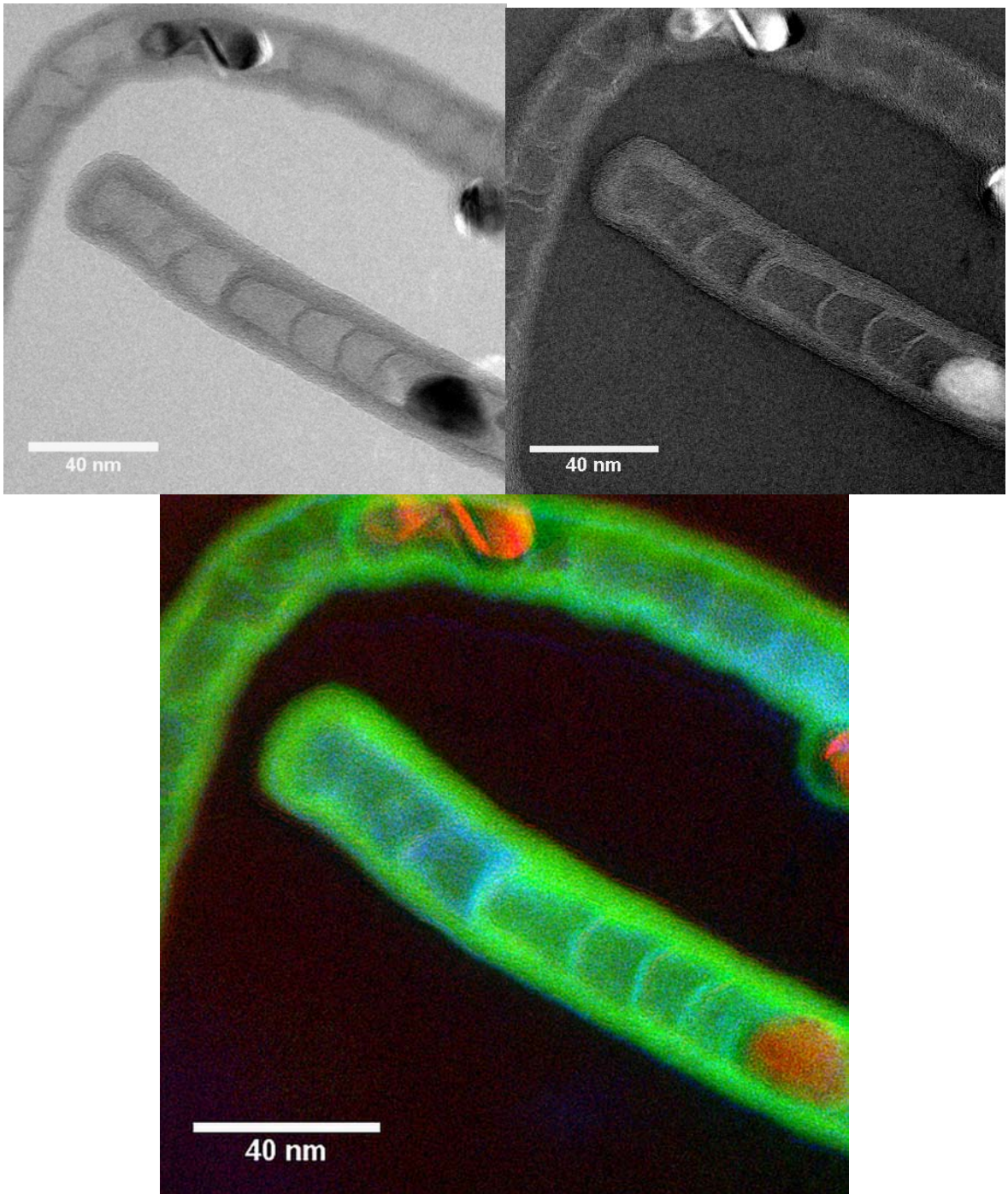


Fig. 11.4. EFTEM images of N-CNTs grown from 5 *wt.%* N-source; (a) bright field, (b) zero loss and (b) false colour EFTEM image with carbon (green), nitrogen (blue) and iron (red).

11.3.4 Fe nanoparticles incorporation in tube

Iron nanoparticles were found to be encapsulated within the individual N-CNT and within the walls. The encapsulated Fe particles are associated with tubes with open ends. Some of these particles were also observed in the wall surfaces of the tubes. Fig. 11.5 shows the interior structure of a N-CNT with Fe particles embedded in the walls.

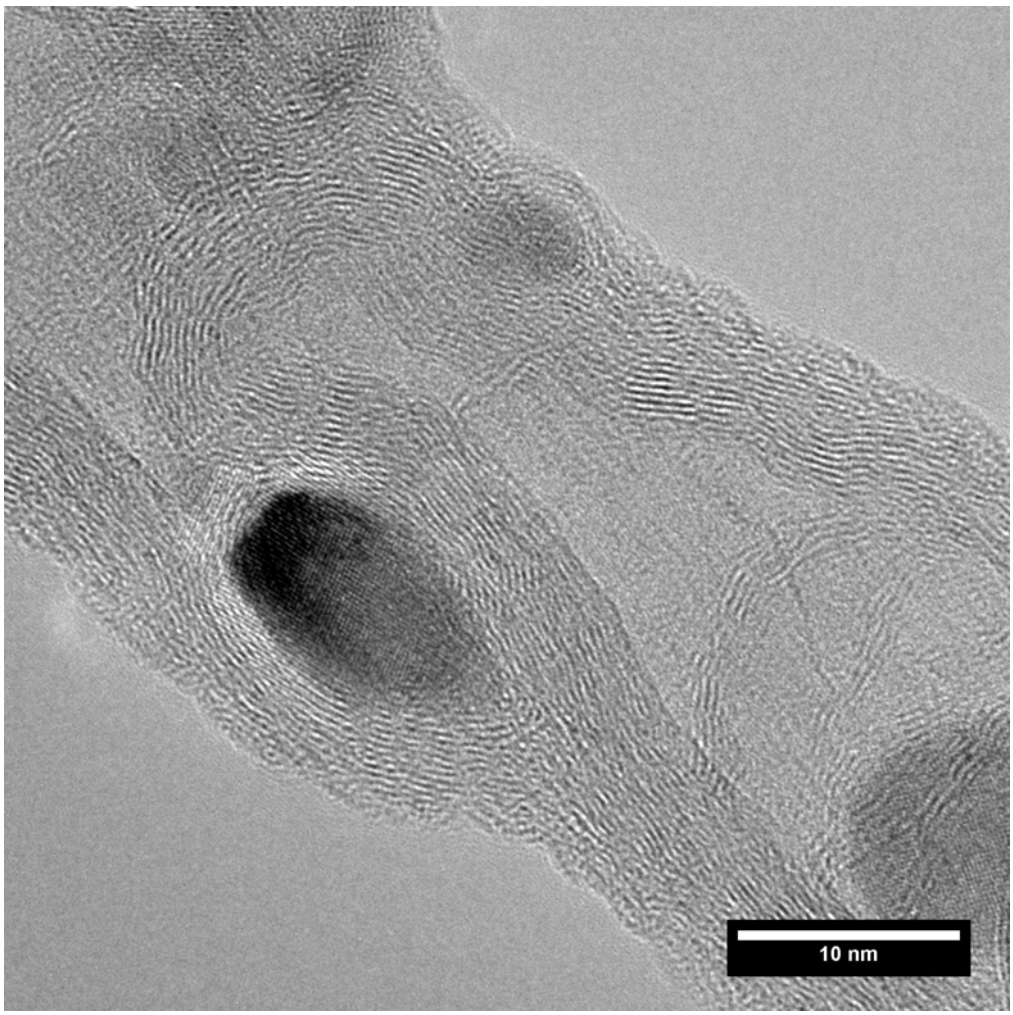


Fig. 11.5. Images of iron nanoparticles in N-CNTs.

It is known that the graphitic layers wrap onto the surface of such nanoparticles. However, in this N-CNT, it was observed that this caused a distortion of the bamboo structure in the walls. Where no Fe particles were involved, the bamboo links were significantly thinner and less direct. HRTEM reveals that the metallic particles (5 - 10 nm) are mainly crystalline.

11.4 Conclusion

We have investigated the surface and interior morphological of N-CNTs and the state of iron nanoparticles encapsulated in the N-CNTs and the location of nitrogen atoms using HRTEM and EFTEM. It has been established that iron nanoparticles can interfere with the interior structure of the bamboo links. Increased concentrations of N were predominantly located in the bamboo linking structures and this controls the thickness of the link. In addition, we employed HRTEM to determine the structural properties of N-CNTs (diameters, number of layers, interlayer spacing, *etc.*) at the different concentration concentrations.

References

1. I. Martin-Gullon, J. Vera, J.A. Conesa, J.L. Gonzalez, C. Merino, Carbon 44 (2006) 1572.

2. J.I. Pascual, J. Mendez, J. Gomez-Herrero, A.M. Baro, N. Garcia, U. Landman, W.D. Luedtke, E.N. Bogachek, H.P. Cheng, Science 267 (1995) 1793.

3. A. Govindaraj, C.N.R. Rao, Pure Appl. Chem. 74 (2002) 1571.

4. P. Ayala, R. Arenal, M.H. Rümmeli, A. Rubio, T. Pichler, Carbon 3 (2010) 575.

5. K. Suenage, M.P. Johansson, N. Hellgren, E. Broitman, L.R. Wallenberg, C. Colliex, J. Sundgren, L. Hultman, Chem. Phys. Lett. 300 (1999) 695.

6. C. Tang, D. Golberg, Y. Bando, F. Xu, B. Liu, Chem. Commun. Cambridge 24 (2003) 3050.

7. M. Glerup, M. Castignolles, M. Holzinger, G. Hug, A. Loiseau, P. Bernier, Chem. Commun. Cambridge 20 (2003) 2542.

8. S. Trasobares, O. Stephan, C. Colliex, W.K. Hsu, H.W. Kroto, J. Chem. Phys. 116 (2002) 8966.

9. R. Droppa Jr., C.T.M. Ribeiro, A.R. Zanatta, M.C. dos Santos, F. Alvarez, Phys. Rev. B 69 (2004) 045405.

10. J.M. Zuo, I. Vartanyants, M. Gao, R. Zhang, L.A. Nagahara, Science 300 (2003) 1419.

11. N. Anderson, A. Hartschuh, L. Novotny, Nano Lett. 7 (2007) 577.

12. S.M. Bachilo, M.S. Strano, C. Kittrell, R.H. Hauge, R.E. Smalley, R.B. Weisman, Science 298 (2002) 2361.

13. E.N. Nxumalo, V.O. Nyamori, N.J. Coville, J. Organometal. Chem. 693 (2008) 2942.

14. M. Terrones, A.M. Benito, C. Manteca-Diego, W.K. Hsu, O.I. Osman, J.P. Hare, D.G. Reid, H. Terrones, A.K. Cheetham, K. Prassides, H.W. Kroto, D.R.M. Walton, Chem. Phys. Lett. 257 (1996) 576.

15. C.T. Wirth, S. Hofmann, J. Robertson, Diamond Relat. Mater. 18 (2009) 940.

16. E.N. Nxumalo, V.P. Chabalala, V.O. Nyamori, M.J. Witcomb, N.J. Coville, J. Organomet. Chem. 695 (2010) 1451.

17. S. Kuwahara, T. Sugai, H. Shinohara, Nanotechnology 20 (2009) 225702.

18. R. Seidel, M. Mertig, W. Pompe, Surf. Int. Anal. 33 (2002) 15.

19. P.L. Gai, O. Stephan, K. McGuire, A.M. Rao, M.S. Dresselhaus, Mater. Chem. 14 (2004) 669.

20. P. Ghosh, M. Tanemura, T. Soga, M. Zamri, T. Jimbo, Solid State Commun. 147 (2008) 15.

21. R. Xue, Z. Sun, L. Su, X. Zhang, Catal. Lett. 135 (2010) 312.

22. A. Misra, P.K. Tyagi, M.K. Singh, D.S. Misra, Diamond Relat. Mat. 15 (2006) 385

23. L.S. Panchakarla, A. Govindaraj, C. N. R. Rao, ACS Nano 1 (2007) 494.

24. D. Golberg, Y. Bando, L. Bourgeois, K. Kurashima, T. Sato, Carbon 38 (2000) 2017.

25. W. Zhou, X.C. Ma, Z.Y. Yuan, E.G. Wang, Surf. Interface Anal. 32 (2001) 236.

26. R. Xue, Z. Sun, L. Su, X. Zhang, Catal. Lett. 135 (2010) 312.

27. E.M.M. Ibrahim, V.O. Khavrus, A. Leonhardt, S. Hampel, S. Oswald, M.H. Rümmeli, B. Büchner, Diamond Relat. Mater. 19 (2010) 1199.

28. P. Wang, G. Behan, M. Takeguchi, A. Hashimoto, K. Mitsuishi, M. Shimojo, A.I. Kirkland, P.D. Nellist, Phys. Rev. Lett. 104 (2010) 200801.

29. P.J. Thomas, P.A. Midgleyz, Top. Catal. Vol. 21 (2002) 109.

30. Discussion with Mr. Paul Franklyn, School of Chemistry, University of the Witwatersrand, South Africa, 2010.

31. C. Ducati, K. Koziol, S. Friedrichs, T.J.V. Yates, M.S. Shaffer, P.A. Midgley, A.H. Windle, Small 2 (2006) 774.

Chapter 12
Conclusions and perspectives

Nitrogen doped multi-wall carbon nanotubes (N-CNTs) and related nanostructures have been grown by the CVD floating catalyst methods (*i.e.* nebulised spay pyrolysis and injection technique) and autoclaves systems, using ferrocene and substituted ferrocenes as catalyst sources. The experimental investigations presented in this thesis allowed us to obtain a comprehensive impression of the catalytic growth of N-CNTs. In the various chapters, investigations of the diverse morphologies of N-CNTs grown by these methods were discussed. A significant influence of the temperature and the catalyst material on the quality of the carbon nanostructures was observed. The diameter of the nanotubes and the density could be adjusted by choosing the appropriate reaction conditions (temperature, gas flow rates, concentration of the catalyst solution and N source concentration).

The organometallic catalysts employed to form the N-CNTs used in this work were ferrocene (FcH), FcH containing substituents and FcH/N-source mixtures. Depending on the reaction conditions employed, the type of C and N source used and the growth temperature used, these catalysts can be used to synthesize N-CNTs or other SCNMs with defined morphologies. The

information presented in this work indicates that the effect of N concentration on CNT growth is now known - high concentrations of N leads to shorter, thinner tubes with small compartments. However, the shape of the compartment and the mechanism of N-CNT growth thereof still needs to be established.

The N-CNTs and other nanostructures obtained were fully studied using a range of instrumental techniques such as transmission electron microscopy (TEM), scanning electron microscopy (SEM), high resolution TEM (HRTEM), energy filtered TEM, energy dispersive X-ray (EDX) spectroscopy, thermogravimetric analysis (TGA), Raman spectroscopy, BET surface area and porosity analysis, CHN analysis, X-ray photoelectron spectroscopy (XPS) and electron spin resonance (ESR) spectroscopy.

To briefly mention the main highlights of this work:

(i) Successful N-doping was evidenced by the presence of the *so-called* compartmentalized bamboo structures in the CNT walls. The type of catalysts used during the N-CNT growth plays a role in the formation of the compartments as observed under TEM. Further, previous literature observations reinforce our opinion about Fe-catalysed reactions leading to the formation of CNTs bearing bamboo structures.

(ii) Raman spectroscopy investigations revealed that N-CNTs have a low degree of graphitization indicating the presence of defects and disorder in the CNT walls. Further, XPS and CHN analysis demonstrated that N was indeed present in the CNTs in quantifiable amounts and in different bonding configurations.

(iii) The study reveals that the diameters of the tubes can be controlled by changing the N source concentration. More significantly, a higher N content is achieved by using the *substituted ferrocene* as a catalyst when compared to ferrocene/N-source mixtures *i.e.* when the N source is not attached to the catalyst.

(iv) It has also been shown that the position of the methyl group attached to the imidazole can quite significantly influence the size distribution and the type of SCNMs produced in the 'autoclave' system. An analysis of the SCNMs and the bamboo structures reveals that the three structural isomers of methylimidazoles lead to different products; in particular with N-CNTs that contain different amounts of N as determined by measurements of *bamboo compartments* and tube diameters. The results show that the control of N-CNT growth is determined by the decomposition of the N source during the reaction.

(v) The effect of using different N-sources on the production of N-CNTs using a nebulised floating catalyst method was established. From this method, it was found that the increase in concentration of nitrogen containing hydrocarbons during the synthesis of N-CNTs results in an increase in the average outer diameter and an increase in the length of carbon nanotubes at low N concentration. The data shows that the growth rate of CNTs from the pyrolysis of FcH/toluene in the presence of nitrogen containing hydrocarbons decreases with an increase in the addition of nitrogen containing species. Increasing N content in the reactant mixture gives shorter doped tubes and tubes with more disorder. Thus, the effects of N concentration are more significant than the nature and the type of the N source in the formation of N-CNTs.

(vi) Treatment of N-CNTs with nitric acid results in chemically modified/oxidized nanotubes with loss of alignment, decreased stability and an increased number of defects - resulting in tubes with fused/melted looks.

(vii) This thesis also demonstrates that the role of *para*-substituted ferrocene complexes is to provide a source of metal, carbon and heteroatom (O or Br) radicals/atoms/ions. The toluene also provides an extra source of carbon. This mixture of radicals/atoms/ions can act as a precursor for the production of SCNMs. Not unexpectedly, the heteroatoms impact on the catalyst activity and selectivity and thus influence the yields and morphologies of the resulting SCNMs. The overall finding is that the presence of Br and O in the growth environment significantly reduces CNT growth.

(viii) In the ESR results, we have observed variations in the CNT ESR spectral line shape, the *g*-factor shift and the line width at different temperatures. These are attributed to the presence of varying amounts of N in the CNTs. Generally, the undoped CNTs show a weak dependence in their line widths on temperature. A significantly large *g*-factor shift for the N-CNTs grown was observed as analysed in terms of Elliott-Wagoner and the Bottleneck models.

(ix) Au nanoparticles with a wide range of diameters were successfully attached to surfaces of N-CNTs. The method offers some advantages, such as providing Au nanoparticles in good yields and ease of use. More work is still in progress to fully investigate the use of these materials in catalysis.

(x) Investigations of the surface and interior morphology of N-CNTs and the state of iron nanoparticles encapsulated in the N-CNTs were performed using HRTEM. EFTEM demonstrated that increased concentrations of N were found to be predominantly located in the bamboo linking structures and this controls the thickness of the link. It has also been established that iron nanoparticles can interfere with the interior structure of the bamboo links.

The purpose of this study was to synthesize N-CNTs by various CVD techniques and determine the appropriate conditions for the growth of N-CNTs, study N-CNT magnetic properties and use the N-CNTs in the fabrication of Au/N-CNT nanostructured hybrids for use in catalysis. In general, the objectives of the study were accomplished. As with all projects, questions were also raised during the study and many avenues of nanotube research remain open. While progress has been achieved concerning the effects that various dopants have on CNT behaviour and morphology, information in the interactions of N-CNT with metal nanoparticles still remain largely unknown. Work on metal/N-CNT interaction will continue to be a forefront problem in N-CNT research in the foreseeable future. This will lead to a better understanding of their use as catalysts. In particular, it is envisaged that the materials made in this study will be used in (i) solar cells applications, (ii) oxidation and hydrogenation reactions, (iii) sensor applications and (iv) the formation of CNT/membranes for use in water treatment.

Regardless of the outcome of the proposed applications, CNT-related materials have already provided great possibilities in nanotechnology that were not conceived before. Nanotechnologies in the future will be expected to build on the advances made from CNT research. It remains true that these applications will have a positive impact on CNT product development. It is noteworthy that many CNT-derived products are already in the market. However, before we consider commercialization of CNTs a success, some challenges *e.g.* safety issues, needs to be clarified.

To bridge the gap between academia and industry, it is important that the elemental knowledge about nanotechnology and the progresses discussed in this document are transferred to industry, so that nanotechnology products can thrive in the commercial front.

Appendices

A. Figures

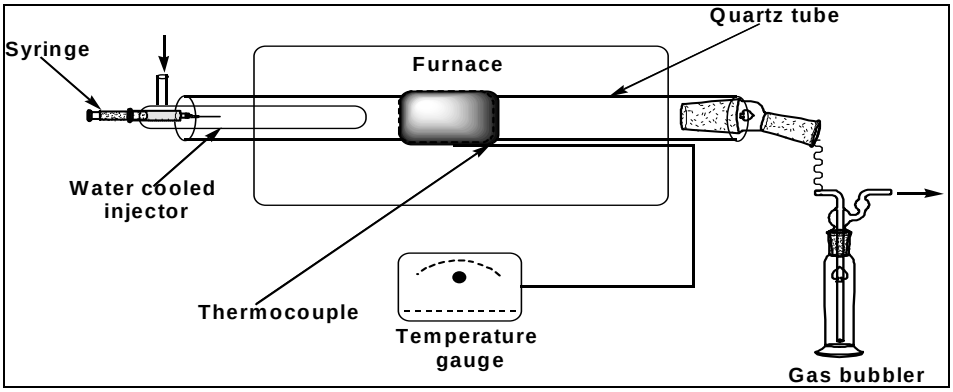


Fig. A5.1. A typical horizontal furnace system used for the synthesis of CNTs.

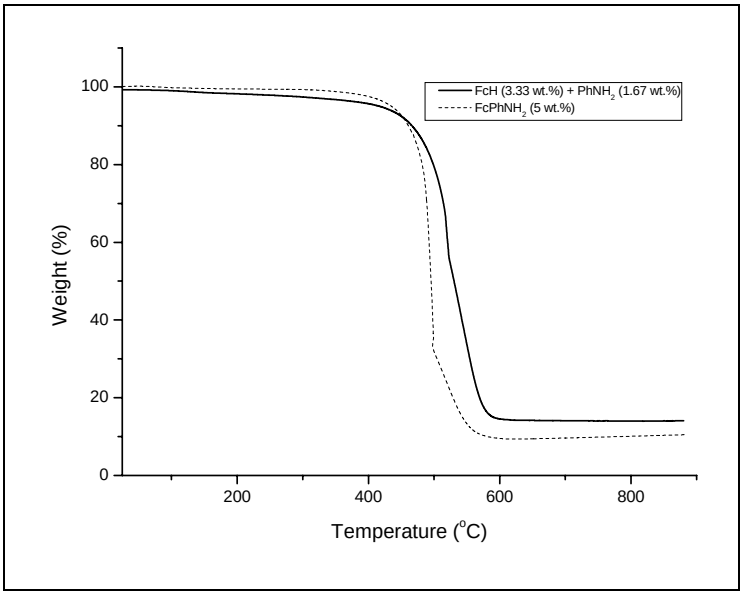


Fig. A5.2. TGA curves of CNTs grown from FcH (3.33 *wt.%*) /$PhNH_2$ (1.67 *wt.%*) and $FcPhNH_2$ (5 *wt.%*).

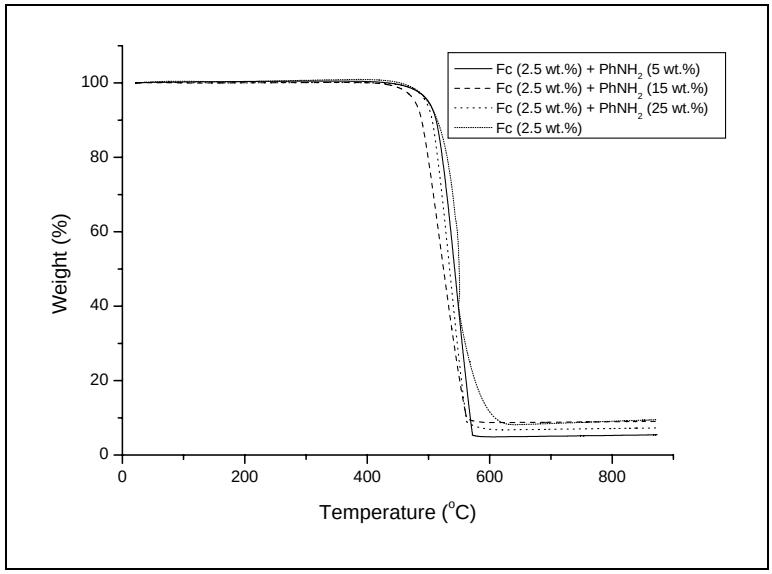


Fig. A5.3. TGA curves of CNTs grown from FcH (2.5 *wt.%*)/$PhNH_2$ (0, 5, 15 and 25 *wt.%* aniline.

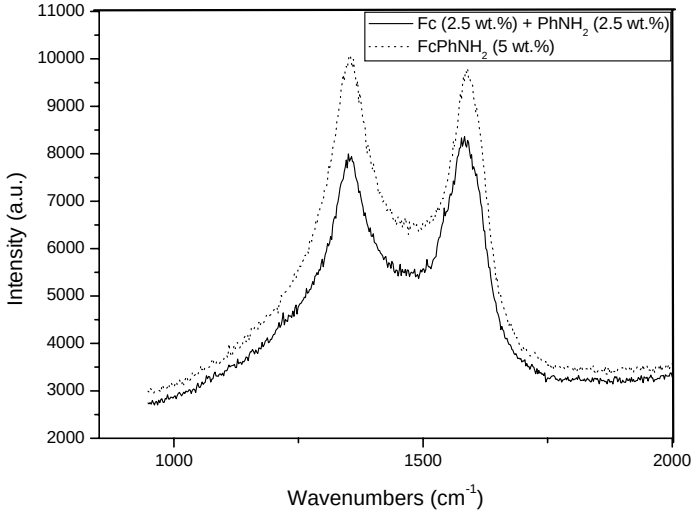


Fig. A5.4. Raman spectra of CNTs grown from FcH (2.5 *wt.%*)/$PhNH_2$ (2.5 *wt.%*) and $FcPhNH_2$ (5 *wt.%*).

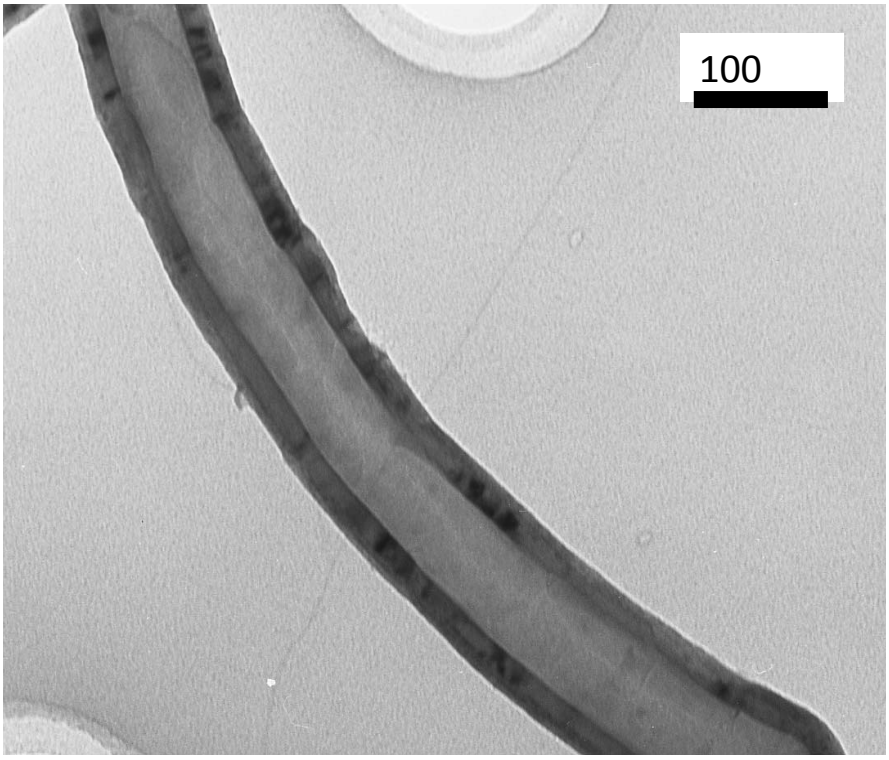


Fig. A6.1. TEM images of CNTs grown from the pyrolysis of FcH (100%).

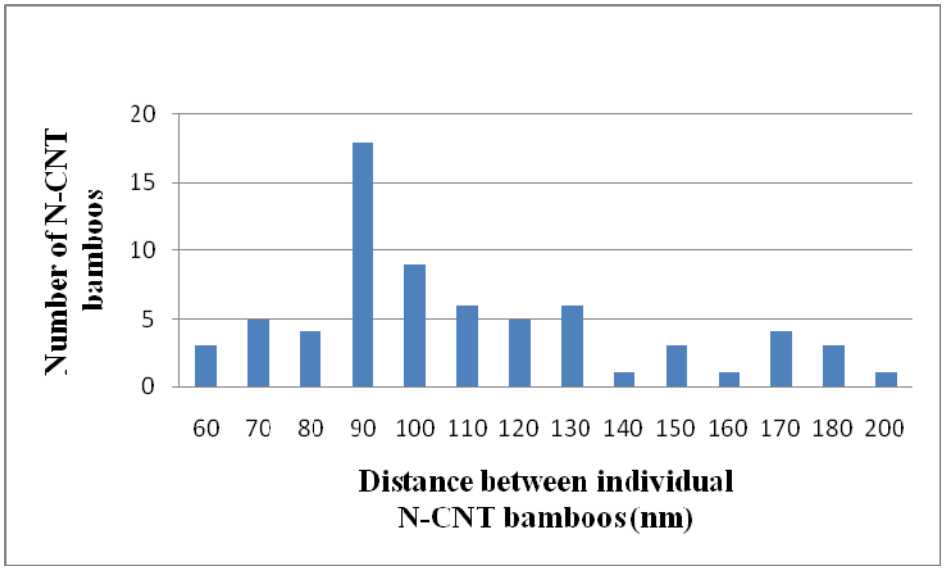


Fig. A6.2. Distance between individual bamboo compartments obtained from the pyrolysis of 2-methylimidazole (50:50).

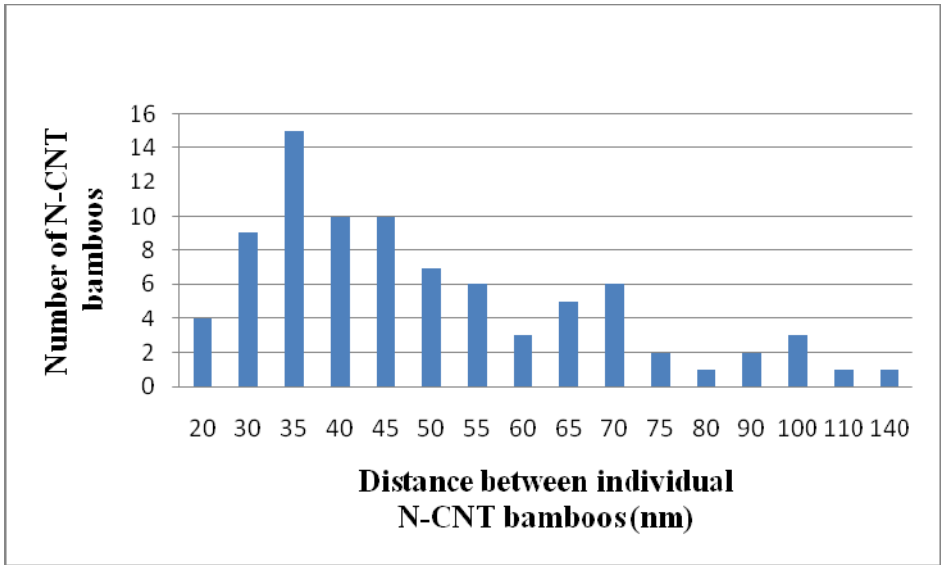


Fig. A6.3. Distance between individual bamboo compartments obtained from the pyrolysis of 4-methylimidazole (50:50).

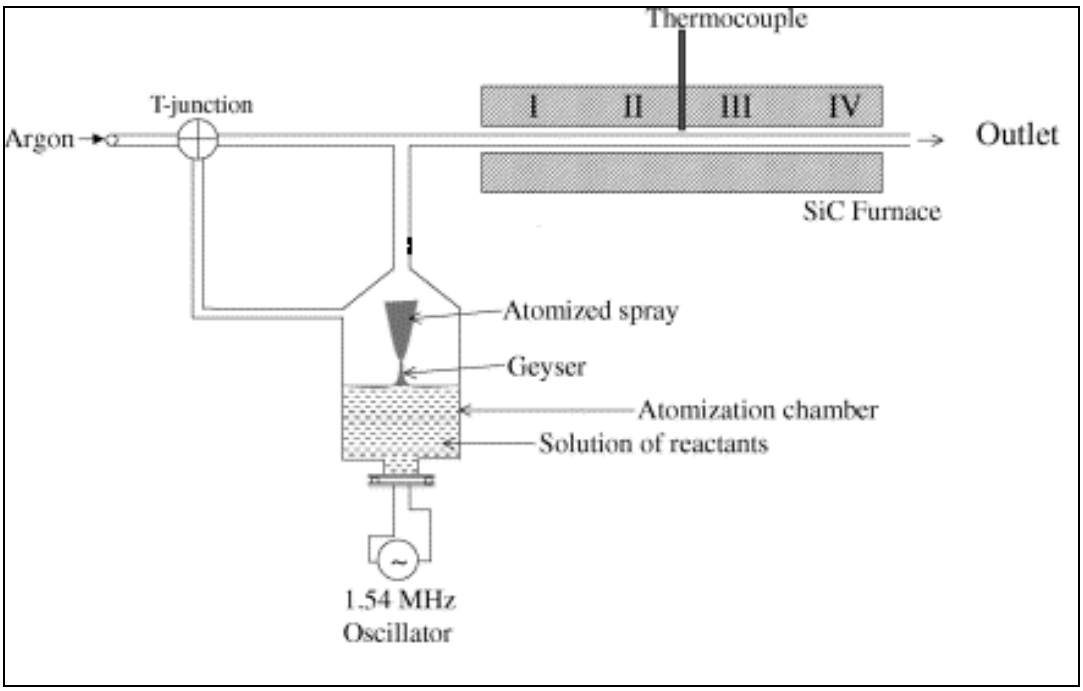


Fig. A7.1. Schematic diagram of the experimental setup for the synthesis of N-CNTs [1,2].

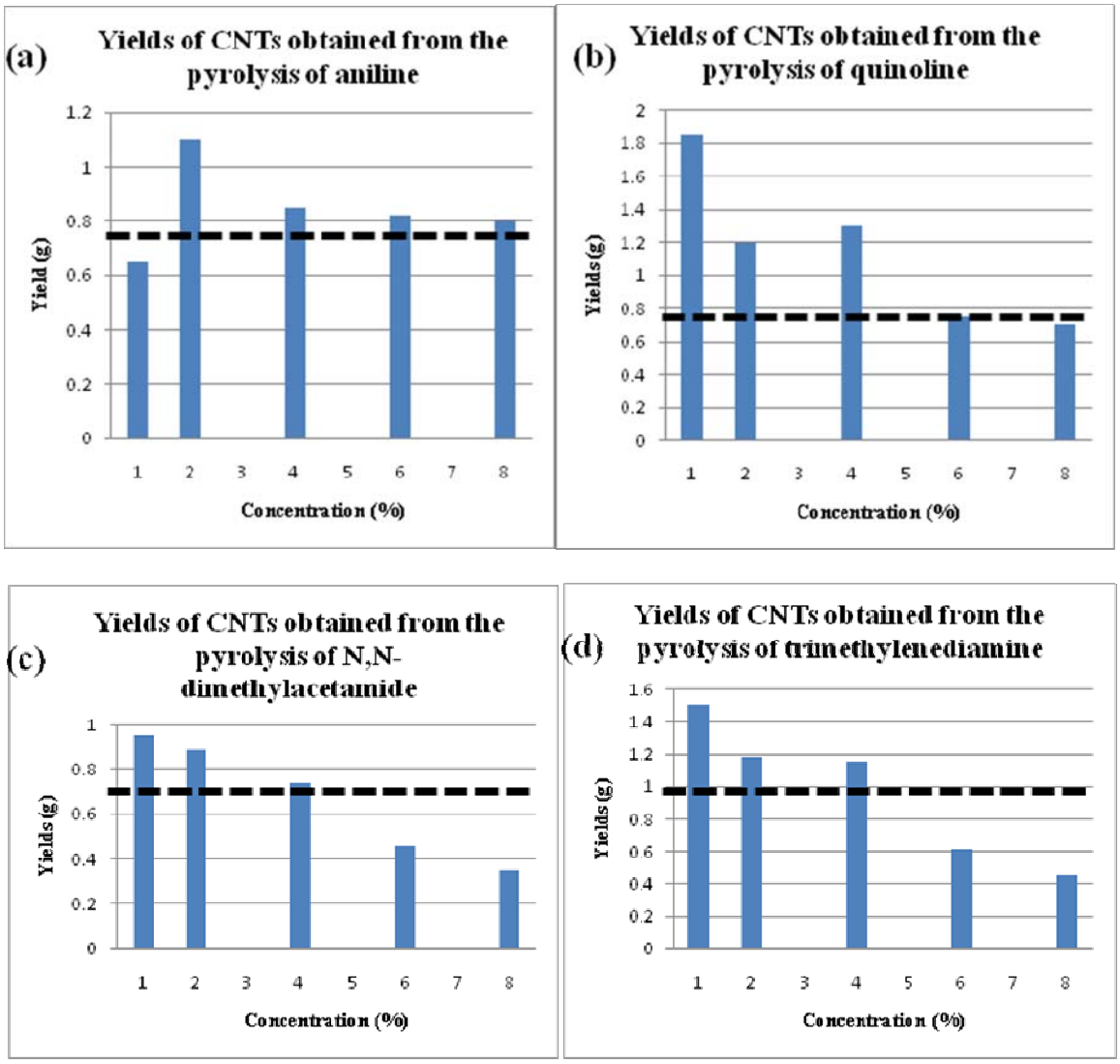


Fig. A7.2. Yield of CNTs obtained from the pyrolysis of toluene and ferrocene in the presence of (a) aniline; (b) quinoline; (c) *N*,*N*-dimethylacetamide; and (d) trimethylenediamine at different concentrations. Horizontal dotted lines indicate yields for ferrocene/toluene CNTs.

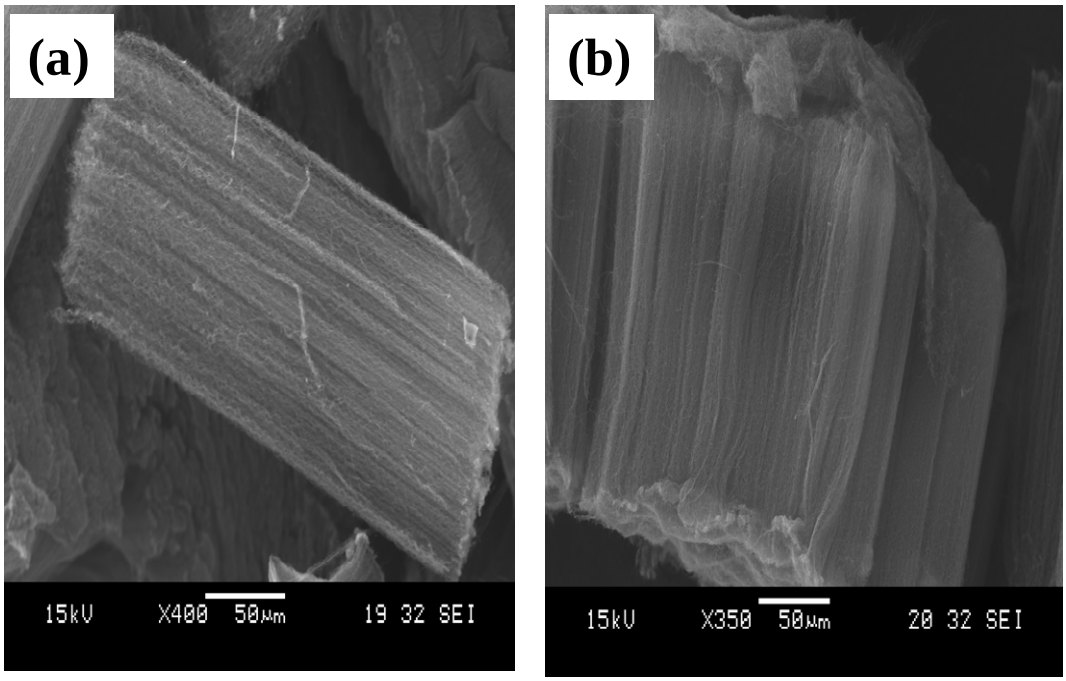


Fig. A7.3. SEM micrographs of CNT obtained from the pyrolysis of toluene and FcH in the presence of (a) 4% and (d) 8% formamide.

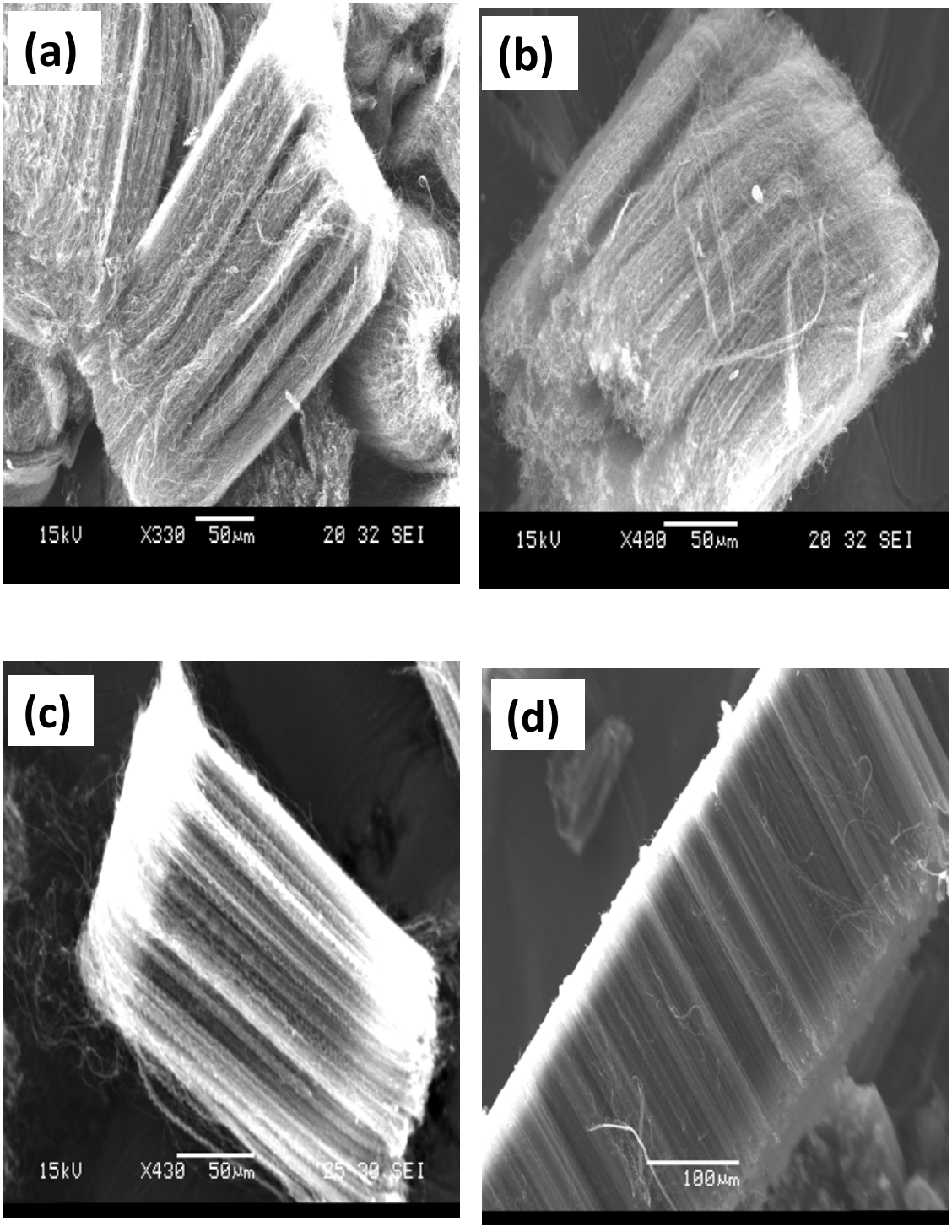


Fig. A7.4. SEM images of CNTs obtained from the pyrolysis of toluene and ferrocene in the presence of (a) 1%; and (b) 8% quinoline; and (c) 1%; and (d) 8% *N*,*N*-dimethylacetamide.

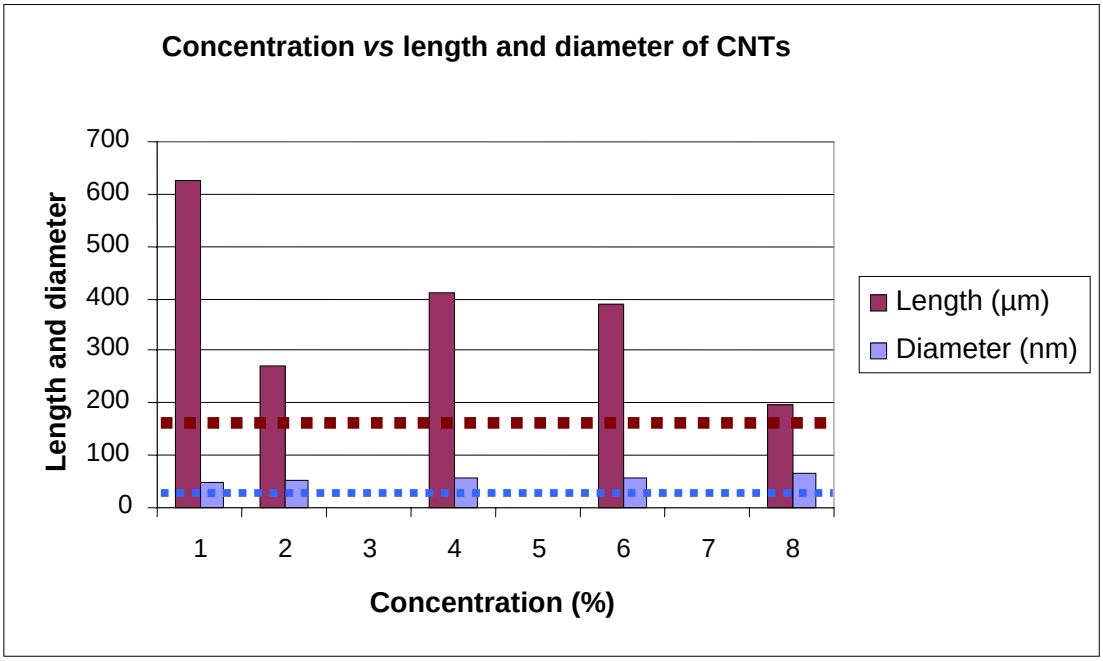


Fig. A7.5. Graph of concentration versus length and diameters of CNTs grown from hexamethylenediamine. Horizontal dotted line indicates lengths and diameters of CNTs obtained from FcH/toluene.

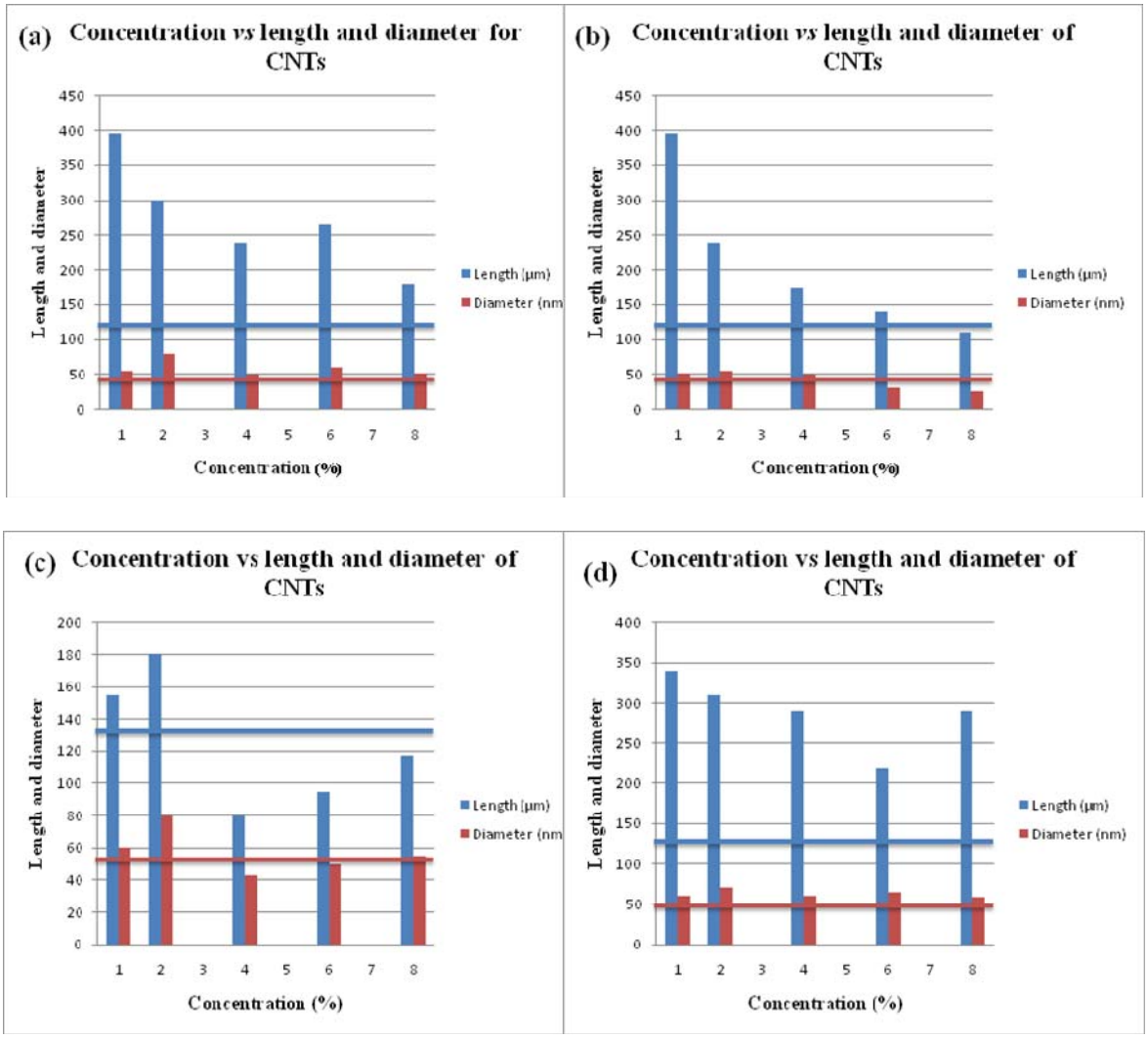


Fig. A7.6. Graph of concentration versus diameter and length of CNTs obtained from the pyrolysis of toluene and ferrocene in the presence of (a) diethylamine; (b) pyridine; (c) 1-methylpiperazine; and (d) formamide. Horizontal bar and dotted line indicate the length and diameter of the CNTs, respectively.

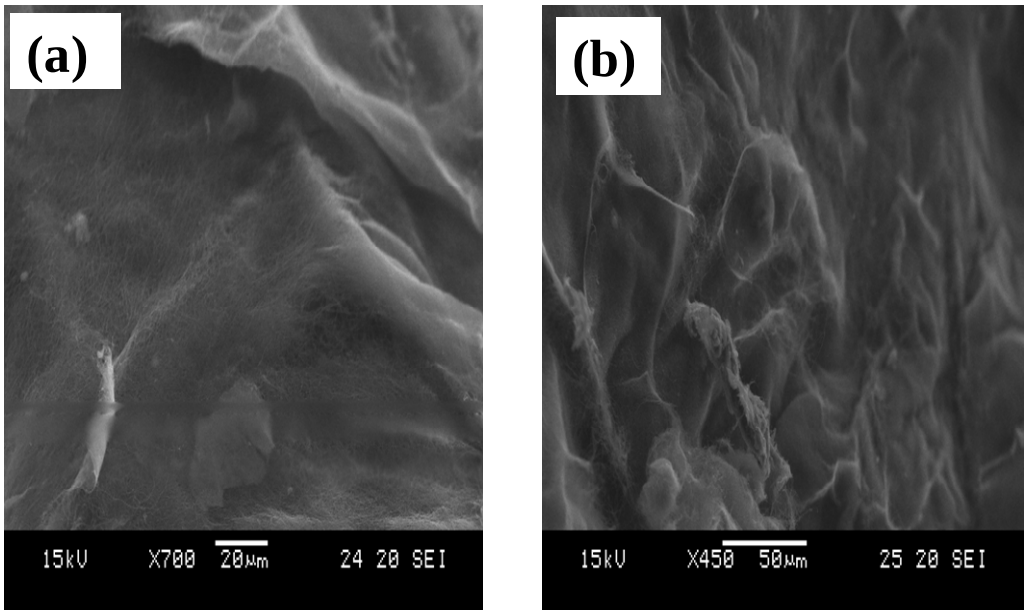


Fig. A7.7. SEM images of acid treated CNTs obtained from the pyrolysis of toluene and FcH in the presence (a) 1% and 8% quinoline.

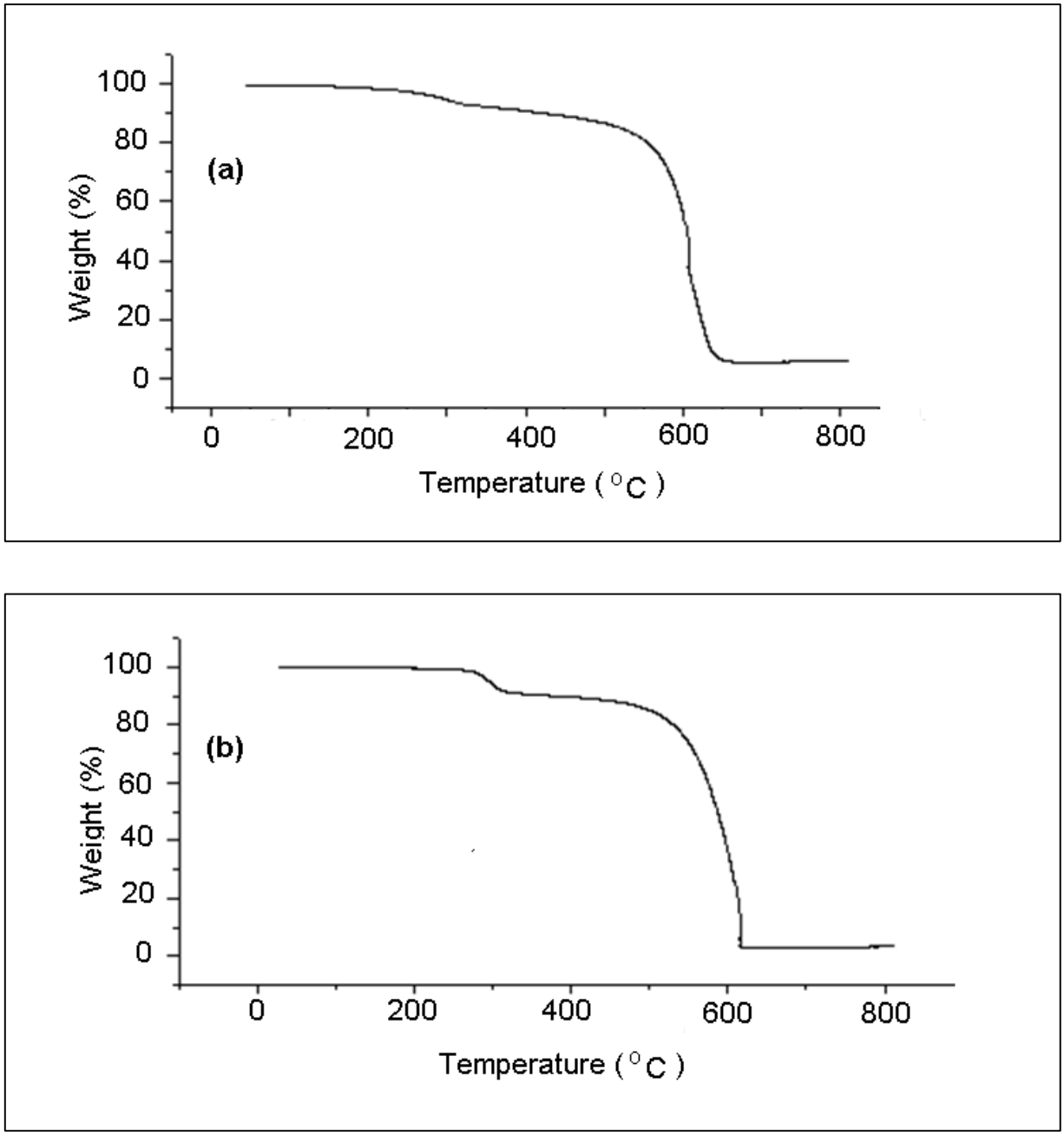


Fig. A7.8. TGA spectra of acid treated CNTs obtained from the pyrolysis of toluene and FcH in the presence of (a) 1%; and (b) 8% hexamethylenediamine.

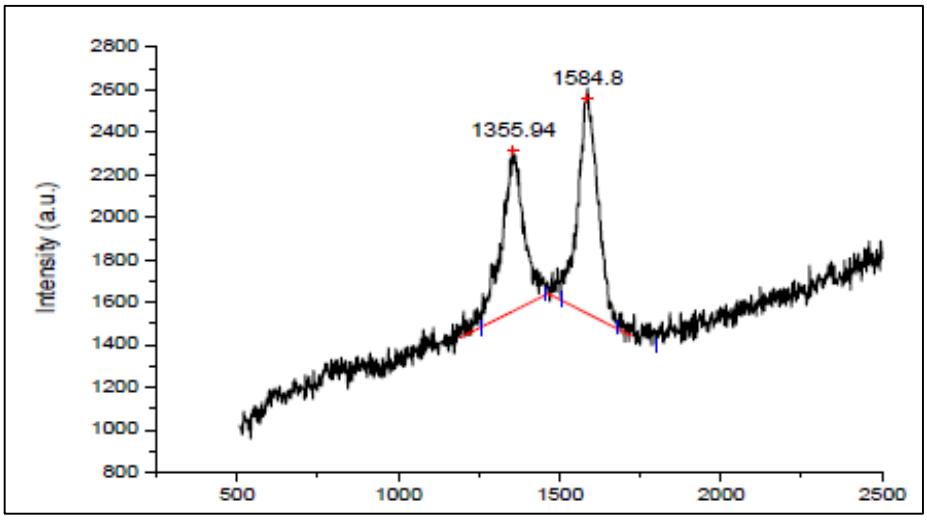


Fig. A7.9. Raman spectrum of CNTs obtained from the pyrolysis of toluene/FcH in the presence of 8% diethylamine.

B. Tables

Table A5.1. Crystal data and structure refinement for 7m_vc3_0a.

Identification code	7m_vc3_0a
Empirical formula	C16 H15 Fe N
Formula weight	277.14
Temperature	173(2) K
Wavelength	0.71073 Å
Crystal system	Orthorhombic
Space group	Pna2(1)
Unit cell dimensions	a = 18.2233(3) Å □= 90°.
	b = 10.9547(2) Å □= 90°.
	c = 6.08920(10) Å □ = 90°.
Volume	1215.59(4) $Å^3$
Z	4
Density (calculated)	1.514 Mg/m^3
Absorption coefficient	1.218 mm^{-1}
F	(000) 576
Crystal size	0.49 x 0.30 x 0.19 mm^3
Theta range for data collection	2.17 to 28.00°.
Index ranges	-24<=h<=24, -14<=k<=13, -8<=l<=7
Reflections collected	12806
Independent reflections	2812 [R(int) = 0.0315]
Completeness to theta	= 28.00° 99.9 %
Absorption correction	Intergration
Max. and min. transmission	0.8015 and 0.5866
Refinement method	Full-matrix least-squares on F^2
Data / restraints / parameters	2812 / 8 / 171
Goodness-of-fit on F^2	1.099

Final R indices [I>2sigma(I)]	R1 = 0.0221, wR2 = 0.0606
R indices (all data)	R1 = 0.0231, wR2 = 0.0611
Absolute structure parameter	0.002(13)
Largest diff. peak and hole	0.199 and -0.385 e.Å^{-3}

Table A5.2. Atomic coordinates (x 10^4) and equivalent isotropic displacement parameters (Å^{2}x 10^3) for 7m_vc3_0a. U(eq) is defined as one third of the trace of the orthogonalized U^{ij} tensor.

	x	y	z	U(eq)
C(1)	1512(1)	5770(2)	3695(3)	35(1)
C(2)	1546(1)	6530(2)	1854(3)	32(1)
C(3)	1069(1)	6074(2)	234(3)	44(1)
C(4)	731(1)	5009(2)	1105(8)	52(1)
C(5)	1006(1)	4831(2)	3238(5)	47(1)
C(6)	2968(1)	4544(1)	951(4)	22(1)
C(7)	2690(1)	4763(1)	-1200(3)	26(1)
C(8)	2163(1)	3838(2)	-1702(3)	30(1)
C(9)	2104(1)	3052(2)	133(3)	29(1)
C(10)	2599(1)	3482(1)	1779(3)	26(1)
C(11)	3548(1)	5245(1)	2086(3)	21(1)
C(12)	3878(1)	6270(1)	1143(3)	25(1)
C(13)	4441(1)	6891(2)	2171(3)	27(1)
C(14)	4699(1)	6511(1)	4220(3)	25(1)
C(15)	4372(1)	5499(2)	5198(3)	26(1)
C(16)	3812(1)	4877(1)	4140(3)	24(1)
Fe(1)	1842(1)	4795(1)	1006(1)	20(1)
N(1)	5255(1)	7148(2)	5302(3)	36(1)

Table A6.1. Raman data of CNTs produced from the pyrolysis of FcH, ferrocenylmethylimidazole and FcH/*i*-methylimidazole at varying ratios.

Catalyst used to grow CNTs	**D-band (cm^{-1})**	**G-band (cm^{-1})**	I_D/I_G **Ratio**
FcH (100%)	1345	1577	1.09
Ferrocenylmethylimidazole (100%)	1348	1595	1.93
FcH/1-methylimidazole (90:10)	1345	1581	1.25
FcH/2-methylimidazole (90:10)	1352	1580	0.75
FcH/4-methylimidazole (90:10)	1342	1577	1.01
FcH/1-methylimidazole (80:20)	1349	1580	1.09
FcH/2-methylimidazole (80:20)	1352	1582	0.65
FcH/4-methylimidazole (80:20)	1345	1581	2.04
FcH/1-methylimidazole (50:50)	1350	1582	0.85
FcH/2-methylimidazole (50:50)	1348	1583	1.53
FcH/4-methylimidazole (50:50)	1343	1601	1.21
FcH/1-methylimidazole (20:80)	1358	1554	2.53
FcH/2-methylimidazole (20:80)	1382	1601	1.89
FcH/4-methylimidazole (20:80)	1379	1600	1.60
FcH/1-methylimidazole (10:90)	1350	1579	0.80
FcH/2-methylimidazole (10:90)	1351	1504	1.42
FcH/4-methylimidazole (10:90)	1369	1533	1.72

Table A7.1. Yield of CNTs obtained from pyrolysis of toluene and FcH in the presence of various N containing reagents at different concentrations.[1]

	Mass (g)				
Reagent	1%	2%	4%	6%	8%
Diethylamine	1.26	1.02	0.89	0.56	0.58
Butylamine	1.28	0.69	0.58	0.61	0.53
Isopropylamine	0.97	0.83	0.55	0.56	0.36
Benzylamine	1.47	1.29	0.94	0.93	0.85
Pyridine	1.67	0.46	0.43	0.43	0.23
Aniline	-	1.09	0.88	0.87	0.81
Quinoline	1.86	1.19	1.28	0.76	0.69
N-benzylmethylamine	0.99	1.27	0.74	0.75	0.63
1-methylpiperazine	1.37	1.10	0.74	0.57	0.42
Hexamethylenediamine	1.07	1.23	1.15	1.32	-
N-methylethylenediamine	1.07	0.74	0.61	0.72	0.33
Trimethylenediamine	1.52	1.16	1.11	0.65	0.53
Formamide	1.53	1.07	0.95	0.68	0.99
N,*N*-dimethylformamide	1.82	0.97	0.57	0.52	0.49
N,*N*-dimethylacetamide	0.94	0.88	0.75	0.46	0.35

[1] FcH/toluene with no added N containing reagent; yield = 0.70 g

Table A7.2. Average diameters of acid treated CNTs obtained from the pyrolysis of toluene and FcH in the presence of various nitrogen containing hydrocarbons.[1,2]

Nitrogen containing hydrocarbons	Diameter (nm)	
	1%	8%
Diethylamine	48 (58)	42 (54)
Quinoline	43 (59)	49 (62)
Hexamethylenediamine	50 (49)	48 (65)
N,*N*-dimethylacetamide	44 (57)	36 (62)

[1] Toluene/FcH CNTs length = 130 μm (136 μm); diameter = 44 (45) (untreated data in brackets)

[2] Untreated CNT diameters given in brackets

Table A7.3. Mass of CNTs before and after purification; mass difference and percentage difference.

N containing reagent	Mass before purification (g)	Mass after purification (g)	Mass difference (g)	Difference (%)
0%	0.0506	0.0413	0.0093	18.4
1% Diethylamine	0.0512	0.0452	0.0060	11.7
8% Diethylamine	0.0511	0.0422	0.0089	17.4
1% Quinoline	0.0501	0.0424	0.0077	15.4
8% Quinoline	0.0500	0.0322	0.0179	35.8
1% Hexamethylenediamine	0.0500	0.0380	0.012	24.0
8% Hexamethylenediamine	0.0505	0.0431	0.0074	13.4
1% *N*,*N*-dimethylformamide	0.0506	0.0381	0.0121	23.9
8% *N*,*N*-dimethylformamide	0.0514	0.0475	0.0039	7.59

References

1. S.R.C. Vivekchand, L.M. Cele, F.L. Deepak, A.R. Raju, A. Govindaraj, Chem. Phys. Lett. 386 (2004) 313.
2. P. Letsoalo, The effect of nitrogen sources on the synthesis of carbon nanotubes by nebulized spray pyrolysis, MTech dissertation, University of Johannesburg, 2006.